INTRAOPERATIVE FLUORESCENCE IMAGING AND DIAGNOSIS IN CENTRAL AND PERIPHERAL NERVOUS SYSTEM TUMORS: ESTABLISHED APPLICATIONS AND FUTURE PERSPECTIVES

EDITED BY: Francesco Acerbi, Constantinos G. Hadjipanayis, Karl-Michael Schebesch, Morgan Broggi and Talat Kiris

PUBLISHED IN: Frontiers in Oncology and Frontiers in Neurology

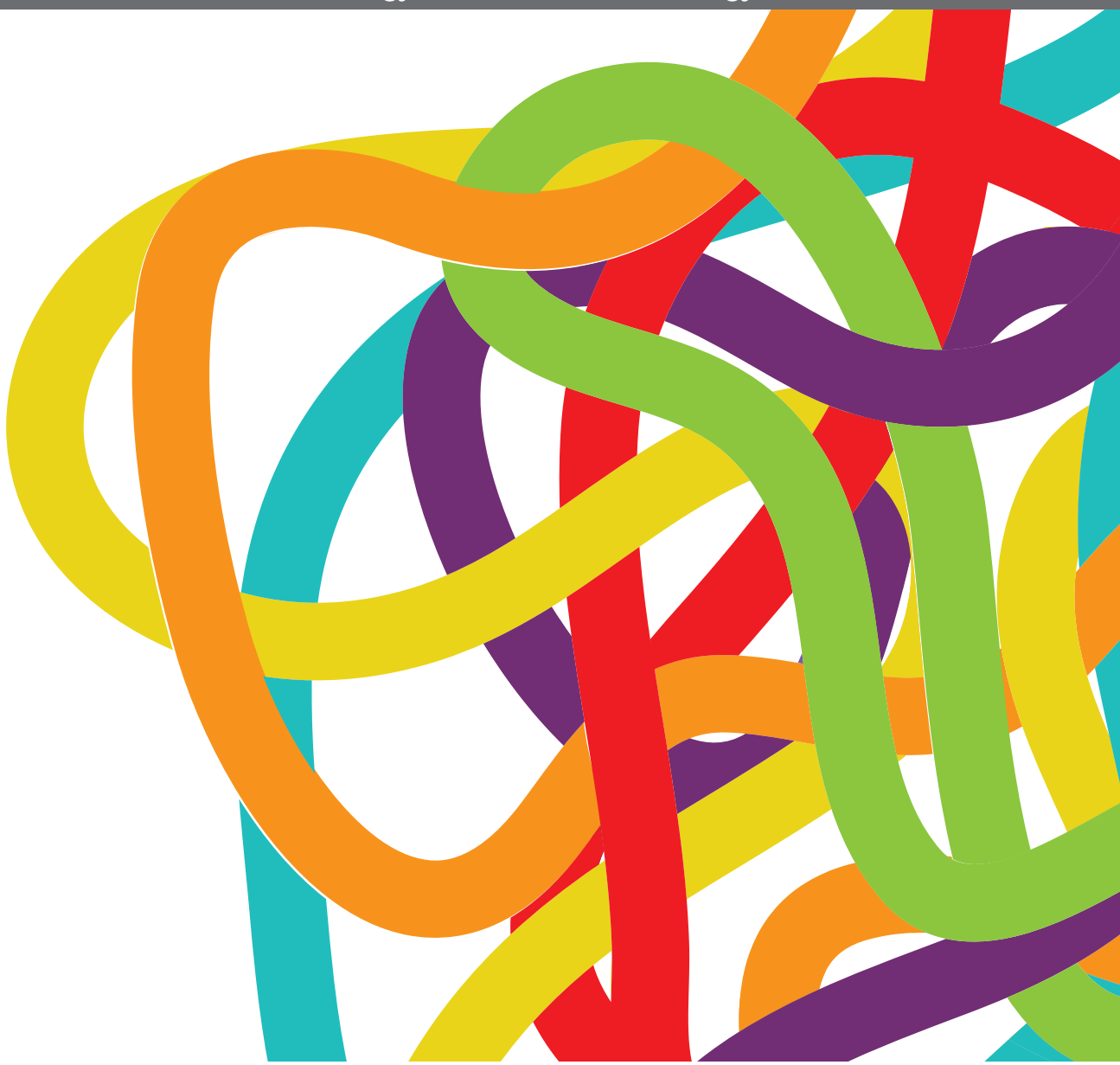

frontiers Research Topics

ISSN 1664-8714
ISBN 978-2-88974-773-3
DOI 10.3389/978-2-88974-773-3

About Frontiers

Frontiers is more than just an open-access publisher of scholarly articles: it is a pioneering approach to the world of academia, radically improving the way scholarly research is managed. The grand vision of Frontiers is a world where all people have an equal opportunity to seek, share and generate knowledge. Frontiers provides immediate and permanent online open access to all its publications, but this alone is not enough to realize our grand goals.

Frontiers Journal Series

The Frontiers Journal Series is a multi-tier and interdisciplinary set of open-access, online journals, promising a paradigm shift from the current review, selection and dissemination processes in academic publishing. All Frontiers journals are driven by researchers for researchers; therefore, they constitute a service to the scholarly community. At the same time, the Frontiers Journal Series operates on a revolutionary invention, the tiered publishing system, initially addressing specific communities of scholars, and gradually climbing up to broader public understanding, thus serving the interests of the lay society, too.

Dedication to Quality

Each Frontiers article is a landmark of the highest quality, thanks to genuinely collaborative interactions between authors and review editors, who include some of the world's best academicians. Research must be certified by peers before entering a stream of knowledge that may eventually reach the public - and shape society; therefore, Frontiers only applies the most rigorous and unbiased reviews.
Frontiers revolutionizes research publishing by freely delivering the most outstanding research, evaluated with no bias from both the academic and social point of view. By applying the most advanced information technologies, Frontiers is catapulting scholarly publishing into a new generation.

What are Frontiers Research Topics?

Frontiers Research Topics are very popular trademarks of the Frontiers Journals Series: they are collections of at least ten articles, all centered on a particular subject. With their unique mix of varied contributions from Original Research to Review Articles, Frontiers Research Topics unify the most influential researchers, the latest key findings and historical advances in a hot research area! Find out more on how to host your own Frontiers Research Topic or contribute to one as an author by contacting the Frontiers Editorial Office: frontiersin.org/about/contact

INTRAOPERATIVE FLUORESCENCE IMAGING AND DIAGNOSIS IN CENTRAL AND PERIPHERAL NERVOUS SYSTEM TUMORS: ESTABLISHED APPLICATIONS AND FUTURE PERSPECTIVES

Topic Editors:
Francesco Acerbi, IRCCS Carlo Besta Neurological Institute Foundation, Italy
Constantinos G. Hadjipanayis, Mount Sinai Health System, United States
Karl-Michael Schebesch, University of Regensburg, Germany
Morgan Broggi, Department of Neurosurgery, IRCCS Carlo Besta Neurological Institute Foundation, Italy
Talat Kiris, Koç University, Turkey

Citation: Acerbi, F., Hadjipanayis, C. G., Schebesch, K.-M., Broggi, M., Kiris, T., eds. (2022). Intraoperative Fluorescence Imaging and Diagnosis in Central and Peripheral Nervous System Tumors: Established Applications and Future Perspectives. Lausanne: Frontiers Media SA. doi: 10.3389/978-2-88974-773-3

Table of Contents

frontiers in Oncology

EDITORIAL
published: 07 February 2022
doi: 10.3389/fonc.2022.845333

Editorial: Intraoperative Fluorescence Imaging and Diagnosis in Central and Peripheral Nervous System Tumors: Established Applications and Future Perspectives

Francesco Acerbi[1*], *Morgan Broggi*[1], *Constantinos G. Hadjipanayis*[2], *Talat Kiris*[3] *and Karl-Michael Schebesch*[4]

[1] Department of Neurosurgery, Foundation IRCCS Neurological Institute Carlo Besta, Milano, Italy, [2] Department of Neurosurgery, Icahn School of Medicine at Mount Sinai, Mount Sinai Health System, New York, NY, United States, [3] Department of Neurosurgery, School of Medicine, Koc University, Istanbul, Turkey, [4] Department of Neurosurgery, University Medical Center Regensburg, Regensburg, Germany

Keywords: CNS tumors, gliomas, PNST, fluorescence, 5-ALA, fluorescein, ICG, confocal endomicroscopy

Editorial on the Research Topic

Intraoperative Fluorescence Imaging and Diagnosis in Central and Peripheral Nervous System Tumors: Established Applications and Future Perspectives

OPEN ACCESS

Edited and reviewed by:
David D. Eisenstat,
Royal Children's Hospital, Australia

***Correspondence:**
Francesco Acerbi
Francesco.Acerbi@istituto-besta.it

Specialty section:
This article was submitted to Neuro-Oncology and Neurosurgical Oncology, a section of the journal Frontiers in Oncology

Received: *29 December 2021*
Accepted: *20 January 2022*
Published: *07 February 2022*

Citation:
Acerbi F, Broggi M, Hadjipanayis CG, Kiris T and Schebesch K-M (2022) Editorial: Intraoperative Fluorescence Imaging and Diagnosis in Central and Peripheral Nervous System Tumors: Established Applications and Future Perspectives. Front. Oncol. 12:845333. doi: 10.3389/fonc.2022.845333

This Research Topic "*Intraoperative Fluorescence Imaging and Diagnosis in Central and Peripheral Nervous System Tumors: Established Applications and Future Perspectives*" consists of 13 articles contributed by 100 authors in the field of Neurosurgery, Neuropathology, Neuro-oncology, Medical Physics, and Biophotonics. Our aim was to provide a comprehensive and up-to-date understanding of the possible utilization of different intraoperative fluorophores for both diagnostic and therapeutic purposes in the field of neuro-oncological surgery, as well as its combined use with other intraoperative tools. Eight of the 13 published papers were addressing the problem of the utilization of different intraoperative fluorophores for tumor visualization and therapeutic purposes.

Schupper et al. performed a review to describe the most currently used fluorophores for glioma surgery [5-aminolevulenic acid (5-ALA), sodium fluorescein (SF), indocyanine green (ICG)], elucidating the current evidence on the perspective of timing for each. In addition, these authors also mentioned current studies on fluorophores with more directed mechanisms of action, such as tozulesteride (BLZ-100), a conjugate of tumor-specific peptide chlorotoxin paired with a near-infrared fluorophore, Alkylphosphocholine analogs (APCs), small synthetic phospholipid ether molecules targeting specific tumor cells, with different fluorescent spectrum, and Epidermal Growth Factor receptor (EGFR) targeted molecules, conjugated with near-infrared fluorophores. Finally, they also provide a summary of the most common Central Nervous System (CNS) tumors or other pathological conditions that can be operated with fluorescence-guided resection.

Other studies concentrated on the use of 5-ALA in neuro-oncological surgery. Maragkos et al. identified 16 patients with high-grade gliomas (HGG) undergoing fluorescence-guided resection more than 6 hours after 5-ALA administration (in one case 27 hours and 46 minutes after). They showed that all cases had adequate intraoperative fluorescence, without toxicity, suggesting that relaxation on restrictions regarding timing of surgery after 5-ALA administration could have a positive impact on

procedure scheduling and workflow, without any additional risks for the patient. Kiesel et al. performed a review on the available literature evaluating the current role, limitations and new approaches of 5-ALA fluorescence during surgery on suspected low-grade gliomas (LGG). They showed that the current 5-ALA technique is limited by the frequent absence of visible fluorescence in pure LGG (i.e. those lesions without any areas of anaplastic transformation), suggesting instead that it could be particularly useful to visualize intratumoral regions with malignant transformation within suspected LGG. Furthermore, they also analyzed possible future approaches to improve intraoperative LGG visualization such as quantitative spectroscopic Protoporphyrin IX (PpIX) measurements, fluorescence lifetime imaging of PpIX, or confocal endomicroscopy.

Four studies focused on the use of SF in CNS tumors and Peripheral Nervous System tumors (PNST). Xu et al. studied the *in vitro* and *ex vivo* optical characteristics of SF to understand its spectroscopic features after biological tissue uptake. They showed that SF exhibits a significant broadening of its emission band together with a batochromic shift after tissue uptake in CNS tumor samples, possibly explained by differences in pH and concentration of the molecule inside the tumoral tissue. Wang et al. discussed the potential role of fluorescein in facilitating targeted supramarginal resection in HGG, by analyzing its strength in tumor identification, also in areas that fail to enhance on T1-weighed MRI, and its limitations. Olguner et al. analyzed the results of fluorescein-guided resection in 49 patients with spinal intradural tumors, 15 being intra- and 34 being extra-medullary. They found a dense and homogenous fluorescence in all extramedullary tumors and in 73.3% of intramedullary tumors, while 13.3% of intramedullary tumors presented lower and more heterogeneous fluorescence. The use of SF was considered helpful to remove the lesion in 95.9% of the cases. Pedro et al. studied the application of low-dosage of SF for fluorescence-guided resection or biopsy of PNST, analyzing a series of 10 patients. The series comprised schwannomas (6 cases), neurofibroma (1 case), malignant PNST (2 cases) and B-cell lymphoma (1 case). In 90% of the cases the surgeon considered the use of SF helpful in performing the surgical procedure. In addition, the authors were able to find specific fluorescence spectra in different histological subtypes and normal nerve fibers by retrospectively analyzing the recorded intraoperative pictures.

Raspagliesi et al. evaluated the feasibility and safety of sonodynamic therapy in a preclinical animal model using both 5-ALA and SF as sonosensitizers. In particular, they showed that it was safe to sonicate the entire brain parenchyma after administration of sonosensitizing agents, demonstrating that no grey or white matter areas were subjected to macro- and microscopic damage.

Five articles focused on the use the confocal laser endomicroscopy (CLE) in neuro-oncological surgery, using SF. Acerbi et al. reported the results of a prospective *ex vivo* study enrolling 15 patients operated on for primary glioblastomas (GBM) with fluorescein-guided technique and using the CONVIVO® system, a new miniature CLE available on the market. Several biopsies both at the tumor central core and at the tumor margins were performed and analyzed by the CONVIVO® system and then submitted for frozen and permanent sections. A blind comparison between confocal images and frozen/permanent section results was then performed. This comparison showed that the CONVIVO® system was revealed to be a quick (mean time for image interpretation was 5.74 minutes) and reliable method to recognize GBM characteristics at the tumor core, raising the possibility to use it as a complementary tool for intraoperative diagnosis. The research group at the Barrow Neurological Institute greatly contributed to this field by presenting three papers. In the paper by Belykh et al., they confirmed the high specificity (90% overall, 94% in gliomas) and positive predictive value of *ex vivo* tissue analysis with CLE in 47 patients (122 biopsies) affected by different brain tumors advocating its early shift to an *in vivo* use. They also introduced the idea of a second SF injection (reported in 7 patients) to improve image quality and consequently CLE diagnostic accuracy. This concept was further investigated by Abramov et al.: they compared the CLE images of six patients in which a second dose of SF was administered during surgery, according to the neurosurgeon's request, because the SF signal did not sufficiently yield clear, interpretable, actionable CLE images, with those of the first initial dose of the same group of patients and with those of another nine patients in which a single dose of SF was used. The article's conclusions were that, when judged necessary especially in prolonged procedures, redosing SF improves the CLE image quality and therefore its usefulness without side effects. Finally, following the very same concept, Belyck et al. reported the application of a high dose of SF (40 mg/Kg) and CLE in a case of a suspected LLG, without contrast-enhancing on preoperative Magnetic Resonance (MR). Very clear and nice images were obtained from the CLE system and were suggestive for a grade 2/3 glioma, confirmed by frozen section; final histology revealed a grade 3 anaplastic oligodendroglioma. The authors encouraged further investigation of this application in non-enhancing "borderline" gliomas. Lastly, in their very interesting paper, Ziebart et al. tried to overcome operator-dependent images interpretation errors by training two different machine learning systems to analyze *ex vivo* 13.972 CLE images obtained from 25 patients with different brain tumors: this residual network model was able to provide automated, real-time analysis of tumors specimen based on CLE images dataset. Once again, *in vivo* studies were warranted to further assess the intraoperative advantages of CLE technique.

Intraoperative tumor visualization represents one of the most important problems in neuro-oncological surgery. The use of intraoperative fluorescence, as also shown by the articles published in this Research Topic, represents one of the most interesting and effective ways to improve the macroscopic and microscopic discrimination between tumoral and non-tumoral tissue at the tumor margin, with a possible impact on patients' prognosis.

AUTHOR CONTRIBUTIONS

FA, MB, CH, TK, and KM-S analyzed the papers published in the Research Topic and contributed to the Editorial.

Conflict of Interest: FA and KM-S received fees from Carl Zeiss Meditec for lectures at International Scientific Meetings. CH is a consultant for NX Development Corporation (NXDC) and Synaptive Medical. NXDC, a privately held company, markets Gleolan (5-ALA, aminolevulinic acid hydrochloride). Gleolan is an optical imaging agent approved for the visualization of malignant tissue during glioma surgery. CH is a consultant for NXDC and receives royalty payments for the sale of Gleolan, has also received speaker fees by Carl Zeiss and Leica.

The remaining authors declare that the research was conducted in the absence of any commercial or financial relationships that could be construed as a potential conflict of interest.

Publisher's Note: All claims expressed in this article are solely those of the authors and do not necessarily represent those of their affiliated organizations, or those of the publisher, the editors and the reviewers. Any product that may be evaluated in this article, or claim that may be made by its manufacturer, is not guaranteed or endorsed by the publisher.

frontiers in Oncology

ORIGINAL RESEARCH
published: 04 December 2020
doi: 10.3389/fonc.2020.599250

Intraoperative Confocal Laser Endomicroscopy *Ex Vivo* Examination of Tissue Microstructure During Fluorescence-Guided Brain Tumor Surgery

*Evgenii Belykh[1], Xiaochun Zhao[1], Brandon Ngo[1], Dara S. Farhadi[1], Vadim A. Byvaltsev[2], Jennifer M. Eschbacher[3], Peter Nakaji[1] and Mark C. Preul[1]**

[1] Department of Neurosurgery, The Loyal and Edith Davis Neurosurgical Research Laboratory, Barrow Neurological Institute, St. Joseph's Hospital and Medical Center, Phoenix, AZ, United States, [2] Department of Neurosurgery and Innovative Medicine, Irkutsk State Medical University, Irkutsk, Russia, [3] Department of Neuropathology, Barrow Neurological Institute, St. Joseph's Hospital and Medical Center, Phoenix, AZ, United States

OPEN ACCESS

Edited by:
Morgan Broggi, Istituto Neurologico Carlo Besta (IRCCS), Italy

Reviewed by:
Alexander Brawanski, University Medical Center Regensburg, Germany
Emanuele La Corte, University of Bologna, Italy

***Correspondence:**
Mark C. Preul
Neuropub@barrowneuro.org

Specialty section:
This article was submitted to Neuro-Oncology and Neurosurgical Oncology, a section of the journal Frontiers in Oncology

Received: *26 August 2020*
Accepted: *26 October 2020*
Published: *04 December 2020*

Citation:
Belykh E, Zhao X, Ngo B, Farhadi DS, Byvaltsev VA, Eschbacher JM, Nakaji P and Preul MC (2020) Intraoperative Confocal Laser Endomicroscopy Ex Vivo Examination of Tissue Microstructure During Fluorescence-Guided Brain Tumor Surgery. Front. Oncol. 10:599250. doi: 10.3389/fonc.2020.599250

Background: Noninvasive intraoperative optical biopsy that provides real-time imaging of histoarchitectural (cell resolution) features of brain tumors, especially at the margin of invasive tumors, would be of great value. To assess clinical-grade confocal laser endomicroscopy (CLE) and to prepare for its use intraoperatively *in vivo*, we performed an assessment of CLE *ex vivo* imaging in brain lesions.

Methods: Tissue samples from patients who underwent intracranial surgeries with fluorescein sodium (FNa)–based wide-field fluorescence guidance were acquired for immediate intraoperative *ex vivo* optical biopsies with CLE. Hematoxylin-eosin–stained frozen section analysis of the same specimens served as the gold standard for blinded neuropathology comparison. FNa 2 to 5 mg/kg was administered upon induction of anesthesia, and FNa 5 mg/kg was injected for CLE contrast improvement. Histologic features were identified, and the diagnostic accuracy of CLE was assessed.

Results: Of 77 eligible patients, 47 patients with 122 biopsies were enrolled, including 32 patients with gliomas and 15 patients with other intracranial lesions. The positive predictive value of CLE optical biopsies was 97% for all specimens and 98% for gliomas. The specificity of CLE was 90% for all specimens and 94% for gliomas. The second FNa injection in seven patients, a mean of 2.6 h after the first injection, improved image quality and increased the percentage of accurately diagnosed images from 67% to 93%. Diagnostic CLE features of lesional glioma biopsies and normal brain were identified. Seventeen histologic features were identified.

Conclusions: Results demonstrated high specificity and positive predictive value of *ex vivo* intraoperative CLE optical biopsies and justify an *in vivo* intraoperative trial. This new portable, noninvasive intraoperative imaging technique provides diagnostic features to discriminate lesional tissue with high specificity and is feasible for

incorporation into the fluorescence-guided surgery workflow, particularly for patients with invasive brain tumors.

Keywords: brain histology, brain tumor, confocal laser endomicroscopy, fluorescein sodium, fluorescence, frozen section, optical biopsy

INTRODUCTION

Complete resection within the bounds of functional safety is the goal of neurosurgical treatment for most brain tumors, especially invasive tumors, such as high-grade glioma (HGG) (1, 2). Of particular importance are intraoperative tools that aid not only in the identification of abnormal brain tissue that should be resected but also in its differentiation from healthy brain tissue that should be preserved (3). Here we report an investigation of a relatively new handheld cellular resolution imaging tool that may prove valuable for intraoperative noninvasive optical biopsy.

Previous generations of the confocal laser endomicroscope (CLE) demonstrated initial feasibility in visualizing brain tumor microstructure with significant diagnostic accuracy (4). However, these designs were largely based on an imaging platform directly adapted from those used for gastrointestinal imaging. Thus, the US Food and Drug Administration (FDA) approved the use of these systems in the brain only for experimental purposes, and previous generations of CLE were used in only three limited trials that included *in vivo* and *ex vivo* intraoperative use (5–7). Disadvantages of the early designs included the necessity to sterilize the scanning probe between procedures; the wide 7-mm diameter of the probe, which limited the use of the CLE within narrow surgical corridors; and the straight profile of the probe as it fit into the surgeon's hand.

The novel-generation commercial clinical grade CLE was developed to address these shortcomings. The FDA-approved CLE system has a 5-mm-diameter probe that is curved like an aspiration instrument, and it has increased imaging resolution and is designed to work with a removable sterile sheet. Since the use of CLE for visualization of brain tumors was first reported, wide-field fluorescence guidance surgery has increased in popularity. Thus, fluorescein sodium (FNa) began to be administered as part of the standard neurosurgical procedure so that the bright glow of FNa fluorescence could be visualized with an operating microscope used in the Yellow560 mode.

To assess the clinical grade CLE and prepare for its intraoperative use *in vivo*, we designed an assessment of its *ex vivo* imaging performance in brain lesions, particularly invasive brain tumors. We studied CLE use during routine fluorescence-guided surgery (FGS) with the operating microscope to visualize and compare CLE tissue-imaging microstructure in *ex vivo* samples with frozen section biopsies of brain tumors. We assessed the feasibility and diagnostic accuracy of CLE optical biopsies of brain lesions to identify relevant practical and methodologic variables for future *in vivo* use in clinical studies.

Abbreviations: 5-ALA, 5-aminolevulinic acid; CI, confidence interval; CLE, confocal laser endomicroscope, confocal laser endomicroscopy; FDA, US Food and Drug Administration; FGS, fluorescence-guided surgery; FNa, fluorescein sodium; H&E, hematoxylin-eosin; HGG, high-grade glioma; ICG, indocyanine green.

MATERIALS AND METHODS

Study Design

This prospective study was conducted at St. Joseph's Hospital and Medical Center with approval from the Institutional Review Board for Human Research (IRB No, 10BN130). All participants gave informed voluntary consent for participation in this study and were recruited from patients who were operated on from August 2016 to May 2019. Patients eligible for inclusion were adults (>18 years old) scheduled at our institution for neurosurgical lesion removal involving FNa contrast administration. This convenience sample of patients with brain lesions, mostly tumors, were enrolled whenever there was availability of CLE for operations conducted by the neurosurgeons participating in the study. Standard intraoperative techniques were used during tumor resection, including neuronavigation, operating microscope, endoscopic assistance, and, in some patients, intraoperative functional mapping. Deidentified brain tumor samples were used for this study. Demographic characteristics were deemed irrelevant to the optical biopsy interpretation and quality-assessment aspects of this study and were not recorded.

FNa Administration

FNa was administered intravenously at the induction of anesthesia to create a contrast for wide-field fluorescence guidance using the Yellow560 mode of the operating microscope. The FNa dose was determined by the operating neurosurgeon. FNa 2 mg/kg was used in patients with gliomas and meningiomas, and FNa 5 mg/kg was used in patients with metastatic lesions. FNa was readministered at a 5-mg/kg dose if deemed necessary by the neurosurgeon. One patient received 40 mg/kg of FNa at the induction of anesthesia only.

Tissue Collection and Processing

Tissue samples that were removed as a part of the standard neurosurgical procedure were obtained during the tumor resection for examination. These samples were separate from those obtained for clinical care (i.e., frozen-section and permanent-section analyses). When possible, multiple biopsies of the tumor core and tumor bed area were acquired. The number of biopsies was determined by the operating neurosurgeon.

Samples were placed on a moisturized nonadherent surgical dressing, transferred to the CLE station (CONVIVO, Carl Zeiss Meditec, AG, Jena, Germany) in the same operating room, and imaged using the CLE probe affixed in a probe holder in an upright position. Tissue samples were imaged with CLE

immediately after acquisition from the brain. The tissue samples were gently placed with microsurgical forceps to obtain optimal imaging. To obtain optimally balanced CLE images, we used a 488 nm excitation laser and a 517.5. to 572.5-nm bandpass filter at 1× zoom with automatic gain, resulting in resolution of 1920 × 1080 pixels and a 267 × 475 μm field of view.

The neurosurgeon was able to review the CLE images during the operation because they were displayed intraoperatively in real time on a large LED screen. When image brightness was not sufficient, the FNa was readministered according to the prescribed dosage at the request of the neurosurgeon.

After CLE imaging, tissue samples were placed on a piece of moistened absorbent cotton material in a plastic container. Samples were then submitted for histologic processing and hematoxylin-eosin (H&E) staining in the neuropathology department.

Image Analysis

The collected CLE images were processed using FIJI open-source software by applying the "despeckle" filter and creating short videos (3–20 frames in length) of select imaging locations. Deidentified CLE optical biopsies and H&E-stained sections were reviewed retrospectively in a blinded fashion by a board-certified neuropathologist (J.E.) competent in interpreting CLE images. The neuropathologist had no clinical information except that the biopsy had been performed during an intracranial procedure for removal of a lesion.

CLE optical biopsies were presented as multiple still images and video-like image loops. A CLE optical biopsy was graded as "lesional" when it was deemed representative of a tumor or necrotic tissue; as "normal" when it was representative of normal or reactive brain tissue; and as "nondiagnostic" when it was not representative of tumor or necrotic tissue (i.e., nondiagnostic of tumor). Seventeen histologic features were identified and assessed as "present" or "absent" in each CLE biopsy. The overall quality of CLE images for each optical biopsy was graded subjectively on a 6-point scale of zero to 5: 0 (not diagnostic or very bad), 1 (bad), 2 (poor), 3 (average), 4 (good), and 5 (very good). This quality assessment based on a subjective interpretation of clarity and brightness of tissue microstructure was performed by a neurosurgeon and a neuropathologist experienced in CLE and other fluorescence cell-imaging technologies.

H&E slides of biopsies were graded as "lesional" when they were representative of tumor tissue useful for diagnosis or interpretations and as "nonlesional" when they were representative of nontumor tissue, such as normal brain or gliotic reactive brain tissue. All H&E slides were useful for such interpretations. Each H&E slide was also labeled on the basis of the most likely diagnosis for a particular slide or as "nondiagnostic."

Image Interpretation

To assess how experience in working with CLE affects the interpretation of CLE images, we assigned two additional appraisers (both experienced senior neurosurgeons) to review a set of CLE images for interpretation. The first neurosurgeon (M.C.P.) was experienced in interpreting CLE images but was blinded to the image acquisition process. The second neurosurgeon (V.A.B.) had limited experience in interpreting CLE images but had assistance from a general pathologist who also lacked experience in interpreting CLE images. Prior to assessment, both neurosurgeons were instructed using a separate set of images on the key histologic features identifiable on CLE images. No information was provided to the neurosurgeons or general pathologist regarding case history, imaging, surgical information, or diagnosis.

Statistical Analysis

Statistical analysis was performed in Excel (Microsoft, Inc., Redmond, WA). The interpretation of CLE images and H&E histologic sections was compared. We also assessed CLE image quality and timing and dose of FNa injection. Exploratory diagnostic accuracy was calculated using a 2×2 table and standard formulas for the sensitivity, specificity, positive predictive value, and negative predictive value; results were reported according to the Standards for Reporting Diagnostic Accuracy Studies guidelines (8). For statistical analysis, CLE optical biopsies that were nondiagnostic of tumor tissue or that were labeled as normal tissue were used as a negative CLE test result. For the purpose of analysis, inconclusive H&E results were treated as "nonlesional."

RESULTS

Descriptive Analysis

Seventy-seven potentially eligible patients provided consent during the study period. CLE imaging was not performed for 13 patients because of surgery cancelation or CLE unavailability. Fourteen patients were excluded because their procedures were endoscopic transsphenoidal surgeries, and three patients were excluded because no biopsy samples were available for analysis. Thus, CLE imaging was available for 47 patients with 122 matched optical and histologic biopsies available for analysis (**Table 1**, **Figure 1**). Preliminary diagnoses by tumor type were as follows: 32 gliomas (19 primary glioblastomas, 5 recurrent glioblastomas, 5 infiltrating gliomas, 3 low-grade gliomas), 7 meningiomas, 4 metastatic brain lesions, 1 choroid plexus carcinoma, 1 craniopharyngioma, 1 schwannoma, and 1 arteriovenous malformation (reactive normal brain). All specimens were successfully analyzed *ex vivo* with CLE immediately after acquisition.

Second Dose of FNa

Resection of the lesion was completed in all patients under operating microscope visualization with and without Yellow560 mode irrespective of regard for *ex vivo* CLE analysis. In 7 cases (5 gliomas, 1 metastasis, and 1 choroid plexus carcinoma), FNa (5 mg/kg) was subsequently administered after the initial resection to evaluate the edge with subsequent biopsy acquisition for CLE analysis. FNa was readministered at a mean (SD) of 157 (52) min after the first administration. Analysis of these specimens showed improved brightness and contrast and improved overall image quality. For the cases in which the reinjection was performed, the percentage of images with an accurate diagnosis increased from 67% (18 of 27) to 93% (14 of 15), and the percentage of nondiagnostic CLE

TABLE 1 | General characteristics on confocal laser endomicroscopy of 122 biopsy specimens from 47 cases.

Final diagnosis	Cases	Biopsies	Biopsies per case, mean	Diagnosis on the basis of H&E staining (no. of biopsies)
GBM	19	52	2.7	HGG (30); infiltrating glioma (12); reactive gliotic brain (5); normal brain (3); necrosis (1); inconclusive (1)
Recurrent GBM	5	24	4.8	HGG (11); infiltrating glioma (10); necrosis (1); reactive gliotic brain (1); inconclusive (1)
Infiltrating glioma	5	13	2.6	Infiltrating glioma (11); reactive gliotic brain (1); normal brain (1)
LGG	3	8	2.7	Infiltrating glioma (4); normal brain (4)
Metastasis	4	9	2.3	Metastasis (8); reactive gliotic brain (1)
Meningioma	7	9	1.3	Meningioma (9)
Choroid plexus carcinoma	1	4	4	Choroid plexus carcinoma (4)
Craniopharyngioma	1	1	1	Craniopharyngioma (1)
Schwannoma	1	1	1	Schwannoma (1)
AVM	1	1	1	Reactive gliotic brain (1)

AVM, arteriovenous malformation; GBM, glioblastoma multiforme; H&E, hematoxylin-eosin; HGG, high-grade glioma; LGG, low-grade glioma.

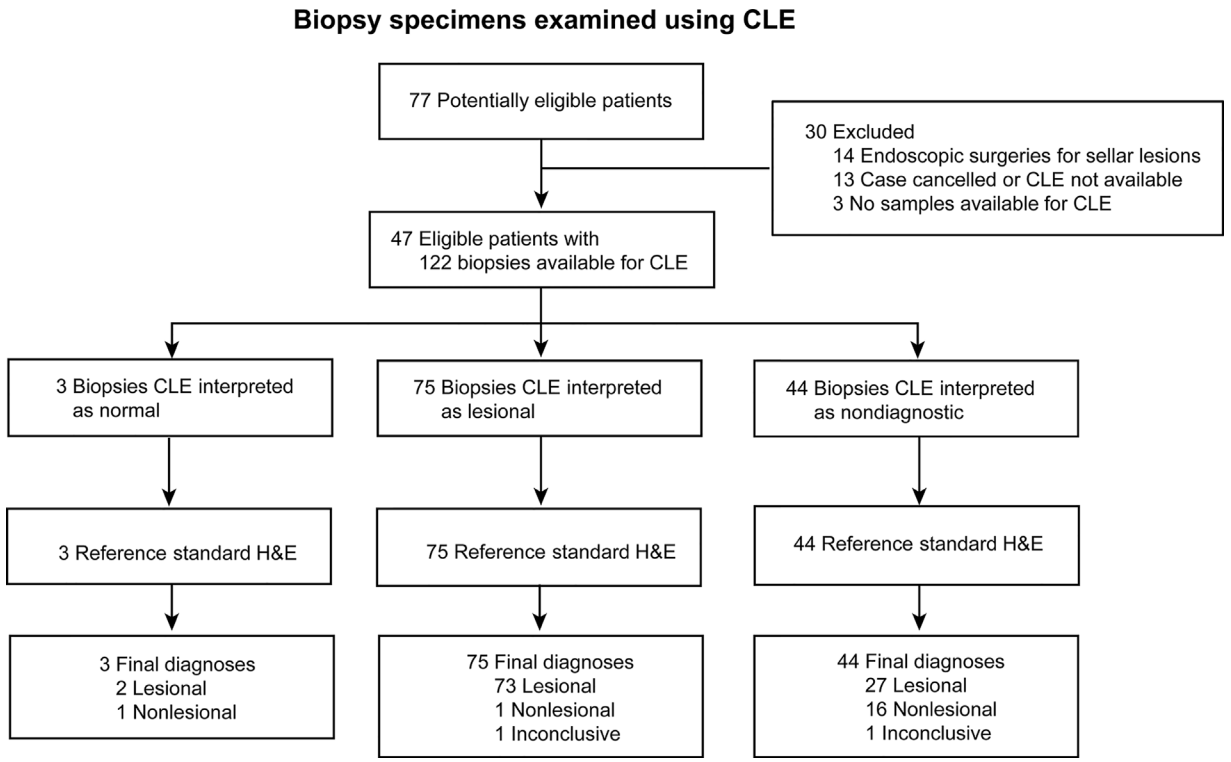

FIGURE 1 | Flowchart of 122 biopsy specimens from 47 patients with brain tumors examined using confocal laser endomicroscopy (CLE). H&E, hematoxylin-eosin. *Used with permission from Barrow Neurological Institute, Phoenix, Arizona.*

decreased from 26% (7 of 27) to 13% (2 of 15), although our study was not powered to detect differences in these subgroups (P=0.11 and P=0.31, respectively, by χ^2 analysis).

Timing of FNa Injection

In many cases, biopsy acquisition occurs more than 90 min after the first FNa administration, which results in suboptimal contrast in CLE images (7). This decrease in image quality was also found for biopsies in the current study when the FNa was injected 1 to 5 min before imaging. However, the analysis of all biopsies, as well as the glioma-only biopsies obtained at different time points after FNa injection, showed no correlation between the timing of FNa administration and image quality (r=−0.14, P>0.05) or with the probability of the CLE optical biopsy being used to diagnose specimens as either lesional or nondiagnostic (logistic regression P=0.93).

CLE Histologic Features

Various histologic features were assessed to elucidate characteristics of diagnostic and nondiagnostic CLE optical biopsies (**Figure 2**).

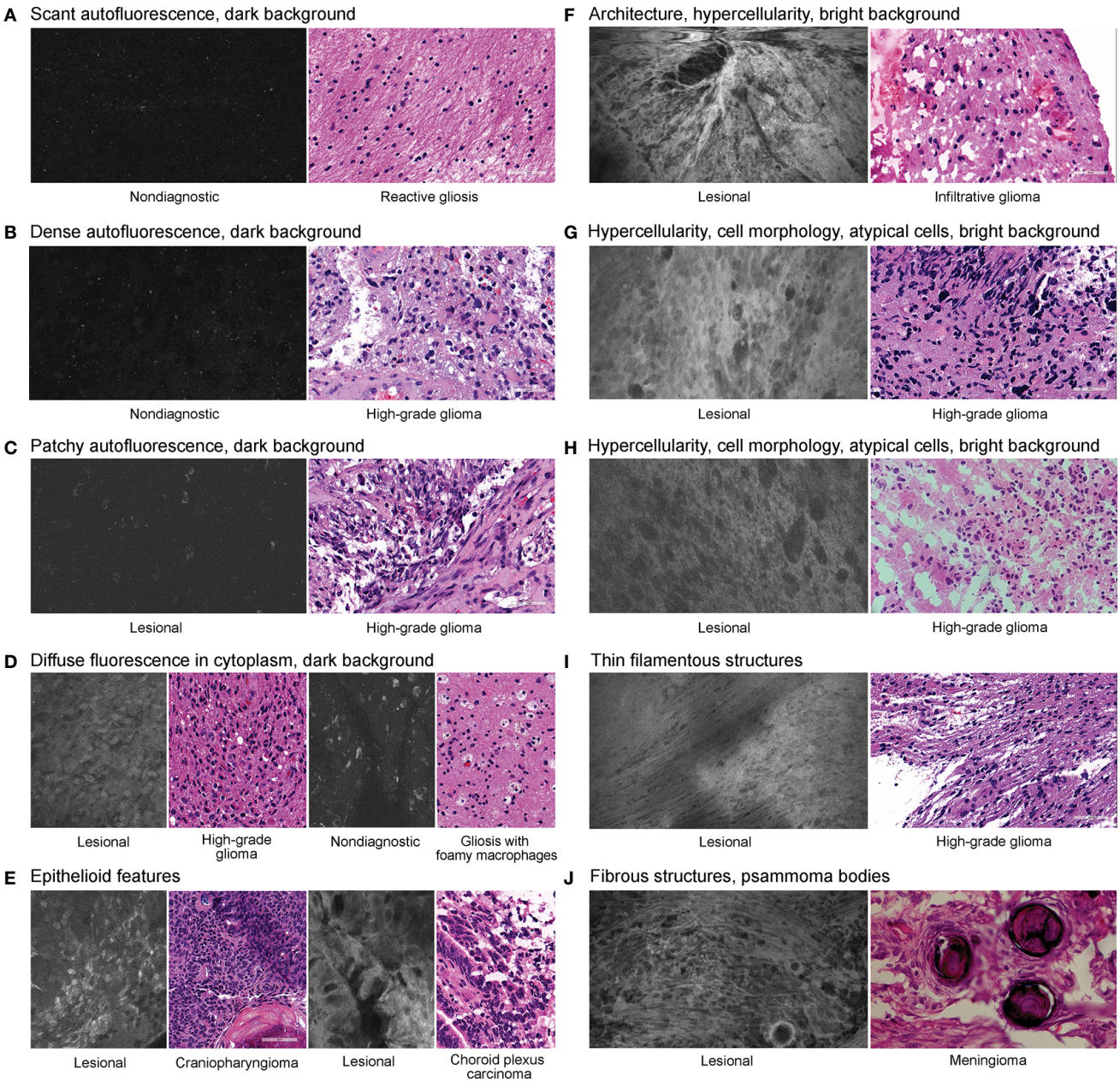

FIGURE 2 | Histologic features identified on confocal laser endomicroscopy images of various brain tumors and matching hematoxylin-eosin images. We identified three types of autofluorescence: scant **(A)**, dense **(B)**, and patchy **(C)**. We also identified the following image characteristics as separate histologic features: diffuse intracytoplasmic fluorescence **(D)**, epithelioid features **(E)**, hypercellularity **(F–H)**, filamentous structures **(I)**, and fibrous structures **(J)**. An example of characteristic identifiable tissue architecture as a histologic feature is shown in **(F)**. Examples of characteristic identifiable features of cell morphology and atypical cells are shown in **(G)** and **(H)**. An example of psammoma bodies is presented in **(J)**. We classified the brightness of background (extracellular space) as dark **(A–D)** or bright **(F–I)**. *Used with permission from Barrow Neurological Institute, Phoenix, Arizona.*

The prevalence of identifiable histologic features on CLE imaging was specifically studied in select biopsies of glioma, reactive gliosis, and normal brain samples (**Figure 3**).

Autofluorescence

Three types of autofluorescence were distinguished: scant, patchy, and dense. Scant autofluorescence was frequently observed in nonglioma samples that were deemed nondiagnostic by CLE ($P<0.001$), but there were no significant differences in the frequencies of patchy and dense fluorescence.

Diffuse Intracellular Fluorescence

In some CLE optical biopsies, cells exhibited diffuse accumulation of FNa in the cytoplasm. This accumulation was

Feature		CLE Lesional				CLE Nondiagnostic				CLE Normal				P Value	
		Glioma (n=53)		Nonglioma (n=0)		Glioma (n=23)		Nonglioma (n=15)		Glioma (n=0)		Nonglioma (n=1)			
		Inf. Glioma (22)	HGG (31)	Gliosis (0)	Normal (0)	Inf. Glioma (14)	HGG (9)	Gliosis (8)	Normal (7)	Inf. Glioma (0)	HGG (0)	Gliosis (1)	Normal (0)	Lesional Glioma vs. Nondiagnostic Glioma	Lesional Glioma vs. Nondiagnostic Nonglioma
Autofluorescence	Scant	5%	19%			14%	22%	63%	57%			0%		0.90	**<.001**
	Dense	27%	26%			43%	44%	25%	14%			0%		0.14	0.87
	Patchy	23%	29%			57%	44%	63%	29%			0%		**0.03**	0.24
Fluorescence diffusely in cytoplasm		32%	10%			7%	22%	25%	14%			100%		0.54	0.78
Background	Dark	14%	26%			57%	78%	100%	86%			100%		**<.001**	**<.001**
	Bright (extravasation)	86%	77%			43%	33%	13%	0%			0%		**0.001**	**<.001**
Architecture		95%	77%			36%	22%	38%	14%			100%		**<.001**	**<.001**
Cell morphology		73%	74%			0%	0%	38%	14%			100%		**<.001**	**<.001**
Atypical cells		38%	48%			0%	0%	0%	0%			0%		**<.001**	**0.004**
Hypercellularity		77%	65%			0%	22%	13%	0%			0%		**<.001**	**<.001**
Epithelial features		0%	0%			0%	0%	0%	0%			0%		NA	NA
Vessels		23%	16%			0%	11%	0%	29%			100%		0.19	0.91
Fibrous structures	Collagen fibers	5%	0%			0%	0%	0%	0%			0%		0.67	0.50
	Thin filamentous structures	0%	3%			7%	0%	0%	0%			100%		0.87	0.50
	Abundant fibrous structures	14%	6%			7%	22%	0%	14%			0%		0.95	0.86
Psammoma bodies		0%	0%			0%	0%	0%	0%			0%		NA	NA
RBC artifacts prevalent		14%	13%			50%	22%	13%	43%			100%		**0.03**	0.39

FIGURE 3 | Prevalence of histologic features among gliomas and normal or reactive brain tissue specimens. This analysis excluded 2 confocal laser endomicroscopy (CLE) optical biopsies with false-positive results, 2 CLE optical biopsies with false-negative results, and 1 nondiagnostic sample stained with hematoxylin-eosin. Table cells are shaded to reflect the prevalence of the specified feature among each group of specimens on a spectrum from red (0%) to green (100%). Boldface type indicates statistical significance. HGG, high-grade glioma; NA, not available; RBC, red blood cell. *Used with permission from Barrow Neurological Institute, Phoenix, Arizona.*

especially noticeable in tissue from carcinomas. In gliomas, however, the frequency of this pattern was not significantly different among nontumor and glioma biopsies.

Background Color

The pattern of CLE images in which the extracellular space was dark, and usually darker than the cells, was significantly more prevalent in nonglioma specimens (P<0.001) and in glioma specimens that were rated nondiagnostic (P<0.001). However, bright background was observed in most glioma samples diagnosed as lesional, and it was almost absent in biopsies from normal and reactive brain (P<0.001).

Cellular Features

Features such as tissue architecture, cell morphology, atypical cells, and hypercellularity were more prevalent in lesional glioma biopsies than in normal and reactive brain (P<0.001 for all). These features were also more prevalent in lesional glioma biopsies than in glioma biopsies that were labeled nondiagnostic on CLE (P<0.001 for all).

Epithelial Features

The pattern of hypercellular areas with cells contacting each other and having glandular or epithelial arrangement was observed in all three metastases, in one choroid carcinoma, and in the epithelial portion of the craniopharyngioma specimen. This feature was not observed in gliomas.

Vessels

Vessels were not frequently identified, most likely because of the lack of blood flow in *ex vivo* samples, which hampered detection. No differences were observed in their frequency of occurrence in the diagnostic, nondiagnostic, and normal brain samples. However, normal capillaries with FNa-stained vessel walls were

deemed more characteristic of normal brain, or possibly of invasive glioma, than of cellular tumor.

Fibrous Structures

Various acellular fibrous structures were encountered, mostly in meningiomas, but were rarely seen in gliomas. However, some thin filamentous structures representing myelinated cell processes could be seen in gliomas. Psammoma bodies were identified in meningiomas as large, round, contrast-impermeable structures.

Red Blood Cell Artifacts

Although red blood cell artifacts are inevitable during CLE imaging, an abundance of blood was encountered significantly more often in nondiagnostic CLE biopsies of gliomas than in lesional CLE biopsies of gliomas (P=0.02).

Blinded Review by Trained Neuropathologist

The overall diagnostic accuracy for all biopsies analyzed by a trained neuropathologist was 75%. Lesional CLE biopsies were used as positive CLE test results; nonlesional CLE, which included nondiagnostic and true negative normal or reactive brain CLE, were used as negative CLE test results (**Table 2**). Diagnostic accuracy in various tumor types was elucidated by performing subgroup analyses in glioma, metastases, and meningioma samples, which confirmed high positive predictive value of CLE optical biopsies (98%, 91%, and 83%, respectively) (**Table 3**). Notably, two CLE optical biopsies that were labeled as lesional had nonlesional H&E labeling such that they might have been true positives, which would further improve specificity and positive predictive value to 100% for all specimens and for gliomas (**Figure 4**).

Blinded Review by Trained and Untrained Appraisers

Overall diagnostic accuracy for all biopsies blinded for analysis by a neurosurgeon with experience interpreting CLE images was 78% vs 71% for the neurosurgeon without CLE image-reading experience. The comparative diagnostic accuracy data are presented in **Figure 5** and **Table 4**. Both the experienced neuropathologist and the experienced neurosurgeon demonstrated higher specificity and positive predictive value for gliomas.

TABLE 2 | Confocal laser endomicroscopy interpretation of 122 biopsy specimens from 47 patients.

H&E Diagnosis	Specimens	Confocal Laser Endomicroscopy Interpretation				
		Lesional		Nonlesional		
				Normal		Nondiagnostic
		TP	FP	TN	FN	
Choroid plexus carcinoma	4	3				1
Craniopharyngioma	1	1				
HGG	41	31			1	9
Infiltrating glioma	37	22			1	14
Meningioma	9	6				3
Metastasis	8	7				1
Necrosis	2	2				
Normal brain	8		1			7
Reactive gliotic brain	9			1		8
Schwannoma	1	1				
Inconclusive	2	1				1

H&E, hematoxylin-eosin; HGG, high-grade glioma: FN, false negative; FP, false positive; TN, true negative; TP, true positive.

TABLE 3 | Diagnostic accuracy of *ex vivo* confocal laser endomicroscopy (CLE) analyzed by a neuropathologist experienced in CLE image interpretation.

Value	All samples	Gliomas	Carcinomas[a]	Meningiomas
Sensitivity	72 (62–80)	66 (55–76)	83 (51–97)	63 (26–90)
Specificity	90 (67–98)	94 (69–100)	94 (69–100)	94 (69–100)
Positive predictive value	97 (90–100)	98 (89–100)	91 (57–100)	83 (36–99)
Negative predictive value	38 (25–54)	37 (23–53)	89 (64–98)	84 (60–96)

Data are reported as percentage (95% confidence interval).
[a]*Carcinomas included metastatic lesions and choroid plexus carcinomas.*

Adverse Effects

No adverse effects due to biopsy acquisition or FNa administration were noted. One patient was inadvertently administered 40 mg/kg of FNa at the induction of anesthesia, resulting in yellowish skin discoloration that resolved uneventfully within 48 h. No other adverse reactions were observed.

DISCUSSION

The projected clinical applications for the use of CLE in neurosurgery are to guide biopsy acquisition, to provide preliminary diagnosis in a manner similar to that of frozen section, and to perform screening for tumor detection during resection. In this study, we evaluated CLE optical biopsies of 122 *ex vivo* brain samples from 47 patients. The results demonstrated high sensitivity for this diagnostic technology in detecting cellular brain tumor tissue, which has significantly informative clinical value.

Image Interpretation

Our results demonstrated that a neuropathologist and neurosurgeons experienced in reading CLE images interpreted images of gliomas with greater specificity than an inexperienced neurosurgeon, even in consultation with an inexperienced pathologist. Previous reports have indicated that special training and experience are necessary to interpret the gray scale confocal images of intravital microscopy (9–13). However, in our study, the scores are not greatly dissimilar among the experienced neuropathologist, the experienced neurosurgeon, and the inexperienced neurosurgeon assisted by a general pathologist. The interpretative accuracy of these scores is surprising, given that no information was provided to the personnel about the clinical or historical nature of the cases. In the normal surgery-pathology workflow, such additional contextual information would be a requisite part of the

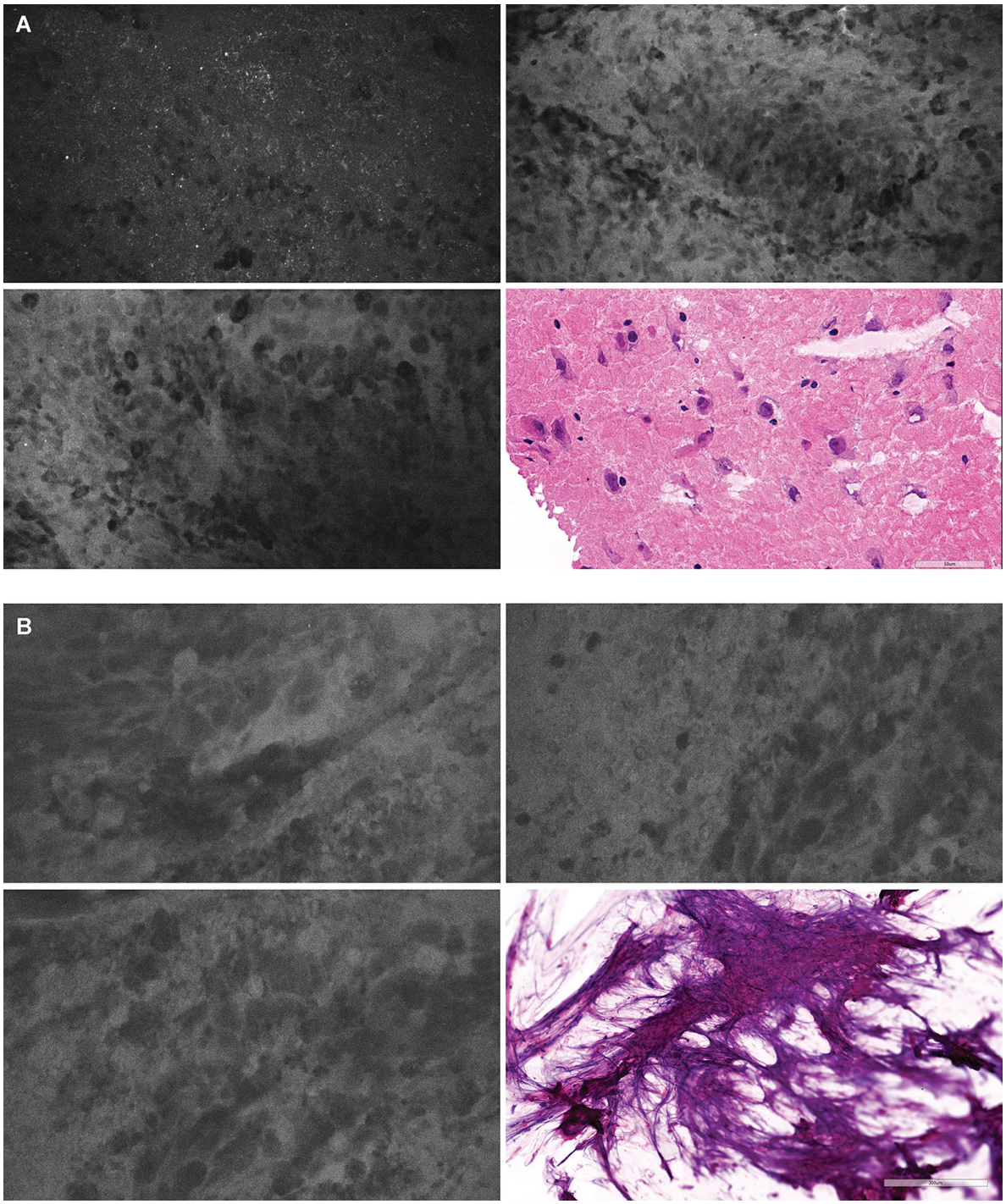

FIGURE 4 | Positive confocal laser endomicroscopy (CLE) optical biopsies with negative hematoxylin-eosin (H&E) stain results. **(A)** In one optical biopsy, extravasation of FNa highlighted the background and revealed hypercellular areas of atypical large cells. Overall, this CLE optical biopsy was thought to be highly representative of a lesional tissue. However, the H&E-stained specimen was read as normal cortex without a tumor. We hypothesized that there might be a sampling error and that the specimen contained a tumor area that had been missed during histologic sectioning. **(B)** This optical biopsy demonstrated extravasation of FNa with hypercellular areas containing large atypical cells highly suggestive of a cellular tumor. However, because of the scant tissue available for histologic processing, the H&E stain results were inconclusive. Both H&E-stained specimens were treated as nonlesional for diagnostic accuracy analysis. However, if these two H&E biopsy specimens had been treated as lesional, then both specificity and positive predictive value would be 100%. *Used with permission from Barrow Neurological Institute, Phoenix, Arizona.*

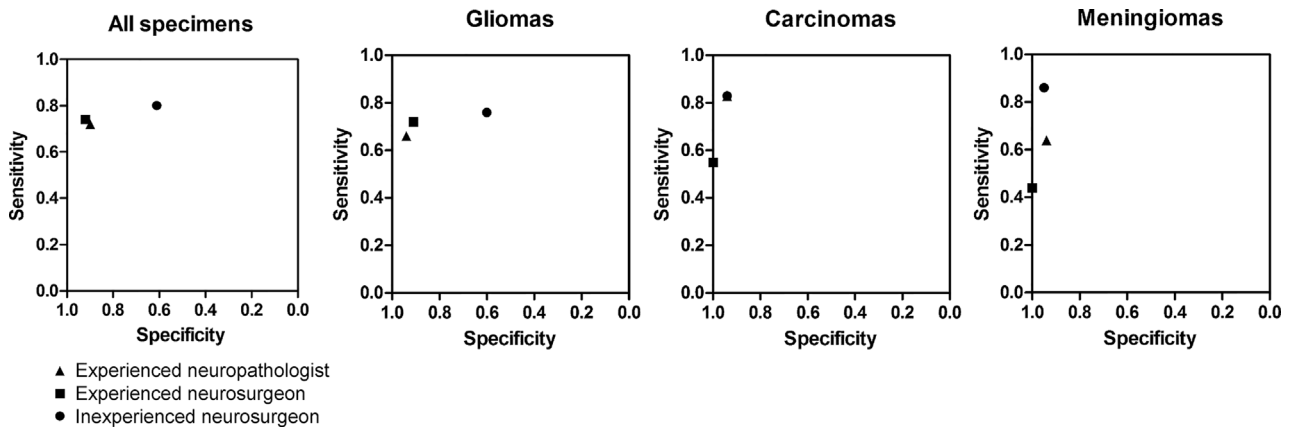

FIGURE 5 | Diagnostic accuracy diagrams for all specimens together and for gliomas, carcinomas, and meningiomas analyzed separately, as assessed by an experienced neuropathologist, an experienced neurosurgeon, and an inexperienced neurosurgeon using confocal laser endomicroscopy. *Used with permission from Barrow Neurological Institute, Phoenix, Arizona.*

TABLE 4 | Diagnostic accuracy of *ex vivo* confocal laser endomicroscopy analyzed by an experienced neuropathologist, an experienced neurosurgeon, and an inexperienced neurosurgeon.

Tissue type, diagnostic parameter	Experienced neuropathologist	Experienced neurosurgeon	Inexperienced neurosurgeon
All samples			
Sensitivity	72 (62–80)	74 (65–83)	80 (70–90)
Specificity	90 (67–98)	92 (69–98)	61 (44–72)
Positive predictive value	97 (90–100)	97 (90–100)	71 (59–80)
Negative predictive value	38 (25–54)	47 (31–61)	72 (56–84)
Glioma			
Sensitivity	66 (55–76)	72 (61–82)	76 (62–87)
Specificity	94 (69–100)	91 (67–98)	60 (42–72)
Positive predictive value	98 (89–100)	96 (87–99)	66 (52–78)
Negative predictive value	37 (23–53)	49 (31–69)	71 (53–84)
Carcinoma[a]			
Sensitivity	83 (51–97)	55 (32–76)	83 (51–97)
Specificity	94 (69–100)	100 (60–100)	94 (68–100)
Positive predictive value	91 (57–100)	100 (68–100)	91 (57–100)
Negative predictive value	89 (64–98)	50 (24–71)	89 (62–98)
Meningioma			
Sensitivity	63 (26–90)	44 (21–69)	86 (42–99)
Specificity	94 (69–100)	100 (63–100)	95 (71–100)
Positive predictive value	83 (36–99)	100 (56–100)	86 (42–99)
Negative predictive value	84 (60–96)	53 (27–73)	95 (71–100)

Data are reported as percentage (95% confidence interval).
[a]*Includes metastatic lesions and choroid plexus carcinoma.*

interpretation of CLE images for diagnosis and surgical guidance (7).

In the future, CLE image interpretation could be augmented by robust automated computer image analysis, which would allow for rapid identification of useful information from among the hundreds to thousands of images that may be acquired from one patient (14–16) and by digital telepathology consultation provided by an expert (17). In addition to confirming the diagnostic value of the new-generation CLE system, this study addresses the implementation of CLE into the surgery-pathology operating room workflow during FGS of the brain. As discussed below, the results provide data that will be helpful in planning future *in vivo* CLE studies in various tumor types.

Implications for Practice: Incorporation of CLE into the Workflow of Fluorescence-Guided Brain Surgery

Building on a previous study in which FNa was administered approximately 5 min before CLE imaging (7), this study demonstrated the feasibility of using CLE in Yellow560 mode during FGS when FNa is administered upon induction of anesthesia. This timing of FNa injection favors navigation using the wide-field fluorescence operative microscope (18, 19), and it has been studied in several clinical trials (20, 21). However, after early administration of FNa, we found that the contrast in CLE images was insufficient in some cases, thus requiring readministration of FNa. Readministration of FNa resulted in improved CLE image quality. Interestingly, we found no correlation between the time of contrast injection and overall image quality, which may be related to the heterogeneity of the tumor tissue or blood artifacts and to the *ex vivo* nature of the study.

Reinjection of FNa showed important benefits for image quality and interpretation. Analysis of these specimens showed improved brightness, contrast, and improved overall image quality. For the cases in which the reinjection was performed, the percentage of images with an accurate diagnosis increased by 50%, and the percentage of nondiagnostic CLE decreased by 50%. In some cases, reinjection allowed us to obtain meaningful interpretation where with only a single injection at the start of

the case, this would not have been possible. Although reinjection of FNa improved CLE image quality, the diffusion of FNa at the resection cavity can hamper the selectivity of Yellow560 wide-field fluorescence guidance, but this hindrance was not a major problem for us. However, there are some relevant considerations for reinjection of FNa. When administered later during surgery FNa extravasates at the regions of surgical injury creating false-positive fluorescence, which was the major critique of FNa as a contrast agent for wide-field fluorescence guidance (22). Future *in vivo* studies should address this problem. Most likely, CLE could best be used after resection under Yellow560 guidance to facilitate inspection of the surgical resection bed at the conclusion of surgery (i.e., to interrogate suspected tumor invasion into eloquent or surrounding cortex). Interestingly, when 40 mg/kg FNa was administered, CLE demonstrated high-quality images with excellent contrast in visualizing tumor cells, further supporting our approach to reinject FNa to increase image contrast and clarity.

Alternatively, FNa could be used for CLE optical biopsy during or at the completion of resection under 5-aminolevulinic acid (5-ALA) guidance. Simultaneous use of 5-ALA and FNa has been reported previously (23). Our experience with the new operating microscope in Blue400 and Yellow560 modes demonstrates that the two channels can be alternated without compromising image quality. Concurrent FNa-contrasted CLE may be advantageous during surgeries performed using near-infrared guidance (e.g., using indocyanine green [ICG]) because of the absence of spectral overlap with FNa (24, 25). Confocal-assisted fluorescence microscopy with ICG as a contrast has also been reported (26, 27). In view of future incorporation of CLE into the workflow of FGS, diagnostic accuracy using CLE should be compared to wide-field fluorescence imaging technology using various diagnostic fluorophore agents, such as FNa, 5-ALA, and ICG.

For safe maximal resection, other techniques should also be considered, particularly intraoperative stimulation and awake brain mapping using fluorescence (28). These and other functional methods are designed to be highly sensitive for eloquent brain areas that should be preserved, whereas the goal of FGS and CLE is to specifically detect and reveal tumor regions for the surgical decision on whether to resect. These two methods can therefore provide mutually complementary information.

The use of CLE requires coordination with the anesthesiologist for timely and accurate administration of the FNa dose. Importantly, we believe that close association with a neuropathologist, either remotely or in the operating room, is necessary, especially at the initial adoption stage of the CLE technology, as was the case for this *ex vivo* application. Coordination and communication between the neurosurgeon in the operating room using the CLE and the neuropathologist providing rapid examination of the images acquired on the fly is fully supported by this CLE technology, and this will be especially advantageous for *in vivo* use. The images can be ported to any computer workstation or even handheld computing device (e.g., "smart phone") supporting image display. CLE systems will require and foster a close partnership and collaboration between the neurosurgeon and neuropathologist.

Diagnostic Accuracy in Different Tumor Types

Because glioma tissue is often challenging to distinguish from normal brain tissue without special or enhanced imaging techniques, *in vivo* CLE optical biopsy of gliomas is of particular interest because it yields histopathologic imaging results immediately. With our experience from experimental animal studies and early clinical studies, we have identified characteristic CLE patterns and have developed confidence in our interpretation of CLE images and in our successful identification of hypercellular HGG samples (5, 29, 30). In contrast to previous studies, this study assessed multiple matched biopsies from the same patient, including multiple samples that were read as gliotic brain without tumor.

CLE images from within a tumor mass may readily display characteristic cellular features that are unique to and therefore diagnostic of the tumor type. However, although imaging within a main tumor mass may be useful for rapid histologic recognition and confirmation, the main purpose and advantage of the CLE is to recognize abnormal histologic features at the marginal regions of tumor to identify regions that can be surgically optimized. Such an imaging situation occurs within the surgical resection bed when assessing whether to extend the tumor removal. The CLE field of view is small (267 × 475 μm), and thus the concentration on identifiable histologic features at the tumor or pathological margins may not include readily visible diagnostic features that inform an exact tumor type. Instead, the focus should be on distinguishing abnormal histoarchitectural features, such as those described in the results.

Coupled with our previous studies on the differentiation of glioma tissue from injured normal brain in the murine model (31), the current work deepens our understanding of the CLE features of nontumor normal and gliotic brain tissue in humans. Most of the specimens of gliotic and normal brain tissue were labeled as nondiagnostic of brain tumor because they lacked typical cellular features and high cellularity, although most of them had dark extracellular backgrounds and some autofluorescent speckles. Normal cells were not clearly visible on these images, which impeded a definitive conclusion that the optical biopsy was representative of normal brain tissue. Interestingly, increased speckles on CLE images obtained with a similar device have previously been observed in low-grade gliomas after administration of 5-ALA (32), but they most likely represented autofluorescence (33). Whether this observation indicates the normal appearance of brain tissue using CLE imaging with FNa contrast is not clear. We believe that future *in vivo* studies should focus on the assessment of marginal tissue to better distinguish normal brain tissue when interpreting a dark CLE optical biopsy with autofluorescence in the absence of cellular architecture features (**Figure 6**).

With respect to metastatic lesions and choroid plexus carcinomas, CLE provides high-contrast, clear, and reliable images of cellular features that are highly diagnostic of cellular tumor. Most nondiagnostic CLE optical biopsies are attributable to blood artifacts that hide the actual tissue or the FNa contrast redistribution over time, which diminishes contrast among cells and among their nuclei, cytoplasm, and extracellular compartments.

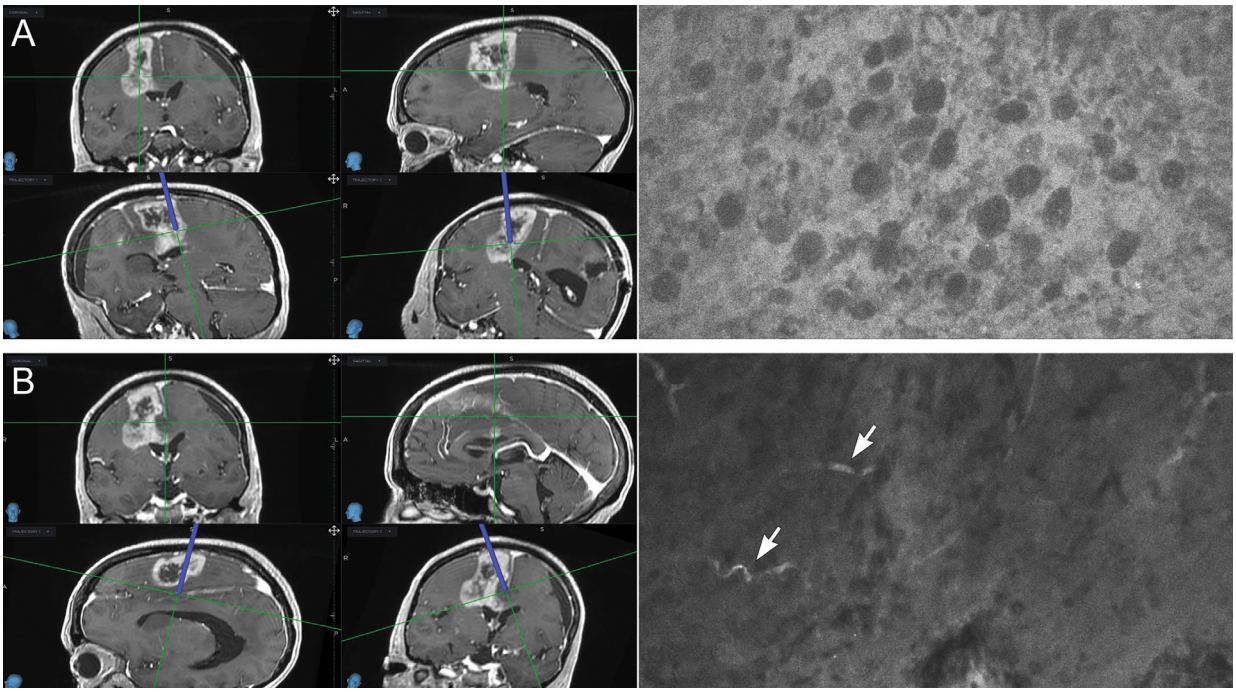

FIGURE 6 | Illustrative example of confocal laser endomicroscopy (CLE) (*right*) used in combination with intraoperative navigation (*left*). Multiple biopsies were performed during resection of a high-grade glioma; two biopsies are shown. **(A)** A biopsy specimen obtained from a deep posterior contrast-enhancing tumor margin. CLE findings were positive for tumor showing atypical cellular features and hypercellularity. A diagnosis of high-grade glioma was made on the basis of hematoxylin-eosin (H&E) staining of this biopsy specimen. Resection was extended further and deeper. **(B)** A biopsy specimen was obtained from a deep noncontrast-enhancing posteromedial tumor margin. CLE had findings negative for tumor and showed normal-appearing vessels (*arrows*). This biopsy specimen was identified as normal cortex with focal vessels on H&E staining. *Used with permission from Barrow Neurological Institute, Phoenix, Arizona.*

In all available meningioma samples, including one composed of 80% dura and 20% invasive meningioma tissue, CLE provided clear high-contrast images of hypercellular tissue with fibrous structures and psammoma bodies, when present. Because normal marginal nonmeningioma samples were not available for CLE assessment, we used normal and gliotic brain tissue as negative controls for calculating the diagnostic accuracy in meningiomas. However, for future *in vivo* studies of meningiomas, multiple biopsies of the dura at the edge of the tumor should be obtained, similar to the tissue acquisition workflow in gliomas. We have thoroughly examined features of normal dura with FNa in a pig model (unpublished data), but its appearance at the marginal tumor regions should be better characterized in future studies.

Study Power Considerations

In this study, the prevalence of lesional samples was 84% (102 of 122) among all samples and 82% (80 of 97) among the glioma samples. The Buderer formula (34), with accuracy set at 0.05, prevalence of disease in the tested population set at 84%, and a sample size of 122, resulted in z=1.127 and confidence interval (CI) within 0.70 to 0.75 for sensitivity and z=1.687 and CI of 0.90 to 0.92 for specificity. For gliomas, the power analysis resulted in z=0.594 with CI of <50% for sensitivity and z=1.307 and CI of 0.80 to 0.85 for specificity. Although our study was underpowered for sensitivity, it is the first feasibility study to provide prevalence and diagnostic accuracy values for the planning of future diagnostic accuracy studies using CLE. For example, assuming 82% prevalence of tumor-positive samples, 94% specificity, and 66% sensitivity, the study size should be 419 for calculation of sensitivity and 103 for specificity to obtain a 95% CI and 0.05 accuracy.

Study Limitations

Factors such as biopsy location, tumor type, the experience of the CLE user, and the extent of the scanned region of interest may have introduced biases and should be controlled for in future studies. This study is limited to *ex vivo* analyses because of the unavailability of the sterile CLE probe sheaths during the time the study was conducted; thus, human *in vivo* use was precluded. However, this situation may be viewed as advantageous because it may have decreased sampling error compared with *in vivo* acquisition for methodologic reasons, as it is more certain that the CLE images were obtained from and directly correlated with the same biopsy region, which is often difficult to accomplish intraoperatively.

Nevertheless, we acknowledge that sampling error is unavoidable with the small field of view of the imaging probe. H&E slides of multiple samples were inhomogeneous when viewed under the microscope: some had areas of necrosis encompassing up to 75% of the whole section, and some had infiltrating tumor in only 20% of their area, with the remaining regions consisting of vessels and hemorrhage. Use of CLE may identify and distinguish tumor cellular areas that are later missed on standard histologic examination (**Figure 4**). Two CLE optical

biopsies that were classified as having normal results (i.e., false-negative results) had dark backgrounds and normal-appearing vessels suggestive of normal brain; however, few regions of interest were imaged with CLE for this sort of optical biopsy, and therefore the infiltrative tumor areas detected on H&E slides may have been missed. To minimize the sampling error, we moved the probe across specimens to visualize larger areas and to identify locations with high-quality confocal images bearing diagnostic features, but the area that is scanned is subject to user bias.

CONCLUSION

Our results demonstrate the feasibility of incorporating CLE assessment of tissue microarchitecture in FGS. CLE optical biopsies showed high specificity and positive predictive value in fresh *ex vivo* glioma samples. These results reinforce the utility of CLE in providing real-time intraoperative cell resolution imaging to the neurosurgeon that is comparable to and faster than conventional histologic analysis from tissue biopsies in the operating room. These results also provide background data for planning future *in vivo* clinical studies.

DATA AVAILABILITY STATEMENT

The original contributions presented in the study are included in the article/supplementary material. Further inquiries can be directed to the corresponding author.

ETHICS STATEMENT

The studies involving human participants were reviewed and approved by St. Joseph's Hospital and Medical Center with approval from the Institutional Review Board for Human Research. The patients/participants provided their written informed consent to participate in this study.

AUTHOR CONTRIBUTIONS

Study planning and coordination: PN, MP, JE, EB. Acquisition of surgical biopsies and patient recruitment: PN. Acquisition of confocal images: EB, XZ. Processing and organizing of the data and confocal images: BN, DF, EB. Assessment of confocal images: EB, MP, VB, JE. Histology processing: EB. Histology reading: JE. Statistical analysis: EB, BN, DF. Writing a draft: BN, DF, EB. Review of the draft: EB, BN, DF, VB, MP, PN. All authors contributed to the article and approved the submitted version.

FUNDING

This research received material support from Carl Zeiss Meditec, AG, and financial support from the Barrow Neurological Foundation and the Newsome Chair in Neurosurgery Research held by Dr. Preul.

ACKNOWLEDGMENTS

The authors thank the Neuroscience Publications staff at Barrow Neurological Institute for assistance with manuscript preparation. We also thank Thomas Chastain and the staff of the pathology department for excellent technical assistance. This work is a part of the doctoral dissertation of EB. Part of this work was presented at the 2019 AANS meeting on April 13 to 17, 2019, in San Diego, California.

REFERENCES

1. D'Amico RS, Englander ZK, Canoll P, Bruce JN. Extent of Resection in Glioma-A Review of the Cutting Edge. *World Neurosurg* (2017) 103:538–49. doi: 10.1016/j.wneu.2017.04.041
2. Sanai N, Berger MS. Glioma extent of resection and its impact on patient outcome. *Neurosurgery* (2008) 62(4):753–64; discussion 264-6. doi: 10.1227/01.neu.0000318159.21731.cf
3. Barbosa BJ, Mariano ED, Batista CM, Marie SK, Teixeira MJ, Pereira CU, et al. Intraoperative assistive technologies and extent of resection in glioma surgery: a systematic review of prospective controlled studies. *Neurosurg Rev* (2015) 38(2):217–26; discussion 26-7. doi: 10.1007/s10143-014-0592-0
4. Belykh E, Cavallo C, Gandhi S, Zhao X, Veljanoski D, Izady Yazdanabadi M, et al. Utilization of intraoperative confocal laser endomicroscopy in brain tumor surgery. *J Neurosurg Sci* (2018) 62(6):704–17. doi: 10.23736/S0390-5616.18.04553-8
5. Sanai N, Eschbacher J, Hattendorf G, Coons SW, Preul MC, Smith KA, et al. Intraoperative confocal microscopy for brain tumors: a feasibility analysis in humans. *Neurosurgery* (2011) 68(2 Suppl Operative):282–90; discussion 90. doi: 10.1227/NEU.0b013e318212464e
6. Eschbacher J, Martirosyan NL, Nakaji P, Sanai N, Preul MC, Smith KA, et al. *In vivo* intraoperative confocal microscopy for real-time histopathological imaging of brain tumors. *J Neurosurg* (2012) 116(4):854–60. doi: 10.3171/2011.12.JNS11696
7. Martirosyan NL, Eschbacher JM, Kalani MY, Turner JD, Belykh E, Spetzler RF, et al. Prospective evaluation of the utility of intraoperative confocal laser endomicroscopy in patients with brain neoplasms using fluorescein sodium: experience with 74 cases. *Neurosurg Focus* (2016) 40(3):E11. doi: 10.3171/2016.1.FOCUS15559
8. Bossuyt PM, Reitsma JB, Bruns DE, Gatsonis CA, Glasziou PP, Irwig L, et al. STARD 2015: an updated list of essential items for reporting diagnostic accuracy studies. *BMJ* (2015) 351:h5527. doi: 10.1136/bmj.h5527
9. Liu JT, Loewke NO, Mandella MJ, Leigh SY, Levenson RM, Crawford JM, et al. Real-time pathology through *in vivo* microscopy. *Stud Health Technol Inform* (2013) 185:235–64. doi: 10.3233/978-1-61499-234-9-235
10. Farnetani F, Scope A, Braun RP, Gonzalez S, Guitera P, Malvehy J, et al. Skin Cancer Diagnosis With Reflectance Confocal Microscopy: Reproducibility of Feature Recognition and Accuracy of Diagnosis. *JAMA Dermatol* (2015) 151(10):1075–80. doi: 10.1001/jamadermatol.2015.0810
11. Rao BK, Mateus R, Wassef C, Pellacani G. *in vivo* confocal microscopy in clinical practice: comparison of bedside diagnostic accuracy of a trained physician and distant diagnosis of an expert reader. *J Am Acad Dermatol* (2013) 69(6):e295–300. doi: 10.1016/j.jaad.2013.07.022

12. Rajadhyaksha M, Marghoob A, Rossi A, Halpern AC, Nehal KS. Reflectance confocal microscopy of skin *in vivo*: From bench to bedside. *Lasers Surg Med* (2017) 49(1):7–19. doi: 10.1002/lsm.22600
13. Wells WA, Thrall M, Sorokina A, Fine J, Krishnamurthy S, Haroon A, et al. *in vivo* and *Ex Vivo* Microscopy: Moving Toward the Integration of Optical Imaging Technologies Into Pathology Practice. *Arch Pathol Lab Med* (2019) 143(3):288–98. doi: 10.5858/arpa.2018-0298-RA
14. Izadyyazdanabadi M, Belykh E, Mooney MA, Eschbacher JM, Nakaji P, Yang Y, et al. Prospects for Theranostics in Neurosurgical Imaging: Empowering Confocal Laser Endomicroscopy Diagnostics via Deep Learning. *Front Oncol* (2018) 8:240. doi: 10.3389/fonc.2018.00240
15. Izadyyazdanabadi M, Belykh E, Mooney M, Martirosyan N, Eschbacher J, Nakaji P, et al. Convolutional neural networks: Ensemble modeling, fine-tuning and unsupervised semantic localization for neurosurgical CLE images. *J Visual Commun Image Represent* (2018) 54:10–20. doi: 10.1016/j.jvcir.2018.04.004
16. Izadyyazdanabadi M, Belykh E, Zhao X, Moreira LB, Gandhi S, Cavallo C, et al. Fluorescence Image Histology Pattern Transformation Using Image Style Transfer. *Front Oncol* (2019) 9:1–7. doi: 10.3389/fonc.2019.00519
17. Fuks D, Pierangelo A, Validire P, Lefevre M, Benali A, Trebuchet G, et al. Intraoperative confocal laser endomicroscopy for real-time *in vivo* tissue characterization during surgical procedures. *Surg Endosc* (2019) 33(5):1544–52. doi: 10.1007/s00464-018-6442-3
18. Acerbi F, Broggi M, Eoli M, Anghileri E, Cavallo C, Boffano C, et al. Is fluorescein-guided technique able to help in resection of high-grade gliomas? *Neurosurg Focus* (2014) 36(2):E5. doi: 10.3171/2013.11.FOCUS13487
19. Acerbi F, Broggi M, Broggi G, Ferroli P. What is the best timing for fluorescein injection during surgical removal of high-grade gliomas? *Acta Neurochir (Wien)* (2015) 157(8):1377–8. doi: 10.1007/s00701-015-2455-z
20. Acerbi F, Broggi M, Schebesch KM, Hohne J, Cavallo C, De Laurentis C, et al. Fluorescein-Guided Surgery for Resection of High-Grade Gliomas: A Multicentric Prospective Phase II Study (FLUOGLIO). *Clin Cancer Res* (2018) 24(1):52–61. doi: 10.1158/1078-0432.CCR-17-1184
21. Falco J, Cavallo C, Vetrano IG, de Laurentis C, Siozos L, Schiariti M, et al. Fluorescein Application in Cranial and Spinal Tumors Enhancing at Preoperative MRI and Operated With a Dedicated Filter on the Surgical Microscope: Preliminary Results in 279 Patients Enrolled in the FLUOCERTUM Prospective Study. *Front Surg* (2019) 6:49. doi: 10.3389/fsurg.2019.00049
22. Stummer W. Poor man's fluorescence? *Acta Neurochirurgica* (2015) 157(8):1379–81. doi: 10.1007/s00701-015-2471-z
23. Schwake M, Stummer W, Suero Molina EJ, Wolfer J. Simultaneous fluorescein sodium and 5-ALA in fluorescence-guided glioma surgery. *Acta Neurochir (Wien)* (2015) 157(5):877–9. doi: 10.1007/s00701-015-2401-0
24. Cho SS, Salinas R, Lee JYK. Indocyanine-Green for Fluorescence-Guided Surgery of Brain Tumors: Evidence, Techniques, and Practical Experience. *Front Surg* (2019) 6:11. doi: 10.3389/fsurg.2019.00011
25. Cho SS, Salinas R, De Ravin E, Teng CW, Li C, Abdullah KG, et al. Near-Infrared Imaging with Second-Window Indocyanine Green in Newly Diagnosed High-Grade Gliomas Predicts Gadolinium Enhancement on Postoperative Magnetic Resonance Imaging. *Mol Imaging Biol* (2019) 22:1427–37. doi: 10.1007/s11307-019-01455-x
26. Charalampaki P, Nakamura M, Athanasopoulos D, Heimann A. Confocal-Assisted Multispectral Fluorescent Microscopy for Brain Tumor Surgery. *Front Oncol* (2019) 9:583:583. doi: 10.3389/fonc.2019.00583
27. Martirosyan NL, Cavalcanti DD, Eschbacher JM, Delaney PM, Scheck AC, Abdelwahab MG, et al. Use of *in vivo* near-infrared laser confocal endomicroscopy with indocyanine green to detect the boundary of infiltrative tumor. *J Neurosurg* (2011) 115(6):1131–8. doi: 10.3171/2011.8.Jns11559
28. Duffau H. Surgery for Malignant Brain Gliomas: Fluorescence-Guided Resection or Functional-Based Resection? *Front Surg* (2019) 6:21:21. doi: 10.3389/fsurg.2019.00021
29. Sankar T, Delaney PM, Ryan RW, Eschbacher J, Abdelwahab M, Nakaji P, et al. Miniaturized handheld confocal microscopy for neurosurgery: results in an experimental glioblastoma model. *Neurosurgery* (2010) 66(2):410–7; discussion 7-8. doi: 10.1227/01.NEU.0000365772.66324.6F
30. Martirosyan NL, Georges J, Kalani MY, Nakaji P, Spetzler RF, Feuerstein BG, et al. Handheld confocal laser endomicroscopic imaging utilizing tumor-specific fluorescent labeling to identify experimental glioma cells *in vivo*. *Surg Neurol Int* (2016) 7(Suppl 40):S995–S1003. doi: 10.4103/2152-7806.195577
31. Belykh E, Miller EJ, Patel AA, Yazdanabadi MI, Martirosyan NL, Yagmurlu K, et al. Diagnostic Accuracy of a Confocal Laser Endomicroscope for *in vivo* Differentiation Between Normal Injured And Tumor Tissue During Fluorescein-Guided Glioma Resection: Laboratory Investigation. *World Neurosurg* (2018) 115:e337–e48. doi: 10.1016/j.wneu.2018.04.048
32. Sanai N, Snyder LA, Honea NJ, Coons SW, Eschbacher JM, Smith KA, et al. Intraoperative confocal microscopy in the visualization of 5-aminolevulinic acid fluorescence in low-grade gliomas. *J Neurosurg* (2011) 115(4):740–8. doi: 10.3171/2011.6.JNS11252
33. Cavallo C, Gandhi S, Zhao X, Belykh E, Valli D, Nakaji P, et al. Applications of Microscope-Integrated Indocyanine Green Videoangiography in Cerebral Revascularization Procedures. *Front Surg* (2019) 6:1–10. doi: 10.3389/fsurg.2019.00059
34. Buderer NM. Statistical methodology: I. Incorporating the prevalence of disease into the sample size calculation for sensitivity and specificity. *Acad Emerg Med* (1996) 3(9):895–900. doi: 10.1111/j.1553-2712.1996.tb03538.x

Conflict of Interest: The authors declare that the research was conducted in the absence of any commercial or financial relationships that could be construed as a conflict of interest.

frontiers in Oncology

ORIGINAL RESEARCH
published: 23 December 2020
doi: 10.3389/fonc.2020.606574

Ex Vivo Fluorescein-Assisted Confocal Laser Endomicroscopy (CONVIVO® System) in Patients With Glioblastoma: Results From a Prospective Study

Francesco Acerbi[1]*, *Bianca Pollo*[2], *Camilla De Laurentis*[1], *Francesco Restelli*[1], *Jacopo Falco*[1], *Ignazio G. Vetrano*[1], *Morgan Broggi*[1], *Marco Schiariti*[1], *Irene Tramacere*[3], *Paolo Ferroli*[1] and *Francesco DiMeco*[1,4]

[1] Department of Neurosurgery, Fondazione IRCCS Istituto Neurologico Carlo Besta, Milan, Italy, [2] Neuropathology Unit, Fondazione IRCCS Istituto Neurologico Carlo Besta, Milan, Italy, [3] Department of Research and Clinical Development, Scientific Directorate, Fondazione IRCCS Istituto Neurologico Carlo Besta, Milan, Italy, [4] Department of Pathophysiology and Transplantation, University of Milano, Milan, Italy

OPEN ACCESS

Edited by:
David D. Eisenstat
University of Alberta, Canada

Reviewed by:
Mark Preul,
Barrow Neurological Institute (BNI), United States
Evgenii Belykh,
Rutgers University, Newark, United States
Muriel Abbaci,
Gustave Roussy Cancer Campus, France

***Correspondence:**
Francesco Acerbi
francesco.acerbi@istituto-besta.it

Specialty section:
This article was submitted to Neuro-Oncology and Neurosurgical Oncology, a section of the journal Frontiers in Oncology

Received: 15 September 2020
Accepted: 19 November 2020
Published: 23 December 2020

Citation:
Acerbi F, Pollo B, De Laurentis C, Restelli F, Falco J, Vetrano IG, Broggi M, Schiariti M, Tramacere I, Ferroli P and DiMeco F (2020) Ex Vivo Fluorescein-Assisted Confocal Laser Endomicroscopy (CONVIVO® System) in Patients With Glioblastoma: Results From a Prospective Study. Front. Oncol. 10:606574. doi: 10.3389/fonc.2020.606574

Background: Confocal laser endomicroscopy (CLE) allowing intraoperative near real-time high-resolution cellular visualization is a promising method in neurosurgery. We prospectively tested the accuracy of a new-designed miniatured CLE (CONVIVO® system) in giving an intraoperative first-diagnosis during glioblastoma removal.

Methods: Between January and May 2018, 15 patients with newly diagnosed glioblastoma underwent fluorescein-guided surgery. Two biopsies from both tumor central core and margins were harvested, dividing each sample into two specimens. Biopsies were firstly intraoperatively *ex vivo* analyzed by CLE, subsequently processed for frozen and permanent fixation, respectively. Then, a blind comparison was conducted between CLE and standard permanent section analyses, checking for CLE ability to provide diagnosis and categorize morphological patterns intraoperatively.

Results: Blindly comparing CONVIVO® and frozen sections images we obtained a high rate of concordance in both providing a correct diagnosis and categorizing patterns at tumor central core (80 and 93.3%, respectively) and at tumor margins (80% for both objectives). Comparing CONVIVO® and permanent sections, concordance resulted similar at central core (total/partial concordance in 80 and 86.7% for diagnosis and morphological categorization, respectively) and lower at tumor margins (66.6% for both categories). Time from fluorescein injection and time from biopsy sampling to CONVIVO® scanning was 134 ± 31 min (122–214 min) and 9.23 min (1–17min), respectively. Mean time needed for CONVIVO® images interpretation was 5.74 min (1–7 min).

Conclusions: The high rate of diagnostic/morphological consistency found between CONVIVO® and frozen section analyses suggests the possibility to use CLE as a complementary tool for intraoperative diagnosis of *ex vivo* tissue specimens during glioblastoma surgery.

Keywords: fluorescein, glioblastoma, CONVIVO®, *ex vivo*, confocal

HIGHLIGHTS

- A high rate of concordance was found comparing CONVIVO® and histology/frozen sections;
- Higher concordance was found at tumor central core;
- CONVIVO® system may help during surgery in obtaining intraoperative diagnosis.

INTRODUCTION

Nowadays, high grade gliomas (HGGs) are the most diagnosed primary central nervous system (CNS) neoplasms (1). Despite therapeutic advancements, prognosis still remains poor (2). Although extent of resection (EOR) has been demonstrated to directly correlate with survival in patients with HGGs (3), achieving a complete tumor removal is not always feasible, since distinction between normal and pathological tissue is difficult, especially at the tumor margins. Moreover, intraoperative diagnosis is sometimes needed to discriminate between HGGs and other mimicking conditions at the pre-operative assessment, such as abscesses, metastases, and lymphomas (4).

While histopathological analysis still remains the gold-standard for diagnosis, frozen section represents nowadays the most used intraoperative histopathological method for obtaining an intraoperative differential diagnosis. This method unfortunately has still some drawbacks: it requires long time to analyze the sample (20–30 min) and it has to be processed and analyzed outside the operating room (OR) (5–7). For these reasons it could not represent the ideal tool to guide the real-time intraoperative choice of treatment and subsequently extent of resection.

In this field, confocal laser endomicroscopy (CLE) represents a recent and interesting development, permitting the visualization of tissues on a microscopic level, without fixation or staining used in classical histological preparations (8–11). Only recently this new technological advancement has been applied to neurosurgery, by using a wide range of fluorescent dyes as contrast enhancers (8, 12). Although such technique is not available yet on a routine basis, its utilization could improve tumor visualization at the tumor margin and quicken intraoperative diagnosis, since the machinery could be used directly in the OR. In particular, few works have studied specificity and sensitivity of first-generation CLE to provide diagnostic information during biopsy or resection of human brain tumors, finding comparable values to frozen sections (6, 13–17). Less data are currently available on CLE analysis at human HGGs margins (8, 18). To overcome the limitations associated with first-generation CLE systems such as un-optimal imaging processing and displaying, low ergonomic position of the handheld probe and the lack of sterile attachments for the imaging probe, a second generation CLE system specifically ideated for neurosurgical use have been recently developed and tested on animal models, with improvement in image quality and fluorescence visualization (15, 19). Nevertheless, although promising, such data are still not confirmed in human brain tumor surgery and never prospectively analyzed. Thus, the aim of this study was to prospectively assess for the first time the accuracy of a newly designed fluorescein-assisted miniatured CLE (CONVIVO® system, *Carl Zeiss, Meditec, Oberkochen, Germany*) in giving *ex vivo* an intraoperative first-diagnosis during surgical removal of glioblastoma (GBM), by comparing CONVIVO® images to permanent and frozen section results.

MATERIAL AND METHODS

Patients and Specimens Handling

Patients of both genders, more than 18 years of age, with newly diagnosed, suspected GBM based on pre-operative radiological study, scheduled for fluorescein-guided removal, were evaluated for inclusion. Exclusion criteria included: a) histological diagnosis different from GBM (grade IV WHO 2016) (20); b) refuse or impossibility to give consent due to cognitive deficits or language disorder; c) known allergy to contrast agents or history of previous anaphylactic shocks, or adverse reactions to sodium fluorescein (SF); d) acute myocardial infarction or stroke in the last 90 days; e) severe renal, hepatic, or heart failure; f) women in first trimester of pregnancy or lactation.

The design of the study was approved by local Ethical Committee. All patients provided two written informed consents in order to authorize enrollment in the present study and use of SF.

Surgery was performed in a standard fashion, following our common institutional practice (microscopic fluorescent-guided technique, Pentero 900 with Y560 filter, *Carl Zeiss, Meditec, Oberkochen, Germany*) (21). At the induction of anesthesia, each patient received 5 mg/kg of intravenous SF, as specified by AIFA (*Agenzia Italiana del Farmaco – Italian Drug Agency*), according to the legislative decree no. 648 (*determination 905/2015, Gazette n.168, 22 July 2015*). During the tumor resection, besides the main specimen designed to diagnostic procedures, two biopsies of about 3–5 mm^3 were harvested from the tumor tissue. A first biopsy specimen, named A, was taken from a central tumor core, as verified by neuronavigation. The specimen was then cut in two halves, labeled A1 and A2, and each of them was analyzed on the workstation of the CONVIVO® system. Therefore, the two biopsies were transferred to the Neuropathology Department for frozen section (A1) and standard permanent section examination (A2).

A second biopsy specimen, named B, was then taken from the tumor margin, as verified by neuronavigation. Such biopsy was voluntarily taken at margin but inside intraoperative SF-confirmed pathological tissue, due to the *ex vivo* nature of the analysis, in order to reduce the possibility to obtain un-conclusive specimens (22, 23). The specimen was cut into biopsy B1 and B2, analyzed following the same protocol as for biopsies A1 and A2.

CONVIVO® Characteristics and Imaging Acquisition

CLE system consists of a miniatured confocal microscope, in which a laser source is used to deliver light *via* an optical fiber coupler and scanned delivery fiber to a lens system. The lens system focuses blue laser light (488 nm wavelength) into the sample to a depth set by a "Z-depth focusing mechanism" (FOV = 475 μm × 267 μm). SF located in the tissue of interest is excited by the laser light. The fluorescence is collected by the lens system and focused onto the tip of the scanned delivery optical fiber. The optical fiber acts as a confocal pinhole rejecting light other than that from the set Z-depth. The fluorescent light is carried to the confocal processor *via* the optical fiber through a fiber based optical coupler and into a detector. The detector synchronously samples the fluorescence providing an electrical representation of the light intensity that is recorded as a digital sample. The digital samples are constructed into an image frame that is sent *via* a digital interface to the integration computer, which uses custom Host software to deliver the image data to a monitor for display. Altering the position of the focal plane provides control of the confocal imaging depth over an estimated range in excess of 250 μm. Confocal image data is collected at user defined scan rate (Aspect Ratio's) between a minimum of 0.7 frames/s (1,920 × 1,080 pixels) to a maximum of 4 frames/s (1,920 × 135 pixels). Images are showed on the CONVIVO® screen (1,980 pixels/line, resolution scale of 475 × 267 μm).

For CLE imaging in the OR, the scanner probe was fixed in a vertical position and one specimen at a time was positioned on the top of the probe for subsequent analysis. The variables of the CONVIVO® system were adjusted based on the first real-time images visible on the monitor. In particular, the standard Z-depth was about 12–15 μm, never more than 30, since the tissue receives a light beam and the more the depth, the most difficult is the path of the light, which means darkness in the image. The laser power was always between 50 and 75%, without leaving the sample in the same position for a prolonged period of time in order to avoid photobleaching. Brightness was kept between 30 to 75%.

The CONVIVO® system gives the possibility to take a single photo on the Z-depth, multiple photos of the same depth in a short period of time, or a "Z-stack sequence," which is a series of photos focused on the Z-depth of interest but including multiple depths, towards the surface and the core of the specimen, at a 4 μm distance.

For each specimen, CONVIVO® analysis was performed from a point of view, then the specimen was rotated of 180° and other images were taken.

Blinded Intraoperative Interpretation of CONVIVO® Images

A dedicated pathologist was asked to judge in near real-time intraoperatively if the tissue represented tumor tissue, to provide a possible intraoperative tumor *diagnosis*, and to categorize eventual *morphological patterns* according to the following categories: tumor tissue, necrosis, reactive changes, marginal infiltrated tissue, vascular proliferation, and healthy tissue. Thus, CONVIVO® images were analyzed before interpretation of permanent or frozen sections, with the pathologist being totally blinded to their results.

All the resulting images were stored digitally. Other variables that were studied included the presence of artifacts from movements from the environment, duration of the operation with CLE, time from SF injection and time from biopsy sampling to CONVIVO® scanning, and median time needed for CONVIVO® images interpretation.

Frozen Section and Histopathological Processing and Interpretation

After CONVIVO® interpretations, specimens A1 and B1 were frozen in 2-methylbutane deep chilled in liquid nitrogen, following standard Institutional protocols; sections were prepared using the cryostat microtome, the slides were stained with hematoxylin-eosin and then analyzed. Specimens A2 and B2 underwent Carnoy's fixation, paraffin embedding, and processing for standard histopathology; 3 μm sections were performed and hematoxylin-eosin staining was performed according to standard protocols. Sections were examined through a conventional optical microscope. Histological diagnosis and analyses were completed according to the 2016 WHO classification (20).

In each biopsy, the elements of the microscopic image were categorized as it had been done intraoperatively with the CONVIVO® system: tumor tissue, necrosis, reactive changes, marginal infiltrated tissue, vascular proliferation, and healthy tissue.

Diagnostic and Morphological Concordance Among CONVIVO® and Frozen Section/Permanent Section Images

All the results were analyzed separately for biopsies taken at the central core or at the tumor margins. Specifically, for diagnosis, total/partial concordance ("+" or "±") or discordance ("−") between CONVIVO® and permanent/frozen section images were defined based on the degree of qualitative similarity among the written interpretation reports. In particular, a total concordance was given if CONVIVO® and permanent/frozen section images gave the same information; a partial concordance was given if similar but not equal information could be found on CONVIVO® and permanent/frozen section images or, more frequently, when at least two tumor characteristics of GBM could be found on CONVIVO® images in cases recognized as GBM on permanent/frozen section. All other cases were considered as discordant. Looking at morphological categorization, the recognition of a specific pattern in both CONVIVO® and permanent/frozen section images was marked with a "+," while the presence of a categorical pattern in one case, without its counterpart in the other image was considered as a "–." Thus, concordance was defined based on the recognition of at least one morphological category in both CONVIVO® and permanent/frozen section images (**Tables 1**, **2**).

Statistical Analysis

The sample size for this study was defined at 15 subjects (2 biopsies for each patient, thus 30 biopsies for concordance with frozen section and 30 biopsies with standard histopathology). With these numbers, with an estimated concordance of 90% the corresponding binomial standard error would be 5%, while with an estimated concordance of 80% the corresponding standard error would be 7%.

Descriptive statistics were provided in terms of absolute numbers and percentages for categorical data, and means with standard deviations (SDs) and value ranges for continuous data.

RESULTS

Hallmarks of GBM in CONVIVO® Images

The qualitative analysis of GBM specimens demonstrated the peculiarities of GBM samples, as can be seen on CLE acquisitions (**Figure 1**).

Based on the *ex vivo* nature of our study, we did not have the opportunity to analyze the characteristics of normal peri-tumoral parenchyma, as it has been done in previous studies (22, 23). On the contrary, tumor tissue presented as agglomerates of large non-uniform non-fluorescent dark circular cells and shadows on a fluorescent background. We noticed that the different times of SF administration from CLE acquisition influenced contrast definition, as when the dye was given closer to CLE acquisition a higher contrast could be seen among black cells and white background. Cellular features and tumor structures in different regions, such as pleomorphism, atypia, hyper-cellularity, and neovascularization, appeared to correlate with the matched permanent sections and known tissue architecture (**Figures 2**, **3**). Sparse fluorescent cells were occasionally seen (**Figure 1**). Necrosis was noted as presence of low cellular density areas on an amorphous tissue characterized by an intermediate fluorescence background (**Figure 4**).

Results of *Ex Vivo* Analysis

A total of 17 patients were prospectively screened between January 15th, 2018 and May 31st, 2018 at our Institution. Two patients were excluded due to the refusal of surgery in one case and the diagnosis of a brain abscess by Aggregatibacter in the second patient. Therefore, the final enrollment comprised 15 patients with confirmed histopathological diagnosis of GBM (grade IV WHO 2016) (20), for a total of 60 specimens, where concordance between CONVIVO® and either frozen section or standard histopathological examination was analyzed.

Comparing CONVIVO® and frozen sections images in biopsies obtained in the central core, total/partial concordance in making intraoperative diagnosis was found in 12 out of 15 patients (80%); concordant morphological categorization was present in 14 cases (93.3%) (**Table 1**). Similar results were obtained at tumor margins: total/partial diagnostic concordance was obtained in 12 out of 15 cases (80%); morphological categorization resulted to be concordant in 80% of patients (**Table 2**).

Equal rate of concordance was obtained comparing the intraoperative diagnosis given on CONVIVO® images with the result of permanent section specimen analysis at the central core of the tumor (12 patients, 80%). In addition, 86.7% (13 patients) of cases were concordant at the morphological analysis (**Table 1**). At the tumor margins, results were lower: 10 out of 15 cases (66.6%) were totally/partially concordant in regard to intraoperative diagnosis and 66.6% were concordant at the morphological categorization (**Table 2**).

Table 3 shows the morphological hallmarks disclosed in CONVIVO®, frozen section, and histology images. To note, the categories "reactive changes" and "healthy tissue" were never described, and we never found uninterpretable patterns, neither in CONVIVO® nor in frozen sections and standard histopathological examinations.

Looking at operative data, time from SF injection to CONVIVO® scanning was 137.96 min for biopsy taken at tumor core (range 84–214 min), 130.76 min for biopsy taken at tumor margin (range 89–201 min) with a mean value of 134 ± 31 min (122–214 min), taken together. Time from biopsy sampling to CONVIVO® scanning was 9.23 min (range 1–17 min). Mean time needed for CONVIVO® images interpretation was 5.74 min (range 1–7 min).

DISCUSSION

In this study we prospectively evaluated the accuracy of a newly designed miniatured CLE (CONVIVO®) in giving *ex vivo* an intraoperative first-diagnosis during GBM removal, by comparing intraoperative CLE and frozen/permanent sections results. To the best of our knowledge, this is the first available study where such aspect was assessed prospectively and based on a near real-time, blinded interpretation of the pathologist during surgery.

In CNS neoplasms surgery, the analysis of frozen section biopsies during tumor removal is still considered the standard method for intraoperative diagnosis (20). However, this procedure presents several limitations: the analysis is typically based on small volumes of tissues from a limited number of specimens; the complete process of tissue transfer and waiting time for evaluation could require up to 30 min; freezing artifacts and tissue sampling errors can occur. Such aspects all contribute to render frozen sections sometimes unsatisfactory to reveal the histological features necessary for the final diagnosis (5–7). Actually, in fact, a diagnostic discrepancy between frozen and permanent sections is reported to be as high as 2.7% for intracranial pathology (7). In addition, given the large amount of time needed to process and interpret images, this technique is not appropriate to guide intraoperative decision regarding EOR.

CLE is a promising method that permits *in vivo* high-resolution cellular visualization in near real-time, without any need for special tissue preparation, raising the possibility to implement such technology during tumor removal in the OR (8, 9, 18). In recent years several teams have evaluated different first-generation CLE systems developed for other applications

TABLE 1 | Comparison between CONVIVO®, frozen section, and permanent section at central core.

CENTRAL CORE													
	DIAGNOSIS						MORPHOLOGICAL CATEGORIZATION					
Pt. n°	**CONVIVO ANALYSIS**	**SAMPLE A1 (FROZEN SECTION)**	**Concordance**	**CONVIVO ANALYSIS**	**SAMPLE A2 (PERMANENT SECTION)**	**Concordance**	**CONVIVO ANALYSIS**	**SAMPLE A1 (FROZEN SECTION)**	**Concordance**	**CONVIVO ANALYSIS**	**SAMPLE A2 (PERMANENT SECTION)**	**Concordance**
1	High grade tumor—high cellularity	High grade glioma	+	High grade tumor—high cellularity	GBM (IV grade WHO 2016)	+/–	Tumor tissue Vascular proliferation	Tumor tissue Vascular proliferation	+ +	Tumor tissue Vascular proliferation	Tumor tissue Vascular proliferation necrosis	+ + –
2	Tumor tissue	Tumor tissue	+	Tumor tissue	GBM (IV grade WHO 2016)	+/–	Tumor tissue	Tumor tissue	+	Tumor tissue	Tumor tissue Necrosis Vascular proliferation	+ + –
3	High-density tumor tissue Presumable necrosis	GBM: large cells and necrosis	+/–	High-density tumor tissue Presumable necrosis	Giant cells GBM (IV Grade WHO 2016)	+/–	Tumor tissue Likely necrosis	Tumor tissue Necrosis	+ +	Tumor tissue Likely necrosis	Tumor tissue Necrosis Vascular proliferation	+ + –
4	Tumor with large cells Presumable necrosis	Giant cells GBM	+	Tumor with large cells Presumable necrosis	Giant cells GBM (IV Grade WHO 2016)	+	Tumor tissue Likely necrosis	Tumor tissue Necrosis Vascular proliferation	+ + -	Tumor tissue Likely necrosis	Tumor tissue Necrosis Vascular proliferation	+ + –
5	Tumor Mostly necrosis	GBM—Mostly necrosis	+/–	Tumor Mostly necrosis	GBM (IV grade WHO 2016)	+/–	Tumor tissue Necrosis	Tumor tissue Necrosis Vascular proliferation	+ + –	Tumor tissue Necrosis	Tumor tissue Necrosis	+ +
6	Necrosis	GBM—Necrosis Nervous tissue slightly infiltrated by tumor cells	–	Necrosis	GBM (IV grade WHO 2016)	–	Necrosis	Necrosis Tumor tissue	+ –	Necrosis	Necrosis Tumor tissue	+ –
7	High-density tumor tissue Pathological blood vessels	HGG Tumor tissue Pathological blood vessels	+	High-density tumor tissue Pathological blood vessels	GBM (IV grade WHO 2016)	+/–	Tumor tissue Vascular proliferation	Tumor tissue Vascular proliferation	+ +	Tumor tissue Vascular proliferation	Tumor tissue Necrosis	+ –
8	Necrosis	Necrosis	+	Necrosis	Necrosis	+	Necrosis	Necrosis	+	Necrosis	Necrosis	+
9	Infiltrated nervous tissue	GBM—Tumor tissue Necrosis	–	Infiltrated nervous tissue	GBM (IV grade WHO 2016)	–	Infiltrated tissue	Tumor tissue Necrosis	–	Infiltrated tissue	Tumor tissue Necrosis Vascular proliferation	–
10	Tumor Necrosis	GBM—Tumor tissue Necrosis	+/–	Tumor Necrosis	GBM (IV grade WHO 2016)	+/–	Tumor tissue Necrosis	Tumor tissue Necrosis Vascular proliferation	+ + –	Tumor tissue Necrosis	Tumor tissue Necrosis Vascular proliferation	+ + –
11	Tumor Necrosis	GBM—Tumor tissue Necrosis, partly fibrotic tissue	+/–	Tumor Necrosis	GBM (IV grade WHO 2016)	+/–	Tumor tissue Necrosis	Tumor tissue Necrosis	+ +	Tumor tissue Necrosis	Tumor tissue Necrosis Vascular proliferation	+ + –

(Continued)

TABLE 1 | Continued

CENTRAL CORE												
	DIAGNOSIS						MORPHOLOGICAL CATEGORIZATION					
Pt. n°	**CONVIVO ANALYSIS**	**SAMPLE A1 (FROZEN SECTION)**	**Concordance**	**CONVIVO ANALYSIS**	**SAMPLE A2 (PERMANENT SECTION)**	**Concordance**	**CONVIVO ANALYSIS**	**SAMPLE A1 (FROZEN SECTION)**	**Concordance**	**CONVIVO ANALYSIS**	**SAMPLE A2 (PERMANENT SECTION)**	**Concordance**
12	Tumor—Necrosis Likely vascular proliferation	GBM Tumor tissue with small necrotic areas	+	Tumor—Necrosis Likely vascular proliferation	GBM (IV grade WHO 2016)	+/–	Tumor Necrosis Likely vascular proliferation	Tumor tissue Necrosis Infiltrated nervous tissue	+ + –	Necrosis Likely vascular proliferation	Tumor tissue Necrosis Vascular proliferation	– + +
13	Infiltrated nervous tissue	GBM Slightly infiltrated nervous tissue Necrosis Tumor tissue Vascular proliferation	–	Infiltrated nervous tissue	GBM (IV grade WHO 2016)	–	Infiltrated nervous tissue	Infiltrated nervous tissue Necrosis Tumor tissue Vascular proliferation	+ – – –	Infiltrated nervous tissue	Tumor tissue Necrosis Vascular proliferation	–
14	Tumor tissue Necrosis	GBM—Tumor tissue Mostly necrosis	+/–	Tumor tissue Necrosis	GBM (IV grade WHO 2016)	+/–	Tumor tissue Necrosis	Tumor tissue Necrosis	+ +	Tumor tissue Necrosis	Tumor tissue Necrosis	+ +
15	Tumor tissue Necrosis	GBM—Tumor tissue Necrosis	+/–	Tumor tissue Necrosis	GBM (IV grade WHO 2016)	+/–	Tumor tissue Necrosis	Tumor tissue Necrosis	+ +	Tumor tissue Necrosis	Tumor tissue Necrosis Vascular proliferation	+ + –

TABLE 2 | Comparison between CONVIVO®, frozen section, and permanent section at the tumor margin.

TUMOR MARGINS												
	DIAGNOSIS						MORPHOLOGICAL CATEGORIZATION					
Pt. n°	**CONVIVO ANALYSIS**	**SAMPLE B1 (FROZEN SECTION)**	**Concordance**	**CONVIVO ANALYSIS**	**SAMPLE B2 (PERMANENT SECTION)**	**Concordance**	**CONVIVO ANALYSIS**	**SAMPLE B1 (FROZEN SECTION)**	**Concordance**	**CONVIVO ANALYSIS**	**SAMPLE B2 (PERMANENT SECTION)**	**Concordance**
1	Tumor	High-grade glioma	+/–	Tumor with blood	GBM (IV grade WHO 2016)	+/–	Marginal infiltrated tissue	Tumor tissue	–	Infiltrated tissue	Tumor tissue Necrosis Vascular proliferation	–
2	Infiltrated nervous tissue Blood	Tumor (anaplastic glioma) Side with infiltrated nervous tissue Blood	+	Infiltrated nervous tissue Blood	HGG	–	Marginal infiltrated tissue	Tumor tissue Infiltrated tissue	– +	Marginal infiltrated tissue	Tumor tissue with blood	–
3	Infiltrated nervous tissue High cellularity	Nervous tissue infiltrated by tumor	+	Infiltrated nervous tissue	Giant cells GBM (IV Grade WHO 2016)	–	Infiltrated tissue	Tumor tissue (mostly) Infiltrated tissue	– +	Infiltrated tissue	Tumor tissue Necrosis Vascular proliferation	–

(Continued)

TABLE 2 | Continued

TUMOR MARGINS												
	DIAGNOSIS						MORPHOLOGICAL CATEGORIZATION					
Pt. n°	**CONVIVO ANALYSIS**	**SAMPLE B1 (FROZEN SECTION)**	**Concordance**	**CONVIVO ANALYSIS**	**SAMPLE B2 (PERMANENT SECTION)**	**Concordance**	**CONVIVO ANALYSIS**	**SAMPLE B1 (FROZEN SECTION)**	**Concordance**	**CONVIVO ANALYSIS**	**SAMPLE B2 (PERMANENT SECTION)**	**Concordance**
4	Tumor (not high cellularity) Presumable necrosis	Giant cells GBM	+/–	Tumor (not high cellularity) Presumable necrosis	Giant cells GBM (IV Grade WHO 2016)	+/–	Infiltrated tissue Likely necrosis	Tumor tissue Necrosis Vascular proliferation	– + –	Infiltrated tissue Likely necrosis	Tumor tissue Necrosis Vascular proliferation	– + –
5	Tumor necrosis	GBM	+/–	Tumor necrosis	GBM (IV grade WHO 2016)	+/–	Tumor tissue Necrosis	Tumor tissue Vascular proliferation	+ –	Tumor tissue Necrosis	Tumor tissue Necrosis	+ +
6	Infiltrated nervous tissue at borders	GBM Micronecrosis	–	Infiltrated nervous tissue at borders	Nervous tissue infiltrated by GBM (IV grade WHO 2016)	+	Infiltrated tissue	Tumor tissue Necrosis Vascular proliferation	–	Infiltrated tissue	Infiltrated tissue	+
7	Infiltrated nervous tissue at borders Blood	HGG Tumor tissue Infiltrated tissue	+/–	Infiltrated nervous tissue at borders Blood	HGG	+/–	Infiltrated tissue	Tumor tissue Infiltrated tissue	– +	Infiltrated tissue	Tumor tissue Infiltrated tissue	– +
8	Tumor tissue on a side Infiltrated nervous tissue and borders on the other side	Tumor tissue on a side Infiltrated nervous tissue and borders on the other side	+	Infiltrated nervous tissue	GBM (IV grade WHO 2016)	–	Tumor tissue Infiltrated tissue	Tumor tissue Infiltrated tissue	+ +	Infiltrated tissue	Tumor tissue Necrosis Vascular proliferation	–
9	Highly infiltrated nervous tissue	GBM—Tumor tissue Necrosis	–	Highly infiltrated nervous tissue	Mostly necrotic tissue with marginal GBM	–	Infiltrated tissue	Tumor tissue Infiltrated tissue	–	Infiltrated tissue	Tumor tissue Necrosis	–
10	Tumor tissue Infiltrated nervous tissue	GBM—Tumor tissue and necrosis	+/–	Tumor tissue Infiltrated nervous tissue	GBM (IV grade WHO 2016)	+/–	Tumor tissue Infiltrated tissue	Tumor tissue Necrosis Vascular proliferation	+ – –	Tumor tissue Infiltrated tissue	Tumor tissue Necrosis Vascular proliferation	+ – –
11	Tumor tissue Infiltrated nervous tissue	GBM—Tumor and necrosis Side with infiltrated nervous tissue	+/–	Tumor tissue Infiltrated nervous tissue	GBM (IV grade WHO 2016)	+/–	Tumor tissue Infiltrated tissue	Tumor tissue Necrosis Infiltrated nervous tissue	+ –	Tumor tissue Infiltrated tissue	Tumor tissue Necrosis Infiltrated nervous tissue	+ – +
12	Tumor tissue Infiltrated nervous tissue	GBM Tumor tissue and infiltrated tissue	+/–	Tumor Infiltrated nervous tissue	GBM (IV grade WHO 2016)	+/–	Tumor tissue Infiltrated tissue	Tumor tissue Infiltrated tissue	+ +	Tumor tissue Infiltrated nervous tissue	Tumor tissue Infiltrated tissue	+ +

(Continued)

TABLE 2 | Continued

	TUMOR MARGINS					MORPHOLOGICAL CATEGORIZATION				
	DIAGNOSIS									
Pt. n°	CONVIVO ANALYSIS	SAMPLE B1 (FROZEN SECTION)	Concordance	CONVIVO ANALYSIS	SAMPLE B2 (PERMANENT SECTION)	Concordance	CONVIVO ANALYSIS	SAMPLE B1 (FROZEN SECTION)	Concordance	CONVIVO ANALYSIS	SAMPLE B2 (PERMANENT SECTION)	Concordance
13	Infiltrated nervous tissue Mostly blood	GBM: slightly infiltrated nervous tissue Tumor tissue: vascular proliferation and blood	–	Infiltrated nervous tissue Mostly blood	GBM (IV grade WHO 2016), but mostly blood	–	Infiltrated nervous tissue Blood	Infiltrated nervous tissue Tumor tissue Vascular proliferation Blood	+ – –	Infiltrated nervous tissue Blood	Tumor tissue Necrosis Vascular proliferation	– + –
14	Tumor tissue	GBM Tumor tissue Necrosis	+/–	Tumor tissue	GBM (IV grade WHO 2016)	+/–	Tumor tissue	Tumor tissue Necrosis	+ –	Tumor tissue	Tumor tissue Necrosis Vascular proliferation	+ – –
15	Infiltrated nervous tissue Tumor tissue	Infiltrated nervous tissue Tumor tissue	+	Infiltrated nervous tissue Tumor tissue	GBM (IV grade WHO 2016)	+/–	Infiltrated nervous tissue Tumor tissue	HGG—Tumor (80%) Infiltrated nervous tissue (20%)	+ +	Infiltrated nervous tissue Tumor tissue	Tumor tissue Necrosis Vascular proliferation	+ – –

(i.e. gastrointestinal and gynecological surgery) for potential use in neurosurgery (8, 12, 24–26), starting from preclinical models (10, 11). The first studies in mouse GBM models were focused on the ability to distinguish normal brain, microvasculature, and tumor margins (18, 23, 27, 28). Then, feasibility of CLE in human brain tumor surgery was studied through both *ex vivo* and *in vivo* experiences (6, 13, 29, 30). Other authors focused instead on the study of different fluorophores to be used as non-tumor specific contrast-enhancer in CLE technology, such as SF, acridine orange, acriflavine, cresyl violet, 5–ALA, and indocyanine green (18, 23). In addition, others have proposed tumor –specific fluorescent molecular labelings (27). Nevertheless, among the abovementioned dyes, SF represents nowadays one of the most used in conjunction to CLE, thanks to its established neuro-oncological use (21), and to the possibility of enhancing non-naturally reflected structures on CLE systems in fluorescence mode (6, 15).

To overcome the various limitations associated with first-generation CLE systems, such as low ergonomic and quality of imaging analysis and processing, a second-generation neurosurgical CLE system (CONVIVO®, *Carl Zeiss, Meditec, Oberkochen, Germany*) was recently developed. Belykh and colleagues investigated its capability to differentiate in glioma models normal brain, injured normal brain, and tumor tissue, during fluorescein-guided resection (19). Then, in 2019, the same authors brilliantly described in a preclinical study the advantages carried by the use of such new system, including a more responsive and intuitive user interface, collection of metadata with each image, automatic Z-stack imaging, sharper images, and a sterile sheath, if compared to old-generation ones (15).

Our work represents the first available study that prospectively assesses the ability of the CONVIVO® system in offering an intraoperative diagnosis during fluorescein-guided GBM removal, based on a near real-time, blinded interpretation by the pathologist, directly in the OR.

From a qualitative point of view, CONVIVO® scanning demonstrated the peculiarities of GBM, as they may be seen on CLE acquisition (**Figure 1**). In particular, tumor cells appeared as large non-uniform dark cells on a bright background, due to the fluorescent dye that leaked into tumor tissue, due to blood-brain barrier (BBB) disruption (21). Among tumor cells, as expected and as confirmed by other authors, single and multiple cells absorbing SF were noted (15, 19). Although the reason for such finding still needs to be clarified, as it has been demonstrated that tumor cells do not uptake SF *in vitro* (31), some authors suggested a passive uptake due to cell membrane disruption caused by mechanical injury. Belykh and colleagues, in fact, found such phenomenon mostly in their *ex vivo* samples (15). On the contrary, the intracellular fluorescence showed by some large singular cells among tumor tissue may be related to the uptake by polymorphonuclear leukocytes (15).

With CONVIVO® imaging we were also able to see irregular neo-angiogenetic vessels inside tumor tissue, with red blood cells (smaller and morphologically regular cells) easily identifiable inside and outside them. With this study we were also interested in categorizing some morphological patterns: cellular features

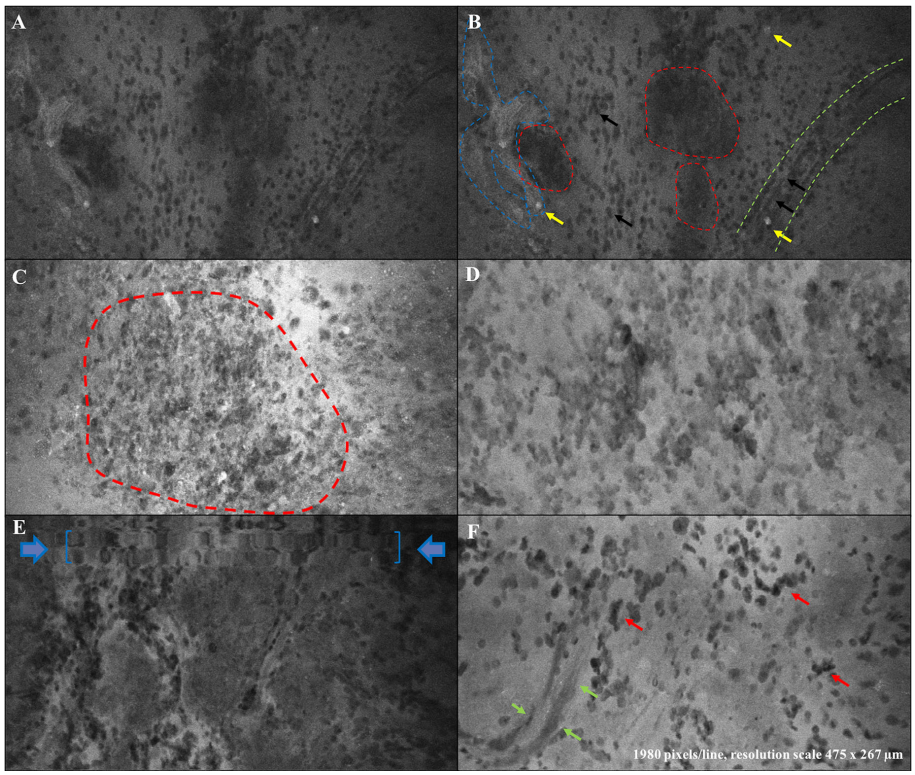

FIGURE 1 | *Ex vivo* confocal hallmarks of GBM. **(A, B)** report the same image of a GBM tumor tissue sample as seen through CONVIVO® system. High-density tumor areas are identifiable as agglomerates of cells appearing darker than the background (red-dotted lines, **B**). As expected, some cells absorbed SF (yellow arrows, **B**). Green-dotted lines in **(B)** delineate the contour of a neo-angiogenetic vessel with erythrocytes inside and outside it (smaller than tumor cells, black arrows). Blue-dotted lines demonstrate SF diffused out of vessels (BBB disruption), creating a fuzzy appearance. **(C)** Another GBM case: high density tumor tissue (red dotted line) appeared brighter due to a closer time between SF injection and sample analysis. **(D)** Another GBM case characterized by high cellularity, pleomorphism with large dysmorphic nuclei and agglomerates of cells. **(E)** A movement artifact on a GBM CLE image (blue arrows and commas). **(F)** Another GBM case with pleomorphic cells (dark nuclei, apparently tumor cells, red arrows) visible on a brighter SF background. Green arrows contour a neoangiogenetic vessel.

and tumor structures, such as pleomorphism, atypia, hypercellularity, and neovascularization appeared to correlate with the matched permanent sections and known tissue architecture. Although quality of images was not as good as the one shown in the paper by Belykh and colleagues (15), CONVIVO® *ex vivo* scanning permitted to clearly identify GBM tissue during surgery, leading to an intraoperative correct diagnosis in a high percentage of cases, fulfilling the primary objective in such study. As a matter of fact, our protocol permitted to the pathologist to analyze CONVIVO® tissue samples in a blinded manner, never knowing anticipately the results from permanent or frozen section images. Thus, the investigator was non-biased and able to focus solely on the CONVIVO® image criteria to diagnose and categorize tissue samples.

Analyzing the quantitative results, CONVIVO® imaging at the central tumor core resulted to be concordant to both frozen section and definitive histology analysis in 80% of the cases, with an even higher ability of defining the morphological categories that were recognized also in frozen section (93.3% of the cases) and permanent section analyses (86.7% of the cases). The morphological pattern majorly described was "tumor tissue," followed by "necrosis" and "vascular proliferation." In addition, when examining the three discordant cases, although the diagnosis was not equal from a qualitative point of view, it was always possible to find some of the characteristic features of GBM, such as necrosis (case 6), or tumor infiltration (cases 9 and 13) (**Table 1**). In previous studies, Breuskin demonstrated a sensitivity and specificity for identification of HGGs of 81 and 85%, respectively (ENDO-MAG1, *ex vivo* analysis) (30), while Martirosyan showed a 91 and 94% of sensitivity and specificity, respectively (Optiscan 5.1, *in vivo* analysis) (6). Using CONVIVO®, in 2018 Belykh and colleagues found an accuracy of 90.2 ± 3.6% in differentiating tumor *versus* no-tumor at the CLE biopsy sites, with high overall sensitivity (86%) and specificity (96%) in differentiating tumor from surrounding brain tissue, in an animal model (19). Hence, it is reasonable to affirm that the slight difference of our results may be partially explained by the *ex vivo* nature of our study. Furthermore, this could be related to the fact that the judgment of discordance was also derived by the application of a strict intraoperative protocol, with CONVIVO® diagnosis expressed upfront directly

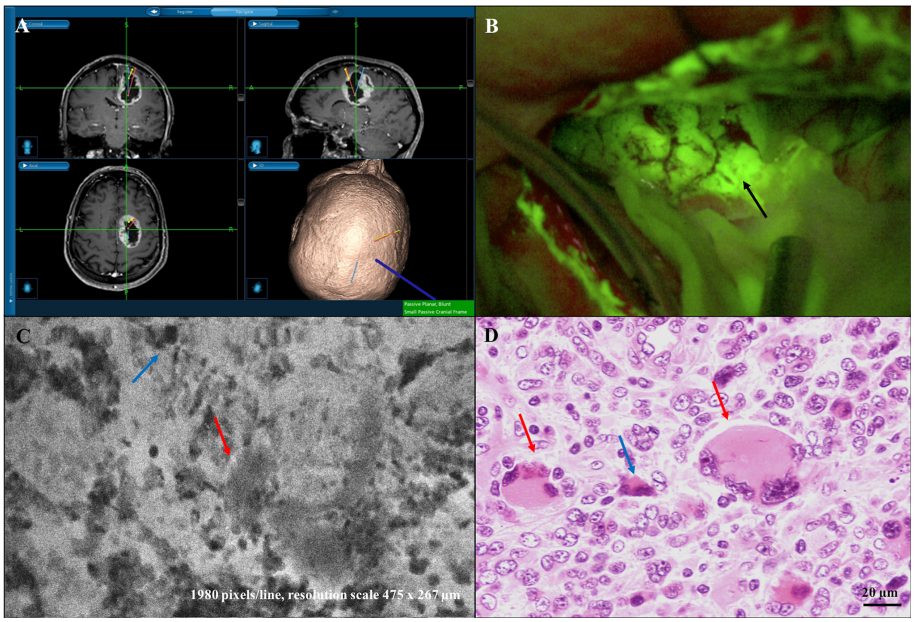

FIGURE 2 | Diagnostic concordant case: right frontal giant-cells GBM (case n. 4). **(A)** Neuronavigation MR images showing the site of "A" biopsy sampling in the GBM core. **(B)** Intraoperative view during tumor removal with SF-guided technique. Yellowish fluorescent areas under Y560 filter activation of the surgical microscope correspond to tumor tissue (site of "A" sampling, black arrow). Both CONVIVO® *ex vivo* images **(C)** and frozen and classical histopathological sections **(D)** confirmed the GBM diagnosis. To note the presence of «giant cells» (red arrows), along with increased cellularity and foci of necrosis with apoptotic cells (blue arrows) in both **(C, D)**.

TABLE 3 | Detailed list of morphological patterns analyzed in CONVIVO®, frozen section, and permanent section images, in both tumor central core and tumor margins specimens.

	TUMOR CENTRAL CORE			TUMOR MARGINS		
	CONVIVO	**FROZEN SECTION (A1)**	**PERMANENT SECTION (A2)**	**CONVIVO**	**FROZEN SECTION (B1)**	**PERMANENT SECTION (B2)**
Tumor tissue	11/15 (73.3%)	14/15 (93.3%)	14/15 (93.3%)	7/15 (46.6%)	15/15 (100%)	14/15 (93.3%)
Necrosis	10/15 (66.6%)	12/15 (80.0%)	15/15 (100%)	2/15 (13.3%)	5/15 (33.3%)	11/15 (73.3%)
Marginal infiltrated tissue	2/15 (13.3%)	2/15 (13.3%)	0/15 (0%)	13/15 (86.6%)	9/15 (60.0%)	4/15 (26.6%)
Vascular proliferation	3/15 (20.0%)	6/15 (40.0%)	10/15 (66.6%)	0/15 (0%)	5/15 (33.3%)	8/15 (53.3%)
Reactive changes	0/15 (0%)	0/15 (0%)	0/15 (0%)	0/15 (0%)	0/15 (0%)	0/15 (0%)
Healthy tissue	0/15 (0%)	0/15 (0%)	0/15 (0%)	0/15 (0%)	0/15 (0%)	0/15 (0%)

in the OR, without knowing the subsequent histological characteristics of the lesion.

Regarding the biopsies taken at tumor margin, as a preliminary consideration it should be said that this work was not designed to calculate a real sensibility and specificity, given the lack of biopsies on healthy brain parenchyma (negatives), as already mentioned. Nonetheless, a high degree of diagnostic and morphological concordance was found when comparing CONVIVO® to frozen sections (80%), but not to standard histology (concordant diagnosis in 66.7% of the cases) (**Table 2**). Nevertheless, the fact that the morphological pattern of samples at the tumor margin in all the diagnostic discordant cases could be classified as "tumoral" by CONVIVO® (**Table 2**) highlights the potentiality of the system to effectively assess the presence of pathology at the tumor margin, to guide also intraoperative decision regarding EOR. Moreover, as mentioned, morphological disparity in all the evaluations performed in this work should be interpreted carefully and optimistically, as the descriptive categories used were voluntarily rigorous and precise, with the aim to increase specificity as much as possible.

There are some intrinsic limitations of the CLE that deserves to be outlined. Its use requires specific training and a learning curve to interpret the acquired information (18, 28). Moreover, it still needs a pathologist in the OR, it requires

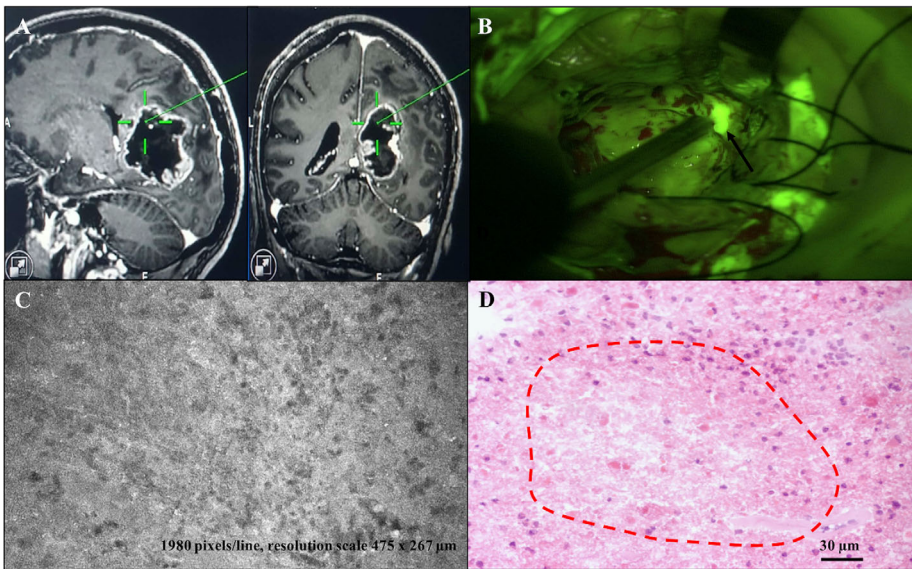

FIGURE 3 | Diagnostic partially concordant case: right parieto-occipital GBM (case n. 14). **(A)** Neuronavigation MR images showing the site of "A" biopsy sampling in the GBM core. **(B)** Intraoperative view during tumor removal with SF-guided technique. Yellowish fluorescent areas under Y560 filter activation of the surgical microscope correspond to tumor tissue (site of "A" sampling, black arrow). **(C, D)** CONVIVO® and permanent section images, respectively, within the biopsy sample, showing an area of tumor tissue with prevalent necrotic aspects, such as low cellular density, prevalence of amorphous tissue on an intermediate fluorescence background **(C)**, confirmed as a low-cellular density necrotic area within the permanent section sample (red-dotted lines in **D**).

established workflows and a real cost-effectiveness analysis has never been performed. In addition, at present time, it is questionable whether CLE could become easily accessible for all neurosurgeons, still making it less competitive to frozen sections. Furthermore, it has to be considered that frozen sections and then permanent sections need gross cut of the tissue block before 3 µm slice performed with cryostat and microtome. Hence, histology sections may be in a Z plan different of Z plan of CLE images. This aspect represents one of the intrinsic limitations that reside behind this technology. There are in fact many more possible Z plans with CONVIVO® scanning than the ones that could be evaluated on permanent/frozen sections. Hence, section comparison between CONVIVO® and histological sections may not be executed exactly in the same plane.

Our study also has some limitations. First of all, the relative low number of patients enrolled, that may affect the further generalization of our results to larger cohorts. Furthermore, from a technical point of view, the amount of time needed from SF injection to image interpretation was relatively high (134 ± 31 min), with peaks up to 214 min. This is surely related to the application in our study of the same protocol of SF injection (i.e. at the time of patient intubation) that we are extensively applying for fluorescein-guided resection of CNS tumors (21, 32), and to the *ex vivo* nature of the study. Given the clear and demonstrated inverted correlation that exists between time from contrast injection to images interpretation and readability of the pictures (less time, clearer images) (6, 27), this aspect may have partially affected readability of CONVIVO® images, especially if such time is summed up to the time needed for subsequent CONVIVO® images interpretation (mean of 5.74 min). This limitation could be partially overcome by a totally *in vivo* setting, which needs a dedicated sterile sheath covering the CONVIVO® probe, allowing for a direct tumor bed analysis, surely much closer to the SF injection time. As a matter of fact, in previous *in vivo* published series, performed with other confocal prototypes, or with CONVIVO® system only in animals (15, 19), the quality of the image related to the improved background fluorescence, is much higher. In addition, other authors suggested to use different protocols of SF injection, right before *in vivo* CLE analysis, with an impact on image quality (6, 13). However, as we consider SF a significant intraoperative adjunct to improve tumor visualization and resection (21, 32), and as we stressed the importance of using the right SF injection timing and dosage to obtain a good discrimination between tumor and normal peritumoral parenchyma (32), we wanted to evaluate if the same protocol could give us similar results in terms of "microscopic" discrimination by using CLE. Another drawback linked to the *ex vivo* sampling and scanning is the small field of views of the confocal imaging, that could limit the identification of important structures that are on the contrary identified on standard histology and frozen section analyses, due to the possibility to enlarge the area of interest in the slide. However, also in this case, *in vivo* analysis could partially address this limitation, by performing multiple virtual biopsies in closer areas of the tumor bed or the brain-tumor interface, enlarging the area of tissue evaluation. Moreover, due to the prospective nature of the

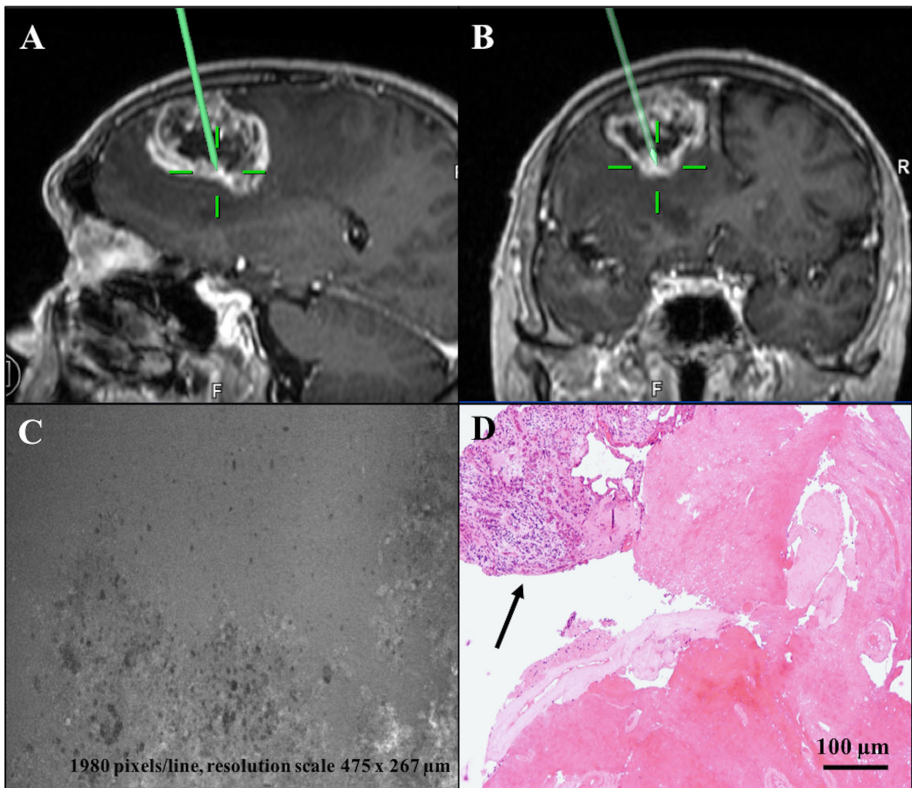

FIGURE 4 | Diagnostic discordant case: left frontal GBM (case n. 6). **(A, B)** Sagittal and coronal T1 after contrast administration images showing location of tissue biopsies sampled at tumor central core, where CONVIVO® scan **(C)** disclosed «necrosis» (amorphous area with few cells and intermediate fluorescence background). **(D)** Definitive histology of the sample showing a small part of tumor tissue (black arrow), adjacent to amorphous material with only some "ghost" cells and vessels, consistent to necrosis and corresponding at the area analyzed by CONVIVO®. Taken together, these features set out the diagnosis of GBM. In this specific case, the discordant results for both tumor diagnosis and morphological categorization at central core were due to a larger field of observation with the optical microscope used at the permanent section examination.

study, with the pathologist that analyzed *a priori* the CONVIVO® images, being blind to the subsequent permanent section analysis, we hypothesize the presence of possible misinterpretations of the CONVIVO® images, that could eventually be reduced if *a posteriori* analysis would have been performed. However, as we were interested in demonstrating the up-front capability of this tool to provide immediate results in the OR setting, this limitation could be interpreted also as a strength of the study.

Then, summed up, our results confirm our initial hypothesis that the CONVIVO® system may definitely help during GBM resection in obtaining a reliable intraoperative diagnosis and to gain more insight in the characteristic histological pattern at the tumor margin.

Future studies are clearly needed to confirm our preliminary results, and to eventually extend such a standardized, prospective and blinded-to-permanent section study in an *in vivo* model, aiming to confirm the potentiality of such new CLE system in helping during intraoperative diagnosis in CNS tumors, and, more importantly, in identifying small residual tissue at the surgical cavity, with a possible impact on EOR. In our Institute, a protocol for *in vivo* CLE study on CNS tumors is already planned and soon to be started.

CONCLUSIONS

The high rate of diagnostic and morphological concordance found between CONVIVO® and frozen section images analysis highlights CLE as a complementary tool during GBM removal, helping in obtaining an intraoperative diagnosis. Future studies are needed to confirm such results and to extend them in an *in vivo* model, aiming to confirm the potentiality of such new CLE system in helping during intraoperative diagnosis and resection of GBM or other CNS tumors.

DATA AVAILABILITY STATEMENT

The original contributions presented in the study are included in the article/supplementary materials. Further inquiries can be directed to the corresponding author.

ETHICS STATEMENT

The studies involving human participants were reviewed and approved by the Ethics Committee, Carlo Besta Neurological Institute. The patients/participants provided their written informed consent to participate in this study.

AUTHOR CONTRIBUTIONS

Substantial contributions to conception and design, acquisition of data, or analysis and interpretation of data: all authors. Drafting the article or revising it critically for important intellectual content: FA, BP, FR, IGV, CD, IT, FD. All authors contributed to the article and approved the submitted version.

FUNDING

The authors declare that this study received funding from Carl Zeiss Meditec. The funder was not involved in the study design, collection, analysis, interpretation of data, the writing of this article or the decision to submit it for publication. This research was partially supported by Carl Zeiss Meditec (Germany) and by Associazione Paolo Zorzi per le Neuroscienze Onlus.

REFERENCES

1. Wen PY, Kesari S. Malignant gliomas in adults. *N Engl J Med* (2008) 359:492–507. doi: 10.1056/NEJMra0708126
2. Stupp R, Mason WP, van den Bent MJ, Weller M, Fisher B, Taphoorn MJ, et al. Radiotherapy plus concomitant and adjuvant temozolomide for glioblastoma. *N Engl J Med* (2005) 352:987–96. doi: 10.1016/j.canrad.2005.05.001
3. Sanai N, Polley M-Y, McDermott MW, Parsa AT, Berger MS. An extent of resection threshold for newly diagnosed glioblastomas. *J Neurosurg* (2011) 115:3–8. doi: 10.3171/2011.2.JNS10998
4. Mabray MC, Barajas RF, Cha S. Modern Brain Tumor Imaging. *Brain Tumor Res Treat* (2015) 3:8–23. doi: 10.14791/btrt.2015.3.1.8
5. Chatterjee S. Artefacts in histopathology. *J Oral Maxillofac Pathol* (2014) 18: S111–6. doi: 10.4103/0973-029X.141346
6. Martirosyan NL, Eschbacher JM, Yashar M, Turner JD, Belykh E, Spetzler RF, et al. Prospective evaluation of the utility of intraoperative confocal laser endomicroscopy in patients with brain neoplasms using fluorescein sodium: Experience with 74 cases. *Neurosurg Focus* (2016) 40:1–8. doi: 10.3171/2016.1.FOCUS15559
7. Plesec TP, Prayson RA. Frozen section discrepancy in the evaluation of central nervous system tumors. *Arch Pathol Lab Med* (2007) 131:1532–40. doi: 10.1043/1543-2165(2007)131[1532:FSDITE]2.0.CO;2
8. Foersch S, Heimann A, Ayyad A, Spoden GA, Florin L, Mpoukouvalas K, et al. Confocal Laser Endomicroscopy for Diagnosis and Histomorphologic Imaging of Brain Tumors In Vivo. *PloS One* (2012) 7:1–11. doi: 10.1371/journal.pone.0041760
9. Breuskin D, Divincenzo J, Kim Y, Urbschat S, Oertel J. Confocal Laser Endomicroscopy in Neurosurgery: A New Technique with Much Potential. *Minim Invasive Surg* (2013) 2013:1–5. doi: 10.1155/2013/851819
10. Dunbar KB, Okolo P, Montgomery E, Canto MI. Confocal laser endomicroscopy in Barrett's esophagus and endoscopically inapparent Barrett's neoplasia: a prospective, randomized, double-blind, controlled, crossover trial. *Gastrointest Endosc* (2009) 70:645–54. doi: 10.1016/j.gie.2009.02.009
11. Tan J, Quinn MA, Pyman JM, Delaney PM, McLaren WJ. Detection of cervical intraepithelial neoplasia in vivo using confocal endomicroscopy. *BJOG* (2009) 116:1663–70. doi: 10.1111/j.1471-0528.2009.02261.x
12. Snuderl M, Wirth D, Sheth SA, Bourne SK, Kwon CS, Ancukiewicz M, et al. Dye-enhanced multimodal confocal imaging as a novel approach to intraoperative diagnosis of brain tumors. *Brain Pathol* (2013) 23:73–81. doi: 10.1111/j.1750-3639.2012.00626.x
13. Pavlov V, Meyronet D, Meyer-Bisch V, Armoiry X, Pikul B, Dumot C, et al. Intraoperative Probe-Based Confocal Laser Endomicroscopy in Surgery and Stereotactic Biopsy of Low-Grade and High-Grade Gliomas: A Feasibility Study in Humans. *Neurosurgery* (2016) 79:604–11. doi: 10.1227/NEU.0000000000001365
14. Osman H, Georges J, Elsahy D, Hattab EM, Yocom S, Cohen-Gadol AA. In Vivo Microscopy in Neurosurgical Oncology. *World Neurosurg* (2018) 115:421–9. doi: 10.1016/j.wneu.2018.03.218
15. Belykh E, Miller EJ, Carotenuto A, Patel AA, Cavallo C, Martirosyan NL, et al. Progress in Confocal Laser Endomicroscopy for Neurosurgery and Technical Nuances for Brain Tumor Imaging With Fluorescein. *Front Oncol* (2019) 9:554. doi: 10.3389/fonc.2019.00554
16. Belykh E, Martirosyan NL, Yagmurlu K, Miller EJ, Eschbacher JM, Izadyyazdanabadi M, et al. Intraoperative Fluorescence Imaging for Personalized Brain Tumor Resection: Current State and Future Directions. *Front Surg* (2016) 3:1–27. doi: 10.3389/fsurg.2016.00055
17. Eschbacher J, Martirosyan NL, Nakaji P, Sanai N, Preul MC, Smith KA, et al. In vivo intraoperative confocal microscopy for real-time histopathological imaging of brain tumors: Clinical article. *J Neurosurg* (2012) 116:854–60. doi: 10.3171/2011.12.JNS11696
18. Martirosyan NL, Georges J, Eschbacher JM, Cavalcanti DD, Elhadi AM, Abdelwahab MG, et al. Potential application of a handheld confocal endomicroscope imaging system using a variety of fluorophores in experimental gliomas and normal brain. *Neurosurg Focus* (2014) 36:E16. doi: 10.3171/2013.11.FOCUS13486
19. Belykh E, Miller EJ, Patel AA, Yazdanabadi MI, Martirosyan NL, Bozkurt B, et al. Diagnostic Accuracy of a Confocal Laser Endomicroscope for In Vivo Differentiation Between Normal Injured And Tumor Tissue During Fluorescein-Guided Glioma Resection: Laboratory Investigation. *World Neurosurg* (2018) 115:E337–48. doi: 10.1016/j.wneu.2018.04.048
20. Louis DN, Perry A, Reifenberger G, Von Deimling A, Figarella D, Webster B, et al. The 2016 World Health Organization Classification of Tumors of the Central Nervous System: a summary. *Acta Neuropathol* (2016) 131:803–20. doi: 10.1007/s00401-016-1545-1
21. Acerbi F, Broggi M, Schebesch K-M, Höhne J, Cavallo C, De Laurentis C, et al. Fluorescein-guided surgery for resection of high-grade gliomas: A multicentric prospective phase II study (FLUOGLIO). *Clin Cancer Res* (2018) 24:52–61. doi: 10.1158/1078-0432.CCR-17-1184
22. Belykh E, Patel AA, Miller EJ, Bozkurt B, Yağmurlu K, Woolf EC, et al. Probe-based three-dimensional confocal laser endomicroscopy of brain tumors: technical note. *Cancer Manag Res* (2018) 10:3109–23. doi: 10.2147/CMAR.S165980
23. Zehri AH, Ramey W, Georges JF, Mooney MA, Martirosyan NL, Preul MC, et al. Neurosurgical confocal endomicroscopy: A review of contrast agents , confocal systems , and future imaging modalities. *Surg Neurol Int* (2014) 5:1–11. doi: 10.4103/2152-7806.131638
24. Peyre M, Clermont-Taranchon E, Stemmer-Rachamimov A, Kalamarides M. Miniaturized handheld confocal microscopy identifies focal brain invasion in a mouse model of aggressive meningioma. *Brain Pathol* (2013) 23:371–7. doi: 10.1111/bpa.12039
25. Belykh E, Cavallo C, Gandhi S, Zhao X, Veljanoski D, Yazdanabadi MI, et al. Utilization of intraoperative confocal laser endomicroscopy in brain tumor surgery. *J Neurosurg Sci* (2018) 62:704–17. doi: 10.23736/S0390-5616.18.04553-8
26. Belykh E, Ngo B, Farhadi DS, Zhao X, Mooney MA, White WL, et al. Confocal Laser Endomicroscopy Assessment of Pituitary Tumor Microstructure: A Feasibility Study. *J Clin Med* (2020) 9:3146. doi: 10.3390/jcm9103146
27. Martirosyan NL, Georges J, Kalani MYS, Nakaji P, Spetzler RF, Feuerstein BG, et al. Handheld confocal laser endomicroscopic imaging utilizing tumor –

specific fluorescent labeling to identify experimental glioma cells in vivo. *Surg Neurol Int* (2016) 7:S995–1003. doi: 10.4103/2152-7806.195577
28. Sankar T, Delaney PM, Ryan RW, Eschbacher J, Abdelwahab M, Nakaji P, et al. Miniaturized handheld confocal microscopy for neurosurgery: Results in an experimental glioblastoma model. *Neurosurgery* (2010) 66:401–17. doi: 10.1227/01.NEU.0000365772.66324.6F
29. Charalampaki P, Nakamura M, Athanasopoulos D, Heimann A. Confocal-Assisted Multispectral Fluorescent Microscopy for Brain Tumor Surgery. *Front Oncol* (2019) 9:583. doi: 10.3389/fonc.2019.00583
30. Breuskin D, Szczygielski J, Urbschat S, Kim Y, Oertel J. Confocal Laser Endomicroscopy in Neurosurgery-An Alternative to Instantaneous Sections? *World Neurosurg* (2017) 100:180–5. doi: 10.1016/j.wneu.2016.12.128
31. Diaz RJ, Dios RR, Hattab EM, Burrell K, Rakopoulos P, Sabha N, et al. Study of the biodistribution of fluorescein in glioma-infiltrated mouse brain and histopathological correlation of intraoperative findings in high-grade gliomas resected under fluorescein fluorescence guidance. *J Neurosurg* (2015) 122:1360–9. doi: 10.3171/2015.2.JNS132507
32. Acerbi F, Broggi M, Broggi G, Ferroli P. What is the best timing for fluorescein injection during surgical removal of high-grade gliomas? *Acta Neurochir (Wien)* (2015) 157:1377–8. doi: 10.1007/s00701-015-2455-z

Conflict of Interest: FA received fees from Carl Zeiss Meditec for lectures at International Congresses.

The remaining authors declare that the research was conducted in the absence of any commercial or financial relationships that could be construed as a potential conflict of interest.

frontiers in Oncology

ORIGINAL RESEARCH
published: 28 January 2021
doi: 10.3389/fonc.2020.618579

Sodium Fluorescein for Spinal Intradural Tumors

Semih Kivanc Olguner, Ali Arslan, Vedat Açık, İsmail İstemen, Mehmet Can, Yurdal Gezercan and Ali İhsan Ökten*

Department of Neurosurgery, Adana City Training and Research Hospital, Adana, Turkey

Technological innovations in spinal intradural tumor surgery simplify treatment. Surgical treatment of cranial benign and malignant pathologies under microscope with sodium (Na)-fluorescein guidance has often been reported, but few studies have focused on spinal intradural tumors. We aimed to investigate the usefulness of Na-fluorescein under yellow filter in intradural spinal tumor surgery by retrospectively reviewing cases involving intramedullary and extramedullary tumors operated under the guidance of Na-fluorescein. Forty-nine adult patients with a diagnosis of spinal intradural tumor operated under a yellow filter (560 nm) microscope using Na-fluorescein dye were included in the study. Demographic data, such as age and sex, neurological status, extent of tumor resection, histopathological diagnosis, Na-fluorescein staining pattern, and its usefulness during surgery were noted and statistically analyzed. Of all recruited patients, 26 women (53.1%) and 23 men (46.9%), were included for analysis. The age range of the patients was 18–64 years, with a mean age of 41.6 ± 13.9. An intradural intramedullary mass was found in 30.6% (n = 15) of the patients, and an intradural extramedullary mass in 69.4% (n: 34). While Na-fluorescein staining was homogeneous in all intradural extramedullary tumors, 73.3% (n: 11) of intradural intramedullary tumors were homogeneous, and 13.3% (n: 2) moderately heterogeneous. In the whole study group, the Na-fluorescein staining pattern was helpful in surgical resection in 47 cases (95.9%). While 34/34 (100%) found it helpful for extramedullary tumors, 13/15 (86.7%) did in intramedullary tumors, and for 2/15 (13.3%) it was not. In conclusion, Na-fluorescein helps in distinguishing tumor from healthy tissue in intradural extramedullary and intramedullary tumor surgery under a yellow filter microscope in most cases, thus providing convenient assistance to surgeons.

Keywords: guidance, surgical resection, spinal tumor, sodium fluorescein, intradural tumor

OPEN ACCESS

Edited by:
Talat Kiris,
Koç University, Turkey

Reviewed by:
Mehmet Osman Akçakaya,
Istanbul Florence Nightingale Hospital, Turkey
Constantin Tuleasca,
Centre Hospitalier Universitaire Vaudois (CHUV), Switzerland

****Correspondence:***
Semih Kivanc Olguner
kivanc3olguner@hotmail.com

Specialty section:
This article was submitted to Neuro-Oncology and Neurosurgical Oncology, a section of the journal Frontiers in Oncology

Received: *17 October 2020*
Accepted: *11 December 2020*
Published: *28 January 2021*

Citation:
Olguner SK, Arslan A, Açık V, İstemen İ, Can M, Gezercan Y and Ökten Aİ (2021) Sodium Fluorescein for Spinal Intradural Tumors. Front. Oncol. 10:618579. doi: 10.3389/fonc.2020.618579

INTRODUCTION

Spinal intradural tumors are rare central nervous system (CNS) diseases categorized as intramedullary and extramedullary according to their location. Treatment of these pathologies is surgical, and in recent years effective results have resulted in tumor surgery from the use of technological innovations. Intraoperative neuromonitorisation (IONM), magnetic resonance (MR) tractography, and ultrasonography (USG) have been used for safe and maximum surgical resection (1–10). Furthermore, surgery under the guidance of Sodium-fluorescein (Na-fluorescein) has

earned a place in neurosurgery for tumor resection and tumor volume reduction. This technique, widely used in intracranial malignant and benign tumor surgery, provides an advantage to the surgical team by staining the tumor tissue in cases where the blood-brain barrier is disrupted (11–16). Similarly, in spinal intradural tumors, another pathology of the central nervous system, the blood-brain barrier is disrupted during neoplasia development. As with intracranial CNS tumors, the main goal is to perform maximal surgical tumor resection within safe limits in spinal intradural masses. Providing gross total resection (GTR) also positively affects the patient's overall quality of life by affecting progression-free survival (PFS) and long-term neurological improvement (LTNI) (17, 18). While tumor margins are clearly monitored in extramedullary tumors, it may not always be possible to find these borders in intramedullary tumors. The most important factor determining the gross total resection is the perioperative tumor cleavage plan (17). For this reason, we assumed that surgery under a yellow filter in the presence of Na-fluorescein might be effective in determining the tumor cleavage plan, especially for spinal intradural tumors. The aim of this study was, therefore, to examine the staining pattern of Na-fluorescein in intradural intramedullary and extramedullary tumors and investigate its suitability for surgery. To our knowledge, only two studies evaluated spinal intradural tumors under yellow filter microscope in the presence of Na-fluorescein (19, 20). Considering the number of published articles evaluating the use of Na-fluorescein in intracranial CNS tumors, this number is very low, pointing to a gap in knowledge we aimed to fill with the data gathered in this study.

MATERIAL AND METHODS

Patients and Data

This study was carried out in accordance with the principles of the Declaration of Helsinki and approved by the Ethics Committee of Adana City Training and Research Hospital. Informed consent was obtained from all patients. Inclusion criteria for the study were adult patients operated under PENTERO 900 (Carl Zeiss, Meditec, Oberkochen, Germany) and a microscope yellow filter (560 nm) using Na-fluorescein dye (5 mg/kg) with a diagnosis of spinal intradural tumor between May 2017 and May 2019. The exclusion criteria for the study were as follows: patients <18 years of age who were not given Na-fluorescein, with known hepatic and renal insufficiency, or those with a history of excessive hypersensitivity-allergic reactions. Besides demographic data such as age and sex of the patients, extent of tumor resection, histopathological diagnosis, Na-fluorescein staining pattern, and neurological status were noted and analyzed. For neurological evaluation, we employed the classification by McCormick et al. (21).

Surgery

In all cases, 5 mg/kg Na-fluorescein was intravenously administered during anesthesia induction and imaging was performed under a microscope with a yellow 560 filter. All surgeries were performed by the same team with continuous intraoperative neuromonitorization (somatosensory evoked potentials, motor evoked potentials, and electromyography). Level determination for tumor localization was performed under lateral view with C-arm fluoroscopy with patients placed in the prone position on the operating table. Following skin incision, the paraspinal muscles were dissected subperiosteally. After hemilaminectomy or laminectomy, the dura was opened, the yellow filter activated, and, if there was Na-fluorescein involvement, extramedullary tumors immediately observed. In intramedullary tumors, after myelotomy, the tumor was observed according to Na-fluorescein involvement, and the tumor-spinal cord tissue demarcation line searched. Tumor excision was performed using the classical microsurgical technique. Additional instrumentation was applied after duraplasty, laminoplasty, or according to the surgical team's preference. The staining pattern was defined by consensus of surgeons performing the surgery. Similar to the classification used in the work by Millesi et al., they were divided into three groups, namely, dense homogeneous, moderate heterogeneous and none (22). If the tumor tissue was in vivid homogenous yellow color, it was determined as "dense homogeneous", if lightly yellow in appearance "moderate heterogeneous" and if there was no staining determined as "none".

Radiological Assessment

Preoperative and postoperative (first 48 h) non-contrast and contrast-enhanced magnetic resonance imaging was performed in all patients, and the amount of resection noted. The basic algorithm preferred by Klekamp et al. was used to define the amount of resection (23). Cases whose tumor tissue was completely excised and no remnant was confirmed by postoperative MRI were called gross total resection (GTR), those with little tumor residue subtotal resection (STR), and those with >50% residual postoperative resection were called partial resection (PR).

Statistical Analysis

Statistical evaluation was performed using the Statistical Package for Social Sciences (SPSS) for Windows 20 (IBM SPSS Inc., Chicago, IL). Normal data distribution was evaluated using the Kolmogorov-Smirnov test. Normally distributed numerical variables are shown as mean ± standard deviation, while numerical variables not showing normal distribution are shown as median (minimum, maximum). Categorical variables are expressed as numbers and percentages. Chi-square and Fisher's exact chi-square tests were used for comparison of categorical data. Student's t-test was used to compare numerical variables showing normal distribution between the two groups. For comparing the postoperative and preoperative period, a repeated mixed model analysis was used. In statistical analysis, a $p < 0.05$ (*) is considered significant.

RESULTS

Between 2017 and 2019, 49 patients, comprising 26 women (53.1%) and 23 men (46.9%), with a diagnosis of spinal

intradural tumor and operated using a yellow filter in the presence of Na-fluorescein, were included in the study. The age range of the patients was 18–64 years, with a mean age of 41.6 ± 13.9. An intradural intramedullary mass was found in 30.6% (n: 15) of patients, and intradural extramedullary mass in 69.4% (n = 34). According to anatomical tumor localizations, 36.7% (n = 18) were found to be cervical, 36.7% (n = 18) thoracic, and 26.6% (n: 13) lumbar. The preoperative McCormick scale was 1.5 ± 0.5 (min: 1; max: 3) and mostly 1.

Age and gender distribution did not differ between patients with intradural intramedullary and intradural extramedullary masses. While Na-fluorescein fluorescence was dense homogeneous in all intradural extramedullary tumors, 73.3% (n: 11) of intradural intramedullary tumors were dense homogeneous, and 13.3% (n: 2) were moderately heterogeneous. All masses with intradural extramedullary location were removed by gross total resection.

Subtotal resection was performed in 20% (n: 3) of intradural intramedullary masses, whereas gross total resection was performed in the others (**Table 1**). In the whole study group, the Na-fluorescein staining pattern was found helpful for surgical resection in 47 cases (95.9%). While in 34/34 (100%) cases it was helpful for all extramedullary tumors, 13/15 (86.7%) were helpful in intramedullary tumors and 2/15 (13.3%) were not helpful at all. In tumors with contrast enhancement on preoperative MRI, Na-fluorescein staining was also observed.

Localization and histopathological distributions in patients with intradural intramedullary and intradural extramedullary masses are shown in **Table 2**. Localization did not significantly differ between groups. Further, there was no allergic hypersensitivity reaction or any complication due to the use of Na-fluorescein.

Preoperative and postoperative McCormick scale scores were significantly higher in the intradural intramedullary group than in the intradural extramedullary group (**Table 3**). The postoperative McCormick scale was significantly increased in all patients compared to the preoperative period (1.5 ± 0.5 vs. 1.8 ± 0.6; p = 0.001). The proportion of patients with preoperative McCormick scale 1 decreased from 67.3 to 55.1% postoperatively, that of patients with McCormick scale 2 increased from 26.5 to 30.6%, as did that with McCormick scale 3 from 6.1 to 12.2% (**Table 4**). While the McCormick scale increased significantly in the postoperative period in the intradural intramedullary group compared to the preoperative period, there was no significant difference in the McCormick scale in the intradural extramedullary group (**Table 4**) (**Figure 1**).

DISCUSSION

This study was conducted to investigate the viability of Na-fluorescein under a yellow filter in intradural spinal tumor surgery. The clinical process was evaluated by examining the tumor staining pattern in tumors with various histopathologies. Na-fluorescein has been used in ophthalmological angiography since 1961 (24). Known as a reliable agent, Na-fluorescein has been used under the YELLOW 560 filter in many pediatric and adult cranial neurooncological pathologies (15, 25–29).

In the literature, there are many studies examining spinal cord intradural tumors with 5-aminolevulinic acid (5-ALA) (30–33), but few on Na-fluorescein. In a comprehensive 5-ALA study, 5-ALA was positive in spinal intramedullary gliomas and the vast majority of intradural meningiomas, and proven to be a useful technique, especially in intramedullary gliomas (33). In the study by Millesi et al., a clinical series including 55 cases was published and 5-ALA evaluated as beneficial in intramedullary tumors (22).

TABLE 1 | Demographic and clinical features.

Variables	Total n = 49	Intramedullary n = 15	Extramedullary n = 34	p
Gender, n(%)				
Female	26(53.1)	8(53.3)	18(52.9)	0.999
Male	23(46.9)	7(46.7)	16(47.1)	
Age, years	41.6 ± 13.9	39.4 ± 13.9	41.1 ± 14.5	0.700
Na-Fl fluorescence, n(%)				
Dense homogeneous (meningioma, schwannoma, ependymoma, non-small cell lung cancer, hemangiopericytoma, ganglioneuroma)	45(91.8)	11(73.3)	34(100.0)	0.006*
Moderate heterogeneous (oligodendroglioma, pilocytic astrocytoma)	2(4.1)	2(13.3)	–	
None (dermoid and epidermoid tumors)	2(4.1)	2(13.3)	–	
Helpful, n(%)				
Helpful	47(95.9)	13(86.7)	34(100.0)	0.164
Not helpful	2(4.1)	2(13.3)	–	
Extent of resection, n(%)				
GTR	46(93.9)	12(80)	34(100.0)	0.164
STR	3(6.1)	3(20)	–	

Numerical variables were expressed as mean ± standard deviation.
Categorical variables were expressed as numbers and percentages.
**p < 0.05 shows statistical significance.*

TABLE 2 | Localization and Histopathological distribution.

Variables	Total n = 49	Intramedullary n = 15	Extramedullary n = 34	p
Localization, n(%)				
Cervical	18(36,7)	8(53,3)	10(29,4)	0,333
Thoracic	18(36,7)	4(26,7)	14(41,2)	
Lumbar	13(26,6)	3(20,0)	10(29,4)	
Histopathology				
Dermoid tm	1(2,0)	1(6,7)	–	< 0,001*
Ependymoma WHO grade 2	10(20,4)	10(66,7)	–	
Epidermoid	1(2,0)	1(6,7)	–	
Ganglioneuroma	1(2,0)	–	1(2,9)	
Meningioma psammomatous grade 1	2(4,0)	–	2(5,8)	
Meningioma transitional grade 1	5(10,2)	–	5(14,8)	
Meningioma meningothelial grade 1	5(10,2)	–	5(14,8)	
Metastasis	1(2,0)	1(6,7)	–	
Mesenchymal non-meningothelial tumor, Hemangiopericytoma WHO grade 1	1(2,0)	–	1(2,9)	
Myxopapillary ependymoma grade 1	1(2,0)	–	1(2,9)	
Oligodendroglioma	1(2,0)	1(6,7)	–	
Pilocytic astrocytoma WHO grade 1	1(2,0)	1(6,7)	–	
Schwannoma	19(38,8)	–	19(55,9)	

Categorical variables were expressed as numbers and percentages.
**p < 0.05 shows statistical significance.*

TABLE 3 | McCormick scale distributions.

McCormick scale	Total n = 49	Intramedullary n = 15	Extramedullary n = 34	p
Preoperative	1,5 ± 0,5	2,0 ± 0,7	1,1 ± 0,3	<0,001*
1	33(67,3)	3(20,0)	30(88,2)	<0,001*
2	13(26,5)	9(60,0)	4(11,8)	
3	3(6,1)	3(20,0)	–	
Postoperative	1,8 ± 0,6	2,5 ± 0,6	1,2 ± 0,4	<0,001*
1	27(55,1)	–	27(79,4)	<0,001*
2	15(30,6)	8(53,3)	7(20,6)	
3	6(12,2)	6(40,0)	–	
4	1(2,0)	1(6,7)	–	

Numerical variables were expressed as mean ± standard deviation.
Categorical variables were expressed as numbers and percentages.
**p < 0.05 shows statistical significance.*

TABLE 4 | Changes in McCormick scale measurements following the treatment.

Group	McCormick scale	Preoperative	Postoperative	p	p_d
Total population	Scale	1,5 ± 0,5	1,8 ± 0,6	0,001*	
	1, n(%)	33(67,3)	27(55,1)	0,001*	–
	2, n(%)	13(26,5)	15(30,6)		
	3, n(%)	3(6,1)	6(12,2)		
	4, n(%)	–	1(2,0)		
Intra	Scale	2,0 ± 0,7	2,5 ± 0,6	0,001*	< 0,001*
medullary	1, n(%)	3(20,0)	–	0,005*	
	2, n(%)	9(60,0)	8(53,3)		
	3, n(%)	3(20,0)	6(40,0)		
	4, n(%)	–	1(6,7)		
Extra	Scale	1,1 ± 0,3	1,2 ± 0,4	0,105	
medullary	1, n(%)	30(88,2)	27(79,4)	0,083	
	2, n(%)	4(11,8)	7(20,6)		
	3, n(%)	–	–		
	4, n(%)	–	–		

Numerical variables were expressed as mean ± standard deviation.
Categorical variables were expressed as numbers and percentages.
**p < 0.05 shows statistical significance.*
pd: Difference between groups of McCormick scale changes after treatment.

In our study, staining accompanied by Na-fluorescein was detected in all extramedullary tumors (34/34) and different degrees of staining in the majority of intramedullary tumors (13/15), and it was found that it helped surgery in 47 of 49 cases.

According to our data, homogeneous Na-fluorescein involvement was detected in all extramedullary tumors (19 schwannomas, 12 meningiomas WHO grade 1, hemangiopericytoma WHO grade 1, ganglioneuroma and myxopapillary epandymoma WHO grade 1). In a prospective study in which Falco et al. evaluated cranial and spinal tumors in the presence of Na-fluorescein, it was reported that two cases of lumbar schwannoma were well stained (20). However, the authors thought that the use of Na-fluorescein in neurinomas was not necessary in surgical treatment because they were easily recognizable tumors, even if stained with Na-fluorescein in homogeneous intensity, and they failed to distinguish non-tumor nerve fibers. In our study, 19 Schwannomas WHO grade 1 were evaluated and, unlike the above view, an effective tumor-non-tumor nerve and fiber distinction could be made in every one of them (**Figures 1**, **2**). The reason for this divergence between the two studies may be that the Schwann cells which conform the tumor form different tumor subtypes. Generally referred to as Schwannoma WHO grade 1, these tumors have many histopathological subtypes (cellular, melanotic, neurofibroma/schwannoma hybrid tumors) (34). Another reason may be the difference in enhancement patterns on

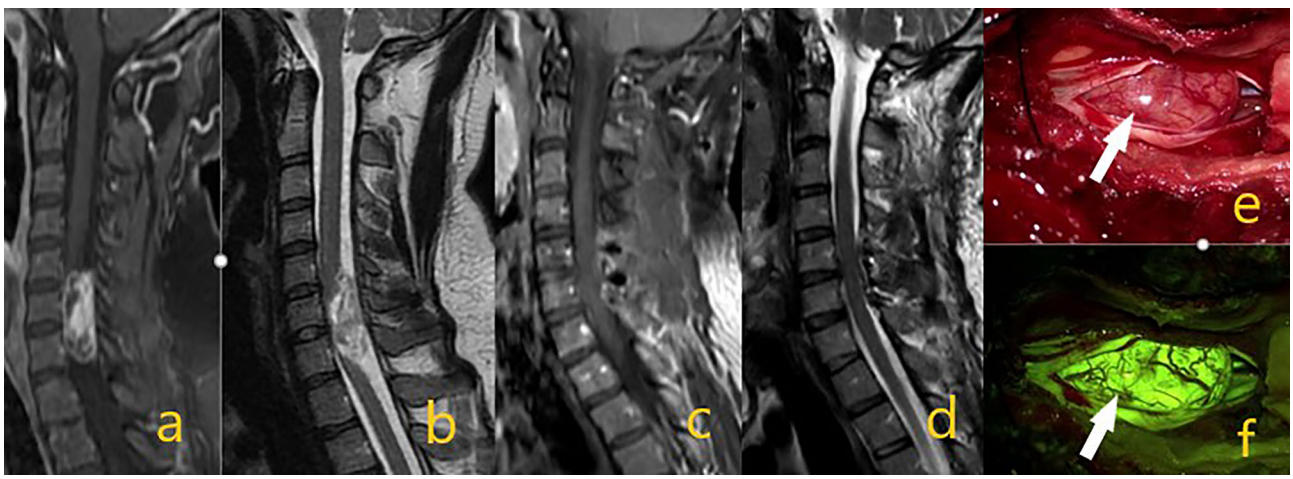

FIGURE 1 | Schwannoma at the C6-7 level in preoperative contrast-enhanced T1 and T2 sequences on images **(A, B)**. On postoperative **(C, D)** images, the mass was totally removed. In intraoperative microscope image **(E)** white arrow shows the mass, while image **(F)** shows tumor homogeneous staining pattern with activated yellow filter.

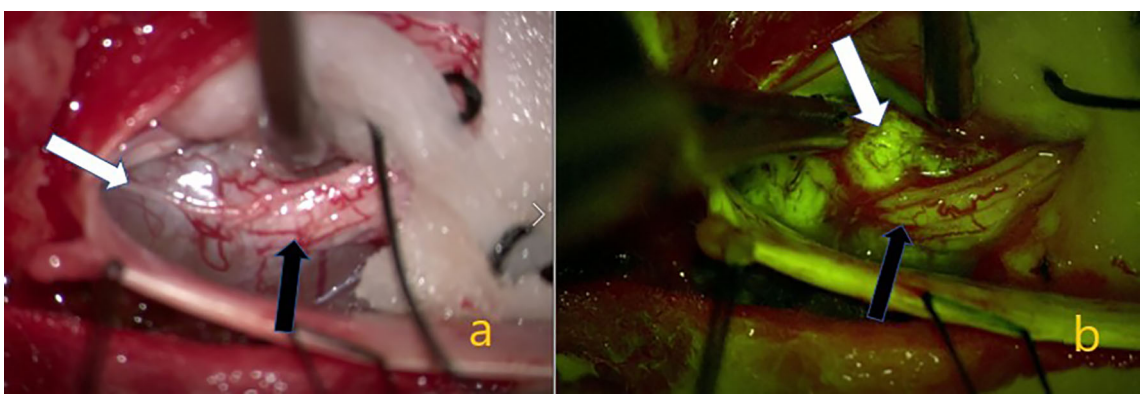

FIGURE 2 | Schwannom located in the lumbar 5. **(A)** White arrow showing the tumor on the intraoperative microscope image. Black arrow indicating the nerve root from which the tumor originated. In **(B)** the yellow filter is activated, the white arrow indicating homogeneous staining of the tumor tissue, and the black arrow indicating weaker staining of the nerve root.

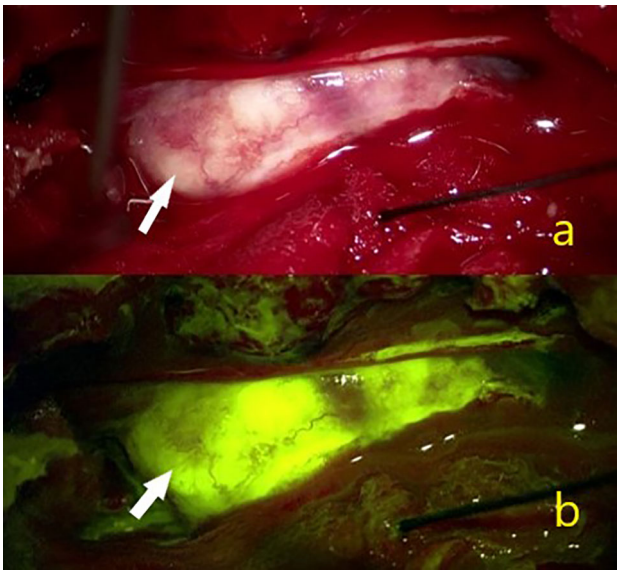

FIGURE 3 | In a 42-year-old female patient **(A)** White arrow showing the intraoperative view of a T11 localized psammomatous meningioma. **(B)** White arrow indicating intense homogeneous Na-fl uptake.

preoperative MRI. Spinal schwannomas have been reported to show different types of enhancement patterns (35, 36). Previous studies have reported that preoperative contrast enhancement is due to disruption of the blood brain barrier and contrast enhancement is correlated with Na-fluorescein involvement (27, 37, 38). Considering the above, we think that the use of Na-fluorescein in spinal Schwannomas is beneficial for tumor resection. In the future, we aim to gather more information on this subject. In our study, in which 12 WHO grade 1 meningiomas were evaluated, there were psammomatous, transitional, and meningothelial subtypes. In all of them, intense homogeneous staining and effective tumor-normal tissue separation were detected (**Figure 3**). All meningiomas were grossly excised. Simpson's classification was used for resection classification of meningiomas, and a Simpson 2 resection was performed for all 12 meningiomas. In the literature, we did not find a single study using a yellow filter in the presence of Na-fluorescein in spinal meningiomas. However, it is known that Na-fluorescein has an intense staining pattern and there are high GTR rates in cranial meningiomas (20, 25). In their study, in which 30 patients were evaluated, Akçakaya et al. reported that surgery under YELLOW-560 filter, accompanied by Na-fluorescein, has an increasing effect on safety and extent of resection. In this context, we think that Na-fluorescein is useful both in preventing vascular injuries and distinguishing between tumor and healthy tissue in meningiomas with dense vascularity.

Gross total resection was performed for all extramedullary tumors (34/34). Except for schwannomas and meningiomas, myxopapillary ependymoma grade 1, hemangiopericytoma,

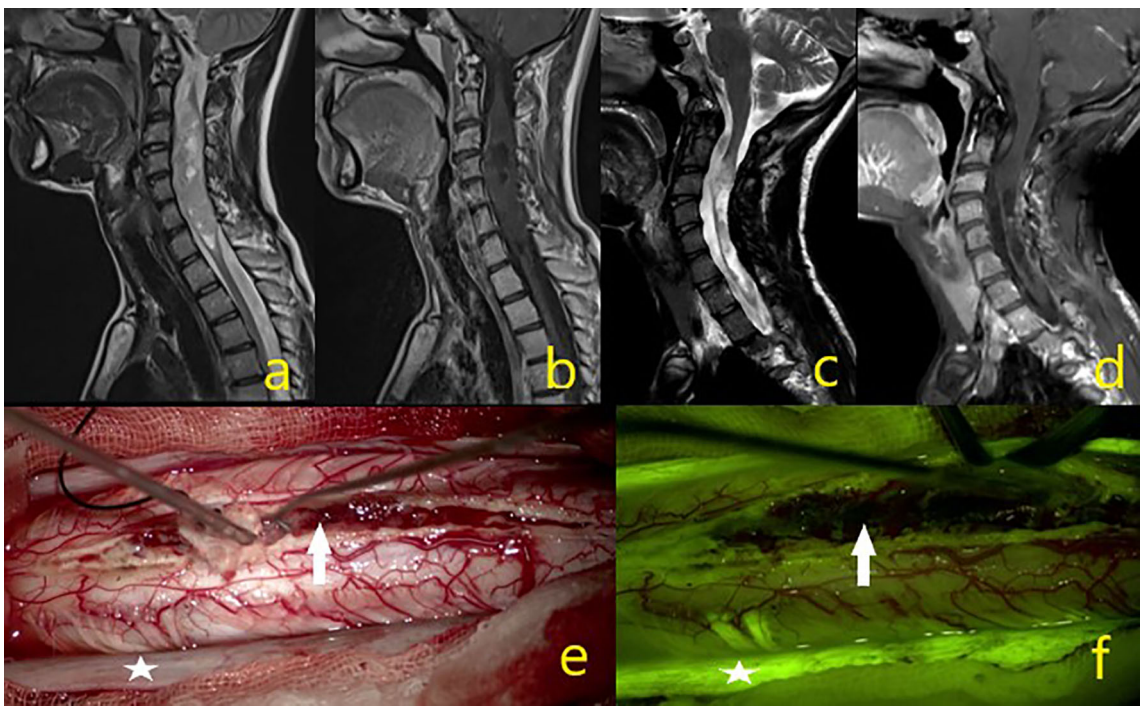

FIGURE 4 | A 23-year-old male patient operated for oligodendroglioma WHO grade 2, but where subtotal excision could not be achieved due to intraoperative IONM signal loss. **(A–D)** Tumor MR sequence images. **(E)** In the intraoperative microscope image, the asterisk is the dura and the white arrow indicates the mass. **(F)** Under the yellow filter, the asterisk shows the dura staining pattern, and the white arrow a moderate heterogeneous stained mass image.

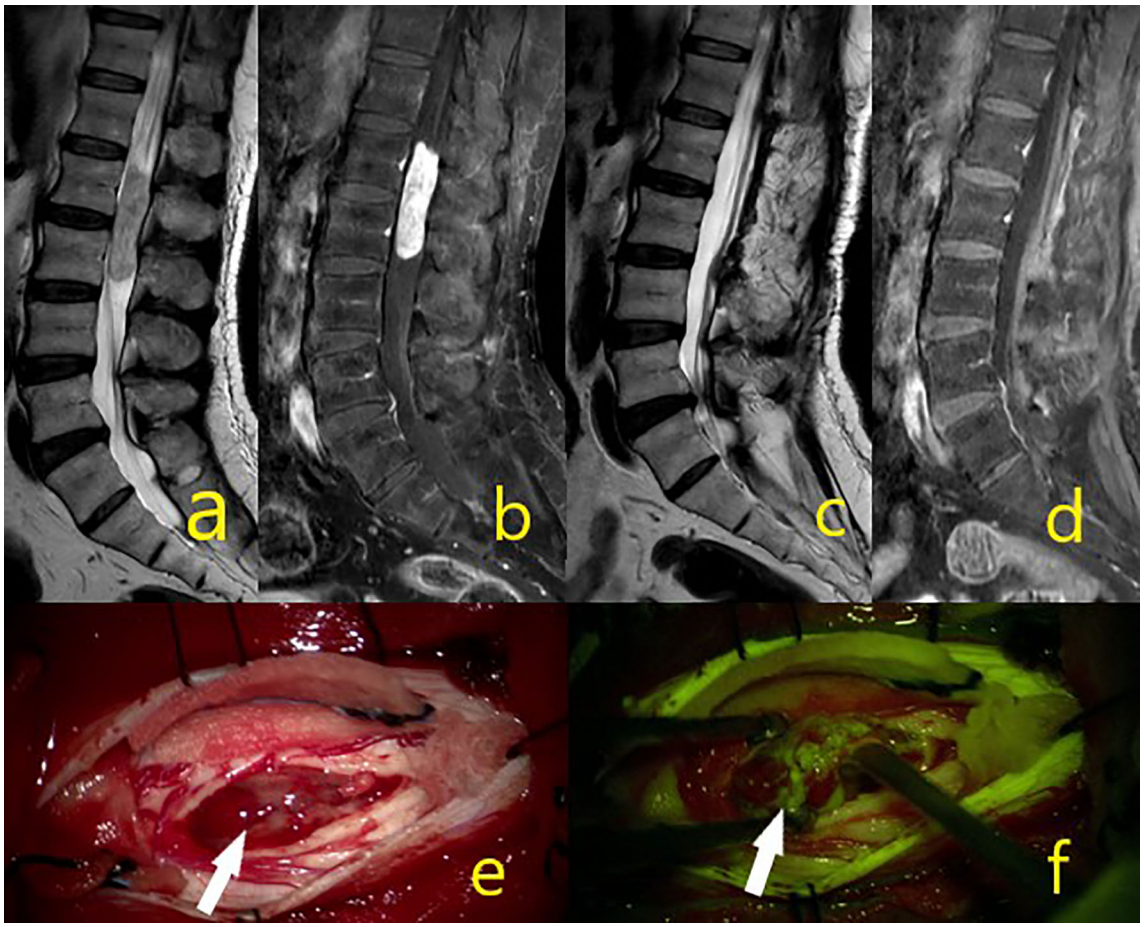

FIGURE 5 | A 44-year-old male patient was operated from epandymoma WHO grade 2 and gross total excision achieved. **(A–D)** Tumor MR sequence images. **(E)** White arrow showing the mass in the intraoperative microscope image**. (F)** White arrow under yellow filter showing the dense homogenous stained mass image.

and ganglioneuroma WHO grade 1 are rare tumors. In our study, these tumors had an intense homogeneous enhancement pattern on preoperative MRI. Under the yellow filter microscope image, an intense Na-fluorescein uptake was detected and the distinction between tumor and spinal cord tissue could be easily reached.

In intramedullary tumors, Na-fluorescein involvement was not detected in two patients (dermoid and epidermoid tumors). Moderate heterogeneous staining was detected in two patients (oligodendroglioma WHO grade 2 and pilocytic astrocytoma WHO grade 1), and the remaining 11 intramedullary tumors (10 ependymomas WHO grade 2, 1 non-small cell lung cancer) were detected with dense homogeneous staining, and the tumor demarcation line found. Among the intramedullary tumors, in a patient with oligodendroglioma WHO grade 2, although the tumor demarcation line was followed, surgery was terminated early due to signal loss in intraoperative neuro-monitorization and subtotal resection performed (**Figure 4**). In two patients diagnosed with ependymoma WHO grade 2, the surgery was terminated by performing subtotal resection due to early motor-evoked potential signal loss, but GTR was provided in all other intramedullary ependymomas. Studies have reported that ependymomas are well stained with 5-ALA and Na-fluorescein, which is useful in determining the tumor cleavage plan by distinguishing the tumor from healthy spinal tissue cord (19, 22, 30). Acerbi et al. presented their first experience of intramedullary tumor surgery under the YELLOW 560 filter with Na-fluorescein (19), wherein a total of 11 patients with various histopathologies were evaluated, all ependymomas (5/5) were homogeneously stained bright and subjected to gross total resection. In our study, 10 ependymomas were intensely stained in WHO grade 2 and GTR applied to eight of them (8/10) (80%) (**Figure 5**). STR had to be applied in two cases due to early signal loss in neuro-monitorization. Klekamp et al., presenting a huge series of 100 patients in intramedullary ependymoma surgery, stated that GTR ratio was 86.3% (23). The GTR rate was reported lower, namely, as 69 and 80% in two other important series (39, 40). The reason for not achieving GTR could be the absence of a tumor cleavage plan in ependymomas, loss of neurophysiological signal during surgery, and overlooking residual tumor tissue

under white light (22, 30). In this study, the staining pattern and GTR rate obtained in ependymomas are satisfactory considering the above, thus, we consider Na-fluorescein useful in the surgical treatment of ependymomas with a yellow filter.

This study has some limitations. Performing a volumetric analysis, especially when reporting extent of resection results, could have yielded more objective results in terms of comparing preoperative and postoperative values. However, the high GTR rate in the study partly compensates for this disadvantage. Furthermore, the retrospective design and the limited number of cases in some of the anatomopathological diagnoses is a disadvantage. The strength of our study is that it is the first to report the results of surgical procedures using a yellow filter microscope to detect Na-fluorescein in a large case series consisting of 49 patients with spinal cord tumors.

In conclusion, an Na-fluorescein staining pattern under the yellow 560 filter in parallel with preoperative MR enhancement could be observed in both extramedullary and intramedullary spinal cord tumors. During surgery of both extramedullary and intramedullary tumors, it facilitates the distinction between intraoperative tumors and healthy tissue. Given the scarcity of research on this topic and its safety, its use in intradural spinal cord tumors will shed light on future studies.

DATA AVAILABILITY STATEMENT

The original contributions presented in the study are included in the article/supplementary materials. Further inquiries can be directed to the corresponding author.

ETHICS STATEMENT

The studies involving human participants were reviewed and approved by Ethics Committee of Adana City Training and Research Hospital. The patients/participants provided their written informed consent to participate in this study.

AUTHOR CONTRIBUTIONS

YG and AÖ constructed the hypothesis. SO, AA, VA, and İİ made data collection and took responsibility in data management and reporting analysis. SO, AA, VA, İİ, and MC made literature review and wrote manuscript. YG and AÖ critically reviewed the article intellectually. All authors contributed to the article and approved the submitted version.

REFERENCES

1. Haciyakupoglu E, Yuvruk E, Onen MR, Naderi S. The use of intraoperative ultrasonography in intradural spinal tumor surgery. *Turk Neurosurg* (2019) 29(2):237–41. doi: 10.5137/1019-5149.JTN.23296-18.3
2. Maiuri F, Iaconetta G, Gallicchio B, Stella L. Intraoperative Sonography for Spinal Tumors. Correlations With MR Findings and Surgery. *J Neurosurg Sci* (2000) 44(3).
3. Maiuri F, Iaconetta G, De Divitiis O. The role of intraoperative sonography in reducing invasiveness during surgery for spinal tumors. *Minim Invasive Neurosurg* (1997) 40(1):8–12. doi: 10.1055/s-2008-1053405
4. Granata F, Racchiusa S, Mormina E, Barres V, Garufi G, Grasso G, et al. Presurgical role of MRI tractography in a case of extensive cervicothoracic spinal ependymoma. *Surg Neurol Int* (2017) 8(1):56. doi: 10.4103/sni.sni_33_17
5. Setzer M, Murtagh RD, Murtagh FR, Eleraky M, Jain S, Marquardt G, et al. Diffusion tensor imaging tractography in patients with intramedullary tumors: Comparison with intraoperative findings and value for prediction of tumor resectability: Presented at the 2009 Joint Spine Section Meeting. *J Neurosurg Spine* (2010) 13(3):371–80. doi: 10.3171/2010.3.SPINE09399
6. Zhao M, Shi B, Chen T, Zhang Y, Geng T, Qiao L, et al. Axial MR diffusion tensor imaging and tractography in clinical diagnosed and pathology confirmed cervical spinal cord astrocytoma. *J Neurol Sci* (2017) 375:43–51. doi: 10.1016/j.jns.2017.01.044
7. Ghadirpour R, Nasi D, Iaccarino C, Romano A, Motti L, Sabadini R, et al. Intraoperative neurophysiological monitoring for intradural extramedullary spinal tumors: Predictive value and relevance of D-wave amplitude on surgical outcome during a 10-year experience. *J Neurosurg Spine* (2019) 30 (2):259–67. doi: 10.3171/2018.7.SPINE18278
8. Scibilia A, Terranova C, Rizzo V, Raffa G, Morelli A, Esposito F, et al. Intraoperative neurophysiological mapping and monitoring in spinal tumor surgery: Sirens or indispensable tools? *Neurosurg Focus* (2016) 41(2):2. doi: 10.3171/2016.5.FOCUS16141
9. Rijs K, Klimek M, Scheltens-de Boer M, Biesheuvel K, Harhangi BS. Intraoperative Neuromonitoring in Patients with Intramedullary Spinal Cord Tumor: A Systematic Review, Meta-Analysis, and Case Series. *World Neurosurg* (2019) 125:498–510.e2. doi: 10.1016/j.wneu.2019.01.007
10. Azad TD, Pendharkar AV, Nguyen V, Pan J, Connolly ID, Veeravagu A, et al. Diagnostic Utility of Intraoperative Neurophysiological Monitoring for Intramedullary Spinal Cord Tumors: Systematic Review and Meta-Analysis. *Clin Spine Surg* (2018) 31(3):112–9. doi: 10.1097/BSD.0000000000000558
11. Shinoda J, Yano H, Yoshimura S-I, Okumura A, Kaku Y, Iwama T, et al. Fluorescence-guided resection of glioblastoma multiforme by using high-dose fluorescein sodium. Technical note. *J Neurosurg* (2003) 99(3):597–603. doi: 10.3171/jns.2003.99.3.0597
12. Koc K, Anik I, Cabuk B, Ceylan S. Fluorescein sodium-guided surgery in glioblastoma multiforme: a prospective evaluation. *Br J Neurosurg* (2008) 22 (1):99–103. doi: 10.1080/02688690701765524
13. Fan C, Jiang Y, Liu R, Wu G, Wu G, Xu K, et al. Safety and feasibility of low-dose fluorescein-guided resection of glioblastoma. *Clin Neurol Neurosurg* (2018) 175:57–60. doi: 10.1016/j.clineuro.2018.10.011
14. Schebesch KM, Hoehne J, Hohenberger C, Proescholdt M, Riemenschneider MJ, Wendl C, et al. Fluorescein sodium-guided resection of cerebral metastases—experience with the first 30 patients. *Acta Neurochir (Wien)* (2015) 157(6):899–904. doi: 10.1007/s00701-015-2395-7
15. Schebesch KM, Proescholdt M, Höhne J, Hohenberger C, Hansen E, Riemenschneider MJ, et al. Sodium fluorescein-guided resection under the YELLOW 560 nm surgical microscope filter in malignant brain tumor surgery - A feasibility study. *Acta Neurochir (Wien)* (2013) 155(4):693–9. doi: 10.1007/s00701-013-1643-y
16. Schebesch KM, Brawanski A, Hohenberger C, Höhne J. Fluorescein sodium-guided surgery of malignant brain tumors: History, current concepts, and future projects. *Turk Neurosurg* (2016) 26(2):185–94. doi: 10.5137/1019-5149.JTN.16952-16.0
17. Garcés-Ambrossi GL, McGirt MJ, Mehta VA, Sciubba DM, Witham TF, Bydon A, et al. Factors associated with progression-free survival and long-term neurological outcome after resection of intramedullary spinal cord tumors: Analysis of 101 consecutive cases - Clinical article. *J Neurosurg Spine* (2009) 11(5):591–9. doi: 10.3171/2009.4.SPINE08159
18. Fehlings MG, Mercier DD. Factors predicting the resectability of intramedullary spinal cord tumors and the progression-free survival following microsurgical treatment. *J Neurosurg Spine* (2009) 11(5):588–9. doi: 10.3171/2009.6.SPINE09360
19. Acerbi F, Cavallo C, Schebesch KM, Akçakaya MO, de Laurentis C, Hamamcioglu MK, et al. Fluorescein-Guided Resection of Intramedullary

Spinal Cord Tumors: Results from a Preliminary, Multicentric, Retrospective Study. *World Neurosurg* (2017) 108:603–9. doi: 10.1016/j.wneu.2017.09.061
20. Falco J, Cavallo C, Vetrano IG, de Laurentis C, Siozos L, Schiariti M, et al. Fluorescein Application in Cranial and Spinal Tumors Enhancing at Preoperative MRI and Operated With a Dedicated Filter on the Surgical Microscope: Preliminary Results in 279 Patients Enrolled in the FLUOCERTUM Prospective Study. *Front Surg* (2019) 6:49. doi: 10.3389/fsurg.2019.00049
21. McCormick PC, Torres R, Post KD, Stein BM. Intramedullary ependymoma of the spinal cord. *J Neurosurg* (1990) 72(4):523–32. doi: 10.3171/jns.1990.72.4.0523
22. Millesi M, Kiesel B, Woehrer A, Hainfellner JA, Novak K, Martínez-Moreno M, et al. Analysis of 5-aminolevulinic acid-induced fluorescence in 55 different spinal tumors. *Neurosurg Focus* (2014) 36(2):E11. doi: 10.3171/2013.12.FOCUS13485
23. Klekamp J. Spinal ependymomas. Part 1: Intramedullary ependymomas. *Neurosurg Focus* (2015) 39(2):E6. doi: 10.3171/2015.5.FOCUS15161
24. Hara T, Inami M, Hara T. Efficacy and safety of fluorescein angiography with orally administered sodium fluorescein. *Am J Ophthalmol* (1998) 126(4):560–4. doi: 10.1016/S0002-9394(98)00112-3
25. Akçakaya MO, Göker B, Kasımcan MÖ, Hamamcıoğlu MK, Kırış T. Use of Sodium Fluorescein in Meningioma Surgery Performed Under the YELLOW-560 nm Surgical Microscope Filter: Feasibility and Preliminary Results. *World Neurosurg* (2017) 107:966–73. doi: 10.1016/j.wneu.2017.07.103
26. Hamamcıoğlu MK, Akçakaya MO, Göker B, Kasimcan MÖ, Kiriş T. The use of the YELLOW 560 nm surgical microscope filter for sodium fluorescein-guided resection of brain tumors: Our preliminary results in a series of 28 patients. *Clin Neurol Neurosurg* (2016) 143:39–45. doi: 10.1016/j.clineuro.2016.02.006
27. Göker B, Kırış T. Sodium fluorescein–guided brain tumor surgery under the YELLOW-560-nm surgical microscope filter in pediatric age group: feasibility and preliminary results. *Child's Nerv Syst* (2019) 35(3):429–35. doi: 10.1007/s00381-018-04037-4
28. Acerbi F, Cavallo C, Broggi M, Cordella R, Anghileri E, Eoli M, et al. Fluorescein-guided surgery for malignant gliomas: a review. *Neurosurg Rev* (2014) 37(4):547–57. doi: 10.1007/s10143-014-0546-6
29. Minkin K, Naydenov E, Gabrovski K, Dimova P, Penkov M, Tanova R, et al. Intraoperative fluorescein staining for benign brain tumors. *Clin Neurol Neurosurg* (2016) 149:22–6. doi: 10.1016/j.clineuro.2016.07.016
30. Wainwright JV, Endo T, Cooper JB, Tominaga T, Schmidt MH. The role of 5-aminolevulinic acid in spinal tumor surgery: a review. *J Neurooncol* (2019) 141(3):575–84. doi: 10.1007/s11060-018-03080-0
31. Krause Molle Z, Gierga K, Turowski B, Steiger H-J, Cornelius JF, Rapp M, et al. 5-ALA-Induced Fluorescence in Leptomeningeal Dissemination of Spinal Malignant Glioma. *World Neurosurg* (2018) 110:345–8. doi: 10.1016/j.wneu.2017.10.069
32. Kamp MA, Krause Molle Z, Munoz-Bendix C, Rapp M, Sabel M, Steiger HJ, et al. Various shades of red—a systematic analysis of qualitative estimation of ALA-derived fluorescence in neurosurgery. *Neurosurg Rev* (2018) 41(1):3–18. doi: 10.1007/s10143-016-0745-4
33. Eicker SO, Floeth FW, Kamp M, Steiger HJ, Hänggi D. The impact of fluorescence guidance on spinal intradural tumour surgery. *Eur Spine J* (2013) 22(6):1394–401. doi: 10.1007/s00586-013-2657-0
34. Röhrich M, Koelsche C, Schrimpf D, Capper D, Sahm F, Kratz A, et al. Methylation-based classification of benign and malignant peripheral nerve sheath tumors. *Acta Neuropathol* (2016) 131(6):877–87. doi: 10.1007/s00401-016-1540-6
35. Kobayashi K, Imagama S, Ando K, Hida T, Ito K, Tsushima M, et al. Contrast MRI findings for spinal schwannoma as predictors of tumor proliferation and motor status. *Spine (Phila Pa 1976)* (2017) 42(3):E150–5. doi: 10.1097/BRS.0000000000001732
36. Ando K, Imagama S, Ito Z, Kobayashi K, Yagi H, Hida T, et al. How do spinal schwannomas progress? The natural progression of spinal schwannomas on MRI. *J Neurosurg Spine* (2016) 24(1):155–9. doi: 10.3171/2015.3.SPINE141218
37. Acerbi F, Broggi M, Schebesch K-M, Höhne J, Cavallo C, De Laurentis C, et al. Fluorescein-Guided Surgery for Resection of High-Grade Gliomas: A Multicentric Prospective Phase II Study (FLUOGLIO). *Clin Cancer Res* (2018) 24(1):52–61. doi: 10.1158/1078-0432.CCR-17-1184
38. Höhne J, Hohenberger C, Proescholdt M, Riemenschneider MJ, Wendl C, Brawanski A, et al. Fluorescein sodium-guided resection of cerebral metastases-an update. *Acta Neurochir (Wien)* (2017) 159(2):363–7. doi: 10.1007/s00701-016-3054-3
39. Hongo H, Takai K, Komori T, Taniguchi M. Intramedullary spinal cord ependymoma and astrocytoma: Intraoperative frozen-section diagnosis, extent of resection, and outcomes. *J Neurosurg Spine* (2019) 30(1):133–9. doi: 10.3171/2018.7.SPINE18230
40. Wostrack M, Ringel F, Eicker SO, Jägersberg M, Schaller K, Kerschbaumer J, et al. Spinal ependymoma in adults: A multicenter investigation of surgical outcome and progression-free survival. *J Neurosurg Spine* (2018) 28(6):654–62. doi: 10.3171/2017.9.SPINE17494

Conflict of Interest: The authors declare that the research was conducted in the absence of any commercial or financial relationships that could be construed as a potential conflict of interest.

frontiers in Oncology

ORIGINAL RESEARCH
published: 09 March 2021
doi: 10.3389/fonc.2021.655392

Intraoperative Sodium-Fluorescence Imaging in Peripheral Nerve Sheath Tumors (PNST)—A New Additional Promising Diagnostic Tool

Maria Teresa Pedro, Nadja Grübel, Gregor Durner, Andrej Pala, Christian Rainer Wirtz and Ralph Werner Koenig*

Klinik für Neurochirurgie, Medizinische Fakultät, Universität Ulm, Ulm, Germany

Background: Through the development and implementation of specific fluorophore filters to microscopes in 2012, sodium fluorescein (SF) is currently experiencing a remarkable renaissance in neurosurgery. The present study examines its intraoperative application during surgical removal of peripheral nerve sheath tumors (PNST) and metastases.

Methods: This single-center study includes 10 cases of benign and malignant tumors as well as metastases of peripheral nerves (in total 11 PNST). Their surgical resections were all performed under microscope-based fluorescence with SF, which was administered intravenously (0.5–1.0 mg/kg body weight) during anesthesia induction. Microsurgical tumor removals were filmed and the collected data were retrospectively analyzed via ImageJ.

Results: Microsurgical tumor preparation was possible under the usage of fluorophore filter. In seven histological confirmed schwannoma ($n = 6$ patients) tissue differentiation between tumor mass and not involved fascicles was statistically significant for the colors green and red. Schwannoma maximum mean for green reached 254.7 pixel and 179.4 pixel for red, whereas passing healthy fascicles revealed a maximum mean for green 94.91 and for red 120.76 pixel. One case of neurofibroma achieved lower amount of pixel. Similar to schwannoma, the two MPNST cases showed a strong homogeneous fluorescence (max. mean green 215 pixel and red 124.51) involving the whole nerve segment. Subcutaneous tumor remnants were visualized and therefore resected. Via fascicular nerve biopsy a B-cell lymphoma of the tibial nerve could be detected. SF led to variable stain intensities in single fascicles. The resected fascicle revealed a max mean green of 100.54 pixel, whereas surrounding fascicles came up with max. mean green of 63.0 pixel.

Conclusions: Intraoperative SF visualization for PNST is feasible and of low risk. During resection of benign PNST, enhanced tissue differentiation between affected and not affected nerve segments is very useful. Tumor remnants can be detected safely and effectively. Its application during resection of malignant PNST is limited. Due to the infiltrative nature of those tumors, intraneural tissue differentiation is not possible.

OPEN ACCESS

Edited by:
Karl-Michael Schebesch, University of Regensburg, Germany

Reviewed by:
Jacopo Falco, Fondazione IRCCS Istituto Neurologio Carlo Besta, Italy
Mehmet Osman Akçakaya, Istanbul Florence Nightingale Hospital, Turkey

****Correspondence:***
Maria Teresa Pedro
maria-teresa.pedro@uni-ulm.de

Specialty section:
This article was submitted to Neuro-Oncology and Neurosurgical Oncology, a section of the journal Frontiers in Oncology

Received: *18 January 2021*
Accepted: *12 February 2021*
Published: *09 March 2021*

Citation:
Pedro MT, Grübel N, Durner G, Pala A, Wirtz CR and Koenig RW (2021) Intraoperative Sodium-Fluorescence Imaging in Peripheral Nerve Sheath Tumors (PNST)—A New Additional Promising Diagnostic Tool. Front. Oncol. 11:655392. doi: 10.3389/fonc.2021.655392

"Fluorescence-guided" biopsy can be regarded as an additional advantage in PNST surgery. Due to the encouraging experience in our institution SF was established as standard visualization tool in PNST surgery.

Keywords: schwannoma, neurofibroma, malignant peripheral nerve sheat tumor, lymphoma, biopsy, sodium-fluorescein

INTRODUCTION

Sodium-Fluorescein

Although an American neurosurgeon was the first one to describe the application of Sodium fluorescein (SF) in brain surgery in 1948 (1), this fluorphore medium fell into oblivion.

Only in 2003 and 2010 Shinoda and Okuda published their results in brain tumor surgeries under the usage of SF (2, 3). Their patients received intravenously a dosage of 20 mg/kg bodyweight which led to a distinct tumor mass fluorescence under white light.

However, since 2012 through the development and implementation of specific fluorophore filters to microscopes (e.g., YELLOW 560 nm filter; Zeiss Meditec, Oberkochen, Germany) its dosage has been significantly reduced to 2–5 mg/kg bodyweight. By this means, until today SF has experienced a tremendous renaissance in neurosurgery (4–8).

Peripheral Nerve Sheath Tumors

Since 2013 the WHO classification has no longer assigned peripheral nerve sheath tumors to tumors of the central nervous system, but to tumors of the soft tissues and bones (9). Schwannoma and neurofibroma each make up about 5% of the soft tissue tumors (10), both rare entities are considered as benign. Their surgical enucleation should not lead to neurological deterioration. But depending on location, size and tissue consistency its surgical preparation may be demanding.

Malignant peripheral nerve sheath tumors (MPNST) are aggressive infiltrative growing tumors leading to a remarkable quickly emerging neurological impairment and resting pain. Until now the only effective therapy is surgical resection with wide negative margins (11). While post-operative radiation is recommended, the efficacy of chemotherapy remains unclear (11, 12).

The present study examines our experience and benefits of intraoperative SF application during surgical removal of different peripheral nerve sheath tumors (PNST) and metastases.

METHODS

Study Group, Dosage, and Technical Equipment

This present single-center study includes 10 cases of benign and malignant tumors as well as metastases of peripheral nerves (in total 11 PNST). Patients over $\geq$ 18 years of age and with suspicion of PNST in MRI were included, whereas patients with history of renal insufficiency or SF intolerance were excluded. Their surgical PNST resections, respectively, biopsies were all performed by one surgeon under microscope-based fluorescence with SF (YELLWO 560 nm filter, Zeiss Meditec, Oberkochen, Germany) between August 2017 and September 2020 (**Table 1**). SF (Fluorescein Alcon 10%, Freiburg, Germany) was administered intravenously (0.5–1.0 mg/kg body weight) directly during anesthesia induction.

Since the application of SF is still restricted to ophthalmologic indications in Germany, the neurosurgical usage was off- label. Therefore, informed written consents were obtained from all patients emphasizing its intraoperative use. As individualized treatment, this study is in accordance with the ethical principles that are reflected in the Declaration of Helsinki.

Image Evaluation

Microsurgical preparation was filmed and the collected data were retrospectively analyzed via ImageJ, an open source Java image processing platform (Version 1.51, National Institutes of Health, Bethesda, Maryland, USA) (13). Therefore, regions of interest

TABLE 1 | Study group overview.

Patient	Age (years); Sex	Affected nerve	Histology	Resection (complete/biopsy)	Surgeon's opinion
1	24 yrs; female	Median nerve	Schwannoma	Complete	Helpful
2	45 yrs; female	Sural nerve	Schwannoma	Complete	Helpful
3	50 yrs; male	Tibial nerve	Schwannoma	Complete	Helpful
4	37 yrs; female	Median nerve	Schwannoma	Complete	Helpful
5	48 yrs; male	Peroneal nerve	2x schwannoma	Complete	Helpful
6	41 yrs; female	Peroneal nerve	Schwannoma	Complete	Helpful
7	45 yrs; male	Median nerve	Neurofibroma	Complete	Helpful
8 Illustrative case	77 yrs; female	Cutanaeus nerve paraspinal	MPNST	Complete	Very helpful
9 Illustrative case	55 yrs; male	Ulnar nerve	MPNST	Biopsy	Not helpful
10	71 yrs; male	Tibial nerve	B-cell lymphoma	Biopsy	Helpful

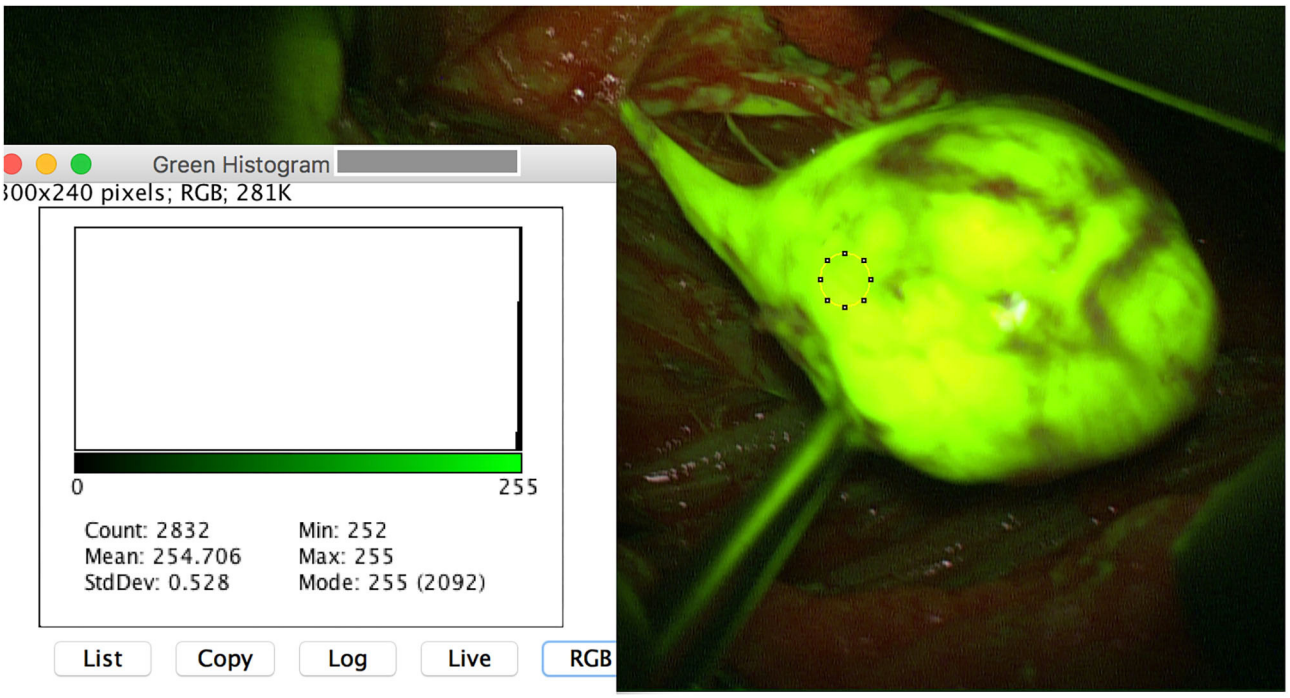

FIGURE 1 | Intraoperative image of a schwannoma of the left tibial nerve after opening of the epineurium. The region of interest (ROI) is set on the tumor mass. ImageJ reveals a $mean_{max}$ for the color green of 255 pixel with a standard deviation of 0.528. Note that the originating fascicle reveals a high yellowish stain.

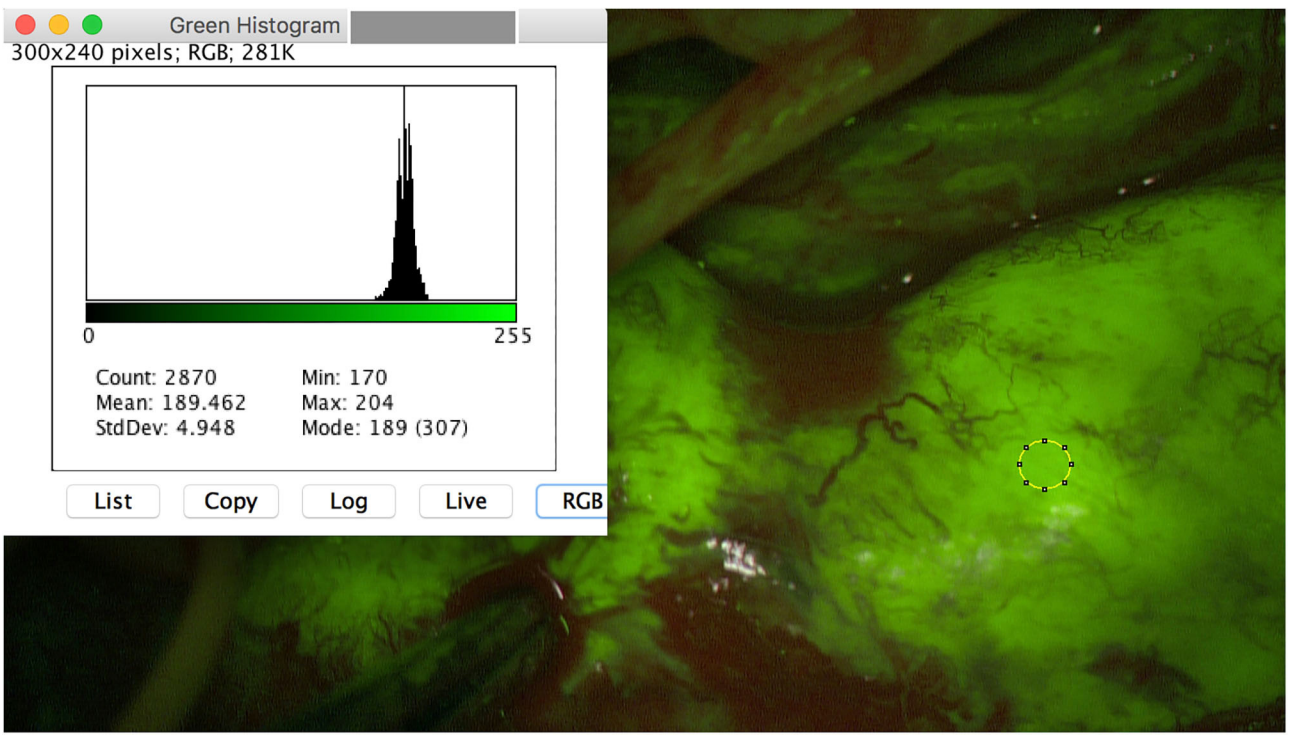

FIGURE 2 | Intraoperative image of a MPNST of the right ulnar arm. A homogeneous fluorescence is seen. $Mean_{max}$ for the color green is 204 pixel.

(ROI) were set on the tumor mass and on inconspicuous nerve segments. For each ROI the quantity of the complementary colors red and green were evaluated.

Data Analysis

For statistical analysis, SAS software version 9.4 (SAS Institute Inc., Cary, North Carolina, USA) was applied. First of all, frequencies, mean values as well as position and dispersion measures were calculated. For the latter, the representation was done with box plot diagrams. The test for normal distribution was carried out with the Shapiro-Wilk test. The non-parametric Mann-Whitney-U test was used to compare interval-scaled variables and the central tendency. The tests were carried out on both sides. $P < 0.05$ ($\alpha = 0.05$) were rated as statistically significant with an error probability of five percent.

RESULTS

General Results

The present cohort consists of each 5 male and female patients ranging in age from 24 to 77 years (mean age, 49 years). In total 11 PNST were histologically examined (7x schwannoma, 1x neurofibroma, 2x MPNST and 1x B-cell lymphoma). Complete tumor resection was performed in 8 patients, whereas 2 cases underwent fascicular biopsy (1x MPNST and 1x B-cell lymphoma). In 9 out of 10 cases (90%) the application of SF during tumor preparation was described as helpful by the surgeon (**Table 1**). No adverse events occurred under the applied dosage of 0.5–1.0 mg/kg bodyweight.

Sodium-Fluorescein Results Correlating to Histopathology

Schwannoma reached a max. $mean_{green}$ of 254.7 pixel and a max. $mean_{red}$ of 179.4 pixel (**Figure 1**). In contrast, the passing healthy fascicles revealed a max. $mean_{green}$ of 94.91 pixel and a max. $mean_{red}$ of 120.76 pixel. The one neurofibroma case achieved a lower amount of fluorescence intensity. Its tumor mass max. $mean_{green}$ reached 140.9 pixel and max. $mean_{red}$ 76.2 pixel. Its not affected fascicles 88.5 (max. $mean_{green}$) and 66.6 (max. $mean_{red}$) pixel.

Similar to schwannoma, the MPNST achieved high SF intensities. One of both MPNST patients revealed an untypical MPNST anamnesis and tumor infestation, so that both cases are highlighted additionally as illustrative cases. MPNST max. $mean_{green}$ was 215 and max. $mean_{red}$ was 124.5 pixel. MPNST fluorescence was homogenous strong involving the whole nerve segment (**Figure 2**). Whereas, the surrounding subcutaneous tissue achieved lower values of 81.4 (max. $mean_{green}$) and 73.4 (max. $mean_{red}$). One patient suffering of a B-cell lymphoma in

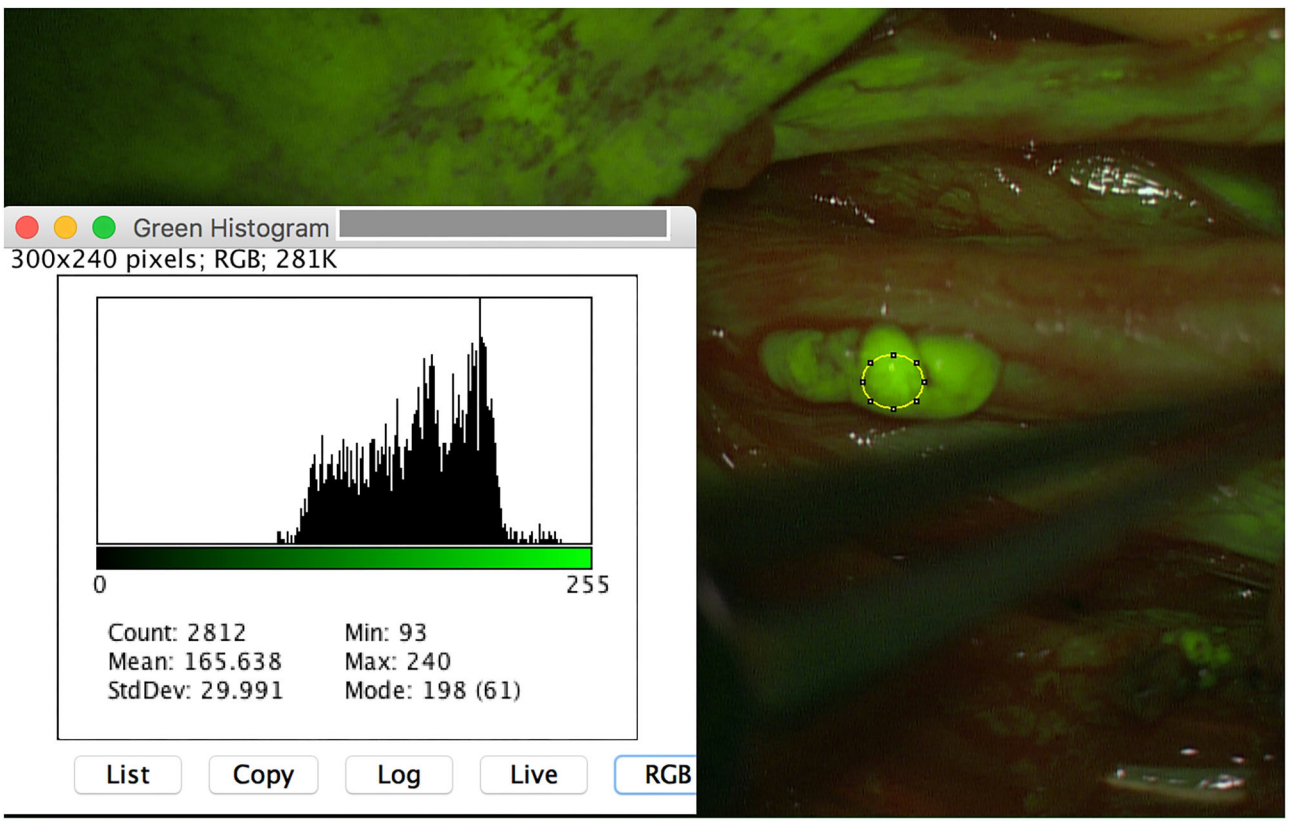

FIGURE 3 | A small schwannoma (3 × 2 mm) of the left peroneal nerve is additionally detected with SF, achieving similar results of $mean_{max}$ as the other schwannoma (240 pixel).

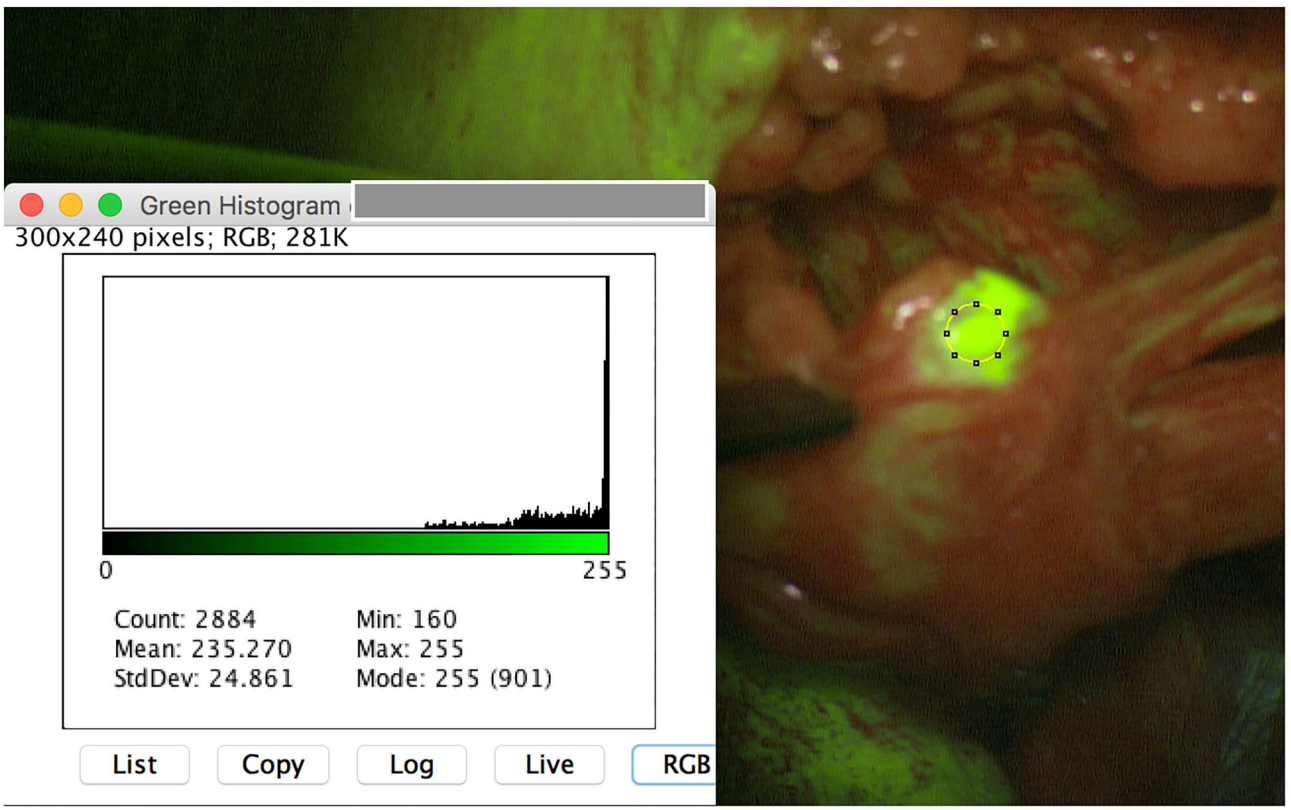

FIGURE 4 | Example of visibility of fluorescent schwannoma remnant of right peroneal nerve.

TABLE 2 | Green and red mean differences between healthy tissue and affected tissue.

	Mean ± SD (Median) Min-Max		
Complementary colors	**Healthy tissue ($n = 11$)**	**Affected issue ($n = 11$)**	***p*-Value**
Green mean value	83.36 ± 24.04 (78.00) 54.17–145.54	198.48 ± 49.97 (189.46) 100.54–254.71	0.0001
Red mean value	78.52 ± 20.13 (83.58) 44.02–120.76	120.16 ± 37.67 (111.94) 57.59–179.41	0.0071

Counts are in pixel, $p < 0.05$ is determined as statistically significant.

his medical history for 3 years, reported of a slowly progressing weakness of his right foot flexion. Since 2017 after chemotherapy he was already suffering a severe polyneuropathy. MRI showed a longitudinal positive contrast enhancement of a thickened tibial nerve. During tibial nerve biopsy, SF led to variable stain intensities in single fascicles. The resected fascicle revealed a max. $mean_{green}$ of 100.54 and max. $mean_{red}$ of 57.6 pixel. Surrounding fascicles came up with max. $mean_{green}$ values of 63 and max. $mean_{red}$ of 44 pixel.

Besides all these results, surgeon described the SF application as useful, since even very small PNST (for instance schwannoma 3 × 2 mm) were safely intraoperatively detected (**Figure 3**). Moreover, tumor remnants were securely depicted and resected (**Figure 4**).

In summary, in this present study group involving different PNST, tissue differentiation via SF was found to be statistically significant for the colors green ($p = 0.0001$) and red ($p = 0.0071$) (**Table 2** and **Figures 5A,B**). Therefore, it is considered as a helpful intraoperative tool.

DISCUSSION

Sodium-Fluorescein in Brain Surgery

The rediscovery and renaissance of SF in neurosurgery, started with its application during brain tumor surgery in the early 2000 (2). Indeed, currently many neurosurgical publications deal with SF. Through technical evolution of specific fluorescence filters and their implementation to microscopes in 2012, SF-visualization was significantly improved whereas its applied dosage was reduced. Subsequently in 2013 Schebesch et al. (14) published their first experience in sodium fluorescein-guided resections of malignant brain tumors. They found SF to be safe and feasible (14). At the same time, similar results were reported

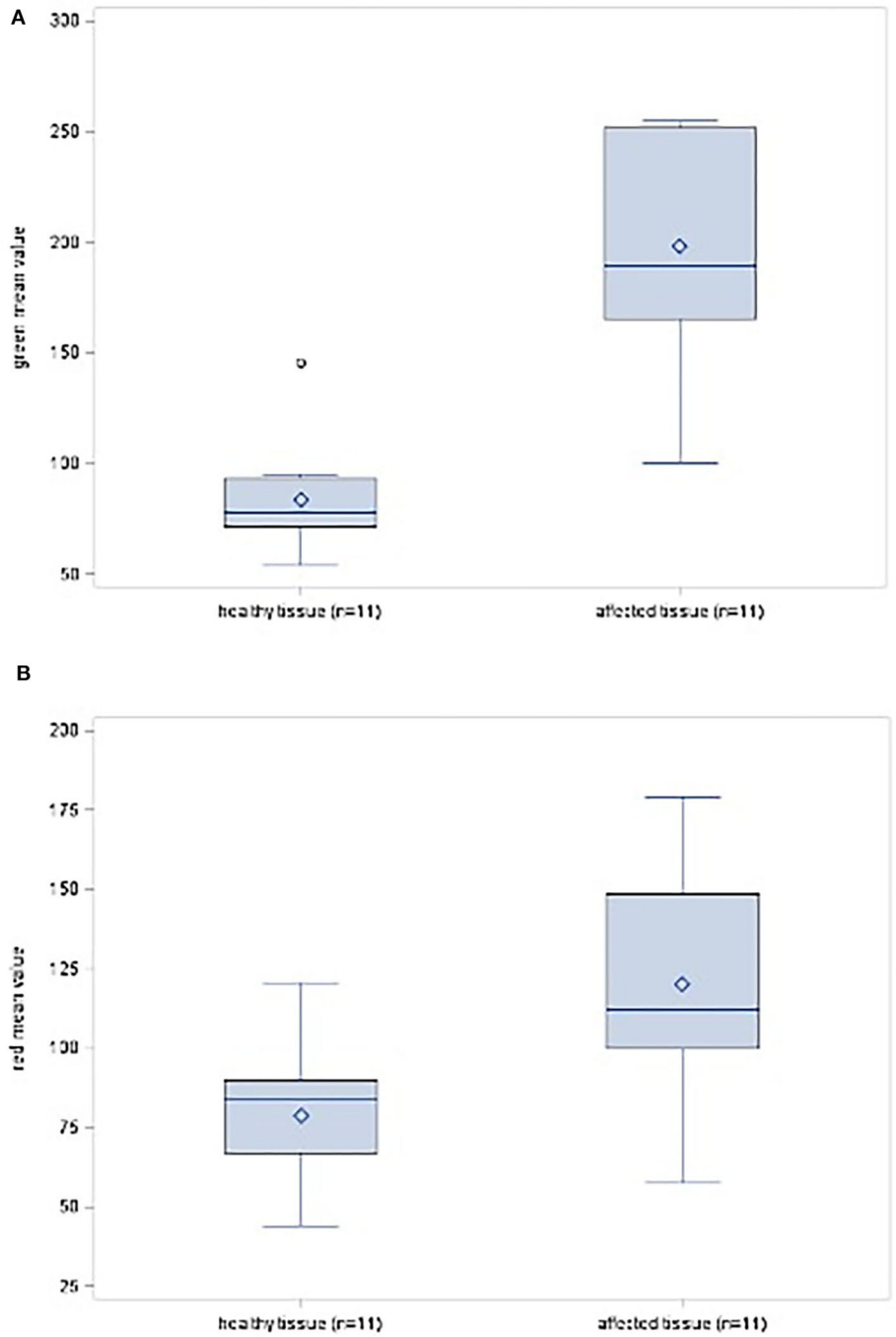

FIGURE 5 | (A) Box-plot diagram showing the distribution scores for the color green in healthy and affected tissues. **(B)** Box-plot diagram showing the distribution scores for the color red in healthy and affected tissues.

by an American group, they even extended SF's application to neurovascular malformations (7). Currently, SF is frequently used in surgeries of high-grade, low-grade gliomas, as well as meningioma or brain metastases (5, 6, 8, 15). Furthermore, SF is meanwhile applied in neuropediatrics (4, 16, 17). Due to this lower dosage of 2.0–5.0 mg/kg bodyweight no adverse events were reported in all those studies.

Nonetheless, the usage of SF in brain surgery has also been criticized by other study groups. In contrast to 5-aminolevulinic acid, SF reveals no glioblastoma cell-specific accumulation (18). After developing several *in vitro* and *in vivo* study models to investigate SF's biodistribution, Diaz et al. (18) came to the conclusion that SF accumulates in the extracellular space most likely due to the blood-brain-barrier dysfunction, similar to

gadolinium contrast enhancement in MRI. Meanwhile, however, a recent study describes via SF a yellowish intraoperative fluorescence during resection of non-gadolinium positive brain tumors. Tumor detection and identification of its margins were possible in those gliomas. As common feature, they were all positive on F-fluoroethyltyrosine positron emission tomography (19).

In their most recent study, Bömers et al. (20) focused on surgeon reported usability of SF during glioblastoma surgery. Similar to the study results of Erdman et al. (16) and de Laurentis et al. (17) a high user satisfaction was observed (20). The identification of tumor location, margins and the secure microsurgical tumor resection under the SF filter was highlighted in all above-mentioned studies. Those results correlate well with our findings during PNST surgery.

Sodium-Fluorescein in Peripheral Nerve Sheath Tumors (PNST)

Meanwhile, the application of SF is becoming a common tool for intraoperative tumor visualization, including intraneural ganglion cysts formations, in peripheral nerve surgery (21–24). According to our present results, it is a safe and useful method, which helps to define clearly tumor borders and hereby achieve gross total resection. Additionally, we were able to quantify these results using an imaging process platform (imageJ) and describe the different spectral ranges within different PNST and healthy tissue. Furthermore, in 10 out of 11 PNST resections, respectively, biopsies surgeon found SF to be helpful in this present analysis. As described in 2019, an application of low dose SF (0.5–1.0 mg/kg bodyweight) in an early stage (i.e., anesthesia induction), leads to a tissue differentiation between schwannoma and en passant fascicles. At the same time the standard principles of PNST microsurgical resection (i.e., direct motoric stimulation, EMG, NAPs, longitudinal dissection) have to be respected to preserve neurological function (21). Similar results were found by an Italian group in 2019. Vetrano et al. (22) examined 25 cases of PNST during surgery under SF. An optimal distinction between tumor and surrounding nerves was observed in 13 out of 14 schwannoma and in all 8 neurofibroma (22). Moreover, they emphasize the fact, that tumor remnants were not seen in 7 cases under white-light, but under SF (22). In contrast to those findings, a French group, examined 5 cases of schwannoma under the same circumstances. They did not see a benefit in between the tumor visualization under white-light and SF (25). Kalamarides stresses the need of intraoperative fascicular mapping and monitoring as stand-alone modality (25). All schwannoma were resected en-bloc, so that the need to depict possible tumor remnants did not arise. As seen in 2019 and in these present results, it is not always possible to detach schwannoma tissue from the healthy fascicles in toto, piecemeal technique has to be applied in some cases. Since a gross-total resection should be achieved, it is definitely reasonable to implement SF during schwannoma, respectively, neurofibroma resection (21, 22, 26).

MPNST are aggressive soft tissue sarcoma that account for ∼5–10% of all cases (27). They mainly arise *de novo* in peripheral nerves or from neurofibroma (28).

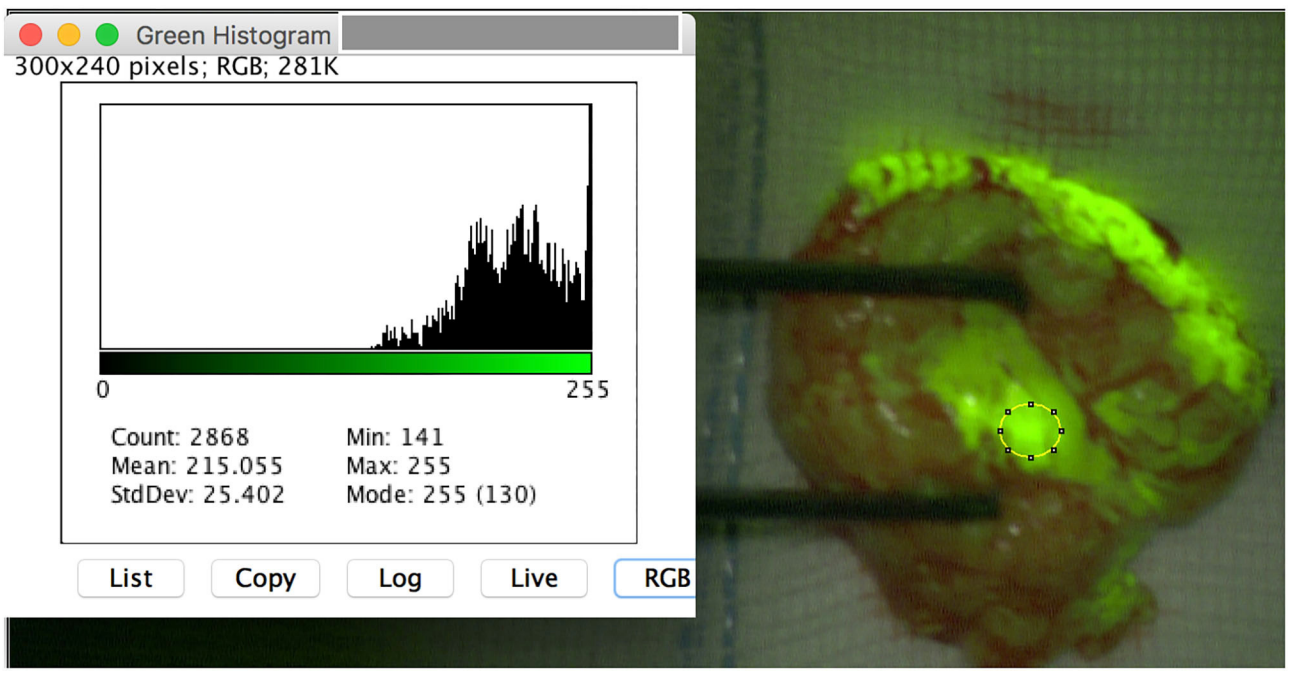

FIGURE 6 | Subcutaneous resected tissue of MPNST of a paraspinal nerve (pat. n° 8). Yellowish tumor remnants became visible.

Until now the only effective therapy and positive predictor of survival is surgical resection with wide negative margins (11, 12). While post-operative radiation is recommended, the efficacy of chemotherapy is controversially discussed (11, 12). As illustrated below, two MPNST patients were operated under the usage of SF. In one case, the whole ulnar nerve achieved a strong homogeneous yellowish stain, so that an intraneural tissue differentiation was not seen under the SF filter. Its usage was considered as not helpful during biopsy. The other case, a MPNST manifestation most likely out of a paraspinal cervical nerve, was operated several times, since under white-light microscopy and frozen section analysis a gross total resection of the surrounding tissue was not achieved. During the third surgery, SF revealed fluorescence of subcutaneous tissue, so that by this means, a complete resection became possible. After radiotherapy the patient reveals no recurrence or metastases until now.

Despite MRI, ultrasound and electrophysiology, there are some cases of peripheral nerve lesions, that need fascicular biopsy for further diagnosis in order to determine the proper therapy (23, 29). Those lesions may look inconspicuous in white-light microscopy, so that the usage of SF has been additionally examined in those cases. As described in 2020, the intraoperative application of SF helps to visualize the most affected fascicles and to determine a target fascicle biopsy (23). In this study group one patient, suffering of a B-cell lymphoma, developed neurological deficits of the tibial nerve. MRI showed a longitudinal nerve enlargement and contrast enhancement. Oncologists set the indication for nerve biopsy. During surgery, different intensities of fluorescence were seen, after motoric mapping of the fascicles, surgeon decided to resect one strong fluorescent fascicle. Histopathology confirmed the manifestation of a B-cell lymphoma.

In summary, SF, applied in low dose and during anesthesia induction, is meaningful and easily feasible during PNST removals or biopsies. No adverse events occurred.

In future, direct implementation of an image processing platform tool into the microscope could additionally enhance the value of this technique. By this means, surgeons would immediately receive mean values of relevant regions of interest in real time. Thereby, differentiated intraoperative decision making would be further simplified and improved.

Illustrative Cases

Patient no. 8 (**Table 1**), a 77 years old female, suffered of a walnut-sized tumorous subcutaneous nuchal formation. She had no pain or neurological deficits. By suspicion of an atheroma she underwent outpatient surgery. Histopathology revealed a MPNST, therefore, she was timely admitted to our clinical center. Up to this point of time, there were no pre-existing neurological diseases, no signs of neurofibromatosis or significant comorbidities.

She was conducted to MRI and FDG-PET. Imaging depicted residual tumor mass and high accumulation of the surrounding tissue. Metastases were not detected. The second tumor

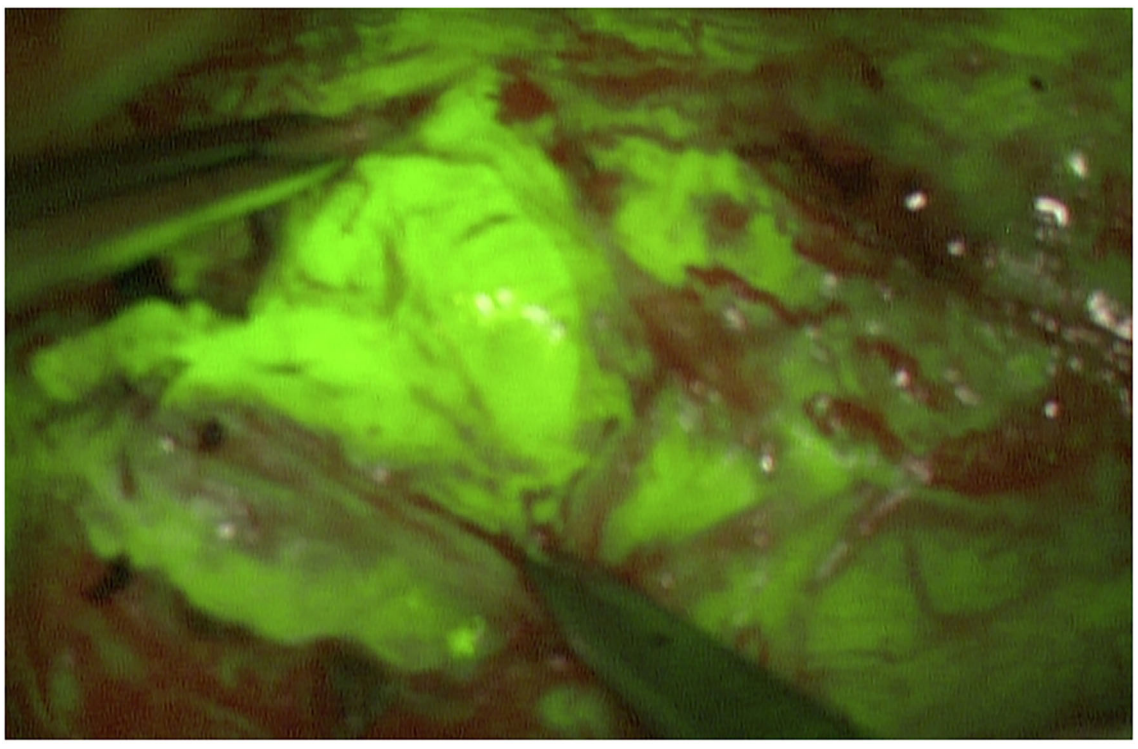

FIGURE 7 | After opening of the epineurium of the ulnare nerve, the complete MPNST tissue reveals a strong homogeneous fluorescence. An intraneural tissue differentiation is not possible via SF (pat. n°9).

resection was performed under white light. However, tumor free margins were not achieved according to the final histopathology results. As consequence, SF was applied during the third tumor resection. Subcutaneous tissue showed different degrees of fluorescence (**Figure 6**). Strong fluorescent areas were all resected. A complete tumor removal was finally confirmed by histopathology. A subsequent radiation followed. Until now, 18 months later, patient reveals no recurrence or metastases in the diagnostic follow-up.

Patient no. 9 (**Table 1**), a 55 years old male, suffered of slow progressing paralysis of his right hand for years. He described an hypesthesia of his ring and small finger, so that on suspicion of a Loge de Guyon entrapment syndrome, he underwent decompression of his right ulnar nerve. Three years later, pain and functional loss increased dramatically. MRI and ultrasound depicted a thickened, strong enhancing ulnar nerve along the complete upper arm. The patient revealed no signs of neurofibromatosis or schwannomatosis. There were no pre-existing diseases. Fascicular biopsy was performed under SF and direct motoric stimulation. After epineurotomy, all fascicles of the ulnar nerve showed a homogenous strong fluorescence. An intraneural tissue differentiation was not recognizable (**Figure 7**).

Histopathology resulted in MPNST. In accordance to the local tumor board, the right arm was amputated. Metastases were not detected at this point. Seven months later, the patient developed pulmonary metastases on both lungs. Besides surgical resection, he died 2 months later.

CONCLUSION

During the resection of benign PNST, tissue differentiation between affected and not affected nerve segments became visible using SF. Tumor remnants were securely detected. This intraoperative visualization method seems to be a helpful tool for surgeons. In contrast, the usage in malignant PNST was limited. In those cases, an intraneural tissue differentiation was not possible, only the extraneural surrounding tissues revealed a far lower fluorescence than the MPNST. Concerning the sciatic infestation of lymphoma, SF was helpful in identifying affected nerve fascicles.

The intraoperative application of SF in PNST surgery has been established as standard visualization tool in the present clinical institution.

DATA AVAILABILITY STATEMENT

The raw data supporting the conclusions of this article will be made available by the authors, without undue reservation.

ETHICS STATEMENT

Ethical review and approval was not required for the study on human participants in accordance with the local legislation and institutional requirements. The patients/participants provided their written informed consent to participate in this study.

AUTHOR CONTRIBUTIONS

MP principal investigator and data analysis. RK conception and ImageJ evaluation. CW study design and counselor. AP data analysis and study design. GD data analysis. NG ImageJ evaluation and study design. All authors contributed to the article and approved the submitted version.

REFERENCES

1. Moore GE, Peyton WT, French LA, Walker WW. The clinical use of fluorescein in neurosurgery; the localization of brain tumors. *J Neurosurg.* (1948) 5:392–8. doi: 10.3171/jns.1948.5.4.0392
2. Shinoda J, Yano H, Yoshimura S, Okumura A, Kaku Y, Iwama T, et al. Fluorescence-guided resection of glioblastoma multiforme by using high-dosage fluorescein sodium. Technical note. *J Neursurg.* (2003) 99:597–603. doi: 10.3171/jns.2003.99.3.0597
3. Okuda T, Kataoka K, Yabuuchi T, Yugami H, Kato A. Fluorescence-guided surgery of metastatic brain tumors using fluorescein sodium. *J Clin Neurosci.* (2010) 17:118–21. doi: 10.1016/j.jocn.2009.06.033
4. Göker B, Kiris T. Sodium fluorescein-guided brain tumor surgery under the Yellow-560-nm surgical microscope filter in pediatric age group: feasibility and preliminary results. *Childs Nerv Syst.* (2019) 35:429–35. doi: 10.1007/s00381-018-04037-4
5. Xiao SY, Zhang J, Zhu ZQ, Li YP, Zhong WY, Chen JB, et al. Application of fluorescein sodium in breast cancer brain-metastasis surgery. *Cancer Manag Res.* (2018) 10:4325–31. doi: 10.2147/CMAR.S176504
6. Schebesch KM, Hoehne J, Hohenberger C, Proescholdt M, Riemenschneider MJ, Wendl C, et al. Fluorescein sodium-guided resection of cerebral metastases- experience with the first 30 patients. *Acta Neurochir.* (2015) 157:899–904. doi: 10.1007/s00701-015-2395-7
7. Rey-Dios R, Cohen-Gadol AA. Technical principles and neurosurgical applications of fluorescein fluorescence using a microscope-integrated fluorescence module. *Acta Neurochir.* (2013) 155:701–6. doi: 10.1007/s00701-013-1635-y
8. Acerbi F, Broggi M, Eoli M, Anghileri E, Cuppini L, Pollo B, et al. Fluorescein-guided surgery for grade IV gliomas with a dedicated filter on the surgical microscope: preliminary results in 12 cases. Acta Neurochir. (2013) 155:1277–86. doi: 10.1007/s00701-013-1734-9
9. Fletcher CDM, Bridge JA, Hogendoorn P, Mertens F. *WHO Classification of Tumours of Soft Tissue and Bone*. 4th ed. Lyon: IARC Press (2013)
10. Kransdorf MJ. Benign soft-tissue tumors in a large referral population: distribution of specific diagnoses by age, sex, and location. *AJR.* (1995) 164:395–402. doi: 10.2214/ajr.164.2.7839977
11. Reilly KM, Kim A, Blakely J, Ferner RE, Gutmann DH, Legius E, et al. Neurofibromatosis type 1- associated MPNST state of the science: outlining a research agenda for the future. *J Natl Cancer Inst.* (2017) 109:djx124. doi: 10.1093/jnci/djx124
12. James AW, Shurell E, Singh A, Dry SM, Eilber FC. Malignant peripheral nerve sheath tumor. *Surg Oncol Clin N Am.* (2016) 25:789–802. doi: 10.1016/j.soc.2016.05.009
13. Schneider CA, Rasband WS, Eliceiri KW. NIH image to ImageJ: 25 years of image analysis. *Nat Methods.* (2012) 9:671–5. doi: 10.1038/nmeth.2089
14. Schebesch KM, Proescholdt M, Hoehne J, Hohenberger C, Hansen E, Riemenschneider MJ, et al. Sodium fluorescein-guided resection under the YELLOW 560 nm surgical microscope filter in malignant brain tumor surgery—a feasibility study. *Acta Neurochir.* (2013) 155:693–9. doi: 10.1007/s00701-013-1643-y

15. Schebesch KM, Brawanski A, Hohenberger C, Hohne J. Fluorescein sodium-guided surgery of malignant brain tumors: history, current concepts, and future project. *Turk Neurosurg.* (2016) 26:185–94. doi: 10.5137/1019-5149.JTN.16952-16.0
16. Erdman CM, Christie C, Iqbal MO, Mazzola CA, Tomycz L. The utilization of sodium fluorescein in pediatric brain stem gliomas: a case report and review of the literature. *Childs Nerv Syst.* (2020). doi: 10.1007/s00381-020-04857-3. [Epub ahead of print].
17. De Laurentis C, Hoehne J, Cavallo C, Restelli F, Falco J, Broggi M, et al. The impact of fluorescein-guided technique in the surgical removal of CNS tumors in a pediatric population: results from a multicentric observational study. *J Neurosurg Sci.* (2019) 63:679–87. doi: 10.23736/S0390-5616.19.04601-0
18. Diaz RJ, Dios RR, Hattab EM, Burell K, Rakopoulos P, Sabha N, et al. Study of the biodistribution of fluorescein in glioma-infiltrated mouse brain and histopathological correlation of intraoperative findings in high-grade gliomas resected under fluorescein fluorescence guidance. *J Neurosurg.* (2015) 122:1360–9. doi: 10.3171/2015.2.JNS132507
19. Schebesch KM, Brawanski A, Doenitz C, Rosengarth K, Proescholdt M, Riemenschneider MJ, et al. Fluorescence-guidance in non-Gadoliniumenhancing, but FET-PET positive gliomas. *Clin Neurol Neurosurg.* (2018) 172:177–82. doi: 10.1016/j.clineuro.2018.07.011
20. Bömers JP, Danielsen ME, Schulz MK, Halle B, Kristensen BW, Sørensen MD, et al. Sodium fluorescein shows high surgeon-reported usability in glioblastoma surgery. *Surgeon.* (2020) 18:344–8. doi: 10.1016/j.surge.2020.01.003
21. Pedro MT, Eissler A, Schmidberger J, Kratzer W, Wirtz CR, Antoniadis G, et al. Sodium fluorescein-guided surgery in peripheral nerve sheath tumors: first experience in 10 cases of schwannoma. *World Neurosurg.* (2019) 17:e513–21. doi: 10.1016/j.wneu.2019.01.010
22. Vetrano IG, Acerbi F, Falco J, Devigili G, Rinaldo GM, Prada F, et al. Fluorescein-guided removal of nerve sheath tumors: a preliminary analysis of 20 cases. *J Neurosurg.* (2019) 6:1–10. doi: 10.3171/2019.9.JNS19970
23. Pedro MT, Eissler A, Scheuerle A, Schmidberger J, Kratzer W, Wirtz CR, et al. Sodium fluorescein as intraoperative visualization tool during peripheral nerve biopsies. *World Neurosurg.* (2020) 133:e513–21. doi: 10.1016/j.wneu.2019.09.081
24. Stone JJ, Graffeo CS, de Ruiter GCW, Rock MG, Spinner RJ. Intraoperative intravenous fluorescein as an adjunct during surgery for peroneal intraneural ganglion cysts. *Acta Neurochir.* (2018) 160:651–4. doi: 10.1007/s00701-018-3477-0
25. Kalamarides M, Bernat I, Peyre M. Extracapsular dissection in peripheral nerve schwannoma surgery using bright light and fluorescein sodium visualization: case series. *Acta Neurochir.* (2019) 161:2447–52. doi: 10.1007/s00701-019-04071-4
26. Vetrano IG, Nazzi V, Acerbi F. What is the advantage of using sodium fluorescein during resection of peripheral nerve tumors? *Acta Neurochir.* (2020) 162:1157. doi: 10.1007/s00701-019-04211-w
27. Fuchs B, Spinner RJ, Rock MG. Malignant peripehral nerve sheath tumors: an update. *J Surg Orthop Adv.* (2005) 14:168–74.
28. Wong WW, Hirose T, Scheithauer BW, Schild SE, Gunderson LL. Malignant peripheral nerve sheath tumor: analysis of treatment outcome. *Int J Radiat Oncol Biol Phys.* (1998) 42:351–60. doi: 10.1016/S0360-3016(98)00223-5
29. Brand C, Pala A, Scheuerle A, Scheglmann K, König R, Kratzer W, et al. Neurolymphomatosis: two case reports. *Nervenarzt.* (2017) 89:701–4. doi: 10.1007/s00115-017-0460-6

Conflict of Interest: The authors declare that the research was conducted in the absence of any commercial or financial relationships that could be construed as a potential conflict of interest.

frontiers in Neurology

ORIGINAL RESEARCH
published: 09 March 2021
doi: 10.3389/fneur.2021.644804

Fluorescence-Guided High-Grade Glioma Surgery More Than Four Hours After 5-Aminolevulinic Acid Administration

Georgios A. Maragkos[1†], Alexander J. Schüpper[1*†], Nikita Lakomkin[1], Panagiotis Sideras[2], Gabrielle Price[1], Rebecca Baron[1], Travis Hamilton[3], Sameah Haider[3], Ian Y. Lee[3], Constantinos G. Hadjipanayis[1,4] and Adam M. Robin[3]*

[1] Department of Neurosurgery, Icahn School of Medicine at Mount Sinai, Mount Sinai Health System, New York, NY, United States, [2] Department of Radiology, Icahn School of Medicine at Mount Sinai, Mount Sinai Health System, New York, NY, United States, [3] Department of Neurosurgery, Henry Ford Health System, Detroit, MI, United States, [4] Department of Neurosurgery, Icahn School of Medicine, Mount Sinai Beth Israel, Mount Sinai Health System, New York, NY, United States

OPEN ACCESS

Edited by:
Jose R. Pineda, University of the Basque Country, Spain

Reviewed by:
Alexander Aleksandrovich Potapov, N.N. Burdenko National Scientific and Practical Center for Neurosurgery, Russia
Rafael García Moreno, Sanitas La Zarzuela Hospital, Spain

***Correspondence:**
Georgios A. Maragkos
georgios.maragkos@mountsinai.org
Alexander J. Schüpper
Alexander.Schupper@mountsinai.org

† These authors have contributed equally to this work and share first authorship

Specialty section:
This article was submitted to Neuro-Oncology and Neurosurgical Oncology, a section of the journal Frontiers in Neurology

Received: 21 December 2020
Accepted: 08 February 2021
Published: 09 March 2021

Citation:
Maragkos GA, Schüpper AJ, Lakomkin N, Sideras P, Price G, Baron R, Hamilton T, Haider S, Lee IY, Hadjipanayis CG and Robin AM (2021) Fluorescence-Guided High-Grade Glioma Surgery More Than Four Hours After 5-Aminolevulinic Acid Administration. Front. Neurol. 12:644804. doi: 10.3389/fneur.2021.644804

Background: Fluorescence-guided surgery (FGS) using 5-aminolevulic acid (5-ALA) is a widely used strategy for delineating tumor tissue from surrounding brain intraoperatively during high-grade glioma (HGG) resection. 5-ALA reaches peak plasma levels ∼4 h after oral administration and is currently approved by the FDA for use 2–4 h prior to induction to anesthesia.

Objective: To demonstrate that there is adequate intraoperative fluorescence in cases undergoing surgery more than 4 h after 5-ALA administration and compare survival and radiological recurrence to previous data.

Methods: Retrospective analysis of HGG patients undergoing FGS more than 4 h after 5-ALA administration was performed at two institutions. Clinical, operative, and radiographic pre- and post-operative characteristics are presented.

Results: Sixteen patients were identified, 6 of them female (37.5%), with mean (SD) age of 59.3 ± 11.5 years. Preoperative mean modified Rankin score (mRS) was 2 ± 1. All patients were dosed with 20 mg/kg 5-ALA the morning of surgery. Mean time to anesthesia induction was 425 ± 334 min. All cases had adequate intraoperative fluorescence. Eloquent cortex was involved in 12 cases (75%), and 13 cases (81.3%) had residual contrast enhancement on postoperative MRI. Mean progression-free survival was 5 ± 3 months. In the study period, 6 patients died (37.5%), mean mRS was 2.3 ± 1.3, Karnofsky score 71.9 ± 22.1, and NIHSS 3.9 ± 2.4.

Conclusion: Here we demonstrate that 5-ALA-guided HGG resection can be performed safely more than 4 h after administration, with clinical results largely similar to previous reports. Relaxation of timing restrictions could improve procedure workflow in busy neurosurgical centers, without additional risk to patients.

Keywords: fluorescence, 5-ALA, glioma, glioblastomas, brain tumors, neuro-oncology, intraoperative imaging

INTRODUCTION

Maximal and safe resection has been established as the initial standard of care for the treatment of high-grade gliomas (HGG) (1–5). Complete resection of the contrast-enhancing tumor (CRET) has been associated with prolonged survival for patients with the most common HGG, glioblastoma (6, 7). Due to the propensity of HGGs involving eloquent regions of the brain, maximal safe resection poses intraoperative challenges for tumor surgeons (8). As a surgical adjunct, the use of fluorescence-guided surgery (FGS) provides surgeons with improved visualization of brain tumors and the infiltrative margin. The use of FGS has been well-studied in the use of HGG resection over the past 20 years and has shown to be an effective tool for resection of HGGs (9, 10).

Multiple fluorophore agents have been studied in the use of FGS for HGGs and each come with their own advantages and disadvantages (11). The most commonly studied fluorophores are 5-aminolevulinic acid (5-ALA), fluorescein and indocyanine green (ICG) (11). 5-ALA is the most widely studied agent for FGS of HGG, and is currently the only agent (Gleolan®) that is approved by the US Food and Drug Administration (FDA) for glioma surgery (9). Administered as an oral solution, 5-ALA is metabolized in the heme biosynthesis pathway to protoporphyrin (PpIX), which accumulates intracellularly in tumor cells (12), absorbing light between 375 and 440 nm and emitting violet-red fluorescence (640–710 nm) (13). 5-ALA has been previously shown in multicenter studies to be safe and effective, with minimal associated side effects (9, 14). Since the completion of the first phase III randomized controlled trial (RCT) for FGS showing improved progression-free survival (PFS) and greater overall tumor resection following FGS (9), 5-ALA has been used broadly across Europe and other countries throughout the world. However, 5-ALA (Gleolan®) only recently has been approved by the FDA in 2017 (15), and is currently being used by neurosurgeons throughout the country.

As part of the FDA approval of 5-ALA (Gleolan®; NX Development Corporation) for glioma surgery, the recommended usage in the label is stated as an "oral dose of ALA HCL solution of 20 mg/kg body weight, administered 3 h (range 2–4 h) prior to induction of anesthesia (16)." These recommendations were established after the RCT led by Stummer et al. (9). The timing of 5-ALA administration was based on rodent experiments in which a fluorescence peak was observed 6 h after administration (17). Oral administration at 3 h (2–4 h) was recommended in order to permit time for anesthesia, positioning, and craniotomy prior to peak intraoperative PpIX fluorescence (9, 10). Recently, however a study by Kaneko et al. found that maximal concentrations of fluorescence intensity were observed after 7–8 h following 5-ALA administration (18), calling for later administration than established in prior studies. In this study, we aim to study a population of patients undergoing glioma surgery beyond the 4 h window (>6 h) following 5-ALA administration as described in the FDA label to determine intraoperative fluorescence, as well as clinical and radiographic outcomes of patients undergoing FGS.

METHODS

Patient Inclusion

Institutional Review Board approval was obtained with waiver of patient informed consent due to the retrospective nature of the study. For the purposes of this study, all patients receiving 5-ALA for resection of radiographic high-grade glioma (HGG) were screened at two separate institutions between 2017 and 2020. Patients were included if they received anesthesia induction more than 4 h following 5-ALA administration. Patients were excluded if they received anesthesia induction within 4 h of 5-ALA, or if they had non-HGG tissue upon histopathology. Patient demographic variables including age, sex, and preoperative functional status as measured by modified Rankin scale (mRS) were collected. Treatment variables included chemotherapy or radiotherapy. Operative variables including anesthesia induction time, incision time, procedure finish time, and time to extubation were collected. Outcome variables included postoperative neurological deficits, mRS scores, Karnofsky Performance Scores (KPS), National Institutes of Health Stroke Scale (NIHSS), 6-month progression-free survival (PFS), and time until death.

Volumetric Analysis

Volumetric analysis from preoperative and postoperative MR imaging was prospectively collected for all patients. Volumetric measurements were made using Olea Sphere (v. 2.3, Olea Medical Solutions, La Ciotat, France) at one institution and Brainlab Elements (Brainlab, Munich, Germany) at the other. Regions of contrast-enhancement were measured in preoperative scans, immediate postoperative scans, and MRIs 6 months following surgery independently by three of the authors (R.B., P.S., S.H.), blinded to the clinical characteristics of the patient cohort, one being a neuroradiology fellow at the time of assessment. One patient volume required confirmation by a senior author (A.R.) who was not previously blinded to patient characteristics.

Statistical Analysis

Clinical, operative, and radiographic pre- and post-operative characteristics are presented as frequencies and percentages for categorical variables, and means and standard deviations for continuous variables. Descriptive statistics were used to analyze both categorical and continuous variables. All statistical analyses were performed on Statistical Analysis Software version 9.4 (SASv9.4 - Cary, NC). Significance for all statistical testing was determined by $p < 0.05$.

RESULTS

Patient Demographics and Tumor Characteristics

A total of 16 patients met the inclusion criteria (**Table 1**), 6 of them female (37.5%), with a mean (SD) age of 59.3 ± 11.5. Preoperative mean modified Rankin score (mRS) was 2 ± 1. All 16 patients received chemotherapy and/or radiation therapy in addition to resection for treatment of their brain tumor. Average tumor volume was 24.9 ± 24.6 cc. Fifteen (93.8%) patients' tumors were diagnosed as glioblastoma (GBM)

TABLE 1 | Patient baseline characteristics.

Variable	Patients, % (*N* = 16)
Age, years (mean, SD)	59.3 ± 11.5
Female sex	6 (37.5)
Preoperative mRS (mean, SD)	2 ± 1
5-ALA dose	
20 mg/kg	16 (100)
Timing from 5-ALA, hours:min (mean, SD)	
Time to intubation	7:04 ± 5:34
Time to incision	8:26 ± 5:43
Time to procedure finish	12:46 ± 6:35
Time to extubation	13:06 ± 6:34
Intraoperative Fluorescence	
Signal presence	16 (100)

TABLE 2 | Lesion characteristics.

Variable	Patients, % (*N* = 16)
Lesion pathology	
Glioblastoma multiforme	15 (93.7)
Anaplastic astrocytoma	1 (6.3)
Ge IDH mutation	2 (12.5)
Tumor location*	
Frontal	3 (18.8)
Temporal	8 (50)
Parietal	4 (25)
Occipital	4 (25)
Eloquent cortex	12 (75)
Lesion depth from cortex (mm)	6.8 ± 7.2
Lesion maximal diameter, mm (mean, SD)	49.4 ± 17.2
Lesion volume (mL) [volumetric]	24.9 ± 24.6

**Three lesions occupied both parietal and occipital lobes.*

on histopathology (one patient had anaplastic astrocytoma), 13 (86.7%) were IDH1 wild-type and 2 (13.3%) were IDH1 mutants. Nine (56.3%) tumors were primary and seven (43.7%) were recurrent HGGs (**Table 2**). Twelve (75%) tumors involved eloquent cortex. The mean extent of resection (EOR) was 91.5%, with 13 (81.3%) cases having residual contrast enhancement on postoperative MRI, and a mean residual volume of 1.16 ± 1.11 cc.

5-ALA Administration and Tumor Fluorescence

All patients were dosed with 20 mg/kg 5-ALA the morning of surgery. The mean time from 5-ALA administration to incision was 507 ± 344 min and time to closure was 767 ± 395, therefore the fluorescence guided surgery was performed after >6 h in all cases. The longest time between 5-ALA administration and anesthesia induction was 27 h and 46 min. This patient received 5-ALA prior to scheduled surgery but was found to have a fever, had a full workup over the ensuing day, then proceeded to have FDG surgery the next day, with adequate fluorescence intraoperatively. All cases had adequate intraoperative fluorescence. No patients in the series experienced 5-ALA-related toxicity. All sixteen patients' tumors demonstrated intraoperative fluorescence *in situ* (**Figures 1**, **2**).

Patient Outcomes

Five (26.7%) patients had postoperative neurological deficits, defined as decrements in the NIHSS more than one point during the initial hospitalization (**Table 3**). Mean progression-free survival was 5 ± 3 months. During the study period, 6 (37.5%) patients died, mean mRS is 2.3 ± 1.3, mean Karnofsky score was 71.9 ± 22.1, and mean NIHSS was 3.9 ± 2.4. Six-month progression-free survival was seen in 46.2% (6) patients. Overall survival following surgery was 6.3 ± 4.9 months (**Figure 3**).

DISCUSSION

5-ALA is a well-studied intraoperative adjunct for the resection of HGGs that helps differentiate tumor from surrounding brain parenchyma and has been shown to improve gross total resection rates as well as overall patient survival (9, 19–32). Despite its widespread use, limited data exists regarding the best timing for administration of 5-ALA prior to surgery. The current guidelines set forth by the Food and Drug Administration (FDA) state that the substance should be administered "3 h (range 2–4 h) before anesthesia (16)." However, the exact fluorescence kinetics regarding PpIX accumulation within tumor tissue are currently unclear. In the current study, the safety and efficacy of 5-ALA use beyond the established time of administration was assessed. In patients administered 5-ALA over 6 h prior to the start of tumor resection, 5-ALA was not only safe to use during this time window, but also efficacious in both in diagnostic accuracy and the extent of resection.

The currently limited data regarding fluorescence kinetics of 5-ALA seem to indicate a more delayed fluorescence peak within HGGs than previously thought. In an early study utilizing an orthotopic brain tumor model, the maximum fluorescence intensity was shown to be around 6 h after administration (17). The recommended time of administration used in the summary of the product characteristics (SPC) for FDA approval (Gleolan©) was based upon animal studies showing that fluorescence peaked 6 h after administration (33). Extrapolated from these experiments, the parameter of administration of 3–4 h prior to anesthesia would allow time for operating room set up and resection in ample time for peak fluorescence during tumor resection (18). As a result, 5-ALA clinical trials, including the RCT, have utilized this parameter (9, 19–32). In the FDA New Drug Application (NDA), six clinical trials were included that used this parameter, all of which were conducted in Germany (34). Prior to this study, only one clinical trial recommended administration of 5-ALA 3–5 h prior to surgery. No studies have assessed a longer time interval.

Other studies have suggested that 5-ALA induced fluorescence may peak beyond the previously studied time window of 2–4 h. Studies measuring PpIX concentration in other parts of the human body have shown a peak in the plasma to be around 8 h (32), and in the skin to be 6.5 to 9.8 h (35). In a later study

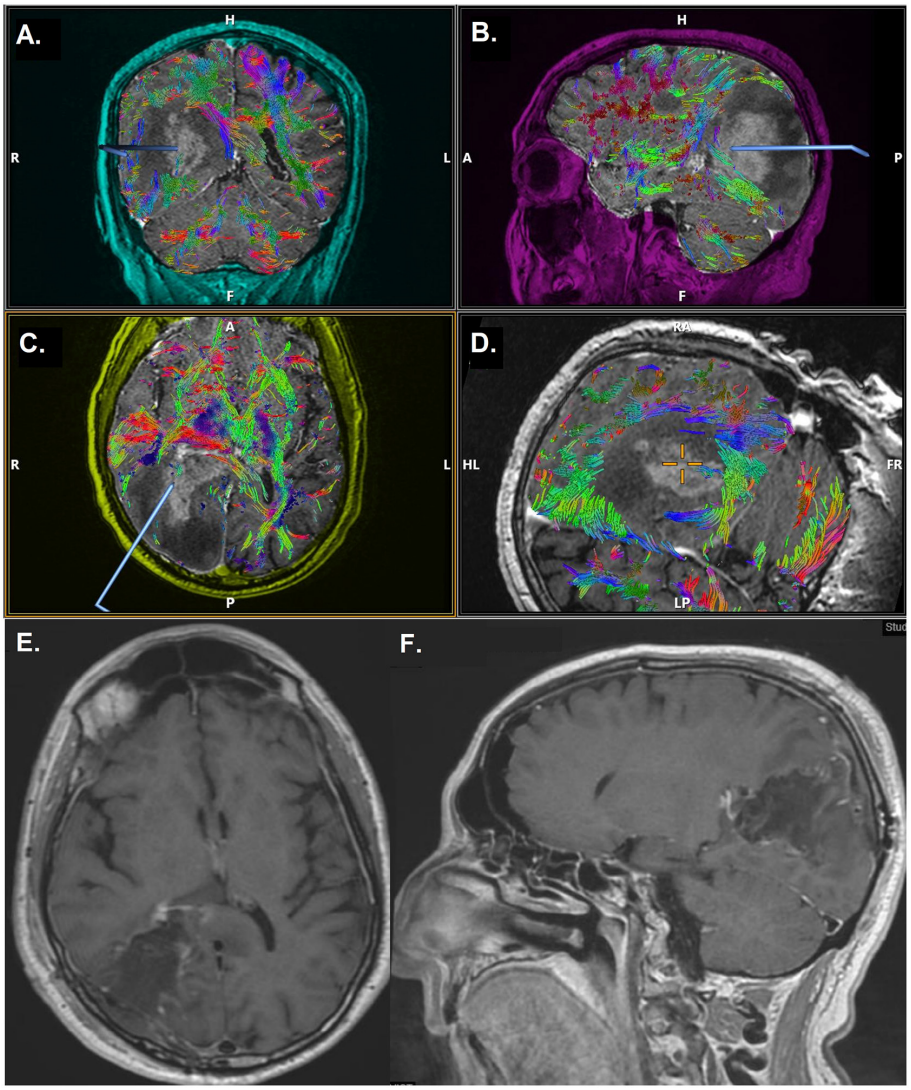

FIGURE 1 | Case demonstration of a 69-year-old male with glioblastoma multiforme, undergoing 5-ALA FGS. Time from 5-ALA administration to anesthesia induction was 7 h and 48 min, time to incision was 9 h and 4 min and time to closure was 12 h and 14 min. **(A–D)** Preoperative MRI with DTI. Axial **(E)** and sagittal **(F)** postoperative MRI scan, after 5-ALA FGS, demonstrating gross total resection of the lesion. 5-ALA, 5-aminolevulinic acid; FGS, fluorescence-assisted glioma surgery; MRI, magnetic resonance imaging; DTI, diffusion tensor imaging.

of 201 samples from 68 patients, Kaneko et al. investigated the time dependency of protoporphyrin IX (PpIX) by measuring fluorescence intensity in tumor biopsy samples at various time points during HGG surgery (18). The authors recorded the time-fluorescence curves in their ex-situ study, demonstrating that the peak intensity may be 7–8 h after 5-ALA administration, and suggested that 5-ALA be administered earlier than what is currently suggested by the FDA, specifically 4–5 h prior to anesthesia induction (18). In line with their work, we found that there was adequate intraoperative fluorescence to guide HGG resection in all our cases that were induced to anesthesia more than 4 h after imbibing 5-ALA. Our results confirm that tumor fluorescence is even present more than 24 h after oral administration in some cases.

The identification of the ideal timing of 5-ALA administration prior to surgery is of high importance for multiple reasons. In everyday practice, where operations may be postponed for various logistical reasons (staffing, cleaning of the operating room, emergent cases), it would be useful to know if any such delay could adversely affect intraoperative fluorescence and, possibly, patient outcomes. Individual institutions and surgeons should account for the time needed for exposure or mapping, and plan accordingly. For tumors known to demonstrate less fluorescence (e.g., WHO grade III gliomas), for tumor margins and in deep-seated gliomas, resection during the peak of fluorescence intensity would be ideal. Another important aspect regarding administration of 5-ALA is the timing of 5-ALA and PpIX clearance from the tumor bed.

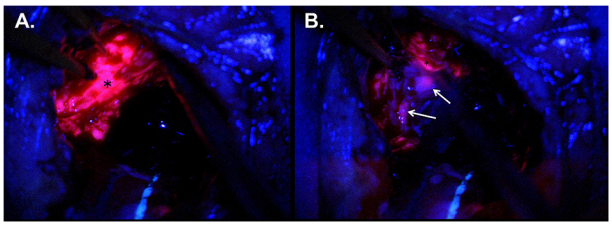

FIGURE 2 | Intraoperative imaging for case demonstration patient. **(A)** Tumor bulk fluorescence after 5-ALA administration (asterisk). **(B)** Infiltrative margin fluorescence after 5-ALA administration (white arrows).

Interestingly, glioblastomas seem to maintain up to 65% of their maximal fluorescence even 10 h after 5-ALA administration (18), confirming that fluorescence clearance may be much slower than its accumulation. Kaneko et al. found that tumor type may predict clearance time of fluorescence (18), which may advocate for further investigation on establishing different time periods for administration based upon pathology. Additionally, the infiltrative tumor margin may have a later peak at around 8–9 h, further corroborating the need for more delayed administration (18, 33). However, the exact timing of fluorescence clearance from the tumor bed is not currently known and further study is warranted to determine the true extent of the 5-ALA time window in order to demonstrate *in situ* results regarding when fluorescence is no longer visible.

The current study did not demonstrate any concerns with patient safety, and had comparable outcomes to prior studies. Of the 16 patients included between two centers, there were no photosensitivity reactions or other 5-ALA-related toxicities noted. The average extent of resection was over 90%, defined as a gross total resection. This compares to other observational and clinical trials showing GTR rates ranging between 25 and 94% with 5-ALA (9–11). In terms of patient outcomes, patients saw an average progression-free survival (PFS) rate of 5 months, with a 6-month PFS rate of 46.2%, which is comparable to previous studies showing a 6-month PFS rate of 46% (22) and average PFS of 8.6 months (36). In our cohort, overall survival was 6.3 ± 4.9 months, which is less than prior studies on 5-ALA FGS (9–11), and may be explained by the patients in the current study. Twelve (75%) patients had tumors in eloquent cortex, which may be less amenable to maximal resection, therefore conferring a lower overall survival. Additionally, multiple patients in the cohort had surgery for recurrent GBM, which is also associated with a lower overall survival rate (37, 38). While this cohort is smaller than prior clinical trials, it did not appear that earlier administration of 5-ALA had an impact on both surgical factors and patient outcomes.

LIMITATIONS

Despite the strengths of this study, there are limitations that must be addressed. The most significant limitation to the present study is the design. As a small, retrospective, single-arm study, the level of evidence is limited, and patient and clinical variables were not able to be controlled. Historical controls were used rather than a randomized control group, and therefore findings from our study may only be assessed as associations, rather than causational. Additionally, the current study was performed at two centers over a 2-year period, and therefore the results may not be representative of other centers. Intraoperative fluorescence was assessed by the primary surgeon and verified by a second surgeon, and no quantified data was

TABLE 3 | Radiographic and clinical patient outcomes.

Variable	Patients, % (*N* = 16)
5-ALA-related toxicity	0 (0)
Residual contrast enhancement on postoperative MRI	13 (81.3)
Residual volume, cc (mean, SD)	1.16 ± 1.11
Percent extent of resection (EOR, mean, SD)	91.5 ± 10.7
Chemotherapy or radiation received	15 (93.8)
Total clinical follow-up, months (mean, SD)	5.7 ± 4.4
New neurological deficit	4 (26.7)
mRS	2.3 ± 1.3
Karnofsky score	71.9 ± 22.1
NIHSS	3.9 ± 2.4
Total radiographic follow-up, months (mean, SD)	3.8 ± 3.1
Radiographic recurrence or progression	8 (50.0)
Time to recurrence or progression, months (mean, SD)[$]	5 ± 3
Mortality	6 (37.5)
Time to mortality, months (mean, SD)[#]	6.3 ± 4.9
6-month progression-free survival[@]	6 (46.2)

Missing data: [$]Out of 4 patients that had recurrence/progression. [#]Out of 3 patients that died. [@]Missing 2 patients operated on <6 months ago.

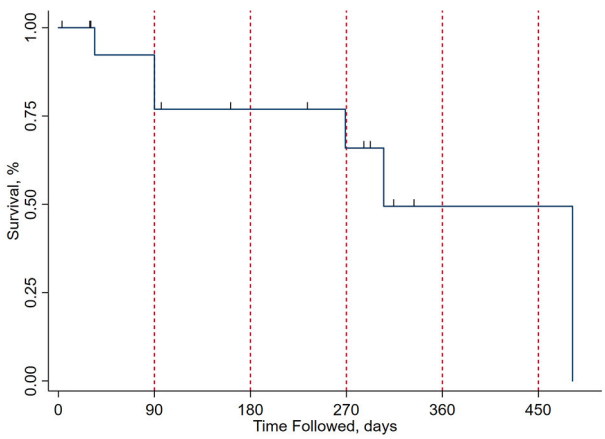

FIGURE 3 | Kaplan-Meier curve for survival after surgical excision on the present cohort. The x axis represents time from surgical excision in days, with red vertical dashed lines at the 3-, 6-, 9-, 12-, and 15-month marks. The y axis represents the percentage of patients surviving at each time point. Drop points in the curve represent patient mortality and the short vertical lines represent subject concealment from further calculations due to end of follow-up, with patients either lost to follow-up or being operated on recently from the time of analysis.

obtained, therefore, there may be an observer bias as there were no controls and subjects were not blinded. To address many of these limitations, a larger, multicenter randomized controlled trial is warranted to determine the safety and efficacy of 5-ALA administration at a longer time window between administration and surgical resection.

CONCLUSION

In this preliminary case series, we demonstrate that 5-ALA FGS can be carried out safely more than 6 h after administration of the substance, with clinical results being largely similar to previous reports. The relaxation on restrictions regarding timing of surgery after 5-ALA administration could have positive implications on procedure scheduling and workflow in busy neurosurgical centers, without any additional risk to patient safety and surgical outcomes.

DATA AVAILABILITY STATEMENT

The raw data supporting the conclusions of this article will be made available by the authors, without undue reservation.

ETHICS STATEMENT

The studies involving human participants were reviewed and approved by Mount Sinai Institutional Review Board. Written informed consent for participation was not required for this study in accordance with the national legislation and the institutional requirements.

AUTHOR CONTRIBUTIONS

All authors listed have made a substantial, direct and intellectual contribution to the work, and approved it for publication.

REFERENCES

1. Stupp R, Mason WP, van den Bent MJ, Weller M, Fisher B, Taphoorn MJ, et al. Radiotherapy plus concomitant and adjuvant temozolomide for glioblastoma. *N Engl J Med.* (2005) 352:987–96. doi: 10.1056/NEJMoa043330
2. Cairncross JG, Wang M, Jenkins RB, Shaw EG, Giannini C, Brachman DG, et al. Benefit from procarbazine, lomustine, and vincristine in oligodendroglial tumors is associated with mutation of IDH. *J Clin Oncol.* (2014) 32:783–90. doi: 10.1200/JCO.2013.49.3726
3. van den Bent MJ, Brandes AA, Taphoorn MJ, Kros JM, Kouwenhoven MCM, Delattre JY, et al. Adjuvant procarbazine, lomustine, and vincristine chemotherapy in newly diagnosed anaplastic oligodendroglioma: long-term follow-up of EORTC brain tumor group study 26951. *J Clin Oncol.* (2013) 31:344–350. doi: 10.1200/JCO.2012.43.2229
4. Wick W, Roth P, Hartmann C, Stockhammer F, Sabel MC, Wick A, et al. Long-term analysis of the NOA-04 randomized phase III trial of sequential radiochemotherapy of anaplastic glioma with PCV or temozolomide. *Neuro Oncol.* (2016) 18:1529–37. doi: 10.1093/neuonc/now133
5. Chang S, Zhang P, Cairncross JG, Gilbert MR, Bahary JP, Dolinskas CA, et al. Phase III randomized study of radiation and temozolomide versus radiation and nitrosourea therapy for anaplastic astrocytoma: results of NRG Oncology RTOG 9813. *Neuro Oncol.* (2017) 19:252–58. doi: 10.1093/neuonc/now313
6. Lacroix M, Abi-Said D, Fourney DR, Gokaslan ZL, Shi W, DeMonte F, et al. A multivariate analysis of 416 patients with glioblastoma multiforme: prognosis, extent of resection, and survival. *J Neurosurg.* (2001) 95:190–8. doi: 10.3171/jns.2001.95.2.0190
7. Marko NF, Weil RJ, Schroeder JL, Lang FF, Suki D, Sawaya RE. Extent of resection of glioblastoma revisited: personalized survival modeling facilitates more accurate survival prediction and supports a maximum-safe-resection approach to surgery. *J Clin Oncol.* (2014) 32:774–82. doi: 10.1200/JCO.2013.51.8886
8. Orringer D, Lau D, Khatri S, Zamora-Berridi GJ, Zhang K, Wu C, et al. Extent of resection in patients with glioblastoma: limiting factors, perception of resectability, and effect on survival. *J Neurosurg.* (2012) 117:851–9. doi: 10.3171/2012.8.JNS12234
9. Stummer W, Pichlmeier U, Meinel T, Wiestler OD, Zanella F, Reulen HJ, et al. Fluorescence-guided surgery with 5-aminolevulinic acid for resection of malignant glioma: a randomised controlled multicentre phase III trial. *Lancet Oncol.* (2006) 7:392–401. doi: 10.1016/S1470-2045(06)70665-9
10. Stummer W, Novotny A, Stepp H, Goetz C, Bise K, Reulen HJ. Fluorescence-guided resection of glioblastoma multiforme by using 5-aminolevulinic acid-induced porphyrins: a prospective study in 52 consecutive patients. *J Neurosurg.* (2000) 93:1003–13. doi: 10.3171/jns.2000.93.6.1003
11. Senders JT, Muskens IS, Schnoor R, Karhade AV, Cote DJ, Smith TR, et al. Agents for fluorescence-guided glioma surgery: a systematic review of preclinical and clinical results. *Acta Neurochir.* (2017) 159:151–67. doi: 10.1007/s00701-016-3028-5
12. Colditz MJ, Leyen K, Jeffree RL. Aminolevulinic acid (ALA)-protoporphyrin IX fluorescence guided tumour resection. Part 2: theoretical, biochemical and practical aspects. *J Clin Neurosci.* (2012) 19:1611–6. doi: 10.1016/j.jocn.2012.03.013
13. Zehri AH, Ramey W, Georges JF, Mooney MA, Martirosyan NL, Preul MC, et al. Neurosurgical confocal endomicroscopy: a review of contrast agents, confocal systems, and future imaging modalities. *Surg Neurol Int.* (2014) 5:60. doi: 10.4103/2152-7806.131638
14. Teixidor P, Arraez MA, Villalba G, Garcia R, Tardáguila M, González JJ, et al. Safety and efficacy of 5-aminolevulinic acid for high grade glioma in usual clinical practice: a prospective cohort study. *PLoS ONE.* (2016) 11:e0149244. doi: 10.1371/journal.pone.0149244
15. Hadjipanayis CG, Stummer W. 5-ALA and FDA approval for glioma surgery. *J Neurooncol.* (2019) 141:479–86. doi: 10.1007/s11060-019-03098-y
16. CDC. Aminolevulinic acid hydrochloride, known as ALA HCl (Gleolan, NX Development Corp.) as an optical imaging agent indicated in patients with gliomas (2017). Available online at: https://www.fda.gov/drugs/resources-information-approved-drugs/aminolevulinic-acid-hydrochloride-known-ala-hcl-gleolan-nx-development-corp-optical-imaging-agent (accessed June 3, 2020).
17. Stummer W, Stocker S, Novotny A, Heimann A, Sauer O, Kempski O, et al. *In vitro* and *in vivo* porphyrin accumulation by C6 glioma cells after exposure to 5-aminolevulinic acid. *J Photochem Photobiol B.* (1998) 45:160–9. doi: 10.1016/S1011-1344(98)00176-6
18. Kaneko S, Suero Molina E, Ewelt C, Warneke N, Stummer W. Fluorescence-based measurement of real-time kinetics of protoporphyrin IX after 5-aminolevulinic acid administration in human in situ malignant gliomas. *Neurosurgery.* (2019) 85:E739–46. doi: 10.1093/neuros/nyz129
19. Pichlmeier U, Bink A, Schackert G, Stummer W, the ALA Glioma Study Group. Resection and survival in glioblastoma multiforme: an RTOG recursive partitioning analysis of ALA study patients. *Neuro Oncol.* (2008) 10:1025–34. doi: 10.1215/15228517-2008-052
20. Stummer W, Suero Molina E. Fluorescence imaging/agents in tumor resection. *Neurosurg Clin N Am.* (2017) 28:569–83. doi: 10.1016/j.nec.2017.05.009
21. Stummer W, Tonn JC, Goetz C, Ullrich W, Stepp H, Bink A, et al. 5-Aminolevulinic acid-derived tumor fluorescence: the diagnostic accuracy of visible fluorescence qualities as corroborated by spectrometry and histology and postoperative imaging. *Neurosurgery.* (2014) 74:310–9. doi: 10.1227/NEU.0000000000000267

22. Stummer W, Tonn JC, Mehdorn HM, Nestler U, Franz K, Goetz C, et al. Counterbalancing risks and gains from extended resections in malignant glioma surgery: a supplemental analysis from the randomized 5-aminolevulinic acid glioma resection study. *Clinical article. J Neurosurg.* (2011) 114:613–23. doi: 10.3171/2010.3.JNS097
23. Valdes PA, Fan X, Ji S, Harris BT, Paulsen KD, Roberts DW. Estimation of brain deformation for volumetric image updating in protoporphyrin IX fluorescence-guided resection. *Stereotact Funct Neurosurg.* (2010) 88:1–10. doi: 10.1159/000258143
24. Valdes PA, Kim A, Brantsch M, Niu C, Moses ZB, Tosteson TD, et al. delta-aminolevulinic acid-induced protoporphyrin IX concentration correlates with histopathologic markers of malignancy in human gliomas: the need for quantitative fluorescence-guided resection to identify regions of increasing malignancy. *Neuro Oncol.* (2011) 13:846–56. doi: 10.1093/neuonc/nor086
25. Valdes PA, Leblond F, Kim A, Harris BT, Wilson BC, Fan X, et al. Quantitative fluorescence in intracranial tumor: implications for ALA-induced PpIX as an intraoperative biomarker. *J Neurosurg.* (2011) 115:11–7. doi: 10.3171/2011.2.JNS101451
26. Jaber M, Wolfer J, Ewelt C, Holling M, Hasselblatt M, Niederstadt T, et al. The value of 5-aminolevulinic acid in low-grade gliomas and high-grade gliomas lacking glioblastoma imaging features: an analysis based on fluorescence, magnetic resonance imaging, 18F-fluoroethyl tyrosine positron emission tomography, and tumor molecular factors. *Neurosurgery*. (2016) 78:401–11. doi: 10.1227/NEU.0000000000001020
27. Johansson A, Palte G, Schnell O, Tonn JC, Herms J, Stepp H. 5-Aminolevulinic acid-induced protoporphyrin IX levels in tissue of human malignant brain tumors. *Photochem Photobiol.* (2010) 86:1373–8. doi: 10.1111/j.1751-1097.2010.00799.x
28. Kaneko S, Kaneko S. Fluorescence-guided resection of malignant glioma with 5-ALA. *Int J Biomed Imaging*. (2016) 2016:6135293. doi: 10.1155/2016/6135293
29. Lau D, Hervey-Jumper SL, Chang S, Molinaro AM, McDermott MW, Phillips JJ, et al. A prospective Phase II clinical trial of 5-aminolevulinic acid to assess the correlation of intraoperative fluorescence intensity and degree of histologic cellularity during resection of high-grade gliomas. *J Neurosurg.* (2016) 124:1300–9. doi: 10.3171/2015.5.JNS1577
30. Roberts DW, Valdes PA, Harris BT, Fontaine KM, Hartov A, Fan X, et al. Coregistered fluorescence-enhanced tumor resection of malignant glioma: relationships between delta-aminolevulinic acid-induced protoporphyrin IX fluorescence, magnetic resonance imaging enhancement, and neuropathological parameters. Clinical article. *J Neurosurg.* (2011) 114:595–603. doi: 10.3171/2010.2.JNS091322
31. Roessler K, Becherer A, Donat M, Cejna M, Zachenhofer I. Intraoperative tissue fluorescence using 5-aminolevolinic acid (5-ALA) is more sensitive than contrast MRI or amino acid positron emission tomography ((18)F-FET PET) in glioblastoma surgery. *Neurol Res.* (2012) 34:314–7. doi: 10.1179/1743132811Y.0000000078
32. Stummer W, Stepp H, Wiestler OD, Pichlmeier U. Randomized, prospective double-blinded study comparing 3 different doses of 5-aminolevulinic acid for fluorescence-guided resections of malignant gliomas. *Neurosurgery*. (2017) 81:230–9. doi: 10.1093/neuros/nyx074
33. Aldave G, Tejada S, Pay E, Marigil M, Bejarano B, Idoate MA, et al. Prognostic value of residual fluorescent tissue in glioblastoma patients after gross total resection in 5-aminolevulinic Acid-guided surgery. *Neurosurgery*. (2013) 72:915–20. doi: 10.1227/NEU.0b013e31828c3974
34. Ballard B. *Center for Drug Evaluation and Research: Clinical Review.* (2015). Available online at: https://www.accessdata.fda.gov/drugsatfda_docs/nda/2017/208630Orig1s000MedR.pdf. (accessed June 15, 2020).
35. Rick K, Sroka R, Stepp H, Kriegmair M, Huber RM, Jacob K, et al. Pharmacokinetics of 5-aminolevulinic acid-induced protoporphyrin IX in skin and blood. *J Photochem Photobiol B.* (1997) 40:313–9. doi: 10.1016/S1011-1344(97)00076-6
36. Eljamel MS, Goodman C, Moseley H. ALA and Photofrin fluorescence-guided resection and repetitive PDT in glioblastoma multiforme: a single centre Phase III randomised controlled trial. *Lasers Med Sci.* (2008) 23:361–7. doi: 10.1007/s10103-007-0494-2
37. Botros D, Dux H, Price C, Khalafallah AM, Mukherjee D. Assessing the efficacy of repeat resections in recurrent glioblastoma: a systematic review. *Neurosurg Rev.* (2020). doi: 10.1007/s10143-020-01331-1. [Epub ahead of print].
38. McNamara MG, Lwin Z, Jiang H, Templeton AJ, Zadeh G, Bernstein M, et al. Factors impacting survival following second surgery in patients with glioblastoma in the temozolomide treatment era, incorporating neutrophil/lymphocyte ratio and time to first progression. *J Neurooncol.* (2014) 117:147–52. doi: 10.1007/s11060-014-1366-9

Conflict of Interest: CH is a consultant for NX Development Corporation (NXDC) and Synaptive Medical. NXDC, a privately held company, markets Gleolan (5-ALA, aminolevulinic acid hydrochloride). Gleolan is an optical imaging agent approved for the visualization of malignant tissue during glioma surgery. CH is a consultant for NXDC and receives royalty payments for the sale of Gleolan. CH receives financial compensation as a consultant and lecturer for Synaptive (manufacturer of the 3D Synaptive MODUS V device). He has also received speaker fees by Carl Zeiss and Leica.

The remaining authors declare that the research was conducted in the absence of any commercial or financial relationships that could be construed as a potential conflict of interest.

frontiers in Oncology

ORIGINAL RESEARCH
published: 10 May 2021
doi: 10.3389/fonc.2021.654300

Optical Characterization of Sodium Fluorescein *In Vitro* and *Ex Vivo*

Ran Xu[1†], Wanda Teich[1†], Florian Frenzel[2], Katrin Hoffmann[2], Josefine Radke[3,4,5], Judith Rösler[1], Katharina Faust[1], Anne Blank[1], Susan Brandenburg[1], Martin Misch[1], Peter Vajkoczy[1], Julia Sophie Onken[1,4‡] and Ute Resch-Genger[2‡]*

[1] Department of Neurosurgery, Charité—Universitätsmedizin Berlin, Corporate Member of Freie Universität Berlin, and Humboldt-Universität zu Berlin, and Berlin Institute of Health, Berlin, Germany, [2] Division Biophotonics, Federal Institute for Materials Research and Testing (BAM), Berlin, Germany, [3] Department of Neuropathology, Charité—Universitätsmedizin Berlin, Corporate Member of Freie Universität Berlin, Humboldt-Universität zu Berlin, and Berlin Institute of Health, Berlin, Germany, [4] German Cancer Consortium (DKTK), Heidelberg, Germany, partner site Charité Berlin, Berlin, Germany, [5] Berlin Institute of Health (BIH), Berlin, Germany

OPEN ACCESS

Edited by:
Karl-Michael Schebesch, University of Regensburg, Germany

Reviewed by:
Julius Höhne, University Medical Center Regensburg, Germany
Jens Gempt, Technische Universität München, Germany

***Correspondence:**
Ran Xu
ran.xu@charite.de

†These authors have contributed equally to this work and share first authorship

‡These authors share last authorship

Specialty section:
This article was submitted to Neuro-Oncology and Neurosurgical Oncology, a section of the journal Frontiers in Oncology

Received: *15 January 2021*
Accepted: *07 April 2021*
Published: *10 May 2021*

Citation:
Xu R, Teich W, Frenzel F, Hoffmann K, Radke J, Rösler J, Faust K, Blank A, Brandenburg S, Misch M, Vajkoczy P, Onken JS and Resch-Genger U (2021) Optical Characterization of Sodium Fluorescein In Vitro and Ex Vivo. Front. Oncol. 11:654300. doi: 10.3389/fonc.2021.654300

Objective: The utilization of fluorescein-guided biopsies and resection has been recently discussed as a suitable strategy to improve and expedite operative techniques for the resection of central nervous system (CNS) tumors. However, little is known about the optical properties of sodium fluorescein (NaFl) in human tumor tissue and their potential impact on *ex vivo* analyses involving fluorescence-based methods.

Methods: Tumor tissue was obtained from a study cohort of an observational study on the utilization of fluorescein-guided biopsy and resection (n=5). The optical properties of fluorescein-stained tissue were compared to the optical features of the dye *in vitro* and in control samples consisting of tumor tissue of high-grade glioma patients (n=3) without intravenous (i.v.) application of NaFl. The dye-exposed tumor tissues were used for optical measurements to confirm the detectability of NaFl emission *ex vivo*. The tissue samples were fixed in 4%PFA, immersed in 30% sucrose, embedded in Tissue-Tek OCT compound, and cut to 10 µm cryosections. Spatially resolved emission spectra from tumor samples were recorded on representative slides with a Confocal Laser Scanning Microscope FV1000 (Olympus GmbH, Hamburg, Germany) upon excitation with λ_{exc} = 488 nm.

Results: Optical measurements of fluorescein in 0.9% sodium chloride (NaCl) under *in vitro* conditions showed an absorption maximum of $\lambda_{max\ abs}$ = 479 nm as detected with spectrophotometer Specord 200 and an emission peak at $\lambda_{max\ em}$ = 538 nm recorded with the emCCD detection system of a custom-made microscope-based single particle setup using a 500 nm long-pass filter. Further measurements revealed pH- and concentration-dependent emission spectra of NaFl. Under ex vivo conditions, confocal laser scanning microscopy of fluorescein tumor samples revealed a slight bathochromic shift and a broadening of the emission band.

Conclusion: Tumor uptake of NaFl leads to changes in the optical properties – a bathochromic shift and broadening of the emission band – possibly caused by the dye's high pH sensitivity and concentration-dependent reabsorption acting as an inner

filter of the dye's emission, particularly in the short wavelength region of the emission spectrum where absorption and fluorescence overlap. Understanding the *ex vivo* optical properties of fluorescein is crucial for testing and validating its further applicability as an optical probe for intravital microscopy, immunofluorescence localization studies, and flow cytometry analysis.

Keywords: sodium fluorescein, spectroscopy, brain tumor, confocal, fluorescein-guided surgery, optical probe pH sensing, NaFl

INTRODUCTION

The utilization of fluorescein as an optical probe for guiding the resection and biopsy of central nervous system (CNS) tumors has been recently proposed as a powerful strategy to improve and expedite operative techniques (1–4). Sodium fluorescein (NaFl) is a fluorescent dye with a molecular weight of 376.3 g/mol that accumulates in tumor tissue where blood brain barrier (BBB) breakdown occurs and thus, enhances tumor visualization, contributing to the extent of resection which is in turn associated with a better overall survival rate (5–9). This dye has been successfully implemented in clinical applications in ophthalmology; in recent years, its implications for CNS tumor resection, as well as for vascular neurosurgery techniques have also been discussed (10–13).

However, little is known about the spectroscopic characteristics of fluorescein after its intravenous (i.v.) application, as it traverses the BBB and accumulates in tumor tissue. The tumor microenvironment is a complex compartment with spatiotemporal variability in tumor cells, acidity, hypoxia, secreted factors, and extracellular matrix proteins. Moreover, it is unknown how the dye is metabolized in this environment. This encouraged us to characterize the *in vitro* and *ex vivo* optical characteristics of NaFl to understand its spectroscopic features after biological tissue uptake with special emphasis on its potential further implications of fluorescent-based assays.

MATERIAL AND METHODS

Patients and Specimen Handling

The study was approved by the local Ethical Committee (EA1/284/20, EA4/219/17 and EA2/101/08) of the Charité University Hospital. All patients gave written consent for the off-label use of i.v. fluorescein-guided surgery or biopsy. All study patients had a contrast-enhancing lesion in which surgical resection was indicated, and their characteristics are listed in **Table 1**. The workflow of the experimental setup of human tissue is shown in **Figure 1**. Briefly, patients received intraoperatively a dosage of 5 mg/kg Fluorescein Alkon i.v. according to our standardized operating procedure for brain tumor surgery (n=5). Tumor surgery was performed in a standard fashion using the Pentero 900 microscope with Y560 filter, Carl Zeiss, Meditec, Oberkochen, Germany. The dye-exposed tumor tissue was brought to the laboratory on ice, and immediately fixed in 4% PFA overnight at 4°C, then immersed in 30% sucrose, and embedded in Tissue-Tek® O.C.T.™ compound. Cryosections were cut into slices of 10 µm thickness. Control samples (n=3) consisted of glioma tumor samples from patients who did not receive fluorescein-guided surgery due to contraindications. Hematoxylin & Eosin (H&E) staining was performed using a standard methodology and staining reagents. Images were collected using a Carl Zeiss Axio observer Z1 inverted immunofluorescence microscope equipped with standard DAPI (filter 49, excitation 365 nm, emission 445 ± 25nm), FITC (filter 38, excitation 470 ± 20nm, emission 525 ± 25nm nm), and Cy3 (filter 43, excitation 545 ± 12.5nm, emission 605 ± 35nm) filters, respectively.

Spectroscopy of NaFl *In Vitro*

The absorbance spectrum of fluorescein in 0.9% NaCl was measured in a cuvette with the spectrophotometer Specord 200. The emission spectrum of fluorescein in 0.9% NaCl under 488 nm laser excitation (Supercontinuum Laser Solea, PicoQuant) was recorded with a custom-made microscope-based single particle setup equipped with a 500 nm long-pass filter using the emCCD detection system (DU970P-BVF, Andor Ltd.).

Concentration- and pH-dependent emission spectra of NaFl *in vitro* were recorded using a spectral scanning Confocal Laser Scanning Microscope (CLSM) FluoView FV1000 (Olympus GmbH, Hamburg, Germany). The emission spectra were measured in droplets of the corresponding NaFl solutions, which were placed on standard microscopy coverslips #1.5 (0.170 mm). A multiline argon ion laser (30 mW) was used as excitation source (λ_{exc} = 488 nm), which was reflected by a beam splitter (BS 20/80) and focused onto the sample through an Olympus objective UPLSAPO 20x (numerical aperture N.A. 0.75). The emitted photons were collected with the same objective, focused onto a photomultiplier (PMT), and recorded in the wavelength range of 500 - 640 nm (spectral resolution of 2.0 nm, step sizes of 2.0 nm).

Spectroscopy of NaFl *Ex Vivo*

Spatially resolved emission spectra of tumor samples were recorded on representative tumor sections. Exemplarily chosen, but representative 10 regions of interests (ROIs) within the tumor tissue and one additional ROI as a blank or baseline control (recording background noise) were measured with the FV1000 (Olympus GmbH, Hamburg, Germany) upon excitation with λ_{exc} = 488 nm under almost the same experimental settings and conditions as described above. The *ex vivo* spectra, however, were measured in derogation through an objective UPLSAPO 20xW/0.75 in the range of 500 nm - 740 nm (spectral resolution of 5.0 nm and step sizes of 2.0 nm).

TABLE 1 | Patient characteristics.

	Age	Gender	Localization	Extent of resection	Histology
Fluorescein	50	M	Left temporolateral	Resection	Glioblastoma, IDH-wildtype (WHO grade IV), MGMT methylated
	58	M	Left temporopolar	Resection	Glioblastoma, IDH-wildtype (WHO grade IV), MGMT methylation
	87	M	Left temporolateral	Biopsy	Glioblastoma, IDH-wildtype (WHO grade IV), MGMT unmethylated
	71	F	Left temporomesial	Biopsy	Diffuse large B-cell lymphoma
	61	M	Left occipital	Resection	Post-transplant lymphoproliferative disorder (PTLD)
Control	24	F	Left temporomesial	Resection	Glioblastoma (WHO grade IV), MGMT unmethylated
	35	F	Right temporolateral	Resection	Glioblastoma (WHO grade IV), MGMT methylation
	64	F	Left frontal operculum	Resection	Glioblastoma (WHO grade IV), MGMT methylation

F, female; M, male.

Statistical Analysis and Figures

Values are generally presented as mean +/- SEM unless otherwise stated. Statistical significance was determined by Student t-test and statistical analysis was performed using Graphpad Prism software (Version 7.0). Elements of **Figures 1** and **5** were composed using BioRender.Com.

RESULTS

NaFl Tumor Samples Show Positive Signal in Both Green and Red Channels

To examine whether NaFl tumor tissue still showed measurable FITC signal after fixation, frozen sections were analyzed in the FITC channel of a fluorescent microscope. Indeed, all the samples exhibited a heterogeneous pattern of FITC signal (**Figure 2**). To clarify that the area of interest was in fact vital tumor tissue, consecutive sections were subjected to Hematoxylin & Eosin (H&E) staining and examined by a consultant neuropathologist to confirm the histopathological diagnosis of the rapid frozen sections (**Figure 2**). However, all samples showed also fluorescence signals in the CY3 channel (**Figure 2**). This observation was surprising since NaFl should not reveal a signal in the CY3 channel separated by the CY3 filter (covering the emission wavelength region of 605 ± 35nm by its transmission profile) under baseline *ex vivo* conditions. The observed changes in the spectroscopic features of NaFl might be of significant relevance in the future, e.g. for the in-depth analysis of *in vivo* tumor imaging using NaFl. To better

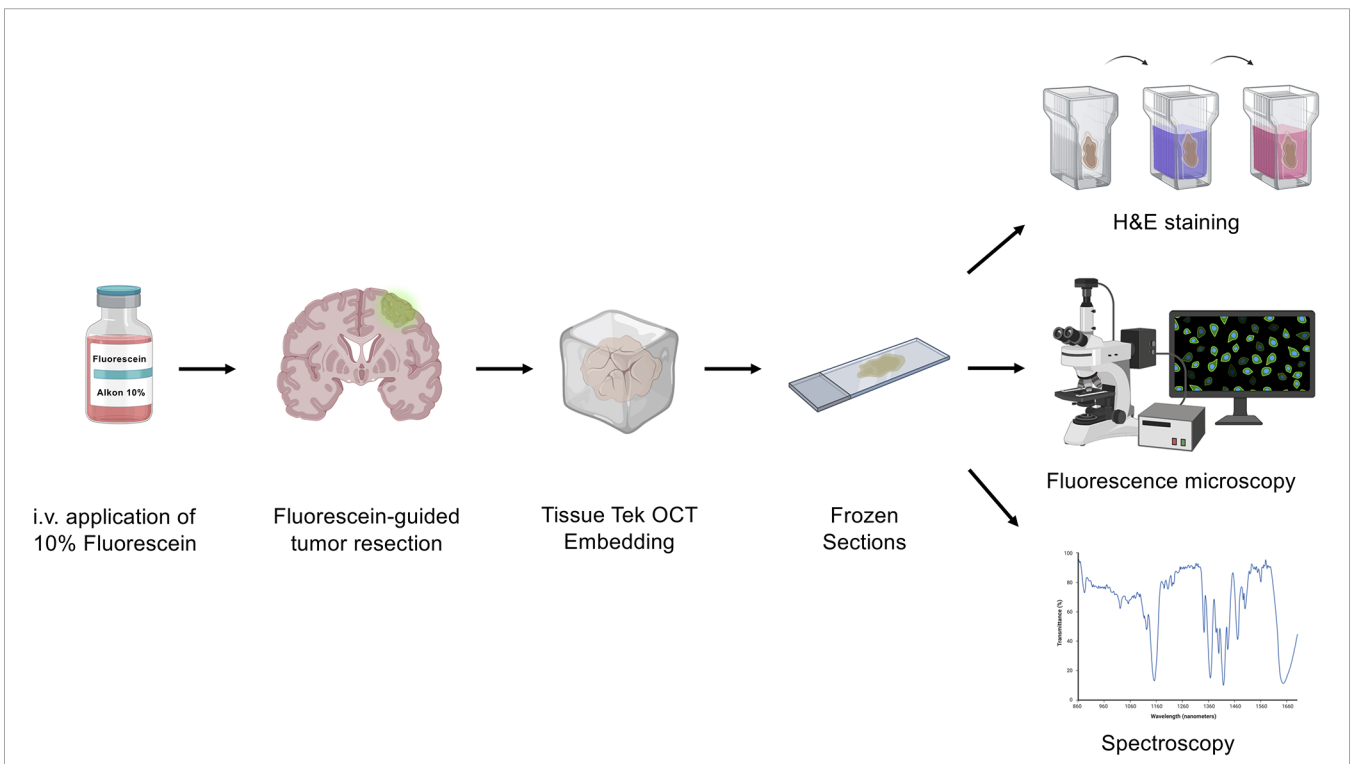

FIGURE 1 | Experimental workflow. Before tumor resection, patients received sodium fluorescein (NaFl) intravenously (i.v.). After fixation in 4% PFA and 30% sucrose immersion, the NaFl-stained tissue was embedded in Tissue-Tek OCT before cryosectioning. Frozen sections were then studied by fluorescence microscopy and spectroscopy measurements.

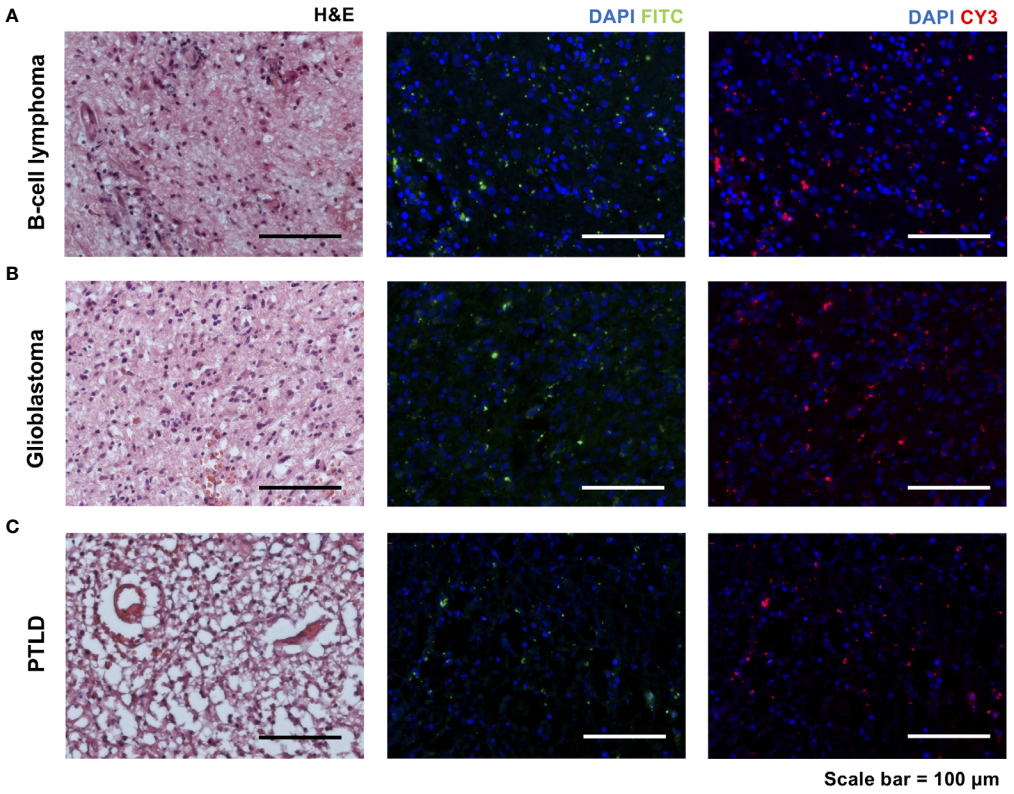

FIGURE 2 | Hematoxylin and eosin (H&E) staining of rapid sections in three different pathologies [**A**, B-cell lymphoma, **B**, glioblastoma, and **C**, posttransplant lymphoproliferative disorder (PTLD)] with consecutive slides using FITC and CY3 filters of an immunofluorescence microscope. All samples showed signals in the FITC channel, and unexpectedly, also in the CY3 channel (scale bar = 100 µm).

understand this shift in emission wavelength we performed a series of *in vitro* and *ex vivo* studies to characterize the optical properties of our optical probe.

Absorbance and Emission of NaFl *In Vitro*

Next, to elucidate the optical properties of NaFl *in vitro*, we measured absorbance and emission spectra of NaFl under *in vitro* conditions. Here, we observed a typical absorbance peak at $\lambda_{max\ abs}$ = 479 nm and an emission peak at $\lambda_{max\ em}$ = 538 nm (**Figure 3A**). These absorbance and emission maxima match well with the previously reported spectroscopic features of fluorescein (14).

Fluorescein-Stained Tumor Tissue Shows a Bathochromic Shift in Emission *Ex Vivo*

We next compared the *in vitro* emission spectra of NaFl to the corresponding emission spectra obtained *ex vivo* to better understand the optical behavior of this dye within the tumor core. Interestingly, in representative tumor samples, we observed a broadening of the dye's emission band and a slight, but significant spectral shift to longer wavelengths, also known as a bathochromic shift, compared to NaFl in buffer solution pH 8.04 *in vitro* (**Figure 3B**). The control samples showed a significantly lower emission intensity with a mean intensity of 530.6 (± 67.58) a.u. [= arbitrary (or relative) units] compared to 971.1 (± 146.1) a.u. at a wavelength of 540 nm in the NaFl tumor samples (p=0.0441) (**Figures 3C, D**).

pH-Dependent and Concentration-Dependent Emission

Since NaFl showed heterogeneous uptake in tumor tissue, we examined whether this finding could be explained by the characteristic pH-dependent emission features of the dye - also given that previous studies highlighted an acidic milieu of the tumor microenvironment contributing to a change in pH (15, 16). Therefore, we measured the absorbance spectra of NaFl in 0.9% NaCl solution and its emission spectra in different phosphate buffers (pH 5.54, pH 7.35, and pH 8.04). Our results reveal the well-known pH-dependence of the NaFl emission intensity that increases with increasing pH (**Figure 4A**) (17). Also, the heterogeneous uptake of the dye leading to different local NaFl concentrations could contribute to the spectroscopic effects observed *ex vivo*. Hence, we measured the spectra of NaFl *in vitro* at different dye concentrations. Thereby, we noticed not only a concentration-dependent emission intensity of the dye (**Figures 4B, C**), but also observed a red shift in the emission maxima with increasing NaFl concentrations (**Figure 4D**).

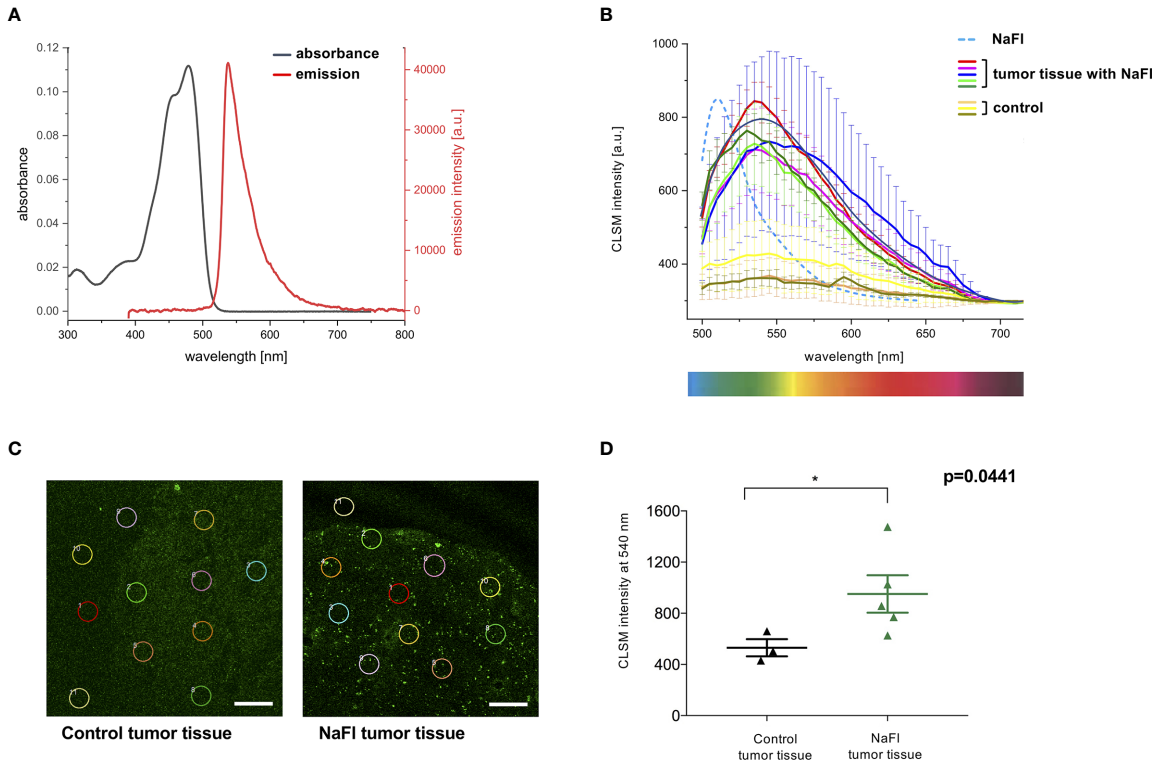

FIGURE 3 | Absorbance and emission of NaFl *in vitro* and *ex vivo*. **(A)** Absorbance (black line) and emission spectra (red line) under *in vitro* conditions show the typical maximum absorbance at $\lambda_{max\ abs}$ = 479 nm and an emission peak at $\lambda_{max\ em}$ = 538 nm. **(B)** Confocal Laser Scanning Microscopy (CLSM) emission spectra of NaFl in phosphate buffer solution at pH 8.04 *in vitro* (blue dashed line) and in *ex vivo* samples (colored solid lines). Exemplary, but representative *ex vivo* tumor samples with NaFl show a broadened, bathochromically shifted NaFl tumor emission (solid lines). A broad but very weak emission in the same wavelength region was also observed for the control samples. **(C, D)** Exemplary, but representative CLSM intensities of 10 regions of interests (ROIs) read out at 540 nm show a significantly higher signal in fluorescein tumor samples (971.1 ± 146.1 a.u.) versus control samples (530.6 ± 67.58 a.u.); p= 0.0441. Values are expressed in average ± S.E.M. (Scale bar = 100 µm).

DISCUSSION

Our results show that NaFl exhibits a significant broadening of its emission band together with a bathochromic shift after tissue uptake in CNS tumor samples. These changes could possibly be explained by the dye's high pH sensitivity and/or concentration-dependent reabsorption effects (**Figure 5**).

Furthermore, our data reveal a very heterogeneous distribution pattern of NaFl in tumor tissue on a microscopic level. This can also be observed intraoperatively by the neurosurgeon on a macroscopic scale. Traditionally, a heterogeneous uptake can be related to a variability in BBB properties and regionally distinct hyperpermeability. Our data show that this heterogeneous emission signal of the dye is also influenced by the dye's high pH sensitivity, potentially caused by the variability of the acidic milieu in the tumor microenvironment. This acidic milieu has also been discussed in the literature as a driver of cancer development (15). The fluorescein molecule can exist in different protonation states which all differ in their fluorescence features; only the dianion and monoanion of fluorescein emit a visible fluorescence of varying fluorescence efficiency or quantum yield while the neutral dye is non-emissive (17). A more acidic extracellular milieu should lead to the formation of the monoanion while a more basic environment favors the formation of the dye's dianion. This goes along with the pH-dependent emission spectra found for the dye in different buffer solutions. Moreover, the heterogeneous appearance of NaFl uptake in tumor tissue is likely caused by the high sensitivity of the NaFl emission behavior to its concentration. This corresponds with the observed decrease in fluorescence intensity with higher local dye concentration due to reabsorption effects. Our data confirm earlier reports that both the pH of the dye's local environment as well as dye concentration can affect the emission of NaFl, which could explain the findings of our *ex vivo* optical measurements, showing a red shift in fluorescence (18, 19).

The change in the intrinsic spectroscopic properties of fluorophores including spectral shifts and changes in the shape of fluorescence emission spectra caused by different environments have been reported before, and the tumor microenvironment is a complex system with a considerable variability in tumor cells, acidity, secretomes, and extracellular compartments that can likely cause changes in the dye's spectroscopic features (4). For example, another study also reported a bathochromic shift for fluorescein ligands bound to rabbit polyclonal anti-Fluorescein Fab fragments (20).

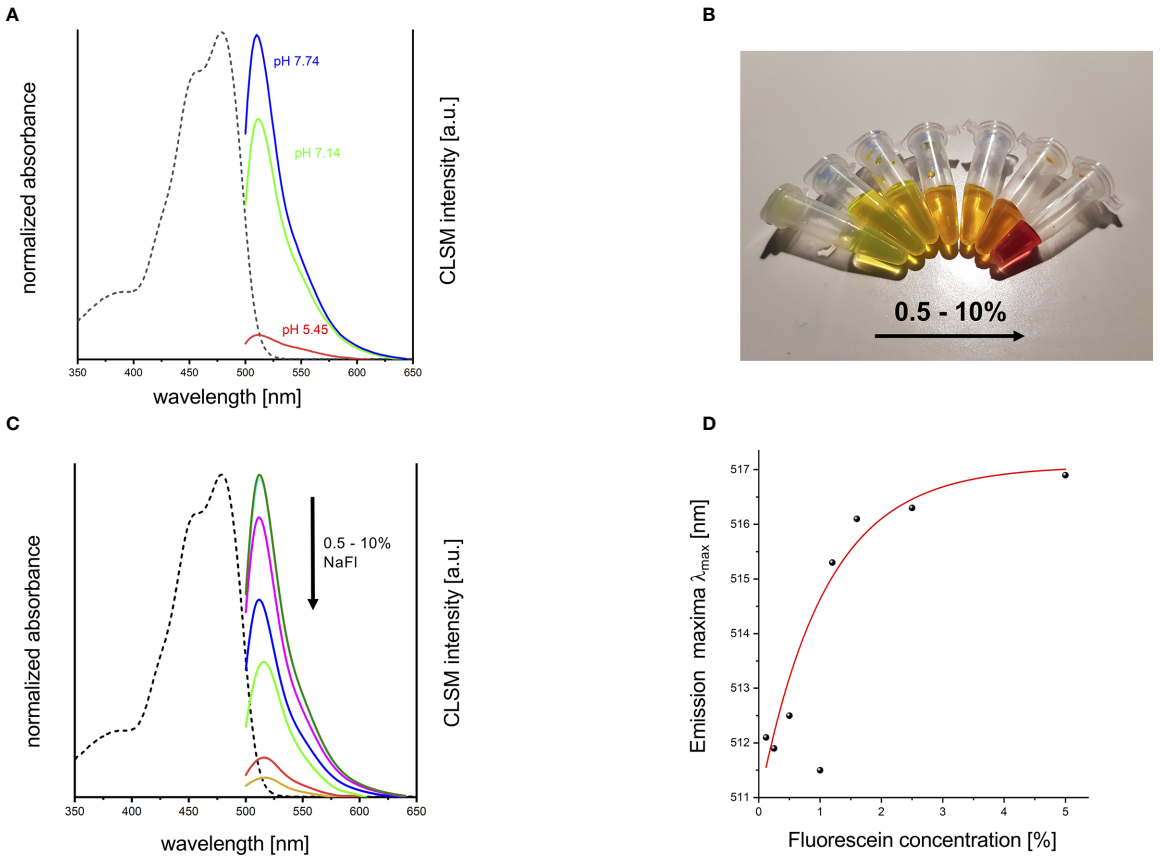

FIGURE 4 | pH- and concentration-dependent emission of NaFl. **(A)** Normalized absorbance (in 0.9% NaCl solution; dashed line) and pH dependent emission spectra of NaFl solutions in different phosphate buffers (phosphate buffer pH 5.54, pH 7.35, and pH 8.04) obtained with a confocal laser scanning microscope (CLSM). **(B)** Concentration series of Na-Fl solutions (in 0.9% NaCl), and **(C)** the corresponding absorbance (in 0.9% NaCl solution; dashed line), and concentration-dependent CLSM emission spectra (solid lines). **(D)** Emission maxima λ_{max} [nm] plotted against NaFl concentration [%] show a concentration-dependent red shift by about 5 nm.

Tumor tissue autofluorescence is a common phenomenon that should be considered, specifically when working with fluorescence-based assays. Some studies even suggest to utilize the spectral characteristics of the autofluorescence signals from glioma cells for diagnostic purposes (21, 22). To verify that autofluorescence signals do not potentially resemble or interfere with the NaFl signal, we measured the emission spectra of native tumor tissue without exposure to NaFl under the same conditions as used for the NaFl measurements. Although this experiment revealed a broad emission band in the green and red wavelength region, control tumor tissue showed only a very weak emission signal compared to the NaFl-stained tumor samples.

Since NaFl has been increasingly used for the guidance of brain tumor resection, it is crucial to understand its *ex vivo* optical properties, since they can impact further in-depth *in vivo* imaging analyses as well as fluorescence-based assays such as FACS analyses, immunofluorescence staining or *in vivo* microscopy (23, 24). The observation in our study that NaFl in tumor tissue revealed signals in the longer wavelength CY3 channel was surprising. The practical implication of these spectral changes is that if further fluorescence-based laboratory studies are conducted on CNS tumor tissue which were resected under fluorescein-guidance, labeling with secondary antibodies using dyes emitting in the FITC or Cy3 channel should be used with care as this can result in spectral interferences and crosstalk. Based on the broadening and bathochromic shift of the emission band, it seems to be more reasonable to switch to secondary antibodies labeled with dyes emitting in the blue (e.g. 350 – 408 nm) or preferably in the far red (630 – 647 nm) and near-IR channels (650 – 750 nm) in assays such as immunofluorescence microscopy and flow cytometry. The implications of the observed changes in optical properties are of relevant nature, especially if these fluorescent-based assays are used for further diagnostic purposes. Furthermore, in the clinical setting, the utilization of NaFl in combination with in-depth *in vivo* and *ex vivo* imaging techniques such as confocal laser endomicroscopy has also been discussed in recent studies in aiding histopathological diagnoses (25, 26). Hence, the increasing role of NaFl in such settings poses increasing interest on NaFl tumor kinetics, and further analysis of its spectroscopic features may help to distinguish its free form from fluorescein metabolites (fluorescein glucuronide).

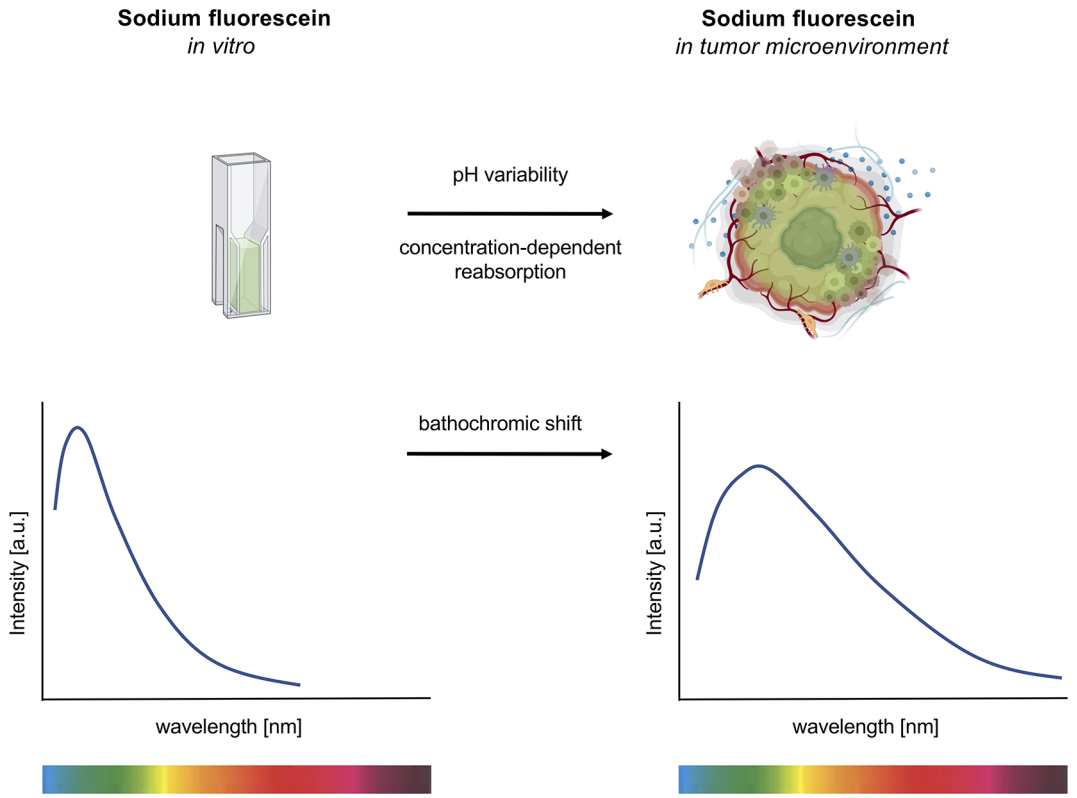

FIGURE 5 | Emission spectroscopy of sodium fluorescein (NaFl) under *in vitro* and *ex vivo* conditions. Exposure of NaFl to the tumor microenvironment shows a broadening and a bathochromic shift of the dye's emission spectrum. The pH sensitivity and the concentration-dependent reabsorption effect of the dye contribute to this red shift.

In summary, our data reveal changes of the spectroscopic properties of NaFl *ex vivo*, particularly a bathochromic shift in emission after tumor uptake, underpinning that the widespread use of fluorescein in neurosurgical procedures requires a detailed study of its optical properties in a clinical setting. Our study is, however, limited by a small sample size, heterogeneity in tumor histology, and the absence of *in vivo* pharmacokinetic properties of NaFl. Further studies are needed to fully understand the exact nature of the changes of the spectroscopic properties of NaFl *ex vivo* and related possible interference with other fluorescence-based assays in tumor tissue.

DATA AVAILABILITY STATEMENT

The raw data supporting the conclusions of this article will be made available by the authors, without undue reservation.

ETHICS STATEMENT

The studies involving human participants were reviewed and approved by Charité's Ethics Committee. The patients/participants provided their written informed consent to participate in this study.

AUTHOR CONTRIBUTIONS

WT, KH, FF, JoR, AB, SB, and RX conducted experiments and analyzed data. RX, JO, and UR-G designed the study. All authors contributed to writing and revising of the manuscript. All authors contributed to the article and approved the submitted version.

FUNDING

RX is supported by the BIH-Charité Clinician Scientist Program funded by the Charité—Universitätsmedizin Berlin and the Berlin Institute of Health. We acknowledge support from the German Research Foundation (DFG) and the Open Access Publication Fund of Charité—Universitaétsmedizin Berlin.

ACKNOWLEDGMENTS

We kindly thank Jimmy LaPrelle for proofreading the manuscript.

REFERENCES

1. Acerbi F, Broggi M, Schebesch KM, Hohne J, Cavallo C, De Laurentis C, et al. Fluorescein-Guided Surgery for Resection of High-Grade Gliomas: A Multicentric Prospective Phase II Study (FLUOGLIO). *Clin Cancer Res* (2018) 24:52–61. doi: 10.1158/1078-0432.CCR-17-1184
2. Rey-Dios R, Hattab EM, Cohen-Gadol AA. Use of Intraoperative Fluorescein Sodium Fluorescence to Improve the Accuracy of Tissue Diagnosis During Stereotactic Needle Biopsy of High-Grade Gliomas. *Acta Neurochir (Wien)* (2014) 156:1071–5. doi: 10.1007/s00701-014-2097-6
3. Stummer W, Novotny A, Stepp H, Goetz C, Bise K, Reulen HJ. Fluorescence-Guided Resection of Glioblastoma Multiforme by Using 5-Aminolevulinic Acid-Induced Porphyrins: A Prospective Study in 52 Consecutive Patients. *J Neurosurg* (2000) 93:1003–13. doi: 10.3171/jns.2000.93.6.1003
4. Hohne J, Acerbi F, Falco J, Akcakaya MO, Schmidt NO, Kiris T, et al. Lighting Up the Tumor-Fluorescein-Guided Resection of Gangliogliomas. *J Clin Med* (2020) 9:2405. doi: 10.3390/jcm9082405
5. Lacroix M, Abi-Said D, Fourney DR, Gokaslan ZL, Shi W, DeMonte F, et al. A Multivariate Analysis of 416 Patients With Glioblastoma Multiforme: Prognosis, Extent of Resection, and Survival. *J Neurosurg* (2001) 95:190–8. doi: 10.3171/jns.2001.95.2.0190
6. 2McGirt MJ, Chaichana KL, Gathinji M, Attenello FJ, Than K, Olivi A, et al. Independent Association of Extent of Resection With Survival in Patients With Malignant Brain Astrocytoma. *J Neurosurg* (2009) 110:156–62. doi: 10.3171/2008.4.17536
7. Brown TJ, Brennan MC, Li M, Church EW, Brandmeir NJ, Rakszawski KL, et al. Association of the Extent of Resection With Survival in Glioblastoma: A Systematic Review and Meta-Analysis. *JAMA Oncol* (2016) 2:1460–9. doi: 10.1001/jamaoncol.2016.1373
8. Stummer W, Reulen HJ, Meinel T, Pichlmeier U, Schumacher W, Tonn JC, et al. Extent of Resection and Survival in Glioblastoma Multiforme: Identification of and Adjustment for Bias. *Neurosurgery* (2008) 62:564–76; discussion 564-76. doi: 10.1227/01.neu.0000317304.31579.17
9. Diaz RJ, Dios RR, Hattab EM, Burrell K, Rakopoulos P, Sabha N, et al. Study of the Biodistribution of Fluorescein in Glioma-Infiltrated Mouse Brain and Histopathological Correlation of Intraoperative Findings in High-Grade Gliomas Resected Under Fluorescein Fluorescence Guidance. *J Neurosurg* (2015) 122:1360–9. doi: 10.3171/2015.2.JNS132507
10. Schebesch KM, Brawanski A, Hohenberger C, Hohne J. Fluorescein Sodium-Guided Surgery of Malignant Brain Tumors: History, Current Concepts, and Future Project. *Turk Neurosurg* (2016) 26:185–94. doi: 10.5137/1019-5149.JTN.16952-16.0
11. Zhao X, Belykh E, Cavallo C, Valli D, Gandhi S, Preul MC, et al. Application of Fluorescein Fluorescence in Vascular Neurosurgery. *Front Surg* (2019) 6:52. doi: 10.3389/fsurg.2019.00052
12. Ward KW. Superficial Punctate Fluorescein Staining of the Ocular Surface. *Optom Vis Sci* (2008) 85:8–16. doi: 10.1097/OPX.0b013e31815ed756
13. Desmettre T, Devoisselle JM, Mordon S. Fluorescence Properties and Metabolic Features of Indocyanine Green (ICG) as Related to Angiography. *Surv Ophthalmol* (2000) 45:15–27. doi: 10.1016/S0039-6257(00)00123-5
14. Sjoback R, Nygren J, Kubista M. Characterization of Fluorescein-Oligonucleotide Conjugates and Measurement of Local Electrostatic Potential. *Biopolymers* (1998) 46:445–53. doi: 10.1002/(SICI)1097-0282(199812)46:7<445::AID-BIP2>3.0.CO;2-5
15. Boedtkjer E, Pedersen SF. The Acidic Tumor Microenvironment as a Driver of Cancer. *Annu Rev Physiol* (2020) 82:103–26. doi: 10.1146/annurev-physiol-021119-034627
16. Petrova V, Annicchiarico-Petruzzelli M, Melino G, Amelio I. The Hypoxic Tumour Microenvironment. *Oncogenesis* (2018) 7:10. doi: 10.1038/s41389-017-0011-9
17. Sjöback R, Nygren J, Kubista M. Absorption and Fluorescence Properties of Fluorescein. *Spectrochim Acta A Mol Biomol Spectrosc* (1995) 51:L7–L21. doi: 10.1016/0584-8539(95)01421-P
18. Doughty MJ. pH Dependent Spectral Properties of Sodium Fluorescein Ophthalmic Solutions Revisited. *Ophthalmic Physiol Opt* (2010) 30:167–74. doi: 10.1111/j.1475-1313.2009.00703.x
19. McLoughlin CK, Kotroni E, Bregnhoj M, Rotas G, Vougioukalakis GC, Ogilby PR. Oxygen- and pH-Dependent Photophysics of Fluorinated Fluorescein Derivatives: Non-Symmetrical vs. Symmetrical Fluorination. *Sensors (Basel)* (2020) 20(18):5172. doi: 10.3390/s20185172
20. Voss EW Jr, Croney JC, Jameson DM. Discrete Bathochromic Shifts Exhibited by Fluorescein Ligand Bound to Rabbit Polyclonal Anti-Fluorescein Fab Fragments. *J Protein Chem* (2002) 21:231–41. doi: 10.1023/a:1019789118530
21. Croce AC, Fiorani S, Locatelli D, Nano R, Ceroni M, Tancioni F, et al. Diagnostic Potential of Autofluorescence for an Assisted Intraoperative Delineation of Glioblastoma Resection Margins. *Photochem Photobiol* (2003) 77:309–18. doi: 10.1562/0031-8655(2003)077<0309:DPOAFA>2.0.CO;2
22. Yuan Y, Yan Z, Miao J, Cai R, Zhang M, Wang Y, et al. Autofluorescence of NADH is a New Biomarker for Sorting and Characterizing Cancer Stem Cells in Human Glioma. *Stem Cell Res Ther* (2019) 10:330. doi: 10.1186/s13287-019-1467-7
23. Mazurek M, Kulesza B, Stoma F, Osuchowski J, Mandziuk S, Rola R. Characteristics of Fluorescent Intraoperative Dyes Helpful in Gross Total Resection of High-Grade Gliomas-a Systematic Review. *Diagnostics (Basel)* (2020) 10(12):1100. doi: 10.3390/diagnostics10121100
24. Stummer W, Koch R, Valle RD, Roberts DW, Sanai N, Kalkanis S, et al. Intraoperative Fluorescence Diagnosis in the Brain: A Systematic Review and Suggestions for Future Standards on Reporting Diagnostic Accuracy and Clinical Utility. *Acta Neurochir (Wien)* (2019) 161:2083–98. doi: 10.1007/s00701-019-04007-y
25. Acerbi F, Pollo B, De Laurentis C, Restelli F, Falco J, Vetrano IG, et al. Ex Vivo Fluorescein-Assisted Confocal Laser Endomicroscopy (Convivo(R) System) in Patients With Glioblastoma: Results From a Prospective Study. *Front Oncol* (2020) 10:606574. doi: 10.3389/fonc.2020.606574
26. Belykh E, Miller EJ, Carotenuto A, Patel AA, Cavallo C, Martirosyan NL, et al. Progress in Confocal Laser Endomicroscopy for Neurosurgery and Technical Nuances for Brain Tumor Imaging With Fluorescein. *Front Oncol* (2019) 9:554. doi: 10.3389/fonc.2019.00554

Conflict of Interest: The authors declare that the research was conducted in the absence of any commercial or financial relationships that could be construed as a potential conflict of interest.

The reviewer JG declared a past co-authorship with the authors to the handling editor.

frontiers in Oncology

ORIGINAL RESEARCH
published: 11 May 2021
doi: 10.3389/fonc.2021.668273

Deep Neural Network for Differentiation of Brain Tumor Tissue Displayed by Confocal Laser Endomicroscopy

Andreas Ziebart[1], Denis Stadniczuk[2], Veronika Roos[1], Miriam Ratliff[1], Andreas von Deimling[3], Daniel Hänggi[1,4] and Frederik Enders[1]*

[1] Department of Neurosurgery, University Hospital Mannheim, Medical Faculty Mannheim, University of Heidelberg, Mannheim, Germany, [2] Department of Software Engineering, Clevertech Inc., New York, NY, United States, [3] Department of Neuropathology, University Hospital Heidelberg, and CCU Neuropathology, DKFZ, Heidelberg, Germany, [4] Department of Neurosurgery, Medical Faculty, Heinrich-Heine-University Düsseldorf, Düsseldorf, Germany

OPEN ACCESS

Edited by:
Francesco Acerbi, Fondazione IRCCS Istituto Neurologico Carlo Besta, Italy

Reviewed by:
Francesco Restelli, Fondazione IRCCS Istituto Neurologico Carlo Besta, Italy
Alexander Brawanski, University Medical Center Regensburg, Germany

***Correspondence:**
Andreas Ziebart
andreas.ziebart@umm.de

Specialty section:
This article was submitted to Neuro-Oncology and Neurosurgical Oncology, a section of the journal Frontiers in Oncology

Received: *15 February 2021*
Accepted: *09 April 2021*
Published: *11 May 2021*

Citation:
Ziebart A, Stadniczuk D, Roos V, Ratliff M, von Deimling A, Hänggi D and Enders F (2021) Deep Neural Network for Differentiation of Brain Tumor Tissue Displayed by Confocal Laser Endomicroscopy. Front. Oncol. 11:668273. doi: 10.3389/fonc.2021.668273

Background: Reliable on site classification of resected tumor specimens remains a challenge. Implementation of high-resolution confocal laser endoscopic techniques (CLEs) during fluorescence-guided brain tumor surgery is a new tool for intraoperative tumor tissue visualization. To overcome observer dependent errors, we aimed to predict tumor type by applying a deep learning model to image data obtained by CLE.

Methods: Human brain tumor specimens from 25 patients with brain metastasis, glioblastoma, and meningioma were evaluated within this study. In addition to routine histopathological analysis, tissue samples were stained with fluorescein *ex vivo* and analyzed with CLE. We trained two convolutional neural networks and built a predictive level for the outputs.

Results: Multiple CLE images were obtained from each specimen with a total number of 13,972 fluorescein based images. Test accuracy of 90.9% was achieved after applying a two-class prediction for glioblastomas and brain metastases with an area under the curve (AUC) value of 0.92. For three class predictions, our model achieved a ratio of correct predicted label of 85.8% in the test set, which was confirmed with five-fold cross validation, without definition of confidence. Applying a confidence rate of 0.999 increased the prediction accuracy to 98.6% when images with substantial artifacts were excluded before the analysis. 36.3% of total images met the output criteria.

Conclusions: We trained a residual network model that allows automated, on site analysis of resected tumor specimens based on CLE image datasets. Further *in vivo* studies are required to assess the clinical benefit CLE can have.

Keywords: confocal laser endomicroscopy, deep neural network, machine learning, brain tumor, fluorescein sodium, image analysis

INTRODUCTION

Intraoperative diagnosis continues to be an essential tool during neurosurgical procedures; nevertheless it remains challenging. Sites frequently lack the possibility of immediate pathologist's interaction and therefore require time for delivery and processing, and the frozen sections are subject to sampling errors (1–3).

Confocal laser endomicroscopy (CLE) can be used for intraoperative visualization in fluorescence guided surgery and offers cellular resolution. CLE has already been successfully applied to facilitate surgery for head and neck neoplasms and urological surgical procedures (4–6). Furthermore, it is used in gastroenterology for diagnosis of Barrett's esophagus and colorectal lesions among others (7, 8). Moreover, the application of CLE showed promising results in thyroid surgery and bronchoscopy including biopsy collection for interstitial lung disease (9, 10).

Since its start, efforts were made matching the features of CLE images to the histopathological sections; however, the transfer of classical neuropathological characteristics of common brain pathologies to CLE images is limited (11, 12). Until recently, application of CLE to central nervous tumors was mostly limited to preclinical studies. The first clinical trials show promising results for CLE to become part of routine intraoperative tumor diagnosis and might help detect tumor remnants in neurosurgery (12, 13). By extending the resection borders at a cellular level, this technique has the promising potential to protect normal brain tissue. However, there is only one optical fluorescence filter available and fluorescein, the most thoroughly investigated fluorescence dye, is not routinely used for brain tumor surgery. Further, for optimal utilization a high amount of intraoperatively collected image data needs to be directly analyzed.

Deep learning models reduce expenditure of time and interobserver-biased evaluation of intricate structures (14). The neural network models are successful where labeled data is available. Multiple recent applications of computer vision and medical imaging have shown cutting-edge performance (15, 16).

We hypothesized that a model integrating features from conventional CLE using a machine learning approach could diagnose tumor origin and identify specific features relevant to the entity.

MATERIAL AND METHODS

Patient Cohort

The training and validation cohort consisted of patients with histologically confirmed glioblastoma, brain metastasis, or meningioma WHO grade I, treated at the neurosurgical department of the University Hospital of Mannheim. The current 2016 WHO classification of brain tumors was used. All patients whose histopathological analyses did not confirm glioblastoma WHO grade IV, brain metastasis, or meningioma WHO grade I were excluded (n = 10). Our final patient cohort included 25 patients (median age 56.3 years; 19–82.2 years, male/female: 9/16).

Tumor Tissue Processing

Brain tumor tissue was collected from 25 adult patients who underwent resection of a brain tumor at the University Hospital Mannheim. Fresh tumor samples were immediately processed and split into sister specimens. Tissue pieces (2–5 mm in diameter) were incubated in fluorescein solution for 30 min (Fluorescein 10%, ALCON Pharma GmbH, Freiburg, Germany, final concentration 0.1 mg/ml, diluted with Ringer's solution) and subsequently washed with Ringer's solution three times for 2 min. As a positive control adjacent tumor specimens were stained with Nuclear Green for 1 min (Abcam, Cambridge, United Kingdom, 50 μM final concentration, diluted with Ringer's solution), incubated for 5 min, and washed once for 5 min with Ringer's solution. All working steps were performed at room temperature. After immediate CLE imaging, tissue samples were analyzed by the Department of Neuropathology of the University Hospital Heidelberg corresponding to routine diagnostics including H&E, immunostaining and in certain cases methylation analysis. Pathology confirmed newly diagnosed glioblastoma in eight patients, brain metastasis in eight patients (six patients presented with non-small cell lung cancer and two with breast cancer) and meningioma WHO grade I in nine patients.

Confocal Laser Endomicroscopy

For CLE imaging the OptiScan System, model CIS-CZM-B-CP (SN R&D 4011-05; Zeiss, Oberkochen, Germany) including a sterile sheath was used. Briefly summarized, light is transmitted by a laser source (488 nm wavelength) through an optical fiber to the hand held scanner probe. The focal signal is detected by exciting the fluorescent dye by laser light. Latter is converted into a digital pattern depending on the amount of emitted fluorescence. This pattern can be transformed into a grayscale image parallel to the lens' plane with adjustable focus depth. Images were acquired immediately after staining. The probe was fixed, and specimens were applied on the lens to minimize motion induced artifacts.

Images were created with 1920 × 1080 pixels and were obtained with 0.75 frames per second and a focus depth of 0 to 120 μm. In a second step, we removed data sets with low imaging quality affecting the whole image due to technical issues, such as blood and motion artifacts or out of focus scanning, from further evaluation.

Image Preprocessing and Convolutional Neural Networks

A convolutional neural network (CNN) is a widely adopted network of machine-learning algorithms to process multiple arrays such as images which detect local conjunctions using convolutional and pooling layers before fully connected layers are following. The given hierarchy in images leads to lower-level features composing higher-level features in a deep neural network. Residual convolutional (ResNet) and Inception networks (InceptionNet) have been applied in clinical classification problems. A ResNet18 and Inception network was constructed with the Pytorch framework (https://pytorch.org/)

written in python as a tensor and dynamic network. ResNet18 has 17 convolutional layers and contains batch normalization and identity mappings, additionally. InceptionNet-v3 was used consisting of seven inception blocks, pooling layers and normalization layers. We used four fully connected layers for both networks. The last fully connected layer gives a classification according to the global features connected from all local features. We used negative log likelihood as loss function and log softmax after the fully connected layers. Stochastic gradient decent was selected for optimization with a learning rate of 0.01 and a momentum of 0.5. We applied data augmentation techniques to enlarge the database with analogical but not identical data. Techniques, such as vertical and horizontal flipping methods, were applied to inflate the size of the training dataset and to reduce overfitting. Images were scaled down to 960 × 540 pixels, and sections of 400 × 400 pixels were chosen randomly. The probability of horizontal and vertical flipping was set to 0.5. Images were fed in batches with a batch size of 32 for ResNet and 16 for InceptionNet, respectively. Eventually, the enhanced training data was fed into the deep learning models for iteration to minimize the loss function. This algorithm was used to classify images obtained by CLE verified as glioblastoma, brain metastases or meningioma.

Image Interpretation by Neurosurgeons

For manual and manual/deep learning combined assessment of CLE images we created a training set, a manual test set, and a ResNet test set, each containing a total of 90 images of balanced proportions of glioblastomas, meningiomas, and metastases. Images containing obvious artifacts (*e.g.* motion artifacts) were excluded previously. The ResNet test set contained only images rated by the ResNet with an output level of 0.99 or higher. In the training set, information about the corresponding histopathologic diagnosis was available for each image, and three experienced neurosurgeons underwent training for CLE image interpretation. Subsequently, images of the two test sets were reviewed by the neurosurgeons in a blinded fashion.

Statistical Analysis

Statistical analysis was performed using GraphPad Prism 8.3.0 (GraphPad Software, San Diego, CA). The overall predictive value was analyzed by area under the receiver operating characteristic curve (AUROC), precision-recall curve, and macro-averaged F1 analysis. For test set accuracy, comparative analysis of deep learning models and neuro-oncological surgeons, the Mann–Whitney test was used. We calculated the accuracies of the three neuro-oncological surgeons using the ratio between the number of correct diagnosed and total CLE images.

RESULTS

To test the hypothesis that CLE could provide an alternative method for intraoperative frozen section histology and facilitate targeted biopsy, we collected surgical specimens from 25 patients and acquired a total of 19,422 images (glioblastoma 5,668, brain metastases 6,814, meningioma 6,960) for the evaluation (**Table 1**). The specimens were either stained with fluorescein dye or nuclear green dye with similar distributed data sets of the three classes. We acquired CLE images of fresh tissue samples, which were free of freezing and additional sectioning artifacts and therefore provided well-preserved tissue architecture. More importantly, fresh tissue imaging mimics intraoperative imaging without complex and time-consuming sample processing (**Supplementary Figure 1**). Representative *ex vivo* CLE images of the three groups are shown in **Supplementary Figure 2**. All glioblastoma *ex vivo* specimens CLE displayed stellate, bright spots.

Differentiation of Malignant Tumors

Conventional magnetic resonance imaging ultimately fails to distinguish between glioblastoma and brain metastases among malignant brain tumors to date. We built a residual network (ResNet18) model for binary classification to demonstrate its diagnostic capability on these highly heterogeneous tumor specimens stained with fluorescein. Specimens from eight patients for each tumor type were used (4,361 images of glioblastoma, 3,503 images of brain metastases). We evaluated CNN-based methods using a leave-one-patient out cross-validation, *i.e.* one patient always represented the test data and all others the training data. This way, inherent correlation within the image sequences did not play a role in the analysis. Receiver operating characteristic curves, corresponding AUC values, and confusion matrix results are shown in **Figures 1A, B**. An average accuracy of 90.9% was achieved following five-fold cross validation. Since fluorescein based CLE imaging is susceptible to artifacts and includes a significant amount of non-diagnostic images, automatic approaches are required to filter relevant data for diagnosis. After we applied a threshold for the output level of the test data of 0.999, the accuracy improved to 100% in this subset (**Table 2**). 35.6% of the images in the test set had an output level of 0.999 or higher, thus providing a potential filter for non-diagnostic images. Next, binary classification for glioblastoma and meningioma as well as brain metastases and meningioma were performed (**Figures 1C, D**). In a test set containing image data of 1,024 images showing glioblastoma and meningioma CLE images, an overall accuracy of 95.5% was achieved. ResNet18 showed 94.3% accuracy for differentiation of brain metastases and meningioma in a test set containing 1,231 CLE images.

TABLE 1 | Patients' characteristics and data composition.

	Training	Test
Total patients	**22**	**3**
Glioblastoma	**7**	**1**
Brain metastases	**7**	**1**
Meningioma	**8**	**1**
Images (fluorescein dye)	**12,273**	**1,699**
Images (nuclear green dye)	**7,151**	**1,291**

Values represent patient numbers for glioblastoma, brain metastasis and meningioma and total image numbers for fluorescein and nuclear green, respectively.

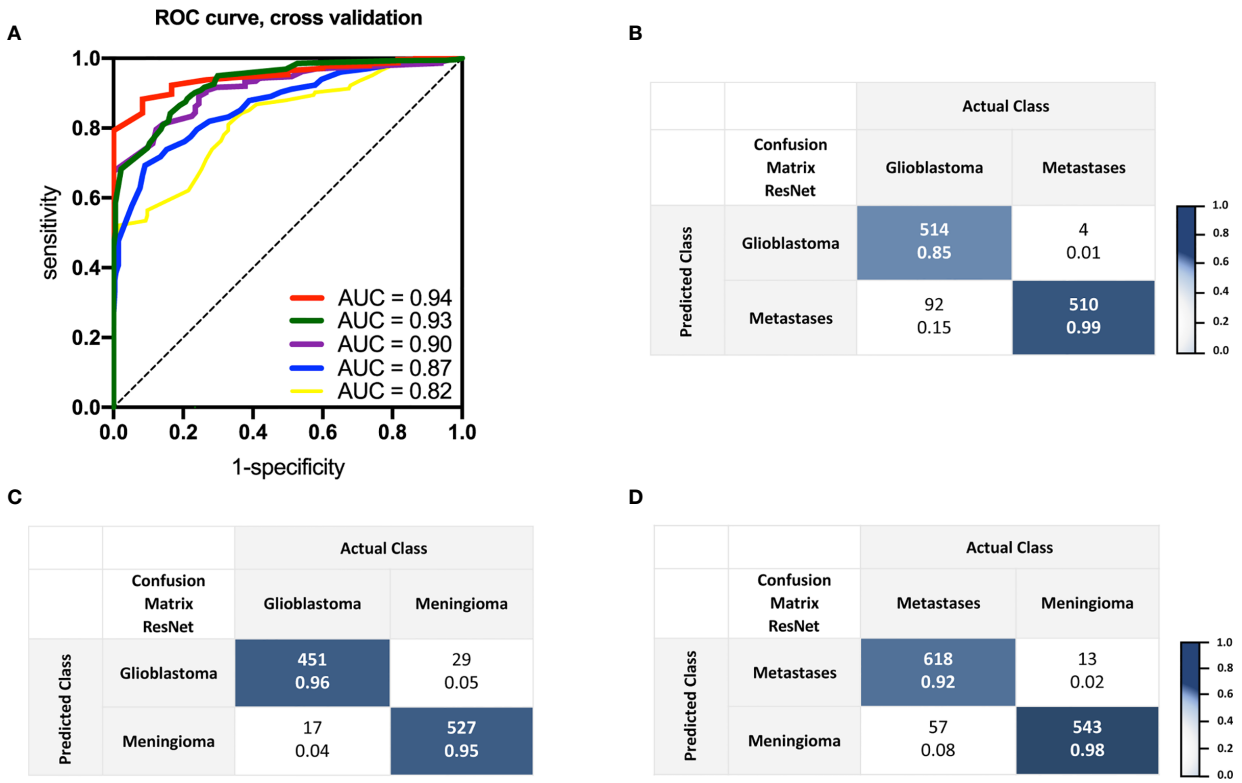

FIGURE 1 | **(A)** Receiver operating curve analysis and corresponding area under the curve values received of a trained two-class residual convolutional network with five-fold cross validation. Images were obtained from seven patients with glioblastoma and brain metastases, respectively. **(B)** Confusion matrix shows outputs and actual labeling for binary classification of an additional test set, including one patient with glioblastoma and another one with brain metastases. **(C, D)** Confusion matrices indicating binary classification results of a test set for glioblastoma and meningioma as well as brain metastases and meningioma, respectively. In each cell, the number above is the count and the number below the normalized count. Images were obtained with CLE following topical *ex vivo* staining with fluorescein dye.

TABLE 2 | Accuracy, macro-averaged F1 and area under the curve analysis of trained networks for multiclass classification (glioblastoma, brain metastasis, and meningioma) and binary classification (glioblastoma and brain metastasis).

Network	Accuracy (%)	F1/AUC	Rate of diagnostic images (%)
ResNet18			
Test total	85.8	92.3% (F1)	32.3
Test confidence > 0.999	93.6		
ResNet18 filtered			
Test total	87.3	93.2% (F1)	36.3
Test confidence > 0.999	98.6		
InceptionNet			
Test total	82.9	90.6% (F1)	17
Test confidence > 0.999	91.1		
ResNet18 binary classification			
Test total	90.9	0.92 (AUC)	35.6
Test confidence > 0.999	100		

ResNet filtered contained manually selected data free of substantial artifacts. The ratio of images rated with an output level of 0.999 or higher and the amount of total images are indicated as diagnostic images. Images were obtained with CLE following topical ex vivo staining with fluorescein dye. Macro-averaged F1 was calculated using the following equation: $2*(precision_m*recall_m)/(precision_m+recall_m)$.

Multiclass Classification With ResNet18 and InceptionNet

For practical reasons, further multiclass classification of common brain neoplasms is needed. Subsequently, we employed a residual network (ResNet18) model and an Inception network (InceptionNet) model to assist the diagnosis of brain tumor tissues including meningiomas based on CLE image data. To train and test the ResNet18 and InceptionNet models, we incorporated CLE images from 25 patients and labeled them as "glioblastoma"(eight patients, 5,322 images), "metastasis" (eight patients, 4,120 images) and "meningioma" (nine patients, 4,529 images), respectively.

The precision-recall curve analysis of concurrent three-class tumor-type prediction showed macro-averaged F1 values of up to 0.92 (**Figure 2**). Importantly, five-fold cross validation confirmed the networks' validity. InceptionNet showed no superior performance with a macro-averaged F1 score of 0.91. ResNet18's overall accuracy of 85.8% for three-class prediction was slightly improved by manually filtering CLE images before employing the ResNet18 model. Considering the network's confidence for the assessment of CLE images provides a possible feasibility for analysis, regarding the lack of

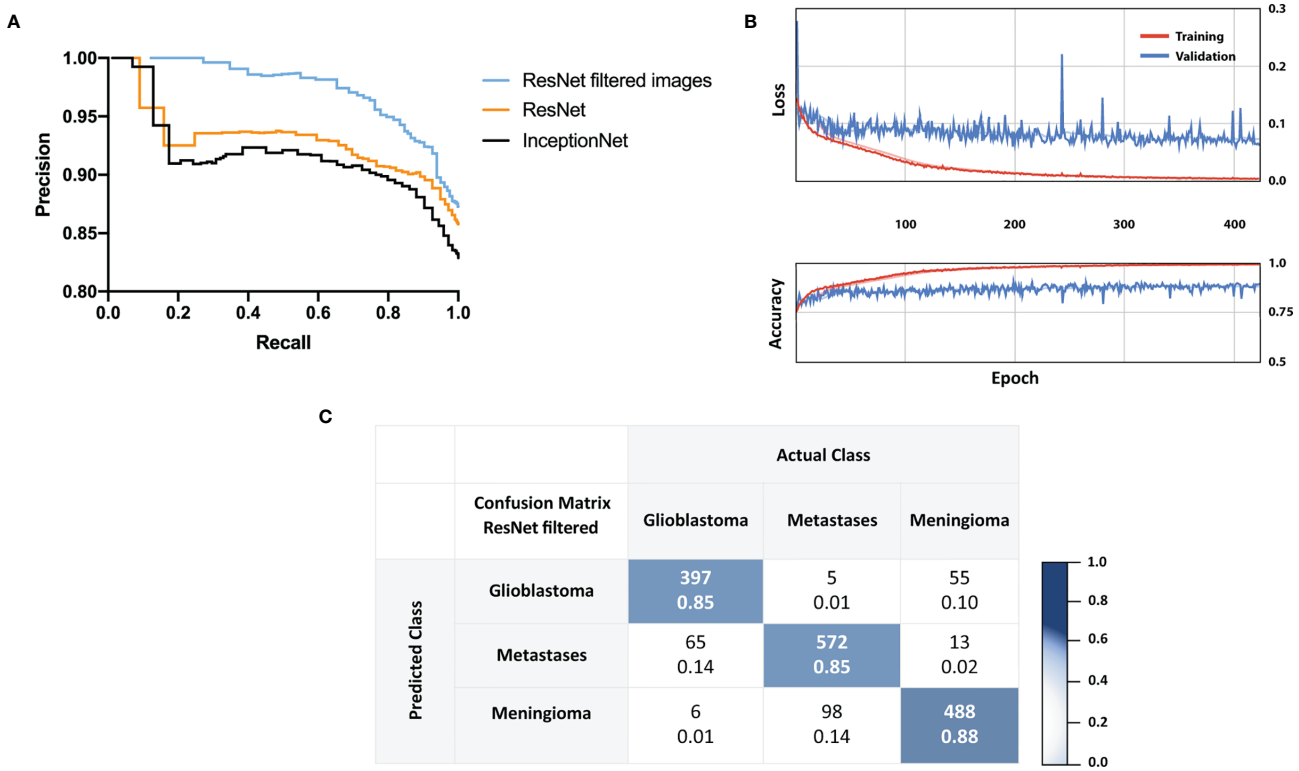

FIGURE 2 | **(A)** Test set results with Precision-Recall curves received for a trained three-class residual convolutional network, Inception network and a trained residual network with manually selected images. In **(A)** 12,273 images were used for training and 1,699 for the test set. In the preselected data set, 5,261 images were found suitable for training, and 647 were available for the test set. **(B)** Five-fold cross validation results. **(C)** Confusion matrix showing ResNet18 outputs and labeling of a test set using preselected images after images including substantial artifacts were manually removed. Images were obtained with CLE following topical *ex vivo* staining with fluorescein dye. In each cell, the number above is the count and the number below the normalized count.

histopathological information in most images. Therefore, we calculated the rate of diagnostic images with high confidence as ratio of images with output levels of 0.999 or higher and the overall amount of images. Results for both the deep learning models and the ResNet18 model with preselected data only are summarized in **Table 2**. Test accuracy was 93.6% when a confidence level of >0.999 was applied. 548 of 1,576 (32.3%) images were marked with a confidence of 0.999 or higher. A ResNet18 model trained and tested with preselected data had an accuracy in the test set of 87.3 and 98.6% for images with a confidence level >0.999. Here 36.7% (355/966) of images had an output level of 0.999 or higher. Test set accuracies for individual classes of glioblastoma, brain metastases, meningioma and the respective rate of diagnostic image data are presented in **Table 3**.

Complementing Manual With Automated Analysis

Since CLE accompanies a high amount of artifacts and potential non-diagnostic images, we had a close look at the output levels, also described as network's confidence for single image analysis. When we analyzed images with output levels of 0.99 or higher,

TABLE 3 | Accuracy analysis of residual neural network with multiclass classification for individual classes.

Class/Network	Accuracy ResNet18 unfiltered	Accuracy ResNet18 unfiltered with threshold >0.999	Rate of diagnostic images
Glioblastoma ResNet18 unfiltered	92.3	93.8	57.5
Metastases ResNet18 unfiltered	89.3	94	20
Meningioma ResNet18 unfiltered	89.9	99.5	25.9
Glioblastoma ResNet18 filtered images only	92.3	98.6	37.8
Metastases ResNet18 filtered images only	93.5	100	53.3
Meningioma ResNet18 filtered images only	88.2	98.6	5.5

The ratio of images rated with an output level of 0.999 or higher and the overall images are indicated as diagnostic images. ResNet18 filtered contained manually selected data free of substantial artifacts. A threshold of >0.999 indicates only images with output values of 0.999 or higher as rated by the network were included in the analysis. Images were obtained with CLE following topical ex vivo staining with fluorescein dye. Percentage values are indicated.

average accuracies of 92.3% were achieved applying ResNet18 for multiclass classification of CLE data. Independent analysis of two neuro-oncological surgeons of these images showed abundant histopathological data compared to the entire data set. Since CLE images are almost immediately displayed during surgery, we wondered if a combination of expert opinion and real-time automated analysis would facilitate decision making. We compared neurosurgical assessment of balanced data sets, containing equal numbers of glioblastoma, brain metastases, and meningioma images to CNN performance (**Figure 3**). There was a tendency towards higher accuracy when images were selected by CNN's output level compared to manually selected images, lacking artifacts or low contrast. However, neuro-oncological surgeons could not achieve accuracies of ResNet18 image analysis rated with an output level of 0.99 or higher.

Convolutional Neural Network for Cell Density and Nuclear Analysis

Staining with nuclear green dye offers a readout for cellular density. CLE images of resected tissue samples stained with nuclear green resulted in image sets with consistently high quality and strong nuclear staining (**Figure 4A**). Exact cell count and morphology might therefore result in sufficient CNN performance (**Figure 4B**). Analysis for binary classification of nuclear green images is presented in **Figures 4C–E** and in **Figure 4F** for multiclass classification. A macro-averaged F1 score of 62% was achieved for classification of the three tumor types. When a threshold of confidence of 0.999 was applied, 124 of 2,990 images were suitable, and an accuracy of 94% resulted in the test set.

Following validation of the neural network models, we created a model for on-site tumor diagnosis of glioblastoma, brain metastases and meningioma. We propose a final evaluation of CLE imaging by the neurosurgeon with the aid of the networks' output levels to estimate diagnostic probability. The output levels do not display percentage of diagnostic probability. Schematic network construction and the proposed streamlined workflow with tissue to diagnose pipeline are shown in **Figure 5**.

DISCUSSION

The neurosurgical workflow and surgical performance could benefit from CLE in at least two aspects. First, its use could substitute for conventional frozen section pathology. Second, it could be used to confirm completeness of the resection by scanning the walls of the resection cavity.

CLE imaging combined with Computer Aided Diagnosis (CAD) successfully predicted the three most common encountered brain tumor entities. Manual preselection of the data showed marginal effect on network accuracy and the rate of diagnostic images. However, there was a limited and probably too small amount of data left for training, affecting the overall output. Further, the selection by a neurosurgeon, focusing on known structures and contrast, might not correlate with the network's criteria used for the output level. Of note, output levels were higher for brain metastases and glioblastoma for two and three-class networks as compared to meningioma. We suspect that the high predictive power of glioblastoma CLE images is due to the characteristic bright spots occurring almost exceptional in glioblastoma specimens. Primarily noted from *ex vivo* imaging, some cells might uptake fluorescein following prolonged exposure to the dye or *via* influx of dye into damaged cells (17). Interestingly, outputs were rather less predictive when nuclear green dye was used. This suggests that in case of fluorescein application other features than nuclear density were chosen.

Diagnostic sensitivity of CLE has been previously described between 52.97 and 90% in case of low grade and high grade gliomas and meningioma *ex vivo* specimens analyzed by neuropathologists and neurosurgeons. Diagnostic sensitivity was only 37% for brain metastases (18, 19). Confocal scanning

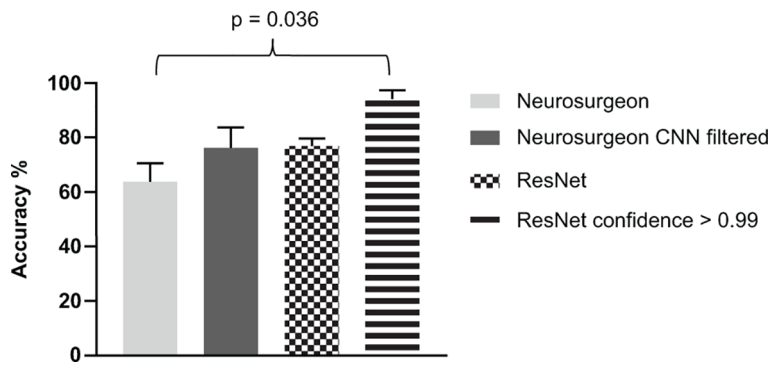

FIGURE 3 | Comparative analysis of manual, deep learning based and combined assessment of glioblastoma, brain metastasis and meningioma images obtained by confocal laser endomicroscopy. Balanced test sets containing 90 images were anonymized and evaluated by trained neuro-oncological surgeons. Results are displayed in the first column. A second test set was evaluated by the surgeons including images rated by the residual network with a confidence of 0.99 or higher (2nd column). Overall accuracies of residual network test set analysis and results of the image subgroup rated with an output level of 0.99 or higher are displayed. Average accuracy of at least three independent experiments and five-fold cross validation are shown, respectively.

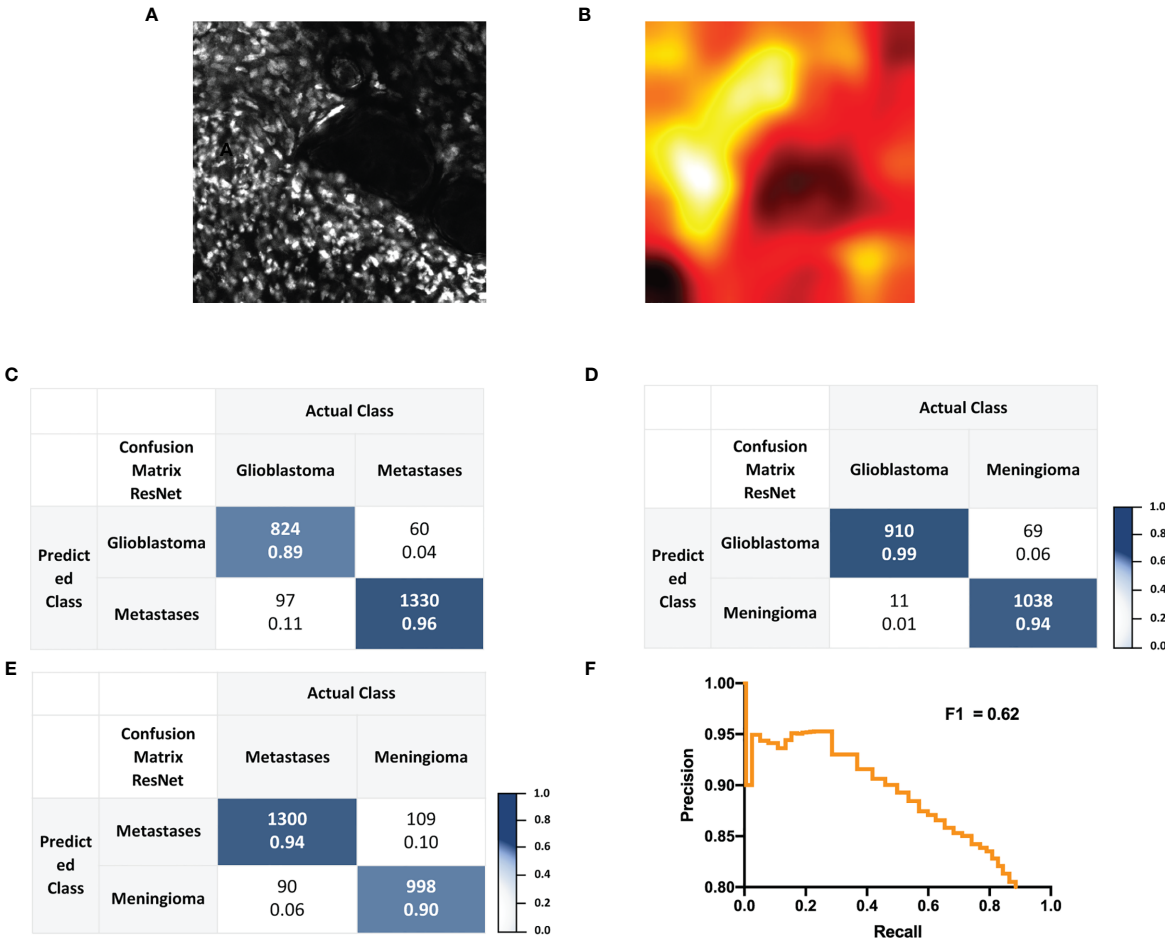

FIGURE 4 | **(A, B)** Representative glioblastoma CLE image following topical staining with nuclear green and corresponding heat map. **(C–E)** Confusion matrix for residual network based binary classification. Images were labeled as "glioblastoma", "brain metastasis" or "meningioma" and were obtained with CLE following topical *ex vivo* staining with nuclear green dye. In each cell, the number above is the count and the number below the normalized count. **(F)** Precision-Recall curve analysis and corresponding macro-averaged F1 score received for a test set of a trained three-class residual network.

microscopy allows rapid histopathological assessment for a variety of brain neoplasms including, gliomas, metastases, and pituitary tumors faster than conventional frozen section (20). However, sifting manually through the images is tedious and impractical for high throughput imaging. Therefore, an upstream network is essential for filtering non-diagnostic images in a fast and feasible manner (21).

The high predictive potential of our network for brain metastases might present an integral part of fully automated diagnosis in the near future, complementing the model with preoperatively diagnosed metastases *via* computer-aided detection in magnetic resonance imaging (22, 23). Izadyyazdanabadi et al. showed promising results applying neural network models to categorize CLE data of brain neoplasms into diagnostic and non-diagnostic images, though not specifying the actual tumor entity (24).

For other fields like Barrett's esophagus, CLE combined with automated image processing approaches has shown not only thorough diagnostic potential, but also decrease of biopsy samples and the ability to classify the pathology (25). CAD of CLE based data also showed promising results in diagnosing inflammatory bowel disease and discriminating neoplastic *versus* non-neoplastic epithelium in head and neck cancer (26, 27). Similar deep networks were used to evaluate cancerous colon tissue following CLE imaging (28).

Kamen et al. early described the use of an automated tissue differentiation algorithm with machine learning in order to classify CLE images of glioblastomas and meningiomas. However, the clinical impact distinguishing solely these tumor types is limited and state-of-the-art CNNs for classification were not used, which resulted in an average accuracy of 84% (29). When aiming for automated tumor diagnosis by CLE image analysis in neurosurgery, multiclass networks need to be designed and trained for multiple tumor types, reactive and normal brain tissues. To our knowledge, such a multiclass classifier has not been applied for CLE image analysis, and

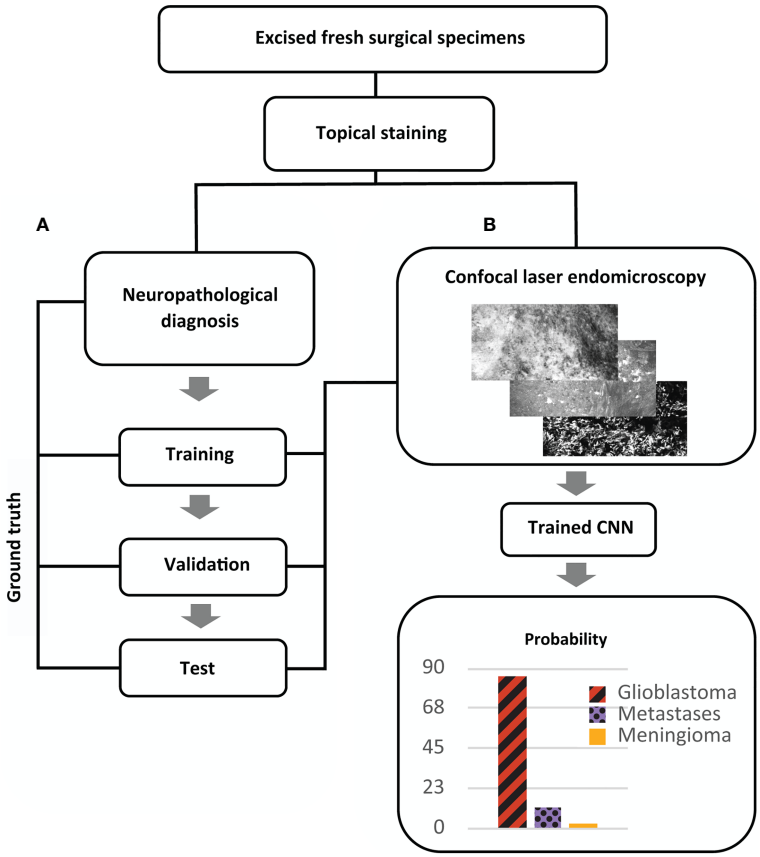

FIGURE 5 | Proposed pipeline for intraoperative diagnosis of brain tumors with confocal laser endomicroscopy after image acquisition, training and test phase of a convolutional neural network (CNN). **(A)** Experimental design for construction and validation of a CNN for multiclass classification of brain tumors. Fresh specimens are stained with fluorescein dye, and images are acquired with confocal laser endomicroscopy (CLE) by a single user. Afterwards the specimens undergo histopathological diagnostics (as described in *Materials and Methods*) providing ground truth for training and validation of the CNN. CLE contained a portable hand held probe and a touch screen. **(B)** Schematic workflow for *ex vivo* brain tumor diagnosis providing CLE images with an additional confidence level. By applying a confidence threshold, non-diagnostic images are not considered for evaluation.

prior studies have not distinguished glioblastoma from cerebral metastases CLE images with machine learning.

We believe CLE based automated data processing is less expensive and more efficient than the current technique, even if time needed for data transfer and consultation with a neuropathologist are included into that consideration. Conventional workflows without automated approaches necessitate a functional network for data transfer and communication, trained and available neuropathologists for image interpretation, time to review single images, and constant technical support. Each step represents a potential economic and technical barrier, while computational costs are limited. Further, the proposed pipeline for *ex vivo* diagnosis is an alternative for neurosurgeons where diagnosis by neuropathologists is not broadly available. The use of CLE-assisted fluorescent surgery not only is an improvement of immediate histological diagnosis as compared to time-consuming hematoxylin and eosin staining, but could also improve representation of the borders of tumor and normal tissues (30).

However, caution is advised in using the networks' confidence for single image analysis. In our opinion, confidence levels provide an aid for intraoperative expert analysis. Multiple images and affiliated output levels should be evaluated in the same region. Further, we acknowledge several limitations to our study. Our model cannot readily be applied to clinical situations yet, unless training for additional tumor types and normal as well as non-tumor mimickers is completed. The current model might be applicable for patients who have high likelihood of glioblastoma, cerebral metastases, or grade I meningioma based on standard radiographic evaluation. The feasibility of CLE-assisted multifluorescent surgery also has to be increased by extending the usability to other fluorescent agents like 5-aminolevulinic acid (30). In order to provide high-quality data *in vivo*, the kinetics of the fluorophore agents and administration techniques have to be taken into account. Furthermore, *in vivo* validation is mandatory, since the study did not utilize intravenous fluorescein application which potentially allows a more homogenous staining than topical application, however

also underlies decreasing fluorescence signal over time after injection (31). Quality of *in vivo* acquired images is limited by the fluorophore kinetics as some dyes, in particular fluorescein, washes out leading to low contrasted tissue if image acquisition is delayed. In contrast, e*x vivo* imaging after topical staining is significantly less affected by the timing of fluorescein administration. Insufficient contrast can be avoided by readministration of fluorescein and thus increase image quality (32). Future analysis will include an assessment of tumor microvasculature in addition to tumor cell morphology and architecture. Interpretation of erythrocyte flow, thrombosis, and velocity changes may help to classify glioma subtypes, normal and injured brain tissues (33). Due to the lack of blood flow in *ex vivo* samples, these features were not included during the CNN training process in this study.

We continue to enlarge our sample size and anticipate to extend the model's labeling ability when a larger data set with different tumor entities will be available. In addition, expert's diagnostic recognition may be improved using machine learning algorithms. For example, Izadyyazdanabadi M. et al. used image style transfer method based on permanent hematoxylin and eosin staining and therefore enhanced diagnostic quality of glioma CLE images (34). Among other factors, colorization of the images provided advantages for the analysis. Therefore image style transfer is a promising tool, which could be integrated into the described workflow for on-the-fly interpretation of CLE images and should also be tested in brain metastases. Additionally, a crucial point for future real-time diagnosis is the automated reduction of artifacts affecting the analysis. Therefore, the use of transfer learning from intermediate endpoints may overcome non-diagnostic image sections and thus improve accuracy as described by Aubreville et al. (35).

CONCLUSIONS

The use of machine-learning algorithms following CLE imaging achieved high accuracy in the prediction of three different brain tumor types when output levels were assessed. The developed algorithm enables CLE to be integrated into the clinical workflow as a tool for almost real-time tissue diagnosis. Beyond simply gaining an orientation about tumor entity, fast high-volume image processing facilitates a high amount of artifact-free digital biopsies. Thereby, intra-tumor heterogeneity and information about resection margins can be taken into account when performing tumor resection or planning postoperative radiation. Further investigations to improve overall performance are needed before the method can become part of neurosurgical routine.

AUTHOR'S NOTE

Portions of this work were presented in abstract form at the 2019 Computer Assisted Radiology and Surgery Conference, Rennes, France, June 20, 2019.

DATA AVAILABILITY STATEMENT

The data associated with the paper are not publicly available but are available from the corresponding author on reasonable request.

ETHICS STATEMENT

The studies involving human participants were reviewed and approved by the Ethics Committee II, University of Heidelberg, Medical Faculty Mannheim. The patients provided their written informed consent to participate in this study.

AUTHOR CONTRIBUTIONS

VR, FE, and AZ performed experiments. DS and AZ analyzed results and prepared figures. FE and DH designed the research. AV provided histopathological analysis, AZ and FE drafted the paper, and all authors reviewed and commented on the report. All authors contributed to the article and approved the submitted version.

SUPPLEMENTARY MATERIAL

The Supplementary Material for this article can be found online at: https://www.frontiersin.org/articles/10.3389/fonc.2021.668273/full#supplementary-material

REFERENCES

1. Tofte K, Berger C, Torp SH, Solheim O. The Diagnostic Properties of Frozen Sections in Suspected Intracranial Tumors: A Study of 578 Consecutive Cases. *Surg Neurol Int* (2014) 5:170. doi: 10.4103/2152-7806.146153
2. Chand P, Amit S, Gupta R, Agarwal A. Errors, Limitations, and Pitfalls in the Diagnosis of Central and Peripheral Nervous System Lesions in Intraoperative Cytology and Frozen Sections. *J Cytol* (2016) 33:93–7. doi: 10.4103/0970-9371.182530
3. Nemoto N, Sakurai I, Baba S, Gotoh S, Osada H. A Study of Intraoperative Rapid Frozen Section Diagnosis Focusing on Accuracy and Quality Assessment. *Rinsho Byori* (1992) 40:1319–28.
4. Goncalves M, Aubreville M, Mueller SK, Sievert M, Maier A, Iro H, et al. Probe-Based Confocal Laser Endomicroscopy in Detecting Malignant Lesions of Vocal Folds. *Acta Otorhinolaryngol Ital* (2019) 39(6):389–95. doi: 10.14639/0392-100X-2121
5. Lee J, Jeh SU, Koh DH, Chung DY, Kim MS, Goh HJ, et al. Probe-Based Confocal Laser Endomicroscopy During Transurethral Resection of Bladder Tumors Improves the Diagnostic Accuracy and Therapeutic Efficacy. *Ann Surg Oncol* (2019) 26:1158–65. doi: 10.1245/s10434-019-07200-6
6. Aubreville M, Knipfer C, Oetter N, Jaremenko C, Rodner E, Denzler J, et al. Automatic Classification of Cancerous Tissue in Laserendomicroscopy Images of the Oral Cavity Using Deep Learning. *Sci Rep* (2017) 7:11979. doi: 10.1038/s41598-017-12320-8

7. Bergenheim F, Seidelin JB, Pedersen MT, Mead BE, Jensen KB, Karp JM, et al. Fluorescence-Based Tracing of Transplanted Intestinal Epithelial Cells Using Confocal Laser Endomicroscopy. *Stem Cell Res Ther* (2019) 10:148. doi: 10.1186/s13287-019-1246-5
8. Wang KK, Carr-Locke DL, Singh SK, Neumann H, Bertani H, Galmiche J-P, et al. Use of Probe-Based Confocal Laser Endomicroscopy (Pcle) in Gastrointestinal Applications. a Consensus Report Based on Clinical Evidence. *United Eur Gastroenterol J* (2015) 3:230–54. doi: 10.1177/2050640614566066
9. Ignat M, Lindner V, Vix M, Marescaux J, Mutter D. Intraoperative Probe-Based Confocal Endomicroscopy to Histologically Differentiate Thyroid From Parathyroid Tissue Before Resection. *Surg Innov* (2019) 26:141–8. doi: 10.1177/1553350618814078
10. Wijmans L, Bonta PI, Rocha-Pinto R, de Bruin DM, Brinkman P, Jonkers RE, et al. Confocal Laser Endomicroscopy as a Guidance Tool for Transbronchial Lung Cryobiopsies in Interstitial Lung Disorder. *Respiration* (2019) 97:259–63. doi: 10.1159/000493271
11. Sanai N, Eschbacher J, Hattendorf G, Coons SW, Preul MC, Smith KA, et al. Intraoperative Confocal Microscopy for Brain Tumors: A Feasibility Analysis in Humans. *Neurosurgery* (2011) 68:282–90:discussion 290. doi: 10.1227/NEU.0b013e318212464e
12. Martirosyan NL, Georges J, Eschbacher JM, Cavalcanti DD, Elhadi AM, Abdelwahab MG, et al. Potential Application of a Handheld Confocal Endomicroscope Imaging System Using a Variety of Fluorophores in Experimental Gliomas and Normal Brain. *Neurosurg Focus* (2014) 36:E16. doi: 10.3171/2013.11.FOCUS13486
13. Belykh E, Cavallo C, Gandhi S, Zhao X, Veljanoski D, Izadyyazdanabadi M, et al. Utilization of Intraoperative Confocal Laser Endomicroscopy in Brain Tumor Surgery. *J Neurosurg Sci* (2018) 62:704–17. doi: 10.23736/S0390-5616.18.04553-8
14. LeCun Y, Bengio Y, Hinton G. Deep Learning. *Nature* (2015) 521:436–44. doi: 10.1038/nature14539
15. He K, Zhang X, Ren S, Sun J. Deep Residual Learning for Image Recognition. *ArXiv [csCV]* (2015) arXiv:1512.03385. doi: 10.1109/CVPR.2016.90
16. Hollon TC, Pandian B, Adapa AR, Urias E, Save AV, Khalsa SSS, et al. Near Real-Time Intraoperative Brain Tumor Diagnosis Using Stimulated Raman Histology and Deep Neural Networks. *Nat Med* (2020) 26:52–8. doi: 10.1038/s41591-019-0715-9
17. Belykh E, Miller EJ, Carotenuto A, Patel AA, Cavallo C, Martirosyan NL, et al. Progress in Confocal Laser Endomicroscopy for Neurosurgery and Technical Nuances for Brain Tumor Imaging With Fluorescein. *Front Oncol* (2019) 9:554. doi: 10.3389/fonc.2019.00554
18. Martirosyan NL, Eschbacher JM, Kalani MYS, Turner JD, Belykh E, Spetzler RF, et al. Prospective Evaluation of the Utility of Intraoperative Confocal Laser Endomicroscopy in Patients With Brain Neoplasms Using Fluorescein Sodium: Experience With 74 Cases. *Neurosurg Focus* (2016) 40:E11. doi: 10.3171/2016.1.FOCUS15559
19. Breuskin D, Szczygielski J, Urbschat S, Kim Y-J, Oertel J. Confocal Laser Endomicroscopy in Neurosurgery—an Alternative to Instantaneous Sections? *World Neurosurg* (2017) 100:180–5. doi: 10.1016/j.wneu.2016.12.128
20. Martirosyan NL, Georges J, Eschbacher JM, Belykh E, Carotenuto A, Spetzler RF, et al. Confocal Scanning Microscopy Provides Rapid, Detailed Intraoperative Histological Assessment of Brain Neoplasms: Experience With 106 Cases. *Clin Neurol Neurosurg* (2018) 169:21–8. doi: 10.1016/j.clineuro.2018.03.015
21. Izadyyazdanabadi M, Belykh E, Mooney M, Martirosyan N, Eschbacher J, Nakaji P, et al. Convolutional Neural Networks: Ensemble Modeling, Fine-Tuning and Unsupervised Semantic Localization for Neurosurgical CLE Images. *J Vis Commun Image Represent* (2018) 54:10–20. doi: 10.1016/j.jvcir.2018.04.004
22. Dikici E, Ryu JL, Demirer M, Bigelow M, White RD, Slone W, et al. Automated Brain Metastases Detection Framework for T1-Weighted Contrast-Enhanced 3D MRI. *IEEE J BioMed Health Inform* (2020) 24 (10):2883–93. doi: 10.1109/JBHI.2020.2982103
23. Zhou Z, Sanders JW, Johnson JM, Gule-Monroe MK, Chen MM, Briere TM, et al. Computer-Aided Detection of Brain Metastases in T1-Weighted MRI for Stereotactic Radiosurgery Using Deep Learning Single-Shot Detectors. *Radiology* (2020) 295(2):407–15. doi: 10.1148/radiol.2020191479
24. Izadyyazdanabadi M, Belykh E, Martirosyan N, Eschbacher J, Nakaji P, Yang Y, et al. Improving Utility of Brain Tumor Confocal Laser Endomicroscopy: Objective Value Assessment and Diagnostic Frame Detection With Convolutional Neural Networks. *Proc SPIE 10134 Med Imaging 2017: Computer-Aided Diagnosis* (2017) 101342J:101342J. doi: 10.1117/12.2254902
25. Ghatwary N, Ahmed A, Grisan E, Jalab H, Bidaut L, Ye X. In-Vivo Barrett's Esophagus Digital Pathology Stage Classification Through Feature Enhancement of Confocal Laser Endomicroscopy. *J Med Imaging* (2019) 6:1. doi: 10.1117/1.jmi.6.1.014502
26. Dittberner A, Rodner E, Ortmann W, Stadler J, Schmidt C, Petersen I, et al. Automated Analysis of Confocal Laser Endomicroscopy Images to Detect Head and Neck Cancer. *Head Neck* (2016) 38 Suppl 1:E1419–26. doi: 10.1002/hed.24253
27. Quénéhervé L, David G, Bourreille A, Hardouin JB, Rahmi G, Neunlist M, et al. Quantitative Assessment of Mucosal Architecture Using Computer-Based Analysis of Confocal Laser Endomicroscopy in Inflammatory Bowel Diseases. *Gastrointest Endosc* (2019) 89:626–36. doi: 10.1016/j.gie.2018.08.006
28. Rasti P, Wolf C, Dorez H, Sablong R, Moussata D, Samiei S, et al. Machine Learning-Based Classification of the Health State of Mice Colon in Cancer Study From Confocal Laser Endomicroscopy. *Sci Rep* (2019) 9:20010. doi: 10.1038/s41598-019-56583-9
29. Kamen A, Sun S, Wan S, Kluckner S, Chen T, Gigler AM, et al. Automatic Tissue Differentiation Based on Confocal Endomicroscopic Images for Intraoperative Guidance in Neurosurgery. *BioMed Res Int* (2016) 2016:6183218. doi: 10.1155/2016/6183218
30. Charalampaki P, Nakamura M, Athanasopoulos D, Heimann A. Confocal-Assisted Multispectral Fluorescent Microscopy for Brain Tumor Surgery. *Front Oncol* (2019) 9:583. doi: 10.3389/fonc.2019.00583
31. Folaron M, Strawbridge R, Samkoe KS, Filan C, Roberts DW, Davis SC. Elucidating the Kinetics of Sodium Fluorescein for Fluorescence-Guided Surgery of Glioma. *J Neurosurg* (2018) 131:724–34. doi: 10.3171/2018.4.JNS172644
32. Belykh E, Zhao X, Ngo B, Farhadi DS, Byvaltsev VA, Eschbacher JM, et al. Intraoperative Confocal Laser Endomicroscopy Ex Vivo Examination of Tissue Microstructure During Fluorescence-Guided Brain Tumor Surgery. *Front Oncol* (2020) 10:599250. doi: 10.3389/fonc.2020.599250
33. Belykh E, Zhao X, Ngo B, Farhadi DS, Kindelin A, Ahmad S, et al. Visualization of Brain Microvasculature and Blood Flow in Vivo: Feasibility Study Using Confocal Laser Endomicroscopy. *Microcirculation* (2021) 11: e12678. doi: 10.1111/micc.12678
34. Izadyyazdanabadi M, Belykh E, Zhao X, Moreira LB, Gandhi S, Cavallo C, et al. Fluorescence Image Histology Pattern Transformation Using Image Style Transfer. *Front Oncol* (2019) 9:519. doi: 10.3389/fonc.2019.00519
35. Aubreville M, Stoeve M, Oetter N, Goncalves M, Knipfer C, Neumann H, et al. Deep Learning-Based Detection of Motion Artifacts in Probe-Based Confocal Laser Endomicroscopy Images. *Int J Comput Assist Radiol Surg* (2019) 14:31–42. doi: 10.1007/s11548-018-1836-1

Conflict of Interest: DS was employed by the company Clevertech Inc.

The remaining authors declare that the research was conducted in the absence of any commercial or financial relationships that could be construed as a potential conflict of interest.

frontiers in Oncology

MINI REVIEW
published: 26 May 2021
doi: 10.3389/fonc.2021.666734

Rationale and Clinical Implications of Fluorescein-Guided Supramarginal Resection in Newly Diagnosed High-Grade Glioma

Linda M. Wang, Matei A. Banu, Peter Canoll and Jeffrey N. Bruce *

Gabriele Bartoli Brain Tumor Laboratory, Department of Neurological Surgery and Department of Pathology and Cell Biology, Columbia University Irving Medical Center, New York, NY, United States

Current standard of care for glioblastoma is surgical resection followed by temozolomide chemotherapy and radiation. Recent studies have demonstrated that >95% extent of resection is associated with better outcomes, including prolonged progression-free and overall survival. The diffusely infiltrative pattern of growth in gliomas results in microscopic extension of tumor cells into surrounding brain parenchyma that makes complete resection unattainable. The historical goal of surgical management has therefore been maximal safe resection, traditionally guided by MRI and defined as removal of all contrast-enhancing tumor. Optimization of surgical resection has led to the concept of supramarginal resection, or removal beyond the contrast-enhancing region on MRI. This strategy of extending the cytoreductive goal targets a tumor region thought to be important in the recurrence or progression of disease as well as resistance to systemic and local treatment. This approach must be balanced against the risk of impacting eloquent regions of brain and causing permanent neurologic deficit, an important factor affecting overall survival. Over the years, fluorescent agents such as fluorescein sodium have been explored as a means of more reliably delineating the boundary between tumor core, tumor-infiltrated brain, and surrounding cortex. Here we examine the rationale behind extending resection into the infiltrative tumor margins, review the current literature surrounding the use of fluorescein in supramarginal resection of gliomas, discuss the experience of our own institution in utilizing fluorescein to maximize glioma extent of resection, and assess the clinical implications of this treatment strategy.

Keywords: fluorescein, supramarginal resection, supramaximal resection, glioblastoma, high-grade glioma, survival, fluorescence-guided surgery

OPEN ACCESS

Edited by:
Talat Kiris, Koç University, Turkey

Reviewed by:
Emanuele La Corte, University of Bologna, Italy
Pawel Tabakow, Wroclaw Medical University, Poland

***Correspondence:**
Jeffrey N. Bruce
jnb2@cumc.columbia.edu

Specialty section:
This article was submitted to Neuro-Oncology and Neurosurgical Oncology, a section of the journal Frontiers in Oncology

Received: *10 February 2021*
Accepted: *10 May 2021*
Published: *26 May 2021*

Citation:
Wang LM, Banu MA, Canoll P and Bruce JN (2021) Rationale and Clinical Implications of Fluorescein-Guided Supramarginal Resection in Newly Diagnosed High-Grade Glioma. Front. Oncol. 11:666734. doi: 10.3389/fonc.2021.666734

INTRODUCTION

Glioblastoma is the most common and aggressive primary brain cancer, with over 12,000 new cases diagnosed each year (1). Current standard of care is surgical resection followed by radiation and temozolomide chemotherapy. Even with maximal therapy, prognosis remains bleak, with a median overall survival of 15 months and a 5-year survival of less than 7% (1–3). Despite focused efforts to

develop new systemic treatment strategies led by an increasingly nuanced understanding of the molecular underpinnings of this disease, this work has yet to translate into significant clinical benefit for the majority of patients.

Surgical resection remains the mainstay of treatment. The only modifiable prognostic indicator of outcome in glioblastoma is extent of resection, which has been shown to correlate closely with improved survival. The current standard of surgical treatment is maximal safe resection (4, 5). However, because of their diffusely infiltrative growth pattern, which results in the microscopic extension of tumor cells along white matter tracts and into adjacent brain parenchyma, gliomas cannot be completely resected. Maximal or gross total resection, therefore, is currently defined as the removal of all contrast-enhancing tumor. Nonetheless, based on multiple studies employing modern histology as well as advanced sequencing methods, numerous and phenotypically diverse infiltrating glioma cells have been identified in the non-enhancing edematous regions adjacent to the tumor core. This infiltrating tumor margin is currently an area of intense research as the putative region of therapeutic resistance and glioma recurrence (6–8).

Despite advances in surgical management, all patients with glioblastoma eventually experience disease recurrence. Importantly, this recurrence almost always arises within 2 cm of the original lesion, thought to be related to the residual microscopic disease (9, 10). More recently, there has been growing interest in exploring the clinical benefit of extending the cytoreductive goal beyond the borders of the contrast-enhancing tumor, so-called supramarginal or supramaximal resection, to target this microscopically infiltrated region surrounding visible tumor. Over the past decade, there have been a number of studies investigating supramarginal resection for the management of high-grade gliomas, many of which have demonstrated that this technique is associated with improvements in survival compared to gross total resection (11). However, as with any surgical approach in the brain, the benefit of supramarginal resection must be balanced against the risk of causing new neurologic deficit. Furthermore, decisions on extent of resection of infiltrative margins have largely been arbitrary. Imaging and/or intraoperative fluorophores, in combination with other novel intraoperative methods such Raman spectroscopy, will increase the efficacy and safety of resection at the infiltrative margins (12, 13).

In pursuit of increasing the safety and accuracy of brain tumor resection, various technologies have been developed with the goal of providing more reliable intraoperative guidance. Frameless stereotactic neuronavigation is the method most typically used in operating rooms today but is not without its weaknesses. This technology relies heavily upon accurate registration prior to surgery, and even with initial accuracy, as tumor resection progresses brain shift inevitably develops and compromises the precision of localization. Compounding this issue is the fact that deeper areas of tumor, which are often the more dangerous areas with the greatest need for reliable guidance due to their proximity to white matter tracts and vascular structures, are most affected by this phenomenon. Intraoperative MRI has been explored as an alternative means of providing more up-to-date navigational information but is disruptive to the operating room workflow; it also fails to provide true real-time information and represents a significant capital investment (14). Intraoperative ultrasound is lower cost, widely available, and produces less interruption of the surgical workflow, but the quality of the scan is operator dependent, and unfamiliarity with the technique due to lack of standard ultrasound training results in difficulty interpreting images and an extended learning curve (15).

Fluorescent agents that selectively localize to pathologic tissue and can be viewed intraoperatively, such as 5-aminolevulinic acid (5-ALA), do provide genuine real-time feedback. 5-ALA has been extensively studied in glioma neurosurgery and is proven to significantly increase extent of resection and improve patient survival (16). Fluorescein is another fluorophore routinely used in ophthalmology with increasing popularity in neurosurgery. Compared to 5-ALA, fluorescein offers several advantages. 5-ALA is expensive, patients must avoid exposure to light after administration due to the risk of severe skin reactions, and significant time must elapse between drug administration and initiation of surgery. 5-ALA can also be disruptive to surgical workflow due to darkening of the surgical field surrounding the tumor, which may necessitate frequent switching between filtered and white light in order to adequately visualize vascular structures or non-tumor tissue (17, 18). In contrast, fluorescein is low-cost, causes few adverse effects, and is conveniently given during induction of anesthesia (17). In our experience, illumination of the surgical field using a specialized filter for fluorescein allows for clear detection of the fluorescent signal as well as good visualization of the relevant surgical anatomy, a finding that has been supported by others (9, 18).

Fluorescein has been shown to reliably correlate with areas of contrast-enhancement on MRI (19). Most interestingly, it has been demonstrated that fluorescein is also able to localize to non-enhancing regions of low-grade and high-grade gliomas, outside of what would traditionally be considered the area representing surgical goal (9). Here we discuss the potential role of fluorescein in facilitating safer and more targeted supramarginal resection in high-grade glioma, as well as the clinical implications of this treatment strategy.

WHAT IS THE CLINICAL BENEFIT OF PURSUING SUPRAMARGINAL RESECTION?

Current Knowledge of the Safety and Feasibility of Supramarginal Resection in Glioblastoma

In its most basic sense, supramarginal resection refers to the removal of tumor exceeding "gross total resection", or, more specifically, the resection of tissue beyond the contrast-enhancing tumor border (11). However, well-defined standardized criteria for what constitutes supramarginal resection have not been established, and different research groups have used different criteria. In their retrospective series of 32 patients, Glenn et al. defined supramarginal resection as the removal of all contrast-enhancing tissue plus at least 1 cm of surrounding brain (20). Studies by Li et al., Mampre et al., and Pessina et al. all based their supramarginal resection on the removal of

additional tissue from the region of FLAIR abnormality, but with differing specifications for what percentage of FLAIR tissue must be removed (21–23). Recently, Certo et al. published a study in which supramarginal resection was guided by FLAIR signal with additional assistance from 5-ALA (24). Perhaps most notably, Roh et al. achieved supramarginal resection by performing either a frontal or temporal lobectomy (25). Still other studies have incorporated the utilization of specific dissection techniques into the definition of supramarginal resection (26).

Despite these differences, almost all clinical studies investigating supramarginal resection for glioblastoma have shown that compared to gross total resection, supramarginal resection correlates with prolonged survival, with reported increases in median overall survival ranging from 5 to 25 months, and increases in progression-free survival as high as 19 months (11, 20, 21, 25). Although these findings are encouraging, it is important to recognize that in addition to the inconsistencies in defining supramarginal resection, much of the existing research investigating this technique comprises small, retrospective studies focusing on a select subset of patients. Before this strategy can find a place in the standard surgical management of glioblastoma, much work remains to be done to further clarify what parameters for supramarginal resection are most clinically useful.

Supramarginal Resection Extends Cytoreduction Into the Peritumoral Tissue, the Putative Driver of Disease Recurrence

Even with complete resection of the contrast-enhancing tumor, glioblastoma invariably recurs, and recurrence is almost always within centimeters of the original lesion, suggesting that the peritumoral region—the region marked by T2/FLAIR signal and lacking contrast enhancement, hence traditionally left behind following surgical resection—plays an important role in this process (6, 27).

The peritumoral region of diffusely infiltrating gliomas contains many different cell populations, both neoplastic and nonneoplastic, that likely contribute to tumor progression and treatment resistance (28). The clinical importance of neoplastic infiltrating cells occupying this region is reflected in evidence suggesting that these cells differ from the neoplastic cells found in the tumor core. Infiltrating glioma cells express genes that may lead to recurrent disease, such as ECM2 and ANGPT1, which play a role cell migration (7). Studies have demonstrated that tumor cells isolated from the resection margins are more invasive than cells sampled from the tumor core (29–32). Using single cell RNA sequencing, Darmanis et al. found that the molecular signature of infiltrating neoplastic cells obtained from the peritumoral tissue was characterized by increased energy production and inhibition of apoptosis, as well as decreased regulation of cell-cell adhesion (7). Moreover, even across distinct patients, the gene expression signatures of infiltrating neoplastic cells displayed a notable degree of homogeneity, possibly implying a shared mechanism of infiltration (7).

Interactions between neurons and glioma cells *via* neuron-glioma synapses may also contribute to tumor progression (33). Depolarization of the glioma cell membrane is known to increase proliferation, referred to as "activity-regulated glioma growth" (33). Gliomas in turn are thought to increase neuronal excitability, creating a positive feedback loop of tumor growth and progression. It stands to reason that these reciprocal interactions predominantly occur at the tumor margin, which is the region where neurons and glioma cells intermingle, and is also the region targeted by supramarginal resection.

While these different cell populations and interactions within the peritumoral environment represent exciting potential targets for medical therapy, more research is needed to bring these findings into the clinical realm. Currently, no known drug can simultaneously target or disrupt all of the elements in the tumor margin that contribute to glioblastoma progression, and the most effective method of addressing these factors remains surgical resection.

Despite the potential benefits of supramarginal resection in glioblastoma, the question remains: how can this technique be effectively and safely carried out? One of the greatest risks of extending surgical resection beyond the area of contrast-enhancement is the possibility of worsening or causing new neurologic deficit. In addition to extent of resection, patient neurological function is closely associated with outcome. Development of a new neurologic deficit after glioblastoma resection has been correlated with a decrease in overall survival, even if the deficit has resolved by as early as the first post-operative visit (11, 34). For this reason, it is crucial to establish clearer, evidence-based guidelines for defining supramarginal resection, and to supplement any attempt at achieving supramarginal resection with appropriate measures to increase safety, such as intraoperative neurophysiological monitoring, image-based navigational guidance, and fluorophores such as fluorescein. Although focused primarily on low-grade gliomas, a 2019 review by Duffau et al. discusses the merits of a functional-based approach for supramarginal resection of diffuse gliomas, where awake brain mapping using direct electrostimulation is combined with intraoperative neurocognitive monitoring to map cortical-subcortical structures, ultimately reducing the risk of malignant transformation while also preserving patient quality of life (35).

HOW CAN FLUORESCEIN FACILITATE SUPRAMARGINAL RESECTION IN HIGH-GRADE GLIOMA?

Fluorescein as a Tool for Achieving Greater Rate of Maximal or "Complete" Resection

Fluorescein sodium is a fluorescent compound with peak excitation in the 460 to 500 nm range and peak emission in the yellow-green part of the spectrum between 540 and 690 nm (36). Though traditionally used in retinal angiography, fluorescein's role in tumor neurosurgery was explored as early as 1947, with studies by Moore et al. investigating the differential retention of fluorescein in malignant versus benign brain tissue (37, 38). Early studies of fluorescein in neurosurgery used doses as high as 20 mg/kg, which enabled visualization under white light illumination (17, 39, 40). With the development of specialized microscopes bearing integrated fluorescence filters, however, doses as low as 3-5 mg/kg are now frequently used, further increasing the safety and tolerability of this agent and bolstering its appeal as a neurosurgical adjunct (17, 18, 41, 42).

Initially, the ability of fluorescein to identify tumor tissue was used for obtaining diagnostic biopsies, but over time interest has grown in its potential to guide resection in high-grade gliomas. Multiple studies have illustrated the utility of fluorescein in improving the rate of gross total resection, with one trial reporting complete resection in over 80% of patients with high-grade gliomas resected using fluorescein, in contrast to the 30-50% rate historically described in patients undergoing surgical resection with white light only (36, 40, 43–45).

Fluorescein is administered intravenously and works not by accumulating within tumor cells, but rather by extravasating in areas of blood brain barrier damage and collecting in the extracellular space (19, 41). This mechanism of action closely mirrors that of gadolinium, and accordingly, much of fluorescein's value as a surgical adjunct has thus far been in its ability to serve as an intraoperative equivalent of the radiologic gadolinium signal, essentially enabling the neurosurgeon to visualize the contrast-enhancing region of tumor in real-time without the pitfalls of traditional neuronavigation such as brain shift or errors in registration (19, 46).

Fluorescein Positivity Extends Beyond the Contrast-Enhancing Region of Tumors and Accurately Predicts Pathologic Tissue

Interestingly, despite the similar mechanism of action shared by fluorescein and gadolinium, studies have pointed to the propensity of fluorescein to localize to areas that fail to enhance on T1-weighted MRI (9, 47, 48). It is not entirely understood why this occurs, although proposed mechanisms include differing degrees of vascular disruption between contrast-enhancing and non-enhancing regions, discrepancies in the vascular permeability of fluorescein and gadolinium, and differences in their patterns of diffusion within the extracellular space (9, 19, 47). Regardless, the same studies have shown that these fluorescein-positive, gadolinium-negative areas do not represent a false positive signal, but in fact frequently identify regions of histologically abnormal tissue. We propose that by staining abnormal tissue beyond what is captured by gadolinium contrast enhancement, fluorescein can extend the surgical resection to include those infiltrated tumor margins that play an important role in disease recurrence.

In 2017, our institution published a study exploring the utility of fluorescein for identifying histopathologic alteration in biopsies obtained from both the contrast-enhancing regions and the non-enhancing margins of high-grade gliomas (9). Neira et al. found that fluorescein staining extended beyond the region of contrast-enhancement and into the non-enhancing infiltrative tumor margins (**Figure 1**). Furthermore, samples from these areas had comparable specificity for tumor tissue compared to samples from contrast-enhancing areas. The positive predictive value of subjectively measured fluorescein positivity for histopathologic alteration was >96% in the non-enhancing areas, and 98.6% across all biopsies regardless of radiographic localization, demonstrating fluorescein's ability to reliably predict glioma-associated pathology in both contrast-enhancing and non-enhancing areas and pointing to its potential role in facilitating more aggressive, supramarginal resection into the non-enhancing margins of high-grade gliomas (9).

Bowden et al. investigated the use of fluorescein in improving diagnostic accuracy of tissue sampling in low-grade gliomas (47). Even in these non-enhancing tumors, fluorescein was able to predict the presence of tissue with pathologic features, once again demonstrating the existence of gadolinium-negative, fluorescein-positive regions that accurately identify pathologic tissue. Although this study sampled only from areas already suspected to be tumor, the authors observed that the fluorescent regions were more likely to demonstrate a greater degree of cytologic atypia, higher cell density, and greater proliferative activity, further supporting our hypothesis that in the absence of contrast enhancement, fluorescein positivity can serve as a marker of areas of interest for surgical resection. In other words, fluorescein can be used to identify regions of high-grade transformation in low-grade gliomas.

In 2018, Schebesch et al. described a series of 5 patients with non-enhancing but positron emission tomography (PET) positive gliomas of varying grade who underwent surgery with fluorescein guidance (48). Specifically, these patients were evaluated with PET using the tracer ^{18}F-fluoroethyl tyrosine (FET), which has increased specificity for glioma tissue (49–51). Histopathologic workup of the fluorescent areas in each case was positive for pathologic tissue. Some lesions demonstrated homogenous fluorescence throughout with clear demarcation of the border between diseased and non-affected brain, while others showed more heterogeneous patterns of staining. However, a common theme across all cases was that the distribution of fluorescence closely aligned with that of FET-PET positivity on preoperative imaging, suggesting that there may be some degree of blood brain barrier disruption that traditional gadolinium contrast-enhanced MRI is not sensitive enough to detect, but that can be predicted to an extent based on FET-PET positivity (48). Notably, it has also previously been found that FET-PET can identify non-enhancing, metabolically active tumor (49, 52).

Limitations of Fluorescein in Achieving Effective Supramarginal Resection

While fluorescein has proven useful in detecting non-contrast-enhancing, glioma-associated tissue, especially at the infiltrative margins, there are limits to this approach. Although fluorescein can certainly contribute to supramarginal resection by identifying regions of interest beyond what is traditionally considered surgical goal, large areas of non-enhancing infiltrated brain that also do not demonstrate fluorescent signal likely remain. In other words, fluorescein does not comprehensively define the boundaries of clinically adequate supramarginal resection. As alluded to earlier, there is still little consensus about what constitutes supramarginal resection, and what definition or criteria best maximizes survival benefit while minimizing patient harm (11). Thus, it will be important to supplement fluorescein with other tools such as intraoperative neurophysiological monitoring (e.g. awake craniotomy, sub-sensory evoked potentials, motor-sensory evoked potentials) and even other fluorescent agents.

FUTURE DIRECTIONS

While studies have investigated different means of achieving supramarginal resection in glioblastoma, perhaps the best way to maximize extent of resection is to combine the various navigational

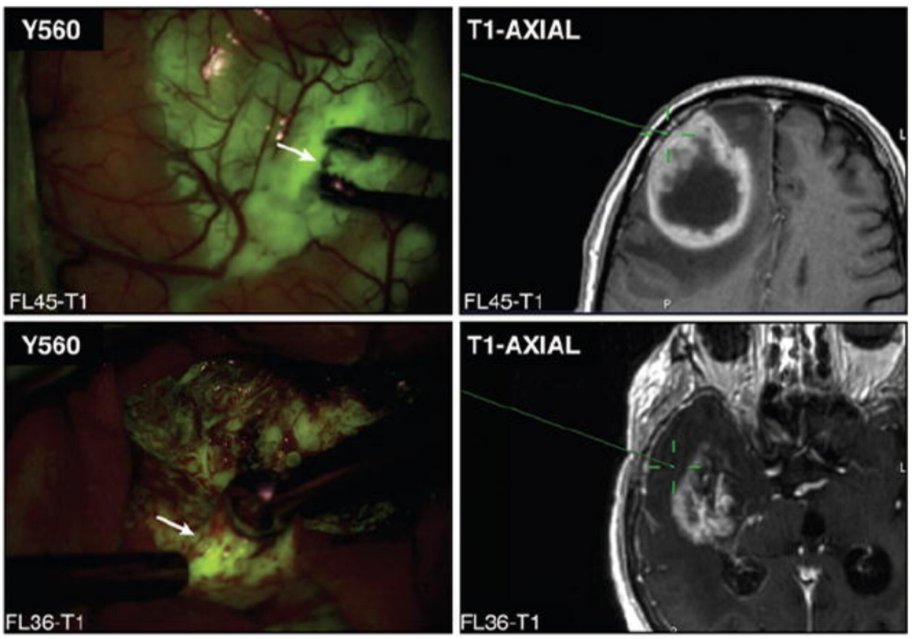

FIGURE 1 | Representative image of biopsy sites (white arrows) from both contrast-enhancing (upper) and non-enhancing (lower) regions, localized using stereotactic guidance with the BrainLab-registered wand indicating the biopsy site on preoperative MRI (green crosshairs). Note that both contrast-enhancing and non-enhancing biopsy sites demonstrate yellow-green fluorescence. Modified from Neira JA: Aggressive resection at the infiltrative margins of glioblastoma facilitated by intraoperative fluorescein guidance. Journal of Neurosurgery 127:111-122, 2017. With permission from Journal of Neurosurgery Publishing Group.

tools at our disposal. 5-ALA and fluorescein have distinct mechanisms of action that complement each other in detecting pathologic tissue, and guidance of supramarginal resection using both fluorophores might prove more effective than using either alone (53, 54). Alternatively, fluorescein could be combined with Raman spectroscopy, which has been shown to accurately delineate tumor versus normal brain at the margins of resection, with superior performance compared to 5-ALA (55). Confocal laser endomicroscopy has also been combined with fluorescein and recently investigated as a means of increasing extent of resection by providing real-time intraoperative verification of pathologic tumor tissue (56–58). Several studies have also mentioned the potential benefit of quantitatively measuring fluorescence intensity and integrating this technology with the operative microscope, which could increase both the safety and the sensitivity of fluorescein as an adjunct for glioma resection (9, 17, 29). The utility of fluorescein for resection of recurrent glioblastoma is beyond the scope of this paper, but fluorescein has shown efficacy in identifying recurrent glioblastoma tissue and improving extent of resection in such cases, and might be of use in distinguishing between active disease and pseudoprogression (59). As shown by Bowden et al. and others, fluorescent agents may also serve as promising adjuncts for guiding resection in non-enhancing low-grade gliomas (47, 60). Finally, the development of novel fluorescent probes with even greater specificity for pathologic tissue, for example by labeling brain tissue based on metabolic or molecular alterations, represents an exciting new advancement in the field of fluorescence-guided surgery (61).

CONCLUSIONS

By localizing to areas of pathologic tissue that fail to enhance on T1-weighted MRI, fluorescein may serve as a way of safely and reliably defining targets for supramarginal resection beyond the traditional contrast-enhancing goal of resection. To maximize patient safety, this strategy must be balanced with other well-established tools for increasing the safety and efficacy of surgical resection. Although supramarginal resection for glioblastoma is a promising treatment approach, larger prospective studies are needed to establish a consistent definition of "supramarginal" and determine the extent of resection that maximizes survival benefit while optimizing patient safety. While prolonged survival is an important outcome measure, it is important that these studies also assess the longer-term effects of supramarginal resection on neurological functioning and patient quality of life.

AUTHOR CONTRIBUTIONS

LW and MB drafted the manuscript. PC and JB supervised and finalized the manuscript. All authors contributed to the article and approved the submitted version.

FUNDING

This research was funded in part through the NIH/NCI Cancer Center Support Grant P30CA013696.

REFERENCES

1. Ostrom QT, Cioffi G, Gittleman H, Patil N, Waite K, Kruchko C, et al. CBTRUS Statistical Report: Primary Brain and Other Central Nervous System Tumors Diagnosed in the United States in 2012–2016. *Neuro-Oncology* (2019) 21(Supplement_5):v1–v100. doi: 10.1093/neuonc/noz150
2. Stupp R, Mason WP, van den Bent MJ, Weller M, Fisher B, Taphoorn MJ, et al. Radiotherapy Plus Concomitant and Adjuvant Temozolomide for Glioblastoma. *N Engl J Med* (2005) 352(10):987–96. doi: 10.1056/NEJMoa043330
3. Koshy M, Villano JL, Dolecek TA, Howard A, Mahmood U, Chmura SJ, et al. Improved Survival Time Trends for Glioblastoma Using the SEER 17 Population-Based Registries. *J Neuro-Oncol* (2012) 107(1):207–12. doi: 10.1007/s11060-011-0738-7
4. Sanai N, Polley MY, McDermott MW, Parsa AT, Berger MS. An Extent of Resection Threshold for Newly Diagnosed Glioblastomas. *J Neurosurg* (2011) 115(1):3–8. doi: 10.3171/2011.2.jns10998
5. Marko NF, Weil RJ, Schroeder JL, Lang FF, Suki D, Sawaya RE. Extent of Resection of Glioblastoma Revisited: Personalized Survival Modeling Facilitates More Accurate Survival Prediction and Supports a Maximum-Safe-Resection Approach to Surgery. *J Clin Oncol* (2014) 32(8):774–82. doi: 10.1200/jco.2013.51.8886
6. Gill BJ, Pisapia DJ, Malone HR, Goldstein H, Lei L, Sonabend A, et al. MRI-Localized Biopsies Reveal Subtype-Specific Differences in Molecular and Cellular Composition At the Margins of Glioblastoma. *Proc Natl Acad Sci* (2014) 111(34):12550–5. doi: 10.1073/pnas.1405839111
7. Darmanis S, Sloan SA, Croote D, Mignardi M, Chernikova S, Samghababi P, et al. Single-Cell RNA-Seq Analysis of Infiltrating Neoplastic Cells At the Migrating Front of Human Glioblastoma. *Cell Rep* (2017) 21(5):1399–410. doi: 10.1016/j.celrep.2017.10.030
8. D'Alessio A, Proietti G, Sica G, Scicchitano BM. Pathological and Molecular Features of Glioblastoma and Its Peritumoral Tissue. *Cancers (Basel)* (2019) 11:(4). doi: 10.3390/cancers11040469
9. Neira JA, Ung TH, Sims JS, Malone HR, Chow DS, Samanamud JL, et al. Aggressive Resection At the Infiltrative Margins of Glioblastoma Facilitated by Intraoperative Fluorescein Guidance. *J Neurosurg* (2017) 127(1):111–22. doi: 10.3171/2016.7.Jns16232
10. Davis ME. Glioblastoma: Overview of Disease and Treatment. *Clin J Oncol Nurs* (2016) 20(5 Suppl):S2–8. doi: 10.1188/16.Cjon.S1.2-8
11. Dimou J, Beland B, Kelly J. Supramaximal Resection: A Systematic Review of Its Safety, Efficacy and Feasibility in Glioblastoma. *J Clin Neurosci* (2020) 72:328–34. doi: 10.1016/j.jocn.2019.12.021
12. Eyüpoglu IY, Hore N, Merkel A, Buslei R, Buchfelder M, Savaskan N. Supra-Complete Surgery Via Dual Intraoperative Visualization Approach (DiVA) Prolongs Patient Survival in Glioblastoma. *Oncotarget* (2016) 7:(18). doi: 10.18632/oncotarget.8367
13. Hollon T, Lewis S, Freudiger CW, Sunney Xie X, Orringer DA. Improving the Accuracy of Brain Tumor Surgery Via Raman-Based Technology. *Neurosurg Focus* (2016) 40(3):E9. doi: 10.3171/2015.12.Focus15557
14. Kubben PL, ter Meulen KJ, Schijns OEMG, ter Laak-Poort MP, van Overbeeke JJ, Santbrink HV. Intraoperative MRI-Guided Resection of Glioblastoma Multiforme: A Systematic Review. *Lancet Oncol* (2011) 12(11):1062–70. doi: 10.1016/S1470-2045(11)70130-9
15. Pino MA, Imperato A, Musca I, Maugeri R, Giammalva GR, Costantino G, et al. New Hope in Brain Glioma Surgery: The Role of Intraoperative Ultrasound. *A Rev Brain Sci* (2018) 8(11):202. doi: 10.3390/brainsci8110202
16. Stummer W, Pichlmeier U, Meinel T, Wiestler OD, Zanella F, Reulen HJ. Fluorescence-Guided Surgery With 5-Aminolevulinic Acid for Resection of Malignant Glioma: A Randomised Controlled Multicentre Phase III Trial. *Lancet Oncol* (2006) 7(5):392–401. doi: 10.1016/s1470-2045(06)70665-9
17. Schebesch KM, Brawanski A, Hohenberger C, Hohne J. Fluorescein Sodium-Guided Surgery of Malignant Brain Tumors: History, Current Concepts, and Future Project. *Turk Neurosurg* (2016) 26(2):185–94. doi: 10.5137/1019-5149.Jtn.16952-16.0
18. Rey-Dios R, Cohen-Gadol AA. Technical Principles and Neurosurgical Applications of Fluorescein Fluorescence Using a Microscope-Integrated Fluorescence Module. *Acta Neurochirurgica* (2013) 155(4):701–6. doi: 10.1007/s00701-013-1635-y
19. Diaz RJ, Dios RR, Hattab EM, Burrell K, Rakopoulos P, Sabha N, et al. Study of the Biodistribution of Fluorescein in Glioma-Infiltrated Mouse Brain and Histopathological Correlation of Intraoperative Findings in High-Grade Gliomas Resected Under Fluorescein Fluorescence Guidance. *J Neurosurg* (2015) 122(6):1360–9. doi: 10.3171/2015.2.Jns132507
20. Glenn CA, Baker CM, Conner AK, Burks JD, Bonney PA, Briggs RG, et al. An Examination of the Role of Supramaximal Resection of Temporal Lobe Glioblastoma Multiforme. *World Neurosurg* (2018) 114:e747–55. doi: 10.1016/j.wneu.2018.03.072
21. Li YM, Suki D, Hess K, Sawaya R. The Influence of Maximum Safe Resection of Glioblastoma on Survival in 1229 Patients: Can We do Better Than Gross-Total Resection? *J Neurosurg* (2016) 124(4):977–88. doi: 10.3171/2015.5.Jns142087
22. Mampre D, Ehresman J, Pinilla-Monsalve G, Osorio MAG, Olivi A, Quinones-Hinojosa A, et al. Extending the Resection Beyond the Contrast-Enhancement for Glioblastoma: Feasibility, Efficacy, and Outcomes. *Br J Neurosurg* (2018) 32(5):528–35. doi: 10.1080/02688697.2018.1498450
23. Pessina F, Navarria P, Cozzi L, Ascolese AM, Simonelli M, Santoro A, et al. Maximize Surgical Resection Beyond Contrast-Enhancing Boundaries in Newly Diagnosed Glioblastoma Multiforme: Is it Useful and Safe? A Single Institution Retrospective Experience. *J Neuro-Oncol* (2017) 135(1):129–39. doi: 10.1007/s11060-017-2559-9
24. Certo F, Altieri R, Maione M, Schonauer C, Sortino G, Fiumano G, et al. Flairectomy in Supramarginal Resection of Glioblastoma Correlates With Clinical Outcome and Survival Analysis: A Prospective, Single Institution, Case Series. *Oper Neurosurg (Hagerstown)* (2020) 20(2):151–63. doi: 10.1093/ons/opaa293
25. Roh TH, Kang SG, Moon JH, Sung KS, Park HH, Kim SH, et al. Survival Benefit of Lobectomy Over Gross-Total Resection Without Lobectomy in Cases of Glioblastoma in the Noneloquent Area: A Retrospective Study. *J Neurosurg* (2019) 312(3):895–901. doi: 10.3171/2018.12.Jns182558
26. Esquenazi Y, Friedman E, Liu Z, Zhu J-J, Hsu S, Tandon N. The Survival Advantage of "Supratotal" Resection of Glioblastoma Using Selective Cortical Mapping and the Subpial Technique. *Neurosurgery* (2017) 81(2):275–88. doi: 10.1093/neuros/nyw174
27. Petrecca K, Guiot MC, Panet-Raymond V, Souhami L. Failure Pattern Following Complete Resection Plus Radiotherapy and Temozolomide Is At the Resection Margin in Patients With Glioblastoma. *J Neurooncol* (2013) 111(1):19–23. doi: 10.1007/s11060-012-0983-4
28. Torres D, Canoll P. Alterations in the Brain Microenvironment in Diffusely Infiltrating Low-Grade Glioma. *Neurosurg Clin N Am* (2019) 30(1):27–34. doi: 10.1016/j.nec.2018.08.001
29. Lemée JM, Clavreul A, Menei P. Intratumoral Heterogeneity in Glioblastoma: Don't Forget the Peritumoral Brain Zone. *Neuro Oncol* (2015) 17(10):1322–32. doi: 10.1093/neuonc/nov119
30. Glas M, Rath BH, Simon M, Reinartz R, Schramme A, Trageser D, et al. Residual Tumor Cells Are Unique Cellular Targets in Glioblastoma. *Ann Neurol* (2010) 68(2):264–9. doi: 10.1002/ana.22036
31. Ruiz-Ontañon P, Orgaz JL, Aldaz B, Elosegui-Artola A, Martino J, Berciano MT, et al. Cellular Plasticity Confers Migratory and Invasive Advantages to a Population of Glioblastoma-Initiating Cells That Infiltrate Peritumoral Tissue. *Stem Cells* (2013) 31(6):1075–85. doi: 10.1002/stem.1349
32. Toussaint LG, Nilson AE, Goble JM, Ballman KV, James CD, Lefranc F, et al. Galectin-1, a Gene Preferentially Expressed At the Tumor Margin, Promotes Glioblastoma Cell Invasion. *Mol Cancer* (2012) 11(1):32. doi: 10.1186/1476-4598-11-32
33. Venkatesh HS, Morishita W, Geraghty AC, Silverbush D, Gillespie SM, Arzt M, et al. Electrical and Synaptic Integration of Glioma Into Neural Circuits. *Nature* (2019) 573(7775):539–45. doi: 10.1038/s41586-019-1563-y
34. Rahman M, Abbatematteo J, De Leo EK, Kubilis PS, Vaziri S, Bova F, et al. The Effects of New or Worsened Postoperative Neurological Deficits on Survival of Patients With Glioblastoma. *J Neurosurg* (2017) 127(1):123–31. doi: 10.3171/2016.7.JNS16396
35. Duffau H. Higher-Order Surgical Questions for Diffuse Low-Grade Gliomas: Supramaximal Resection, Neuroplasticity, and Screening. *Neurosurg Clinics North America* (2019) 30(1):119–28. doi: 10.1016/j.nec.2018.08.009
36. Acerbi F, Broggi M, Schebesch KM, Hohne J, Cavallo C, De Laurentis C, et al. Fluorescein-Guided Surgery for Resection of High-Grade Gliomas: A Multicentric Prospective Phase II Study (Fluoglio). *Clin Cancer Res* (2018) 24(1):52–61. doi: 10.1158/1078-0432.CCR-17-1184

37. Moore GE, Peyton WT, French LA, Walker WW. The Clinical Use of Fluorescein in Neurosurgery. *J Neurosurg* (1948) 5(4):392. doi: 10.3171/jns.1948.5.4.0392
38. MOORE GE. Fluorescein as an Agent in the Differentiation of Normal and Malignant Tissues. *Science* (1947) 106(2745):130–1. doi: 10.1126/science.106.2745.130-a
39. Shinoda J, Yano H, Yoshimura S, Okumura A, Kaku Y, Iwama T, et al. Fluorescence-Guided Resection of Glioblastoma Multiforme by Using High-Dose Fluorescein Sodium. *Tech Note J Neurosurg* (2003) 99(3):597–603. doi: 10.3171/jns.2003.99.3.0597
40. Koc K, Anik I, Cabuk B, Ceylan S. Fluorescein Sodium-Guided Surgery in Glioblastoma Multiforme: A Prospective Evaluation. *Br J Neurosurg* (2008) 22 (1):99–103. doi: 10.1080/02688690701765524
41. Save AV, Gill BJ, D'Amico RS, Canoll P, Bruce JN. Fluorescein-Guided Resection of Gliomas. *J Neurosurg Sci* (2019) 63(6):648–55. doi: 10.23736/S0390-5616.19.04738-6
42. Schebesch KM, Proescholdt M, Höhne J, Hohenberger C, Hansen E, Riemenschneider MJ, et al. Sodium Fluorescein-Guided Resection Under the YELLOW 560 Nm Surgical Microscope Filter in Malignant Brain Tumor Surgery–a Feasibility Study. *Acta Neurochir (Wien)* (2013) 155(4):693–9. doi: 10.1007/s00701-013-1643-y
43. Lacroix M, Abi-Said D, Fourney DR, Gokaslan ZL, Shi W, DeMonte F, et al. A Multivariate Analysis of 416 Patients With Glioblastoma Multiforme: Prognosis, Extent of Resection, and Survival. *J Neurosurg* (2001) 95(2):190–8. doi: 10.3171/jns.2001.95.2.0190
44. McGirt MJ, Chaichana KL, Gathinji M, Attenello FJ, Than K, Olivi A, et al. Independent Association of Extent of Resection With Survival in Patients With Malignant Brain Astrocytoma. *J Neurosurg* (2009) 110(1):156–62. doi: 10.3171/2008.4.17536
45. Acerbi F, Broggi M, Eoli M, Anghileri E, Cuppini L, Pollo B, et al. Fluorescein-Guided Surgery for Grade IV Gliomas With a Dedicated Filter on the Surgical Microscope: Preliminary Results in 12 Cases. *Acta Neurochir (Wien)* (2013) 155(7):1277–86. doi: 10.1007/s00701-013-1734-9
46. Kuroiwa T, Kajimoto Y, Ohta T. Comparison Between Operative Findings on Malignant Glioma by a Fluorescein Surgical Microscopy and Histological Findings. *Neurol Res* (1999) 21(1):130–4. doi: 10.1080/01616412.1999.11740909
47. Bowden SG, Neira JA, Gill BJA, Ung TH, Englander ZK, Zanazzi G, et al. Sodium Fluorescein Facilitates Guided Sampling of Diagnostic Tumor Tissue in Nonenhancing Gliomas. *Neurosurgery* (2018) 82(5):719–27. doi: 10.1093/neuros/nyx271
48. Schebesch KM, Brawanski A, Doenitz C, Rosengarth K, Proescholdt M, Riemenschneider MJ, et al. Fluorescence-Guidance in Non-Gadolinium Enhancing, But FET-PET Positive Gliomas. *Clin Neurol Neurosurg* (2018) 172:177–82. doi: 10.1016/j.clineuro.2018.07.011
49. Lasocki A, Gaillard F. Non-Contrast-Enhancing Tumor: A New Frontier in Glioblastoma Research. *Am J Neuroradiol* (2019) 40(5):758–65. doi: 10.3174/ajnr.A6025
50. Floeth FW, Pauleit D, Wittsack H-J, Langen KJ, Reifenberger G, Hamacher K, et al. Multimodal Metabolic Imaging of Cerebral Gliomas: Positron Emission Tomography With [18F]Fluoroethyl-L-Tyrosine and Magnetic Resonance Spectroscopy. *J Neurosurg* (2005) 102(2):318. doi: 10.3171/jns.2005.102.2.0318
51. Pauleit D, Stoffels G, Bachofner A, Floeth FW, Sabel M, Herzog H, et al. Comparison of 18F-FET and 18F-FDG PET in Brain Tumors. *Nucl Med Biol* (2009) 36(7):779–87. doi: 10.1016/j.nucmedbio.2009.05.005
52. Nowosielski M, DiFranco MD, Putzer D, Seiz M, Recheis W, Jacobs AH, et al. An Intra-Individual Comparison of MRI, [18f]-FET and [18F]-FLT PET in Patients With High-Grade Gliomas. *PloS One* (2014) 9(4):e95830. doi: 10.1371/journal.pone.0095830
53. Coburger J, Engelke J, Scheuerle A, Thal DR, Hlavac M, Wirtz CR, et al. Tumor Detection With 5-Aminolevulinic Acid Fluorescence and Gd-DTPA–Enhanced Intraoperative MRI At the Border of Contrast-Enhancing Lesions: A Prospective Study Based on Histopathological Assessment. *Neurosurg Focus FOC* (2014) 36(2):E3. doi: 10.3171/2013.11.Focus13463
54. Della Puppa A, Munari M, Gardiman MP, Volpin F. Combined Fluorescence Using 5-Aminolevulinic Acid and Fluorescein Sodium At Glioblastoma Border: Intraoperative Findings and Histopathologic Data About 3 Newly Diagnosed Consecutive Cases. *World Neurosurg* (2019) 122:e856–63. doi: 10.1016/j.wneu.2018.10.163
55. Livermore LJ, Isabelle M, Bell IM, Edgar O, Voets NL, Stacey R, et al. Raman Spectroscopy to Differentiate Between Fresh Tissue Samples of Glioma and Normal Brain: A Comparison With 5-ALA–Induced Fluorescence-Guided Surgery. *J Neurosurg JNS* (2020), 1. doi: 10.3171/2020.5.Jns20376
56. Martirosyan NL, Eschbacher JM, Kalani MYS, Turner JD, Belykh E, Spetzler RF, et al. Prospective Evaluation of the Utility of Intraoperative Confocal Laser Endomicroscopy in Patients With Brain Neoplasms Using Fluorescein Sodium: Experience With 74 Cases. *Neurosurg Focus FOC* (2016) 40(3):E11. doi: 10.3171/2016.1.Focus15559
57. Acerbi F, Pollo B, De Laurentis C, Restelli F, Falco J, Vetrano IG, et al. Ex Vivo Fluorescein-Assisted Confocal Laser Endomicroscopy (Convivo® System) in Patients With Glioblastoma: Results From a Prospective Study. *Front Oncol* (2020) 10:2911. doi: 10.3389/fonc.2020.606574
58. Belykh E, Zhao X, Ngo B, Farhadi DS, Byvaltsev VA, Eschbacher JM, et al. Intraoperative Confocal Laser Endomicroscopy Ex Vivo Examination of Tissue Microstructure During Fluorescence-Guided Brain Tumor Surgery. *Front Oncol* (2020) 10:2584. doi: 10.3389/fonc.2020.599250
59. Höhne J, Schebesch K-M, de Laurentis C, Akçakaya MO, Pedersen CB, Brawanski A, et al. Fluorescein Sodium in the Surgical Treatment of Recurrent Glioblastoma Multiforme. *World Neurosurg* (2019) 125:e158–64. doi: 10.1016/j.wneu.2019.01.024
60. Goryaynov SA, Widhalm G, Goldberg MF, Chelushkin D, Spallone A, Chernyshov KA, et al. The Role of 5-ALA in Low-Grade Gliomas and the Influence of Antiepileptic Drugs on Intraoperative Fluorescence. *Front Oncol* (2019) 9:423. doi: 10.3389/fonc.2019.00423
61. Senders JT, Muskens IS, Schnoor R, Karhade AV, Cote DJ, Smith TR, et al. Agents for Fluorescence-Guided Glioma Surgery: A Systematic Review of Preclinical and Clinical Results. *Acta Neurochir (Wien)* (2017) 159(1):151–67. doi: 10.1007/s00701-016-3028-5

Conflict of Interest: The authors declare that the research was conducted in the absence of any commercial or financial relationships that could be construed as a potential conflict of interest.

frontiers in Neurology

REVIEW
published: 16 June 2021
doi: 10.3389/fneur.2021.682151

Fluorescence-Guided Surgery: A Review on Timing and Use in Brain Tumor Surgery

*Alexander J. Schupper[1], Manasa Rao[1], Nicki Mohammadi[1], Rebecca Baron[1], John Y. K. Lee[2], Francesco Acerbi[3] and Constantinos G. Hadjipanayis[1]**

[1] Department of Neurosurgery, Icahn School of Medicine at Mount Sinai, New York, NY, United States, [2] Department of Neurosurgery, University of Pennsylvania School of Medicine, Philadelphia, PA, United States, [3] Department of Neurosurgery, Fondazione Istituto Di Ricovero e Cura a Carattere Scientifico Istituto Neurologico Carlo Besta, Milan, Italy

Fluorescence-guided surgery (FGS) allows surgeons to have improved visualization of tumor tissue in the operating room, enabling maximal safe resection of malignant brain tumors. Over the past two decades, multiple fluorescent agents have been studied for FGS, including 5-aminolevulinic acid (5-ALA), fluorescein sodium, and indocyanine green (ICG). Both non-targeted and targeted fluorescent agents are currently being used in clinical practice, as well as under investigation, for glioma visualization and resection. While the efficacy of intraoperative fluorescence in studied fluorophores has been well established in the literature, the effect of timing on fluorophore administration in glioma surgery has not been as well depicted. In the past year, recent studies of 5-ALA use have shown that intraoperative fluorescence may persist beyond the previously studied window used in prior multicenter trials. Additionally, the use of fluorophores for different brain tumor types is discussed in detail, including a discussion of choosing the right fluorophore based on tumor etiology. In the following review, the authors will describe the temporal nature of the various fluorophores used in glioma surgery, what remains uncertain in FGS, and provide a guide for using fluorescence as a surgical adjunct in brain tumor surgery.

Keywords: fluorescence-guided surgery, 5-ALA, fluorescein, ICG, extent of resection, timing

OPEN ACCESS

Edited by:
Alireza Mansouri, Pennsylvania State University (PSU), United States

Reviewed by:
Marco Riva, University of Milan, Italy
Giovanni Raffa, University of Messina, Italy

***Correspondence:**
Constantinos G. Hadjipanayis constantinos.hadjipanayis@mountsinai.org

Specialty section:
This article was submitted to Neuro-Oncology and Neurosurgical Oncology, a section of the journal Frontiers in Neurology

Received: *17 March 2021*
Accepted: *11 May 2021*
Published: *16 June 2021*

Citation:
Schupper AJ, Rao M, Mohammadi N, Baron R, Lee JYK, Acerbi F and Hadjipanayis CG (2021) Fluorescence-Guided Surgery: A Review on Timing and Use in Brain Tumor Surgery. Front. Neurol. 12:682151. doi: 10.3389/fneur.2021.682151

INTRODUCTION

The single best prognostic factor for patients diagnosed with high-grade gliomas (HGGs) is maximal resection, also known as gross total surgical resection (GTR) (1–3). HGG GTR has been associated with greater overall survival in addition to longer progression-free survival (PFS) (1, 4).In order to maximize the extent of resection (EOR), a number of visualization techniques have been introduced into the field of neurosurgery. Fluorescent agents, also known as fluorophores, aid in the delineation of normal and malignant tumor tissue (5, 6), permitting real-time image guided surgery that can maximize EOR (7).

There are a limited number of fluorophores currently used in clinical practice. Stummer first described the use of 5-aminolevulinic acid (5-ALA) and FGS in glioma patients in 1998. Based on the results of a landmark randomized, Phase III study confirming greater tumor resection and better patient outcomes in comparison to conventional microsurgery, 5-ALA (Gleolan) was approved as an oral intraoperative imaging agent for visualization of malignant tissue during glioma surgery (8–10). The fluorophores have various mechanisms of

action, ranging from intracellular uptake with 5-ALA (11, 12) and ICG (13) to extracellular accumulation with fluorescein sodium (FS) and indocyanine-green (ICG), similar to the contrast enhancement found with gadolinium contrast enhancement found with MR imaging (14–16). FS is administered systemically after the induction of anesthesia while ICG and 5-ALA are given several hours before surgery (11, 15, 17, 18) (**Table 1**).

While each of these agents used for FGS are currently used in patients, there is still ongoing research on the pharmacokinetics of these molecules in order to understand the optimal timing of administration and fluorescence of tumors during surgery. Timing is important with fluorophore administration, as it can be impacted by patient and surgical delays, and may affect the efficacy of the agent. Other new targeted fluorophores are currently being investigated in HGG patients and also require better understanding of optimal administration for FGS. The purpose of this review is to elucidate the current evidence on the perspective of timing for the various fluorophores used in glioma patients for FGS and provide an outline of the literature on the use of the most currently used fluorophores for glioma surgery.

INDOCYANINE GREEN (ICG)

Indocyanine Green (ICG) has been used widely in medical applications, beginning with hepatic and cardiac function measurement, and expanding into ophthalmology indications where it is FDA approved (**Table 2**). Upon systemic administration, as an amphiphilic, tricarbocyanine iodide dye, ICG binds to plasma proteins yielding many advantages including its confinement to the vascular compartment (19). Additionally, it's light excitation and emission in the near-infrared (NIR), low toxicity, and rapid excretion leads to its popularity. ICG has been used as a cerebrovascular intraoperative contrast agent to confirm aneurysm occlusion during surgery. More recently, a more delayed administration of ICG has been described prior to glioma surgery (20). ICG works as a passive targeting agent and requires the breakdown of the BBB to concentrate at the tumor site (19). Unlike 5-ALA and fluorescein, two popular FDA-approved fluorophore agents, ICG is a near-infrared (NIR) fluorophore which presents unique utility in labeling tumor tissue (15, 21). NIR imaging affords higher resolution with increasing tissue penetration depths with excellent signal to noise ratio (SNR) (**Figure 1**).

Both preclinical and clinical studies report the use of ICG for glioma surgery albeit within a few minutes after systemic administration exploiting vascular permeability of glioma compared to normal brain (19, 22). Haglund et al. used ICG for enhanced optical imaging in human gliomas (23). Hansen et al. found that when ICG was injected intravenously into tumor-bearing rats, the tumor fluoresced intensely at 60–120 mg/kg for at least 1 h after injection (24). This study showed the ability of ICG to distinguish rat brain tumor from normal parenchyma with adequate tumor to normal brain background ratio, with minimal post-resection residual tumor cells (24).

ICG intrinsic properties include a plasma half-life of 3–4 min; in preclinical studies after 10 min only a small amount of originally injected ICG volume can be detected in the blood (25). Due to this short half-life, ICG is usually given as a bolus dose of <0.5–1 mg/kg and NIR imaging is performed shortly after (23). Haglund et al. found that ICG fluorescence of glioma tissue, unlike fluorescein, is time-dependent (23). Martirosyan et al. found tissue fluorescence when ICG was injected 15 min prior to visualization, while Haglund et al. found an optical signal between 5 and 10 min after ICG injection (23, 25). The dye uptake rate was shown to be faster in HGGs compared to low-grade gliomas, and this diversity in tumor cell population may explain the time-dependent nature of the ICG peak signal. Studies suggest that as ICG is rapidly being eliminated from the blood at 18–24% per minute, the dye is sequestered into the tumor (23).

More recently, ICG has been administered at higher doses and tumor visualization has been improved by exploiting the enhanced permeability and retention (EPR) of nanoparticle-sized ICG fluorophore within brain tumors (26). Zeh et al. administered doses above the FDA-approved limit of 2 mg/kg in rodents implanted with human glioma xenografts and demonstrated a broad plateau period extending up to 72 h, thus allowing for optimal imaging of glioma as compared to normal brain (20). With the SWIG approach, combining the natural permeability of the tumor vascularity with poor clearance allows for high doses of ICG to penetrate the tumor, a high dose (5 mg/kg) of intravenous ICG is given a day (24 h) prior to surgery, yielding improved intraoperative visualization of the tumor compared to white light (15, 27, 28). In a series of 15 gliomas featuring 11 HGG, sensitivity was 98% and specificity 45% (27).

FLUORESCEIN SODIUM

Fluorescein sodium (FS) is best known for its use in ophthalmology where it is FDA approved for angiography or angioscopy of the retina and iris vasculature (FDA approval letter). Recently, it has been reintroduced into neuro-oncologic surgery for HGG FGS. FS has a molecular weight of 376.27 and is the sodium salt of fluorescein. It was first used to visualize malignant brain tumor in 1948 (29). FS accumulates in HGGs where the BBB is disrupted and provides intra-operative visualization that is similar to pre-operative contrast-enhanced T1 images in which gadolinium accumulation is seen (30–33). FS can be viewed under white light, but the use of an operating microscope fitted with a dedicated filter allows to significantly reduce the dose needed to highlight tumoral tissue (**Figure 2**) (19, 30, 31, 34). FS is excited at 460–500 nm and emits a green, fluorescent emission wavelength at 540–690 nm (19, 35). FS is administered at the time of anesthesia prior to a craniotomy for HGG FGS. Immediately after systemic administration FS flows within the cerebral vasculature and afterwards accumulates in tumoral area where there is a damage of BBB. Fluorescence by FS can be visualized for up to 4 h after administration.

Both preclinical and clinical studies have confirmed that fluorescein, unlike other fluorophores, does not accumulate intracellularly but in the extracellular space in brain tumors (32, 35–37). Instead of tumor-specific uptake, it has been

TABLE 1 | Summary of the properties of fluorophores currently used in fluorescence-guided surgery.

Agent	Excitation (nm)	Emission (nm)	Targeting mode	Administration mode	Dosage (in humans)	Half-life	Time prior to visualization	Time to fluorescence disappearing in target tissue
ICG	778	700–850	Passive	IV	0.2–5 mg/kg	3–4 min	Seconds	Several minutes
Second Window ICG	778	700–850	Passive	IV	2.5–5.0 mg/kg		24 h	>72 h
Fluorescein	460–500	540–690	Passive	IV	2–20 mg/kg	23.5 min	2–4 h	2–4 h
5-ALA	375–440	640–710	Metabolic	Oral	20 mg/kg	1–3 h	2–8 h	22 h
BLZ-100	785	700–850	Molecular	IV	3–30 mg	30 min	3–29 h	48 h
CLR1501	500	517	Molecular	IV	16 mg/kg	4 days	4 days	–
CLR1502	760	778	Molecular	IV	2 mg/kg	4 days	4 days	–
IRDye800CW (EGFR)	–	794	Molecular	IV	Up to 24.5 mg/kg	15–20 min	1 h	3–4 days

ICG, indocyanine green; 5-ALA, 5-aminolevulinic acid; IV, intravenous.

TABLE 2 | Fluorophores currently used in brain tumor surgery and Food and Drug Administration (FDA) use approval.

Agent	Year of FDA approval	Use of FDA approval
ICG	1959	1. Determining cardiac output, hepatic function and liver blood flow. 2. For ophthalmic angiography.
Fluorescein	2006	1. Diagnostic fluorescein angiography or angioscopy of the retina and iris vasculature.
5-ALA	2017	1. Intraoperative optical imaging agent in patients with suspected high-grade gliomas

FDA, Food and Drug Administration; ICG, indocyanine green; 5-ALA, 5-aminolevulinic acid.

demonstrated that fluorescein sodium accumulates at disruptions of the BBB in areas with high- density tumor cells, thereby proving useful for HGG visualization (30–33, 36, 37). Fluorescein sodium has been found to have a sensitivity of 82–94% and a specificity of 90–91% for glioma visualization (19, 31, 32, 38). However, it has also been shown that FS fluorescence might not be limited to tumor tissue. As a matter of fact, some areas, such as dura mater, circumventricular organs and choroid plexus, due to the lack of BBB, appears intensively fluorescent (35). In addition, although the presence of FS fluorescence in normal brain parenchyma close to tumor tissue has been occasionally shown and considered a consequence of direct surgical manipulation (33, 39–41), it has been suggested that the application of a strict intraoperative protocol of FS injection could significantly limit this event (35).

Many studies have reported the safety, efficacy, and convenience of using fluorescein sodium during HGG resection (7, 16, 31, 35, 42–46). Maximal resection or gross-total resection (GTR) of tumors with FS has been reported with an increase in progression-free survival (PFS) (16, 19, 31–33, 35, 39, 40, 44, 45, 47). Additionally, due to concern that fluorescein is non-selective for tumor tissue, one study concluded that dual labeling with 5-ALA and fluorescein allowed for superior visualization in high-grade glioma resection because fluorescein sodium enhanced background tissue and 5-ALA enhanced tumor tissue (48).

Few studies have reported guidelines on when to administer FS for best visualization in the surgical field. Fluorescein distributes to tissues within 10 min and has a plasma half-life of 23.5 min (49). In clinical practice, FS is administered systemically in the operating room either immediately after anesthesia induction or prior to surgical resection (7, 16, 18, 31, 33, 35, 39, 42, 45, 49, 50). In order to elucidate whether fluorescein can be seen in non-tumor tissue, one study evaluated the pharmacokinetics of fluorescein sodium in different preclinical mouse models, without and with xenograft tumor (51). This study established that the majority (up to 70%) of injected fluorescein exists in circulating blood in the unbound form and that only up to 30% result to be protein-bound. Due to its low molecular weight, the circulating unbound form accumulates in normal mice brain tissue without xenograft tumor, with a peak timing of 30 min after injection, particularly if injected at human-equivalent high dosage, and that washout from normal brain seems to be completed 120 min after fluorescein injection. When used in orthotopic glioma models, the presence of unbound fluorescein in normal brain tissue 60 min after injection significantly reduces the tumor-to-normal contrast (51). The study also elucidated the fact that pegylated fluorescein sodium, which better matches gadolinium contrast in sizing, seems to provide more suitable kinetics and a higher ratio of tumor fluorescence compared to normal brain tissue in othotopic glioma models (51). There is a paucity of clinical data on the best timing of FS administration. Some studies have reported administration of fluorescein after incision of the dura with resection beginning as early as 10 or 20 min after injection (7, 16, 33, 39, 42, 44). However, in more recent

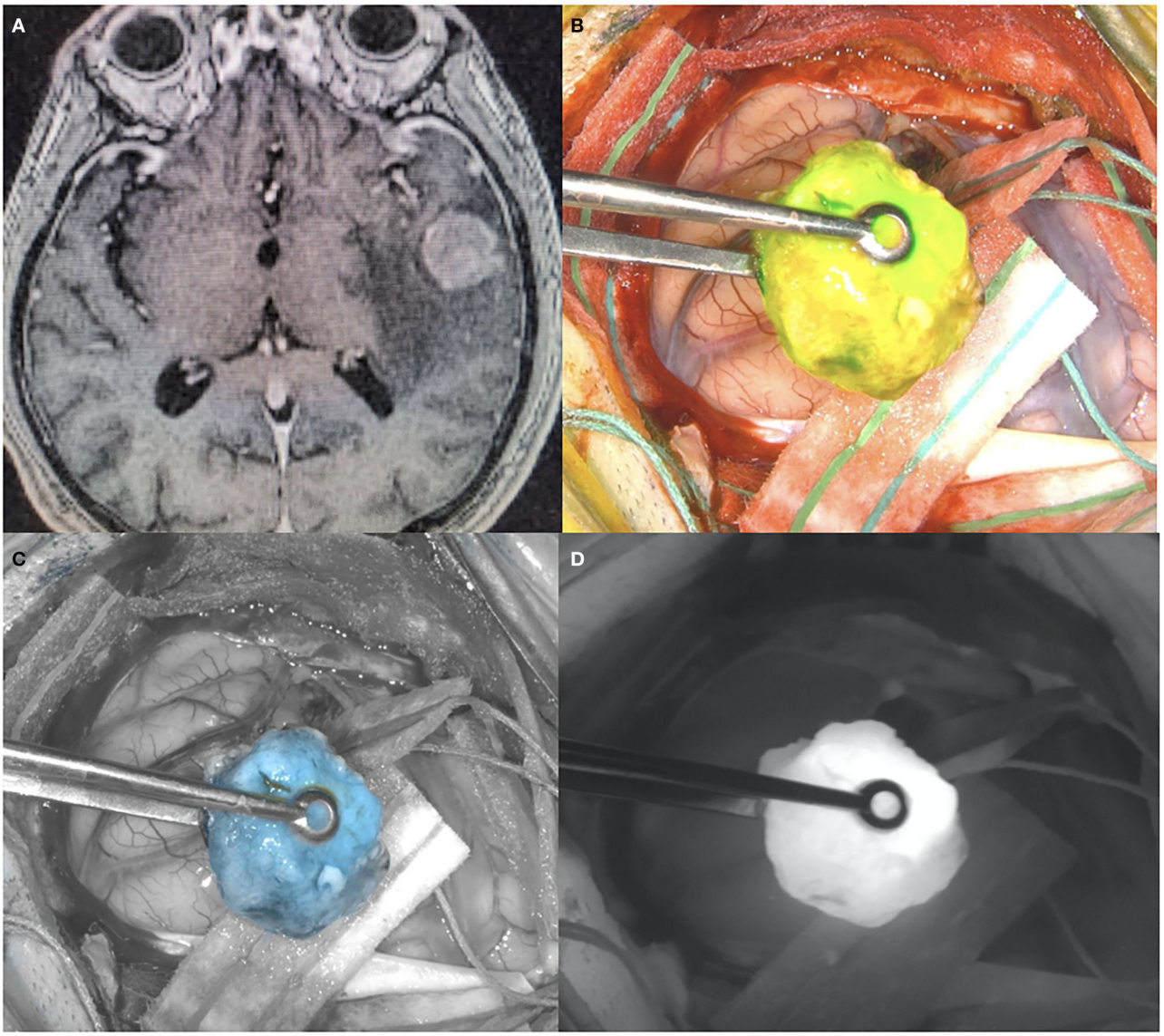

FIGURE 1 | (A) Pre-operative T1 post-contrast MR, showing a left temporal lesion with surrounding vasogenic edema. Histological diagnosis showed a metastatic lung adenocarcinoma. **(B)** Intraoperative picture during the surgical removal of the same case depicted in **(A)**, showing the ICG uptake by the tumor visualized with yellow-green excitation. **(C)** Intraoperative picture during the surgical removal of the same case depicted in **(A)**, showing the ICG uptake by the tumor with blue excitation. **(D)** Intraoperative picture during the surgical removal of the same case depicted in **(A)**, showing the ICG uptake by the tumor visualized with near-infrared excitation.

experiences it has been suggested to use low dose (5 mg/kg) of fluorescein, with intravenous injection performed after patient intubation, thus in most of the cases around 1 h before incision of dura mater (18, 31, 35). More specifically, it has been shown that the optimal strategy to optimize fluorescent contrast during surgery is to use lower dose (1–5 mg/kg) to minimize unspecific extravasation, administered 2–4 h before visualization, which corresponds to the wash-out period of the FLS (43). Surely, a need for further investigation of the clinically-relevant pharmacokinetics of optimal fluorescein sodium administration remains.

5-AMINOLEVULINIC ACID (5-ALA)

5-ALA, a precursor metabolized in the heme biosynthesis pathway to protoporphyrin (PPIX), accumulates intracellularly in tumor cells, and has a high affinity for high-grade glioma tissue (52). PPIX absorbs light between 375 and 440 nm and emits a violet-red fluorescence at 635 nm (**Figure 3**) (11) 5-ALA is the most well-studied fluorescent agent in glioma surgery that has been granted FDA approval (54, 55). A landmark randomized controlled study (RCT) was performed where HGG patients were randomized to FGS or conventional microsurgery (8) 5-ALA FGS

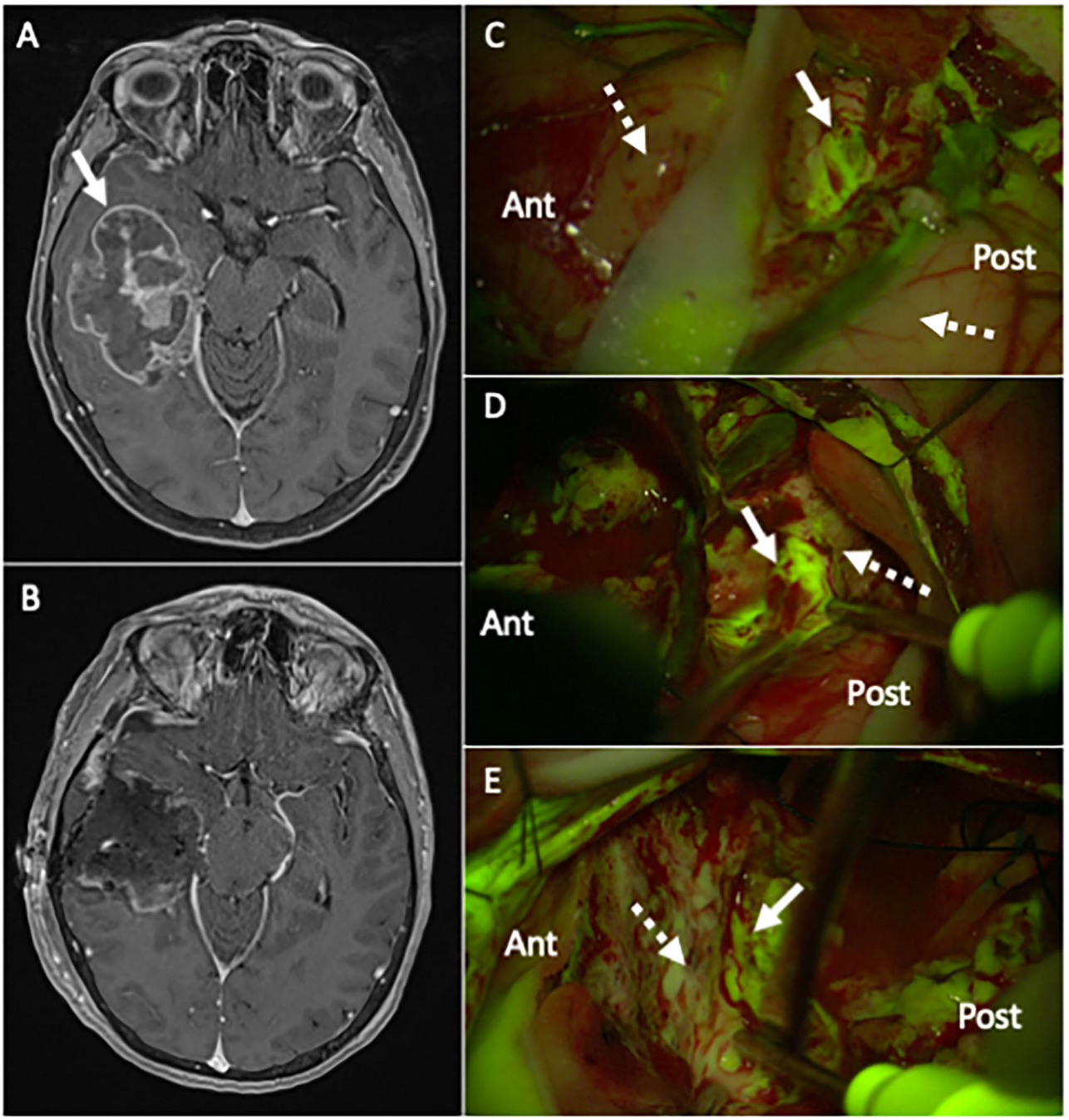

FIGURE 2 | (A) Pre-operative T1 post-contrast MR, showing a large right temporal lesion (white arrow), with irregular enhancement and mass effect, compatible with the suspect of high-grade glioma. **(B)** Post-operative T1 post-contrast MR, performed 24 h after surgery, confirming a gross-total resection (GTR) of the lesion (histological diagnosis showed a Glioblastoma, IDH wild-type). **(C–E)** Intraoperative picture during the surgical removal of the same case depicted in **(A)**, taken with the Y560 filter activated (Pentero 900 microscope, Carl Zeiss Meditec, Oberkochen, Germany): after a small corticectomy **(C)**, the pathological tissue is clearly visible as a bright green-yellow fluorescent area (white arrow), while the non-pathological temporal cortex (dotted white arrow) anteriorly and posteriorly is non-fluorescent (for orientation, Ant is anterior and Post is posterior temporal lobe); during surgical removal with ultrasonic aspirator (Sonoca 300, Soring, Quickborn, Germany), subcortical tumoral tissue is clearly discernible from normal peri-tumoral parenchyma by its bright green-yellow fluorescence (white arrow in **(D)** at the posterior border and in **(E)** at the anterior border), compared to pinkish peritumoral parenchyma (dotted white arrow).

was associated with improved progression-free survival (PFS) and greater overall tumor resection compared to white light control. 5-ALA FGS has been shown to be both safe and effective, with minimal side effects (8, 56, 57).

Since the publication of the RCT, the widespread use of 5-ALA globally has been based upon the same drug administration criteria used in the trial. An oral dose of ALA HCL solution of 20 mg/kg body weight, is administered 3 h (range 2–4 h) prior to induction of anesthesia (8) 5-ALA is rapidly absorbed into the blood after ingestion within 1 h and is metabolized quickly thereafter in brain tumors to its fluorescent PPIX metabolite. This dosing regimen was based upon rodent experiments in which there was a fluorescence peak observed 6 h after administration (10). The decision to have the patient ingest the medication at 3 h (with a range of 2–4 h) prior to surgery was recommended to allow ample time for anesthesia, monitoring and performing the craniotomy, in order for peak intraoperative PPIX fluorescence to be present during tumor resection (8, 56). As a result of this RCT and other European multicenter trials, the same administration criterion was used for the Food and Drug Administration (FDA) approval of 5-ALA (Gleolan®) in 2017 [(54); FDA approval] (58).

Recent studies have suggested that 5-ALA fluorescence may have a longer window of detection than previously described. In a prospective study of 68 patients and 201 tumor samples, Kaneko et al. found that maximal fluorescence intensity was observed 7–8 h following 5-ALA administration, and weak fluorescence peaked later than strong fluorescence, at 8–9 h (59). While prior animal studies have suggested an earlier fluorescence peak, there is now evidence that a longer latency time might lead to stronger fluorescence of HGG tissue. In a retrospective study of 16 patients who received 5-ALA over 4 h prior to anesthesia induction, our group found that adequate intraoperative fluorescence was seen up to almost 28 h post-ingestion, with no 5-ALA-related toxicity (53). Understanding the time window for 5-ALA PpIX fluorescence is clinically relevant, as surgeries are not uncommonly delayed due to emergent cases, staffing issues or other logistical challenges, and it is important to know if intraoperative fluorescence may be utilized despite delays in surgery. Unlike fluorescein and ICG which may be given in the operating room after induction of anesthesia, 5-ALA requires oral administration, and therefore there exists an element of anticipating time of surgery. Having a less narrow window of adequate intraoperative fluorescence allows surgeons greater flexibility with using 5-ALA for glioma surgery.

TARGETED FLUOROPHORES

In addition to the fluorophores mentioned above, there are current studies on fluorophores with more directed mechanisms of action, such as specific receptor targets. Below is a description of several targeted agents currently under clinical investigation.

BLZ-100

A conjugate of tumor-specific peptide chlorotoxin paired with a near-infrared fluorophore, BLZ-100 (tozuleristide, Blaze Bioscience Inc, Seattle, Washington) is visualized with a NIR camera (60). A recent phase I trial demonstrated safety and efficacy for the use of BLZ-100 in patients with primary and recurrent glioblastoma (60). Ongoing evaluation of the conjugate is currently being studied in both adult and pediatric brain tumors (NCT02234297, NCT02462629). BLZ-100 has the same benefits as ICG in the NIR spectrum, however, it adds further tumor specificity with chlorotoxin, a scorpion venom. Given intravenously, BLZ-100, also known as The Tumor Paint©, can safely be given to adults in doses ranging from 3 to 30 mg (60). In this trial, BLZ-100 was administered as a slow IV bolus injection over 1–5 min 3–29 h before surgery. It has a serum half-life of ∼30 min, however, unlike 5-ALA, has been shown to be retained in tumors for over 24 h, particularly in doses over 9 mg or greater in World Health Organization (WHO) grade III and IV gliomas (60). Its length of time in tumor tissue is currently unknown. Further study is required on a larger patient sample, however, depending upon the sensitivity of specificity of BLZ-100, it may provide a useful fluorophore given its high intensity of fluorescence and prolonged retention in glioma tissue.

Alkyl Phosphocholine Analogs

Alkylphosphocholine analogs (APCs) are small synthetic phospholipid ether molecules, which may target specific tumors types, including osteosarcoma, pancreatic adenocarcinoma and glioblastoma (61). Due to lipid raft expression, APCs are able to remain intracellular for prolonged periods of time (61), providing a theoretical advantage for FGS. To date, there are no published clinical results on APC use in gliomas, however, in a proof-of-principle preclinical study, high glioblastoma cell selectivity has been shown with two APCs (CLR1501 and CLR1502, Cellectar Biosciences, Madison, Wisconsin) (62). In the xenograft model, the two APCs were given intravenously in doses ranging from 2 to 16 mg/kg 4 days prior to sacrifice. CLR1501 (green spectrum) showed a tumor to brain fluorescence ratio comparable to 5-ALA, while CLR1502 (NIR) had a superior tumor to brain fluorescence ratio (62).

Epidermal Growth Factor Receptor (EGFR) Targeted Fluorophores

Expressed as cell-surface receptors in many cancers including gliomas, epidermal growth factor receptor (EGFR) may be conjugated with fluorescent dyes, allowing for targeted cell-surface fluorescence (63). In an *in vivo* animal study of IRDye800CW labeled with anti-EGFR antibodies, there was a 100% sensitivity and specificity for distinguishing GBM-specific mutated EGFR positive from EGFR negative cell lines (64). While no clinical studies have been performed to date, preclinical studies have administered intravenous anti-EGFR fluorescence conjugates into rats, and observed safe doses up to 24.5 mg/kg of an IRDye800CW anti-EGFR antibody (ABY-029, Affibody, Sweden) (65). However, due to its short half-life it will need to be given during surgery in humans, and in preclinical investigation had poor fluorescent intensity in the brain (65). Based upon this preclinical trial, it was determined that ABY-029 can be administered within minutes to hours of the surgery start time, and fluorescence was still observed 48 h post-administration (66).

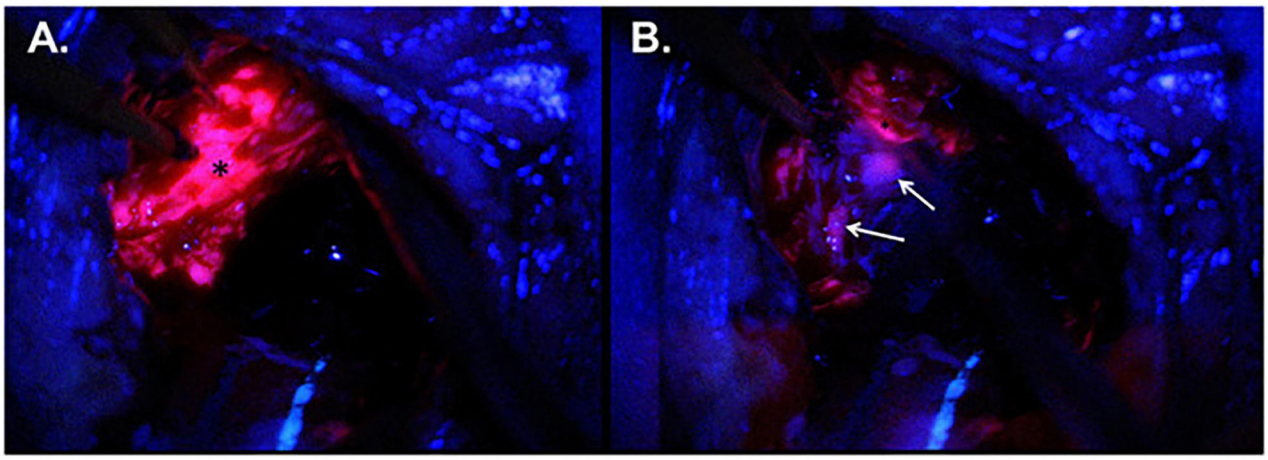

FIGURE 3 | Intraoperative imaging for case demonstration patient. **(A)** Tumor bulk fluorescence after 5-ALA administration (asterisk). **(B)** Infiltrative margin fluorescence after 5-ALA administration (white arrows). Taken with permission from Maragkos et al. (53).

Cetuximab, an EGFR monoclonal antibody, when conjugated with fluorescent IRDye 800CW, fluoresces in the NIR, and has been shown in preclinical studies to be effective for glioma surgery (67). In a first-in-human study, cetuximab-IRDye800 demonstrated both safety and efficacy, with high signal to background ration aiding in glioblastoma visualization (68). Larger studies are warranted to better underwent the use of cetuximab conjugates for FGS.

CHOOSING THE RIGHT FLUOROPHORES: PROPOSED SUGGESTIONS

While all fluorophores provide varying degrees of intraoperative fluorescence during brain tumor surgery, the various mechanisms of action make certain fluorophores better choices for different tumor types. Below is an outline for the different fluorophores currently available for use in FGS, based upon tumor pathology.

High-Grade Gliomas

High-grade gliomas (HGG) are the most widely studied tumor type in FGS. The three most commonly studied fluorophores, 5-ALA, fluorescein and ICG, have all been used in HGG surgery. 5-ALA has been the most robustly studied fluorophore in malignant gliomas. PPIX specifically accumulates in the tumor intracellular space, resulting in a robust red fluorescence in the tumor bulk, and a surrounding lighter pink fluorescence peripherally, representing surrounding infiltrative tumor cells (69, 70). This selective uptake in tumor cells results in high sensitivity and specficity, with prior studies showing mean sensitivity and specificity for delineating tumor tissue vs. surrounding brain to be 83–87% and 89–100%, respectively (6, 10, 71, 72). Additionally, 5-ALA has a strong positive predictive value, with multiple studies finding 100% PPV for solid fluorescence in both primary and recurrent HGG (70, 73, 74). Beyond histologic accuracy of 5-ALA PPIX fluorescence, correlations have been made between fluorescence intensity and histological grading, suggesting the ability to approximate grade by fluorescent signal (75, 76).

In addition to being safe for use in HGG surgery, 5-ALA has also shown to improve patient outcomes. In a phase III randomized controlled trial of 322 HGG patients randomized to 5-ALA FGS or white light surgery, Stummer et al. found that patients who received 5-ALA experience more complete resections of contrast-enhancing tumor (65 vs. 36%, $p < 0.0001$), and higher 6-month progression-free survival (41.0 vs. 21.1%, $p = 0.0003$) (8). In a retrospective study of glioblastoma patients that had undergone surgery with 5-ALA, those patients without residual tissue fluorescence had greater median overall survival compared to those with residual fluorescence (27 vs. 17.5 months, $p = 0.015$) (77).

Despite the advantages of 5-ALA for HGG surgery, the agent is expensive and not universally available. Following a series of successful clinical trials in 5-ALA, FGS researchers tested the safety and efficacy of other more widely accessible fluorophores for HGG resections. Several recent studies have assessed the use of fluorescein sodium, and found that fluorescein improves extent of resection and rates of gross total resection, with GTR rates up to 80% (7, 30, 31, 78). Despite being selective for areas of blood-brain barrier breakdown, rather than tumor tissue itself, fluorescein fluorescent signal has been shown to correlate with contrast-enhancement on preoperative MR imaging (32, 40). To date, there are no randomized controlled trials for fluorescein-guided tumor surgery, however, in a recent multicenter phase II study, Acerbi et al. found that fluorescein was safe and effective in HGG surgery, with a GTR rate of 82.6% and 6-month progression-free survival of 56.6% (35). ICG, a fluorophore used primarily in angiography, has recently been implemented in brain tumor surgery, for its enhanced permeability retention (EPR) effect as a result of BBB disruption. The second window ICG (SWIG) technique allows for ICG accumulation in HGG

tissue, allowing for improved visualization (15, 28). While this technique has not yet been widely studies, in a recent case series of 11 HGG, SWIG was found to be highly sensitive for HGG tissue, and fluorescent signal correlated with MR imaging (27). While safely tolerated, the major disadvtange of ICG is that unlike 5-ALA and fluorescein, it emits in the near infrared spectrum, making it logistically difficult to operate while visualizing the signal.

Low-Grade Gliomas

Low-grade gliomas have created a larger challenge for FGS compared to HGG, as the lower grade tumors do not have as robust areas of BBB breakdown and contrast uptake compared to more infiltrative lesions. While historically "watch and wait" was the treatment paradigm for these lesions, there is now strong evidence for early, maximal safe resection (74, 79, 80). However, these tumors may be difficult to remove completely, as their appearance may only appear slightly different compared to normal brain, and therefore 5-ALA has been implemented. While initially researchers were doubtful that there would be any 5-ALA PPIX uptake in LGG cells due to less BBB breakdown, the differences appear quantitative, rather than qualitative (81). Although initial studies showed no fluorescence in LGG patients (82, 83). Widhalm et al. found a subset of non-contrast-enhancing LGG patients with 5-ALA-induced fluorescence (84). In the largest series to date, Jaber et al. found visible fluorescence in only 13 of 82 WHO grade II gliomas, and concluded that the majority of LGG do not show visible fluorescence (85). However, the value in use of 5-ALA for LGG surgery may be in the histological heterogeneity of these tumors, as areas of malignant transformation, or anaplastic foci, are characteristic for LGGs (86). By fluorescing areas of contrast-enhancement, 5-ALA can help identify areas of higher metabolic activity and subsequently greater proliferation (87).

Meningiomas

Meningiomas are the most common benign brain tumors, and with the propensity to enhance on contrasted imaging, they have been studied in the field of FGS. While the three major fluorophores, 5-ALA, ICG, and fluorescein, have all been studied in the visualization of meningiomas, 5-ALA has been most widely studied, with over 10 clinical studies to date (88). The largest study of FGS use in meningiomas is by Millesi et al., where after administration of 5-ALA to 204 meningioma patients, visible fluorescent signal was found in 91% of tumors, and 100% positive preductive value for bone infiltration (89). In a study of 12 meningioma patients, seven skull base and five convexity, Della Puppa et al. found 89% sensitivity and 100% specificity for 5-ALA detecting bone invasion (90). Additionally, in a small series of eight intradural spinal meningiomas using 5-ALA, there was a positive predictive value of 100% (91).

ICG and fluorescein have also been used in the resection of meningiomas. ICG in particular has been found to be helpful in cases where the tumor invades the dural sinuses, and helps visualize venous collaterals, the surrounding patent sinuses and the pial vascular supply (92–94). In these cases, however, ICG is being used as a vascular contrast agent with visualization within minutes of IV bolus dosing. In contrast, Lee et al., employed the high dose, delayed second window ICG technique found that 78% meningiomas exhibited more fluorescent signal than surrounding brain, with a sensitivity of 96.4%, but only 39% specificity (95). Fluorescein, like ICG, accumulates within tumor regions rapidly, however, the fluorescent signal may persist for hours, aiding in the visualization of meningiomas (54). In a recent study of 30 patients with meningiomas undergoing resection, Akcakaya et al. found that 88% of meningiomas demonstrate diffuse homogenous intraoperative enhancement, yielding a resection rate of 87% (96). With fluorescein, confocal microscopy can help illuminate meningiomas on the cellular level, with a confocal/histology concordance of 90%, with identification of dural invasion (97).

Brain Metastases

As the most common brain tumors in adults, the treatment paradigm for cerebral metastases has been widely studied. Depending on the size, location and quantity of CNS metastatic lesions, treatment options may include chemotherapy, radiation modalities such as stereotactic radiosurgery (SRS) and whole brain radiation therapy (WBRT), and surgical resection. For symptomatic tumors causing mass effect and cerebral compression, complete resection of metastatic lesions is always the goal when attainable (98). Despite the non-infiltrative nature of these lesions (compared to gliomas), 30% of resections are incomplete, which may explain the 60% local recurrence rate (99, 100), providing a rationale for use of an adjunct such as FGS.

5-ALA has been shown to fluoresce in metastatic lung, breast, colon, bladder, melanoma and other primary cancers with brain metastases (101–104). First studied in 2007, 5-ALA for brain metastases has not been widely studied, with only several large patient studies (54, 105). In the largest experience to date of 157 patients with known metastatic lesions undergoing resection with 5-ALA, Marhold et al. concluded that 66% of tumors exhibited fluorescence, with ductal breast cancer having the highest rate of fluorescence (106). In addition to having variable rates of fluorescence, 5-ALA has shown fluorescence in extra-tumoral edema in cases where the tumor core demonstrated poor fluorescence, making FGS less reliable in these cases (107). Further study is warranted on determining predictors of fluorescence among different primary cancers with brain metastases, as well as a more specified use for FGS in metastatic disease.

Fluorescein sodium has been broadly studied for its use in resection of brain metastases. In a series of 30 patients, Schebesch et al. found fluorescence in 90% of tumors, leading to an 83.3% GTR rate (108, 109). In a follow up study expanding upon this initial experience, Hohne et al. found a 95% fluorescence rate in 95 patients, with an 86% rate of no residual contrast enhancement. In this series, lung adenocarcinoma, melanoma and renal cell carcinoma were the only primary cancers that did not consistency exhibit fluorescein fluorescence (110). As part of the FLUOCERTUM Prospective Study, 25 metastastic lesions were included, of which 24 showed heterogenous enhancement (111). From these primary experiences and others, fluorescein appears to be a reliable fluorophore for brain metastasis surgery.

Second Window ICG technique appears to have advantages for visualization of brain metastasis as most of these tumors have a disrupted BBB and thus accumulate ICG (**Figure 1**). In a recent publication, Teng et al. demonstrated improved survival in patients with resection of all near infrared fluorescent signal in patients undergoing craniotomy for brain metastasis (112). In 47 patients who underwent resection of 51 metastatic lesions, all tumors demonstrated quantifiable NIR fluorescence with a mean SBR of 4.9. Diagnostic accuracy was improved by changing the threshold signal as compared to normal brain background, and a lack of residual NIR fluorescence not only predicted the postoperative MRI gadolinium findings but also predicted progression free survival at 1 year. ICG may prove to have its greatest role in resection of these tumors.

Pediatric Brain Tumors

Similar to the adult literature, maximal safe resection is the standard of care in pediatric HGG. However, unlike the adult literature, we lack randomized controlled trial data for using FGS in the treatment of pediatric brain tumors. The use of 5-ALA for brain tumor surgery in children was first reported by Ruge et al., where 5-ALA was used to resect in a 9-year-old with a right temporal lobe pleomorphic xantoastrocytoma (PXA) (113). There have been no large single center studies currently, however, in 78 patients among 20 European centers, Stummer et al. found that 85% HGG and 80% ependymomas showed fluorescence, and that most primitive neuro-ectodermal tumors (PNET), gangliogliomas, medulloblastomas and pilocytic astrocytomas did not fluoresce (70). Other studies have shown robust fluorescence in HGG, with inconsistent fluuoresence in medulloblastoma, which may be related to underlying subtype (21, 114). While the safety data for 5-ALA use has been well-established in the adult literature, it is less studied in pediatric patients, and there has prior suggestion of increased liver enzyme values with decreasing patient age (115). In a multicenter study of 24 pediatric patients, de Laurentis et al. found fluorescence in 77.8% of tumors, and found fluorescence to be "helpful" in half of the cases (116). BLZ-100 has recently shown to be safe and effective in the treatment of both HGG and LGG in adults, and is currently under investigation for pediatric brain tumors (60).

Spinal Cord Intramedullary Tumors

In the resection of intramedullary spinal cord tumors, establishing the margin between tumor and spinal cord is essential to minimize the risk of spinal cord injury. Ependymomas and astrocytomas, two of the most common intramedullary tumors, both have robust uptake of 5-ALA, and therefore it has studied for this use. Gross total resection of ependymomas is especially crucial, as it is a potentially curable lesion. The first series of intramedullary ependymomas using 5-ALA was published in 2013, when Inoue et al. found that 77% of ependymomas demonstrated fluorescence, leading to a GTR in 80% of cases (117). In a study of 52 patients with 55 spinal tumors including 12 ependymomas, Millesi et al. found 5-ALA to be a safe and effective adjunct in cases of ependymomas, meningiomas, hemangiopericytomas and drop metastases, with a GTR rate of 75% ependymomas (118). With spinal astrocytomas, the margins are less defined, and surgeons are faced with a more difficult situation in where to end a subtotal resection, at the expense of sensorimotor function. 5-ALA may help in identifying tumor margins, and to aid in deciding where to limit cytoreduction, to preserve high-level functionality.

Fluorescein sodium has been shown to be effective for intramedullary tumors in several studies. Acerbi et al. found fluorescence in 82% of tumors, including ependymomas, hemangioblastomas, astrocytoma, and a glioneuronal tumor forming rosettes (119). In a study of 34 intradural extramedullary and 15 intramedullary lesions, surgeons found fluorescein helpful in delineating tumor from surrounding tissue in 96% cases (120).

ICG has additionally been used for intramedullary tumors, specifically vascular spinal cord lesions, such as hemangioblastoma and cavernous angioma (54). In these cases, identifying the feeding and draining veins of these tumors can help surgeons safely remove the lesion. In the case of cavernous angiomas, the surrounding spinal cord takes up the ICG fluorescence, however, the angioma remains avascular, providing surgeons with a nice margin for resection (121).

Primary CNS Lymphoma and Stereotactic Biopsy

Safety and accuracy are the two most important objectives for stereotactic biopsy of cerebral lesions. Fluorescein has been shown to be effective in predicting tumor pathology, especially in contrast-enhancing lesions (122), and in a proof-of-concept study, Lynagh et al. found that *in vivo* fluorescein signal was strongly predictive of tumor tissue, and could be used to identify tumor prior to biopsy (123). Additionally, 5-ALA and ICG have been shown to be effective in identifying tumoral vessels, and 5-ALA, ICG and fluorescein can accurately detect tumor tissue prior to biopsy (124). By coupling fluorescence with confocal microscopy, identifying tumor tissue may now be feasible in real time without a frozen section (124), and may even increase the diagnostic yield, with Malinova et al. finding that 5-ALA fluorescence had a higher sensitivity and negative predictive value for unclear cerebral pathologies compared to frozen section (125). Second Window ICG has also been successfully used in stereotactic biopsy procedures, to assure the surgeon that the contrast-enhancing portion of the tumor has been biopsied (126).

Several case series have shown a potential role for 5-ALA PpIX fluorescence in primary CNS lympoma (127, 128). Lymphoma may mimic HGG radiographically, and therefore PpIX and other fluorophores have been used in cases of presumed HGG. However, the standard of care for primary CNS lymphoma is chemotherapy and radiotherapy following diagnostic biopsy (129), creating a potential role for 5-ALA in improving the diagnostic yield of lymphoma tissue. In the largest series to date on stereotactic biopsies for primary CNS lymphoma, Yamamoto et al. found that 34 of 41 lesions showed fluorescent signal, with a true-positive rate of 82.9% (128). Kiesel et al. found fluorescence in 79% primary lymphoma lesions, and it has recently been proposed that if a lesion demonstrates strong fluorescence, that it may not require intraoperative histopathology, potentially making biopsies safer by decreasing number of biopsy samples

and reducing length of stay (130). Fluorescein has also been used to effectively delinate lymphoma tissue vs. normal brain in two case series, where lesions were preoperatively diagnosed as HGG (47, 108). Further study is required to better understand the role for fluorescein in primary CNS lymphoma. In addition, Second Window ICG accumulates dramatically as expected in primary CNS lymphoma, and may be effective in identifying this tissue for biopsy (131).

Other Tumors and Pathological Conditions Requiring Surgery

In addition to the aforementioned CNS tumors, there are several other tumor types that have been studied in the FGS literature.

Peripheral nerve sheath tumors (PNST), comprised of mostly schwannomas, may be difficult to distinguish from surrounding tissues, allowing for a potential role for FGS guidance. In a series of 25 PNST, Vetrano et al. found that fluorescein showed fluorescence in 13 of 14 schwannomas, and allowed for further resection leading to a GTR in six neurofibroma cases and one schwannoma case (132). In a series by Marbacher et al. of 458 tumors receiving 5-ALA PpIX, zero of seven schwannomas showed fluorescence (133). To our knowledge, there have not been studied conducted evaluating SWIG for these tumors.

Sellar tumors, in particular pituitary adenomas, have not been reported to demonstrate strong fluorescent signal, and therefore, not much research has been studied on these tumors. In the Marbacher et al. series, only one of 12 pituitary adenomas demonstrated fluorescence (133). Falco et al. found fluorescence in one of one patients studies in the FLUOCERTUM cohort (111). The role of SWIG in these lesions may be limited, as the pituitary gland is a normal structure that fluoresces with ICG (54). Despite this potential limitaions, ICG endoscopy has been proposed for resection of skull base surgery, and techniques for use have been described (134), with distinguishable margins able to be identified in both functional and non-functional pituitary lesions (135).

Hemangioblastomas may be an important tumor for FGS, as subtotal resection may lead to local recurrence, and FGS may help visualize the intramural nodule within the associated peritumoral cyst. As part of the FLUOCERTUM prospective study of 279 patients receiving fluorescein-guided tumor resection, seven patients with hemangioblastoma were included, all of which demonstrated fluorescence (111). Utsuki et al. used 5-ALA fluorescence, and showed strong fluorescence in all nine hemangioblastoma cases (136). The use of ICG has been rarely reported for both brain and intramedullary hemangioblastoma resections (137, 138).

Several other tumor types have shown potential promise in FGS, such as strong fluorescence observed in fourth ventricle subependymomas (139), germ cell tumors undergoing endoscopic biopsy (140). Further research is warranted on these rarer tumors, to better understand which fluorophores may be implored for use.

CONCLUSION

Understanding the administration and properties of the various fluorophores used in glioma surgery is essential for its use as a surgical adjunct. Fluorophores may target areas of blood-brain barrier breakdown, areas of inflammation, or specifically glioma cells. Fluorophores are administered by different routes, and surgeons should be aware of the relationship between fluorophore administration and tumor fluorescence. ICG and fluorescein work by passive targeting, and have the benefit of IV administration in the operating room within seconds (ICG as vascular angiography agent) to a couple hours (fluorescein), to the next day (Second Window ICG as an EPR accumulated agent). As an oral agent, 5-ALA is consumed prior to anesthseia, and is able to persist in target tissue for longer, allowing for logistical delays. Newly studied molecular targets, such as BLZ-100 and EGFR conjugates, are also given in the operating room, but may last in tumor tissue for up to several days.

AUTHOR CONTRIBUTIONS

AS and CH: conceptualization and investigation. AS, MR, NM, RB, JL, FA, and CH: writing—original draft preparation, writing—review, and editing. AS: visualization. CH: supervision and project. All authors have read and agreed to the published version of the manuscript.

REFERENCES

1. Brown TJ, Brennan MC, Li M, Church EW, Brandmeir NJ, Rakszawski KL, et al. Association of the extent of resection with survival in glioblastoma: a systematic review and meta-analysis. *JAMA Oncol*. (2016) 2:1460–9. doi: 10.1001/jamaoncol.2016.1373
2. Fernandes C, Costa A, Osório L, Lago RC, Linhares P, Carvalho B, et al. *Current Standards of Care in Glioblastoma Therapy*. Glioblastoma: Codon Publications. (2017).
3. Haj A, Doenitz C, Schebesch KM, Ehrensberger D, Hau P, Putnik K, et al. Extent of resection in newly diagnosed glioblastoma: impact of a specialized neuro-oncology care center. *Brain Sci*. (2018) 8:5. doi: 10.3390/brainsci8010005
4. Yamada S, Muragaki Y, Maruyama T, Komori T, Okada Y. Role of neurochemical navigation with 5-aminolevulinic acid during intraoperative MRI-guided resection of intracranial malignant gliomas. *Clin Neurol Neurosurg*. (2015) 130:134–9. doi: 10.1016/j.clineuro.2015.01.005
5. Zhang ZZ, Shields LB, Sun DA, Zhang YP, Hunt MA, Shields CB. The art of intraoperative glioma identification. *Front Oncol*. (2015) 5:175. doi: 10.3389/fonc.2015.00175
6. Su X, Huang Q-F, Chen H-L, Chen J. Fluorescence-guided resection of high-grade gliomas: a systematic review and meta-analysis. *Photodiagn Photodyn Therapy*. (2014) 11:451–8. doi: 10.1016/j.pdpdt.2014.08.001
7. Neira JA, Ung TH, Sims JS, Malone HR, Chow DS, Samanamud JL, et al. Aggressive resection at the infiltrative margins of glioblastoma facilitated by intraoperative fluorescein guidance. *J Neurosurg*. (2016) 127:111–22. doi: 10.3171/2016.7.JNS16232
8. Stummer W, Pichlmeier U, Meinel T, Wiestler OD, Zanella F, Reulen HJ, et al. Fluorescence-guided surgery with 5-aminolevulinic acid for resection of

malignant glioma: a randomised controlled multicentre phase III trial. *Lancet Oncol*. (2006) 7:392–401. doi: 10.1016/S1470-2045(06)70665-9
9. Hadjipanayis CG, Stummer W. *Fluorescence-Guided Neurosurgery: Neuro-Oncology and Cerebrovascular Applications*. New York, NY: Thieme. (2019). doi: 10.1055/b-0038-164181
10. Stummer W, Stocker S, Novotny A, Heimann A, Sauer O, Kempski O, et al. *In vitro* and *in vivo* porphyrin accumulation by C6 glioma cells after exposure to 5-aminolevulinic acid. *J Photochem Photobiol B*. (1998) 45:160–9. doi: 10.1016/S1011-1344(98)00176-6
11. Hadjipanayis CG, Widhalm G, Stummer W. What is the surgical benefit of utilizing 5-aminolevulinic acid for fluorescence-guided surgery of malignant gliomas? *Neurosurgery*. (2015) 77:663–73. doi: 10.1227/NEU.0000000000000929
12. Bottomley, S. S. Pathophysiology of heme synthesis. *Semin Hematol*. (1988) 25:282–302.
13. Onda N, Kimura M, Yoshida T, Shibutani M. Preferential tumor cellular uptake and retention of indocyanine green for *in vivo* tumor imaging. *Int J Cancer*. (2016) 139:673–82. doi: 10.1002/ijc.30102
14. Francaviglia N, Iacopino DG, Costantino G, Villa A, Impallaria P, Meli F, et al. Fluorescein for resection of high-grade gliomas: a safety study control in a single center and review of the literature. *Surg Neurol Int*. (2017) 8:17. doi: 10.4103/sni.sni_89_17
15. Cho SS, Salinas R, Lee JY. Indocyanine-green for fluorescence-guided surgery of brain tumors: evidence, techniques, and practical experience. *Front Surg*. (2019) 6:11. doi: 10.3389/fsurg.2019.00011
16. Okuda T, Yoshioka H, Kato A. Fluorescence-guided surgery for glioblastoma multiforme using high-dose fluorescein sodium with excitation and barrier filters. *J Clin Neurosci*. (2012) 19:1719–22. doi: 10.1016/j.jocn.2011.12.034
17. Haglund MM, Hochman DW, Spence AM, Berger MS. Enhanced optical imaging of rat gliomas and tumor margins. *Neurosurgery*. (1994) 35:930–41. doi: 10.1227/00006123-199411000-00019
18. Acerbi F, Broggi M, Broggi G, Ferroli P. What is the best timing for fluorescein injection during surgical removal of high-grade gliomas? *Acta Neurochir*. (2015) 157:1377–8. doi: 10.1007/s00701-015-2455-z
19. Senders JT, Muskens IS, Schnoor R, Karhade AV, Cote DJ, Smith TR, et al. Agents for fluorescence-guided glioma surgery: a systematic review of preclinical and clinical results. *Acta Neurochir*. (2017) 159:151–67. doi: 10.1007/s00701-016-3028-5
20. Zeh R, Sheikh S, Xia L, Pierce J, Newton A, Predina J, et al. The second window ICG technique demonstrates a broad plateau period for near infrared fluorescence tumor contrast in glioblastoma. *PLoS ONE*. (2017) 12:e0182034. doi: 10.1371/journal.pone.0182034
21. Zhang C, Boop FA, Ruge J. The use of 5-aminolevulinic acid in resection of pediatric brain tumors: a critical review. *J Neurooncol*. (2019) 141:567–73. doi: 10.1007/s11060-018-03004-y
22. Eyüpoglu IY, Hore N, Fan Z, Buslei R, Merkel A, Buchfelder M, et al. Intraoperative vascular DIVA surgery reveals angiogenic hotspots in tumor zones of malignant gliomas. *Sci Rep*. (2015) 5:1–7. doi: 10.1038/srep07958
23. Haglund MM, Berger MS, Hochman DW. Enhanced optical imaging of human gliomas and tumor margins. *Neurosurgery*. (1996) 38:308–17. doi: 10.1097/00006123-199602000-00015
24. Hansen DA, Spence AM, Carski T, Berger MS. Indocyanine green (ICG) staining and demarcation of tumor margins in a rat glioma model. *Surg. Neurol*. (1993) 40:451–6. doi: 10.1016/0090-3019(93)90046-4
25. Martirosyan NL, Cavalcanti DD, Eschbacher JM, Delaney PM, Scheck AC, Abdelwahab MG, et al. Use of *in vivo* near-infrared laser confocal endomicroscopy with indocyanine green to detect the boundary of infiltrative tumor: laboratory investigation. *J Neurosurg*. (2011) 115:1131–8. doi: 10.3171/2011.8.JNS11559
26. Maeda H, Tsukigawa K, Fang J. A retrospective 30 years after discovery of the enhanced permeability and retention effect of solid tumors: next-generation chemotherapeutics and photodynamic therapy–problems, solutions, and prospects. *Microcirculation*. (2016) 23:173–82. doi: 10.1111/micc.12228
27. Lee JY, Thawani JP, Pierce J, Zeh R, Martinez-Lage M, Chanin M, et al. Intraoperative near-infrared optical imaging can localize gadolinium-enhancing gliomas during surgery. *Neurosurgery*. (2016) 79:856–71. doi: 10.1227/NEU.0000000000001450
28. Cho SS, Salinas R, De Ravin E, Teng CW, Li C, Abdullah KG, et al. Near-infrared imaging with second-window indocyanine green in newly diagnosed high-grade gliomas predicts gadolinium enhancement on postoperative magnetic resonance imaging. *Mol Imaging Biol*. (2020) 22:1427–37. doi: 10.1007/s11307-019-01455-x
29. Moore GE, Peyton WT. The clinical use of fluorescein in neurosurgery; the localization of brain tumors. *J Neurosurg*. (1948) 5:392–8. doi: 10.3171/jns.1948.5.4.0392
30. Schebesch K, Brawanski A, Hohenberger C, Hohne J. Fluorescein sodium-guided surgery of malignant brain tumors: history, current concepts, and future projects. *Turkish Neurosurg*. (2016) 26:185–94. doi: 10.5137/1019-5149.JTN.16952-16.0
31. Acerbi F, Broggi M, Eoli M, Anghileri E, Cavallo C, Boffano C, et al. Is fluorescein-guided technique able to help in resection of high-grade gliomas? *Neurosurg Focus*. (2014) 36:E5. doi: 10.3171/2013.11.FOCUS13487
32. Diaz RJ, Dios RR, Hattab EM, Burrell K, Rakopoulos P, Sabha N, et al. Study of the biodistribution of fluorescein in glioma-infiltrated mouse brain and histopathological correlation of intraoperative findings in high-grade gliomas resected under fluorescein fluorescence guidance. *J Neurosurg*. (2015) 122:1360–9. doi: 10.3171/2015.2.JNS132507
33. Shinoda J, Yano H, Yoshimura S, Okumura A, Kaku Y, Iwama T, et al. Fluorescence-guided resection of glioblastoma multiforme by using high-dose fluorescein sodium: technical note. *J Neurosurg*. (2003) 99:597–603. doi: 10.3171/jns.2003.99.3.0597
34. Valli D, Belykh E, Zhao X, Gandhi S, Cavallo C, Martirosyan NL, et al. Development of a simulation model for fluorescence-guided brain tumor surgery. *Front Oncol*. (2019) 9:748. doi: 10.3389/fonc.2019.00748
35. Acerbi F, Broggi M, Schebesch KM, Höhne J, Cavallo C, De Laurentis C, et al. Fluorescein-guided surgery for resection of high-grade gliomas: a multicentric prospective phase II study (FLUOGLIO). *Clin Cancer Res*. (2018) 24:52–61. doi: 10.1158/1078-0432.CCR-17-1184
36. Belykh E, Miller EJ, Patel AA, Yazdanabadi MI, Martirosyan NL, Yagmurlu K, et al. Diagnostic accuracy of a confocal laser endomicroscope for *in vivo* differentiation between normal injured and tumor tissue during fluorescein-guided glioma resection: laboratory investigation. *World Neurosurg*. (2018) 115:e337–48. doi: 10.1016/j.wneu.2018.04.048
37. Ichioka T, Miyatake S, Asai N, Kajimoto Y, Nakagawa T, Hayashi H, et al. Enhanced detection of malignant glioma xenograft by fluorescein–human serum albumin conjugate. *J Neurooncol*. (2004) 67:47–52. doi: 10.1023/B:NEON.0000021783.62610.1b
38. Martirosyan NL, Eschbacher JM, Kalani MY, Turner JD, Belykh E, Spetzler RF, et al. Prospective evaluation of the utility of intraoperative confocal laser endomicroscopy in patients with brain neoplasms using fluorescein sodium: experience with 74 cases. *Neurosurg Focus*. (2016) 40:E11. doi: 10.3171/2016.1.FOCUS15559
39. Kuroiwa T, Kajimoto Y, Ohta T. Development of a fluorescein operative microscope for use during malignant glioma surgery: a technical note and preliminary report. *Surg Neurol*. (1998) 50:41–9. doi: 10.1016/S0090-3019(98)00055-X
40. Chen B, Wang H, Ge P, Zhao J, Li W, Gu H, et al. Gross total resection of glioma with the intraoperative fluorescence-guidance of fluorescein sodium. *Int J Med Sci*. (2012) 9:708–14. doi: 10.7150/ijms.4843
41. Roberts DW, Olson J. Fluorescein guidance in glioblastoma resection. *N Engl J Med*. (2017) 376:e36. doi: 10.1056/NEJMicm1611258
42. Bowden SG, Neira JA, Gill, B. J. A., Ung TH, Englander ZK, Zanazzi G, et al. Sodium fluorescein facilitates guided sampling of diagnostic tumor tissue in non-enhancing gliomas. *Neurosurgery*. (2018) 82:719–27. doi: 10.1093/neuros/nyx271
43. Belykh E, Shaffer KV, Lin C, Byvaltsev VA, Preul MC, Chen L. Blood-brain barrier, blood-brain tumor barrier, and fluorescence-guided neurosurgical oncology: delivering optical labels to brain tumors. *Front Oncol*. (2020) 10:739. doi: 10.3389/fonc.2020.00739
44. Koc K, Anik I, Cabuk B, Ceylan S. Fluorescein sodium-guided surgery in glioblastoma multiforme: a prospective evaluation. *Br J Neurosurg*. (2008) 22:99–103. doi: 10.1080/02688690701765524
45. Schebesch KM, Proescholdt M, Höhne J, Hohenberger C, Hansen E, Riemenschneider MJ, et al. Sodium fluorescein-guided resection under the YELLOW 560 nm surgical microscope filter in malignant brain

tumor surgery–a feasibility study. *Acta Neurochir*. (2013) 155:693–9. doi: 10.1007/s00701-013-1643-y
46. Zhang DY, Singhal S, Lee JYK. Optical principles of fluorescence-guided brain tumor surgery: a practical primer for the neurosurgeon. *Neurosurgery*. (2019) 85:312–24. doi: 10.1093/neuros/nyy315
47. Hamamcioglu MK, Akçakaya MO, Göker B, Kasimcan MÖ, Kiriş T. The use of the YELLOW 560 nm surgical microscope filter for sodium fluorescein-guided resection of brain tumors: our preliminary results in a series of 28 patients. *Clin Neurol Neurosurg*. (2016) 143:39–45. doi: 10.1016/j.clineuro.2016.02.006
48. Suero Molina E, Wölfer J, Ewelt C, Ehrhardt A, Brokinkel B, Stummer W. Dual-labeling with 5-aminolevulinic acid and fluorescein for fluorescence-guided resection of high-grade gliomas: technical note. *J Neurosurg*. (2018) 128:399–405. doi: 10.3171/2016.11.JNS161072
49. Ung TH, Kellner C, Neira JA, Wang SH, D'Amico R, Faust PL, et al. The use of fluorescein sodium in the biopsy and gross-total resection of a tectal plate glioma. *J Neurosurg Pediatr*. (2015) 16:732–5. doi: 10.3171/2015.5.PEDS15142
50. Xiang Y, Zhu XP, Zhao JN, Huang GH, Tang JH, Chen HR, et al. Blood-brain barrier disruption, sodium fluorescein, and fluorescence-guided surgery of gliomas. *Br J Neurosurg*. (2018) 32:141–8. doi: 10.1080/02688697.2018.1428731
51. Folaron M, Strawbridge R, Samkoe KS, Filan C, Roberts DW, Davis SC. Elucidating the kinetics of sodium fluorescein for fluorescence-guided surgery of glioma. *J Neurosurg*. (2018) 131:724–34. doi: 10.3171/2018.4.JNS172644
52. Stummer W, Tonn JC, Goetz C, Ullrich W, Stepp H, Bink A, et al. 5-Aminolevulinic acid-derived tumor fluorescence: the diagnostic accuracy of visible fluorescence qualities as corroborated by spectrometry and histology and postoperative imaging. *Neurosurgery*. (2014) 74:310–9. doi: 10.1227/NEU.0000000000000267
53. Maragkos GA, Schupper AJ, Lakomkin N, Sideras P, Price G, Baron RB, et al. Fluorescence-guided high-grade glioma surgery more than 4 h after 5-aminolevulinic acid administration. *Front Neurol*. (2021) 2021:644804. doi: 10.3389/fneur.2021.644804
54. Hadjipanayis CG, Stummer W. Fluorescence-guided neurosurgery: neuro-oncology and cerebrovascular applications. *Thieme*. (2019).
55. Hadjipanayis CG, Stummer W. 5-ALA and FDA approval for glioma surgery. *Neurooncol*. (2019) 141:479–86. doi: 10.1007/s11060-019-03098-y
56. Stummer W, Novotny A, Stepp H, Goetz C, Bise K, Reulen HJ. Fluorescence-guided resection of glioblastoma multiforme by using 5-aminolevulinic acid-induced porphyrins: a prospective study in 52 consecutive patients. *J Neurosurg*. (2000) 93:1003–13. doi: 10.3171/jns.2000.93.6.1003
57. Teixidor P, Arráez MÁ, Villalba G, Garcia R, Tardáguila M, González JJ, et al. Safety and efficacy of 5-aminolevulinic acid for high grade glioma in usual clinical practice: a prospective cohort study. *PLoS ONE*. (2016) 11:e0149244. doi: 10.1371/journal.pone.0149244
58. Center for Drug Evaluation and Research. *Aminolevulinic Acid Hydrochloride, Known as ALA HCl (Gleolan, NX Development Corp.) as an Optical Imaging Agent Indicated in Patients With Gliomas*. (2017). Available online at: https://www.fda.gov/drugs/resources-information-approved-drugs/aminolevulinic-acid-hydrochloride-known-ala-hcl-gleolan-nx-development-corp-optical-imaging-agent (accessed June 3, 2020).
59. Kaneko S, Suero Molina E, Ewelt C, Warneke N, Stummer W. Fluorescence-based measurement of real-time kinetics of protoporphyrin IX after 5-aminolevulinic acid administration in human *in situ* malignant gliomas. *Neurosurgery*. (2019) 85:E739–46. doi: 10.1093/neuros/nyz129
60. Patil CG, Walker DG, Miller DM, Butte P, Morrison B, Kittle DS, et al. Phase 1 safety, pharmacokinetics, and fluorescence imaging study of tozuleristide (BLZ-100) in adults with newly diagnosed or recurrent gliomas. *Neurosurgery*. (2019) 85:E641–9. doi: 10.1093/neuros/nyz125
61. Weichert JP, Clark PA, Kandela IK, Vaccaro AM, Clarke W, Longino MA, et al. Alkylphosphocholine analogs for broad-spectrum cancer imaging and therapy. *Sci Transl Med*. (2014) 6:240ra75. doi: 10.1126/scitranslmed.3007646
62. Swanson KI, Clark PA, Zhang RR, Kandela IK, Farhoud M, Weichert JP, et al. Fluorescent cancer-selective alkylphosphocholine analogs for intraoperative glioma detection. *Neurosurgery*. (2015) 76:115–24. doi: 10.1227/NEU.0000000000000622
63. Seekell K, Lewis S, Wilson C, Li S, Grant G, Wax A. Feasibility study of brain tumor delineation using immunolabeled gold nanorods. *Biomed. Opt. Express*. (2013) 4:2284–95. doi: 10.1364/BOE.4.002284
64. Davis SC, Samkoe KS, O'Hara JA, Gibbs-Strauss SL, Payne HL, Hoopes PJW, et al. MRI-coupled fluorescence tomography quantifies EGFR activity in brain tumors. *Acad Radiol*. (2010) 17:271–6. doi: 10.1016/j.acra.2009.11.001
65. Samkoe KS, Gunn JR, Marra K, Hull SM, Moodie KL, Feldwisch J, et al. Toxicity and pharmacokinetic profile for single-dose injection of ABY-029: a fluorescent anti-EGFR synthetic affibody molecule for human use. *Mol Imaging Biol*. (2017) 19:512–21. doi: 10.1007/s11307-016-1033-y
66. de Souza AL, Marra K, Gunn J, Samkoe KS, Hoopes PJ, Feldwisch J, et al. Fluorescent affibody molecule administered *in vivo* at a microdose level labels EGFR expressing glioma tumor regions. *Mol Imaging Biol*. (2017) 19:41–8. doi: 10.1007/s11307-016-0980-7
67. Warram JM, de Boer E, Korb M, Hartman Y, Kovar J, Markert JM, et al. Fluorescence-guided resection of experimental malignant glioma using cetuximab-IRDye 800 CW. *Br J Neurosurg*. (2015) 29:850–8. doi: 10.3109/02688697.2015.1056090
68. Miller SE, Tummers WS, Teraphongphom N, van den Berg NS, Hasan A, Ertsey RD, et al. First-in-human intraoperative near-infrared fluorescence imaging of glioblastoma using cetuximab-IRDye800. *J Neurooncol*. (2018) 139:135–43. doi: 10.1007/s11060-018-2854-0
69. Schipmann S, Schwake M, Suero Molina E, Stummer W. Markers for identifying and targeting glioblastoma cells during surgery. *J Neurol Surg A Cent Eur Neurosurg*. (2019) 80:475–87. doi: 10.1055/s-0039-1692976
70. Stummer W, Rodrigues F, Schucht P, et al. Predicting the "usefulness" of 5-ALA-derived tumor fluorescence for fluorescence-guided resections in pediatric brain tumors: a European survey. *Acta Neurochir*. (2014) 156:2315–24. doi: 10.1007/s00701-014-2234-2
71. Zhao S, Wu J, Wang C, Liu H, Dong X, Shi C, et al. Intraoperative fluorescence-guided resection of high-grade malignant gliomas using 5-aminolevulinic acid-induced porphyrins: a systematic review and meta-analysis of prospective studies. *PLoS ONE*. (2013) 8:e63682. doi: 10.1371/journal.pone.0063682
72. Eljamel S. 5-ALA fluorescence image guided resection of glioblastoma multiforme: a meta-analysis of the literature. *Int J Mol Sci*. (2015) 16:10443–56. doi: 10.3390/ijms160510443
73. Diez Valle R, Tejada Solis S, Idoate Gastearena MA, Garcia de Eulate R, Dominguez Echavarri P, and Aristu Mendiroz, J. Surgery guided by 5-aminolevulinic fluorescence in glioblastoma: volumetric analysis of extent of resection in single-center experience. *J Neurooncol*. (2011) 102:105–13. doi: 10.1007/s11060-010-0296-4
74. Lau D, Hervey-Jumper SL, Chang S, Molinaro AM, McDermott MW, Phillips JJ, et al. A prospective Phase II clinical trial of 5-aminolevulinic acid to assess the correlation of intraoperative fluorescence intensity and degree of histologic cellularity during resection of high-grade gliomas. *J Neurosurg*. (2016) 124:1300–9. doi: 10.3171/2015.5.JNS1577
75. Idoate MA, Diez Valle R, Echeveste J, Tejada S. Pathological characterization of the glioblastoma border as shown during surgery using 5-aminolevulinic acid-induced fluorescence. *Neuropathology*. (2011) 31:575–82. doi: 10.1111/j.1440-1789.2011.01202.x
76. Roberts DW, Valdés PA, Harris BT, Fontaine KM, Hartov A, Fan X, et al. Coregistered fluorescence-enhanced tumor resection of malignant glioma: relationships between delta-aminolevulinic acid-induced protoporphyrin IX fluorescence, magnetic resonance imaging enhancement, and neuropathological parameters. Clinical article. *J Neurosurg*. (2011) 114:595–603. doi: 10.3171/2010.2.JNS091322
77. Aldave G, Tejada S, Pay E, Marigil M, Bejarano B, Idoate MA, et al. Prognostic value of residual fluorescent tissue in glioblastoma patients after gross total resection in 5-aminolevulinic Acid-guided surgery. *Neurosurgery*. (2013) 72:915–20. doi: 10.1227/NEU.0b013e31828c3974
78. Rey-Dios R, Hattab EM, Cohen-Gadol AA. Use of intraoperative fluorescein sodium fluorescence to improve the accuracy of tissue diagnosis during stereotactic needle biopsy of high-grade gliomas. *Acta Neurochir*. (2014) 156:1071–5. doi: 10.1007/s00701-014-2097-6

79. Jakola AS, Myrmel KS, Kloster R, Torp SH, Lindal S, Unsgård G, et al. Comparison of a strategy favoring early surgical resection vs. a strategy favoring watchful waiting in low-grade gliomas. *JAMA*. (2012) 308:1881–8. doi: 10.1001/jama.2012.12807
80. Smith JS, Chang EF, Lamborn KR, Chang SM, Prados MD, Cha S, et al. Role of extent of resection in the longterm outcome of low-grade hemispheric gliomas. *J Clin Oncol*. (2008) 26: 1338–45. doi: 10.1200/JCO.2007.13.9337
81. Teng L, Nakada M, Zhao SG, Endo Y, Furuyama N, Nambu E, et al. Silencing of ferrochelatase enhances 5-aminolevulinic acid-based fluorescence and photodynamic therapy efficacy. *Br J Cancer*. (2011) 104:798–807. doi: 10.1038/bjc.2011.12
82. Hefti M, von Campe G, Moschopulos M, Siegner A, Looser H, Landolt H. 5-aminolevulinic acid induced protoporphyrin IX fluorescence in high-grade glioma surgery: a one-year experience at a single institutuion. *Swiss Med Wkly*. (2008) 138:180–5.
83. Utsuki S, Oka H, Sato S, Suzuki S, Shimizu S, Tanaka S, et al. Possibility of using laser spectroscopy for the intraoperative detection of non-fluorescing brain tumors and the boundaries of brain tumor infiltrates. Technical note. *J Neurosurg*. (2006) 104:618–20. doi: 10.3171/jns.2006.104.4.618
84. Widhalm G, Wolfsberger S, Minchev G, Woehrer A, Krssak M, Czech T, et al. 5-Aminolevulinic acid is a promising marker for detection of anaplastic foci in diffusely infiltrating gliomas with non-significant contrast enhancement. *Cancer*. (2010) 116:1545–52. doi: 10.1002/cncr.24903
85. Jaber M, Wölfer J, Ewelt C, Holling M, Hasselblatt M, Niederstadt T, et al. The value of 5-aminolevulinic acid in lowgrade gliomas and high-grade gliomas lacking glioblastoma imaging features: an analysis based on fluorescence, magnetic resonance imaging, 18F-fluoroethyl tyrosine positron emission tomography, and tumor molecular factors. *Neurosurgery*. (2016) 78:401–11. doi: 10.1227/NEU.0000000000001020
86. Paulus W, Peiffer J. Intratumoral histologic heterogeneity of gliomas. A quantitative study. *Cancer*. (1989) 64:442–7. doi: 10.1002/1097-0142(19890715)64:2<442::AID-CNCR2820640217>3.0.CO;2-S
87. Widhalm G, Kiesel B, Woehrer A, Traub-Weidinger T, Preusser M, Marosi C, et al. 5-Aminolevulinic acid induced fluorescence is a powerful intraoperative marker for precise histopathological grading of gliomas with non-significant contrast-enhancement. *PLoS ONE*. (2013) 8:e76988. doi: 10.1371/journal.pone.0076988
88. Kamp MA, Krause Molle Z, Munoz-Bendix C, Rapp M, Sabel M, Steiger HJ, et al. Various shades of red-a systematic analysis of qualitative estimation of ALA-derived fluorescence in neurosurgery. *Neurosurg Rev*. (2018) 41:3–18. doi: 10.1007/s10143-016-0745-4
89. Millesi M, Kiesel B, Mischkulnig M, Martínez-Moreno M, Wöhrer A, Wolfsberger S, et al. Analysis of the surgical benefits of 5-ALA-induced fluorescence in intracranial meningiomas: experience in 204 meningiomas. *J Neurosurg*. (2016) 125:1408–19. doi: 10.3171/2015.12.JNS151513
90. Della Puppa A, Rustemi O, Gioffrè G, Troncon I, Lombardi G, Rolma G, et al. Predictive value of intraoperative 5-aminolevulinic acid-induced fluorescence for detecting bone invasion in meningioma surgery. *J Neurosurg*. (2014) 120:840–5. doi: 10.3171/2013.12.JNS131642
91. Eicker SO, Floeth FW, Kamp M, Steiger HJ, Hänggi D. The impact of fluorescence guidance on spinal intradural tumour surgery. *Eur Spine J*. (2013) 22:1394–401. doi: 10.1007/s00586-013-2657-0
92. d'Avella E, Volpin F, Manara R, Scienza R, Della Puppa A. Indocyanine green videoangiography (ICGV)-guided surgery of parasagittal meningiomas occluding the superior sagittal sinus (SSS). *Acta Neurochir*. (2013) 155:415–20. doi: 10.1007/s00701-012-1617-5
93. Ueba T, Okawa M, Abe H, Nonaka M, Iwaasa M, Higashi T, et al. Identification of venous sinus, tumor location, and pial supply during meningioma surgery by transdural indocyanine green videography. *J Neurosurg*. (2013) 118:632–6. doi: 10.3171/2012.11.JNS121113
94. Han SJ, Magill ST, Tarapore PE, Horton JC, McDermott MW. Direct visualization of improved optic nerve pial vascular supply following tuberculum meningioma resection: case report. *J Neurosurg*. (2016) 125:565–9. doi: 10.3171/2015.6.JNS15765
95. Lee JYK, Pierce JT, Thawani JP, Zeh R, Nie S, Martinez-Lage M, et al. Near-infrared fluorescent image-guided surgery for intracranial meningioma. *J Neurosurg*. (2018) 128:380–90. doi: 10.3171/2016.10.JNS161636
96. Akçakaya MO, Göker B, Kasimcan MÖ, Hamamcioglu MK, Kiriş T. Use of sodium fluorescein in meningioma surgery performed under the YELLOW-560 nm surgical microscope filter: feasibility and preliminary results. *World Neurosurg*. (2017) 107:966–73. doi: 10.1016/j.wneu.2017.07.103
97. Eschbacher J, Martirosyan NL, Nakaji P, Sanai N, Preul MC, Smith KA, et al. *In vivo* intraoperative confocal microscopy for real-time histopathological imaging of brain tumors. *J Neurosurg*. (2012) 116:854–60. doi: 10.3171/2011.12.JNS11696
98. Al-Shamy G, Sawaya R. Management of brain metastases: the indispensable role of surgery. *J Neurooncol*. (2009) 92:275–82. doi: 10.1007/s11060-009-9839-y
99. Kamp MA, Rapp M, Bühner J, Slotty PJ, Reichelt D, Sadat H, et al. Early postoperative magnet resonance tomography after resection of cerebral metastases. *Acta Neurochir*. (2015) 157:1573–80. doi: 10.1007/s00701-015-2479-4
100. Patchell RA, Tibbs PA, Walsh JW, Dempsey RJ, Maruyama Y, Kryscio RJ, et al. A randomized trial of surgery in the treatment of single metastases to the brain. *N Engl J Med*. (1990) 322:494–500. doi: 10.1056/NEJM199002223220802
101. Gamarra F, Lingk P, Marmarova A, Edelmann M, Hautmann H, Stepp H, et al. 5-Aminolevulinic acid-induced fluorescence in bronchial tumours: dependency on the patterns of tumour invasion. *J Photochem Photobiol B*. (2004) 73:35–42. doi: 10.1016/j.jphotobiol.2003.09.009
102. Moan J, Bech O, Gaullier JM, Stokke T, Steen HB, Ma LW, et al. Protoporphyrin IX accumulation in cells treated with 5-aminolevulinic acid: dependence on cell density, cell size and cell cycle. *Int J Cancer*. (1998) 75:134–9. doi: 10.1002/(SICI)1097-0215(19980105)75:1<134::AID-IJC20>3.0.CO;2-F
103. Riedl CR, Daniltchenko D, Koenig F, Simak R, Loening SA, Pflueger H. Fluorescence endoscopy with 5-aminolevulinic acid reduces early recurrence rate in superficial bladder cancer. *J Urol*. (2001) 165:1121–3. doi: 10.1016/S0022-5347(05)66442-7
104. Tsai T, Ji HT, Chiang PC, Chou RH, Chang WS, Chen CT. ALA-PDT results in phenotypic changes and decreased cellular invasion in surviving cancer cells. *Lasers Surg Med*. (2009) 41:305–15. doi: 10.1002/lsm.20761
105. Utsuki S, Miyoshi N, Oka H, Miyajima Y, Shimizu S, Suzuki S, et al. Fluorescence-guided resection of metastatic brain tumors using a 5-aminolevulinic acid-induced protoporphyrin IX: pathological study. *Brain Tumor Pathol*. (2007) 24:53–5. doi: 10.1007/s10014-007-0223-3
106. Marhold F, Mercea PA, Scheichel F, Berghoff AS, Heicappell P, Kiesel B, et al. Detailed analysis of 5-aminolevulinic acid induced fluorescence in different brain metastases at two specialized neurosurgical centers: experience in 157 cases. *J Neurosurg*. (2019) 27:1–12. doi: 10.3171/2019.6.JNS1997
107. Kamp MA, Grosser P, Felsberg J, Slotty PJ, Steiger HJ, Reifenberger G, et al. 5-aminolevulinic acid (5-ALA)-induced fluorescence in intracerebral metastases: a retrospective study. *Acta Neurochir*. (2012) 154:223–8. doi: 10.1007/s00701-011-1200-5
108. Schebesch KM, Hoehne J, Hohenberger C, Acerbi F, Broggi M, Proescholdt M, et al. Fluorescein sodium-guided surgery in cerebral lymphoma. *Clin Neurol Neurosurg*. (2015) 139:125–8. doi: 10.1016/j.clineuro.2015.09.015
109. Schebesch KM, Hoehne J, Hohenberger C, Proescholdt M, Riemenschneider MJ, Wendl C, et al. Fluorescein sodium-guided resection of cerebral metastases—experience with the first 30 patients. *Acta Neurochir*. (2015) 157:899–904. doi: 10.1007/s00701-015-2395-7
110. Höhne J, Hohenberger C, Proescholdt M, Riemenschneider MJ, Wendl C, Brawanski A, et al. Fluorescein sodium-guided resection of cerebral metastases-an update. *Acta Neurochir*. (2017) 159:363–7. doi: 10.1007/s00701-016-3054-3
111. Falco J, Cavallo C, Vetrano IG, de Laurentis C, Siozos L, Schiariti M, et al. Fluorescein application in cranial and spinal tumors enhancing at preoperative MRI and operated with a dedicated filter on the surgical microscope: preliminary results in 279 patients enrolled in the FLUOCERTUM prospective study. *Front Surg*. (2019) 6:49. doi: 10.3389/fsurg.2019.00049
112. Teng CW, Cho SS, Singh Y, De Ravin E, Somers K, Buch L, et al. Second window ICG predicts gross-total resection and progression-free survival during brain metastasis surgery. *J Neurosurg*. (2021) 2:1–10. doi: 10.3171/2020.8.JNS201810

113. Ruge JR, Liu J. Use of 5-aminolevulinic acid for visualization and resection of a benign pediatric brain tumor. *J Neurosurg Pediatr*. (2009) 4:484–6. doi: 10.3171/2009.6.PEDS08428
114. Preuss M, Renner C, Krupp W, Christiansen H, Fischer L, Merkenschlager A, et al. The use of 5-aminolevulinic acid fluorescence guidance in resection of pediatric brain tumors. *Childs Nerv Syst*. (2013) 29:1263–7. doi: 10.1007/s00381-013-2159-8
115. Offersen CM, Skjoeth-Rasmussen J. Evaluation of the risk of liver damage from the use of 5-aminolevulinic acid for intra-operative identification and resection in patients with malignant gliomas. *Acta Neurochir*. (2017) 159:145–50. doi: 10.1007/s00701-016-3014-y
116. de Laurentis C, Höhne J, Cavallo C, Restelli F, Falco J, Broggi M, et al. The impact of fluorescein-guided technique in the surgical removal of CNS tumors in a pediatric population: results from a multicentric observational study. *J Neurosurg Sci*. (2019) 63:679–87. doi: 10.23736/S0390-5616.19.04601-0
117. Inoue T, Endo T, Nagamatsu K, Watanabe M, Tominaga T. 5-aminolevulinic acid fluorescence-guided resection of intramedullary ependymoma: report of 9 cases. *Neurosurgery*. (2013) 72:ons159–68. doi: 10.1227/NEU.0b013e31827bc7a3
118. Millesi M, Kiesel B, Woehrer A, Hainfellner JA, Novak K, Martínez-Moreno M, et al. Analysis of 5-aminolevulinic acid–induced fluorescence in 55 different spinal tumors. *Neurosurg Focus*. (2014) 36:E11. doi: 10.3171/2013.12.FOCUS13485
119. Acerbi F, Cavallo C, Schebesch KM, Akçakaya MO, de Laurentis C, Hamamcioglu MK, et al. Fluorescein-guided resection of intramedullary spinal cord tumors: results from a preliminary, multicentric, retrospective study. *World Neurosurg*. (2017) 108:603–9. doi: 10.1016/j.wneu.2017.09.061
120. Olguner SK, Arslan A, Açik V, Istemen I, Can M, Gezercan Y, et al. Sodium fluorescein for spinal intradural tumors. *Front Oncol*. (2021) 10:618579. doi: 10.3389/fonc.2020.618579
121. Endo T, Aizawa-Kohama M, Nagamatsu K, Murakami K, Takahashi A, Tominaga T. Use of microscope-integrated near-infrared indocyanine green videoangiography in the surgical treatment of intramedullary cavernous malformations: report of eight cases. *J Neurosurg Spine*. (2013) 18:443–9. doi: 10.3171/2013.1.SPINE12482
122. Nevzati E, Chatain GP, Hoffman J, Kleinschmidt-DeMasters BK, Lillehei KO, Ormond DR. Reliability of fluorescein-assisted stereotactic brain biopsies in predicting conclusive tissue diagnosis. *Acta Neurochir*. (2020) 162:1941–7. doi: 10.1007/s00701-020-04318-5
123. Lynagh R, Ishak M, Georges J, Lopez D, Osman H, Kakareka M, et al. Fluorescence-guided stereotactic biopsy: a proof-of-concept study. *J Neurosurg*. (2019) 1–7.
124. Akshulakov SK, Kerimbayev TT, Biryuchkov MY, Urunbayev YA, Farhadi DS, Byvaltsev VA. Current Trends for improving safety of stereotactic brain biopsies: advanced optical methods for vessel avoidance and tumor detection. *Front Oncol*. (2019) 9:947. doi: 10.3389/fonc.2019.00947
125. Malinova V, von Eckardstein K, Mielke D, Rohde V. Diagnostic yield of fluorescence-assisted frame-based stereotactic biopsies of intracerebral lesions in comparison with frozen-section analysis. *J Neurooncol*. (2020) 149:315–23. doi: 10.1007/s11060-020-03608-3
126. Li C, Sullivan PZ, Cho S, Nasrallah MP, Buch L, Isaac Chen HC, et al. Intraoperative molecular imaging with second window indocyanine green facilitates confirmation of contrast-enhancing tissue during intracranial stereotactic needle biopsy: a case series. *World Neurosurg*. (2019) 126:e1211–8. doi: 10.1016/j.wneu.2019.02.231
127. Evers G, Kamp M, Warneke N, Berdel W, Sabel M, Stummer W, et al. 5-aminolaevulinic acid-induced fluorescence in primary central nervous system lymphoma. *World Neurosurg*. (2017) 98:375–80. doi: 10.1016/j.wneu.2016.11.011
128. Yamamoto T, Ishikawa E, Miki S, Sakamoto N, Zaboronok A, Matsuda M, et al. Photodynamic diagnosis using 5-aminolevulinic acid in 41 biopsies for primary central nervous system lymphoma. *Photochem Photobiol*. (2015) 91:1452–7. doi: 10.1111/php.12510
129. Batchelor T, Loeffler JS. Primary CNS lymphoma. *J Clin Oncol*. (2006) 24:1281–8. doi: 10.1200/JCO.2005.04.8819
130. Millesi M, Kiesel B, Wöhrer A, Mercea PA, Bissolo M, Roetzer T, et al. Is intraoperative pathology needed if 5-aminolevulinic-acid-induced tissue fluorescence is found in stereotactic brain tumor biopsy? *Neurosurgery*. (2020) 86:366–73. doi: 10.1093/neuros/nyz086
131. Henderson F Jr, Brem S, Hussain J, Buch L, Maloney E, Singhal S, et al. Second window indocyanine green localizes CNS lymphoma in real time in the operating room: report of two cases. *Br J Neurosurg*. (2020) 3:1–5. doi: 10.1080/02688697.2020.1716945
132. Vetrano IG, Acerbi F, Falco J, Devigili G, Rinaldo S, Messina G, et al. Fluorescein-guided removal of peripheral nerve sheath tumors: a preliminary analysis of 20 cases. *J Neurosurg*. (2019) 6:1–10. doi: 10.3171/2019.9.JNS19970
133. Marbacher S, Klinger E, Schwyzer L, Fischer I, Nevzati E, Diepers M, et al. Use of fluorescence to guide resection or biopsy of primary brain tumors and brain metastases. *Neurosurg Focus*. (2014) 36:E10. doi: 10.3171/2013.12.FOCUS13464
134. Inoue A, Kohno S, Ohnishi T, Nishida N, Suehiro S, Nakamura Y, et al. Tricks and traps of ICG endoscopy for effectively applying endoscopic transsphenoidal surgery to pituitary adenoma. *Neurosurg Rev*. (2020). doi: 10.1007/s10143-020-01382-4
135. Amano K, Aihara Y, Tsuzuki S, Okada Y, Kawamata T. Application of indocyanine green fluorescence endoscopic system in transsphenoidal surgery for pituitary tumors. *Acta Neurochir*. (2019) 161:695–706. doi: 10.1007/s00701-018-03778-0
136. Utsuki S, Oka H, Kijima C, Miyajima Y, Hagiwara H, Fujii K. Utility of intraoperative fluorescent diagnosis of residual hemangioblastoma using 5- aminolevulinic acid. *Neurol India*. (2011) 59:612–5. doi: 10.4103/0028-3886.84349
137. Molina CA, Pennington Z, Ahmed AK, Westbroek E, Goodwin ML, Tamargo R, et al. Use of intraoperative indocyanine green angiography for feeder vessel ligation and en bloc resection of intramedullary hemangioblastoma. *Oper Neurosurg*. (2019) 17:573–9. doi: 10.1093/ons/opz053
138. Singh YB, Cho SS, Blue R, Teng CW, De Ravin E, Buch L, et al. Second-window indocyanine green for visualization of hemangioblastoma: a case report with two-dimensional operative video. *Oper Neurosurg*. (2021) 20:E229–33. doi: 10.1093/ons/opaa392
139. Bernal García LM, Cabezudo Artero JM, Marcelo Zamorano MB, Gilete Tejero, I. Fluorescence-guided resection with 5-aminolevulinic acid of subependymomas of the fourth ventricle: report of 2 cases: technical case report. *Neurosurgery*. (2015) 11(suppl.2):E364–71. doi: 10.1227/NEU.0000000000000682
140. Takeda J, Nonaka M, Li Y, et al. 5-ALA fluorescence-guided endoscopic surgery for mixed germ cell tumors. *J Neurooncol*. (2017). 134:119–24. doi: 10.1007/s11060-017-2494-9

Conflict of Interest: CH is a consultant for NX Development Corporation (NXDC) and Synaptive Medical. NXDC, a privately held company, markets Gleolan (5-ALA, aminolevulinic acid hydrochloride). Gleolan is an optical imaging agent approved for the visualization of malignant tissue during glioma surgery. CH is a consultant for NXDC and receives royalty payments for the sale of Gleolan, has also received speaker fees by Carl Zeiss and Leica. FA has received speaker's fees from Carl Zeiss Meditec, Oberkochen, Germany.

The remaining authors declare that the research was conducted in the absence of any commercial or financial relationships that could be construed as a potential conflict of interest.

frontiers in Oncology

ORIGINAL RESEARCH
published: 21 June 2021
doi: 10.3389/fonc.2021.679989

Intracranial Sonodynamic Therapy With 5-Aminolevulinic Acid and Sodium Fluorescein: Safety Study in a Porcine Model

Luca Raspagliesi[1†], Antonio D'Ammando[1†], Matteo Gionso[2], Natasha D. Sheybani[3], Maria-Beatriz Lopes[4], David Moore[5], Steven Allen[6], Jeremy Gatesman[7], Edoardo Porto[1,8], Kelsie Timbie[5], Andrea Franzini[9], Francesco Di Meco[1,8,10], Jason Sheehan[11], Zhiyuan Xu[11] and Francesco Prada[1,5,11,12]*

[1] Neurosurgery Department, Fondazione IRCCS Istituto Neurologico Carlo Besta, Milan, Italy, [2] Humanitas University, Pieve Emanuele, Italy, [3] Division of Oncology, Department of Medicine, Stanford Cancer Institute, Stanford University, Stanford, CA, United States, [4] Department of Pathology, University of Virginia, Charlottesville, VA, United States, [5] Focused Ultrasound Foundation, Charlottesville, VA, United States, [6] Department of Biomedical Engineering, University of Virginia, Charlottesville, VA, United States, [7] Center for Comparative Medicine, University of Virginia, Charlottesville, VA, United States, [8] Department of Health Sciences, University of Milan, Milan, Italy, [9] Department of Neurosurgery, Humanitas Clinical and Research Center, Milan, Italy, [10] Department of Neurological Surgery, Johns Hopkins Medical School, Baltimore, MD, United States, [11] Department of Neurological Surgery, University of Virginia, Charlottesville, VA, United States, [12] Acoustic Neuroimaging and Therapy Laboratory, Fondazione IRCCS Istituto Neurologico Carlo Besta, Milan, Italy

Background: Sonodynamic therapy (SDT) is an emerging ultrasound-based treatment modality for malignant gliomas which combines ultrasound with sonosensitizers to produce a localized cytotoxic and modulatory effect. Tumor-specificity of the treatment is achieved by the selective extravasation and accumulation of sonosensitizers in the tumor-bearing regions. The aim of this study is to demonstrate the safety of low-intensity ultrasonic irradiation of healthy brain tissue after the administration of FDA-approved sonosensitizers used for SDT in experimental studies in an *in vivo* large animal model.

Methods: In vivo safety of fluorescein (Na-Fl)- and 5 aminolevulinic acid (5-ALA)-mediated low-intensity ultrasound irradiation of healthy brain parenchyma was assessed in two sets of four healthy swine brains, using the magnetic resonance imaging (MRI)-guided Insightec ExAblate 4000 220 kHz system. After administration of the sonosensitizers, a wide fronto-parietal craniotomy was performed in pig skulls to allow transmission of ultrasonic beams. Sonication was performed on different spots within the thalamus and periventricular white matter with continuous thermal monitoring. Sonication-related effects were investigated with MRI and histological analysis.

Results: Post-treatment MRI images acquired within one hour following the last sonication, on day one, and day seven did not visualize any sign of brain damage. On histopathology, no signs of necrosis or apoptosis attributable to the ultrasonic treatments were shown in target areas.

OPEN ACCESS

Edited by:
Constantinos G. Hadjipanayis, Mount Sinai Health System, United States

Reviewed by:
Michael Edward Ivan, University of Miami Health System, United States
Nader Sanai, Barrow Neurological Institute (BNI), United States
David W. Roberts, Dartmouth College, United States

***Correspondence:**
Francesco Prada
francesco.prada@istituto-besta.it

[†]These authors have contributed equally to this work and share first authorship

Specialty section:
This article was submitted to Neuro-Oncology and Neurosurgical Oncology, a section of the journal Frontiers in Oncology

Received: *12 March 2021*
Accepted: *25 May 2021*
Published: *21 June 2021*

Citation:
Raspagliesi L, D'Ammando A, Gionso M, Sheybani ND, Lopes M-B, Moore D, Allen S, Gatesman J, Porto E, Timbie K, Franzini A, Di Meco F, Sheehan J, Xu Z and Prada F (2021) Intracranial Sonodynamic Therapy With 5-Aminolevulinic Acid and Sodium Fluorescein: Safety Study in a Porcine Model. Front. Oncol. 11:679989. doi: 10.3389/fonc.2021.679989

Conclusions: The results of the present study suggest that either Na-FL or 5-ALA-mediated sonodynamic therapies under MRI-guidance with the current acoustic parameters are safe towards healthy brain tissue in a large *in vivo* model. These results further support growing interest in clinical translation of sonodynamic therapy for intracranial gliomas and other brain tumors.

Keywords: safety, brain tumors, ultrasound, sonodynamic therapy (SDT), fluorescein (FL), fluorescein 5-aminolevulinic acid (5-ALA), focused ultrasound (FUS)

INTRODUCTION

High-grade gliomas (HGGs) are the most common and aggressive group of primary tumors of the brain deriving from glial cells, with an incidence of 3-5 cases per 100,000 inhabitants in the United States (1, 2). These tumors are characterized by an infiltrative and diffuse nature, which results in unavoidable early recurrences and a poor overall survival (2, 3). Indeed, current therapeutic schemes, often involving maximal surgical resection, subsequent irradiation and cytotoxic chemotherapy, have little influence on the outcome of HGGs, due to chemo- and radio-resistance of tumor stem cells, rapid infiltration of tumor cells into normal brain tissue through axonal pathways, and low chemotherapy penetration through intact blood-brain barrier (BBB) in the peritumoral region, where tumor stem cells often reside (4–6).

Over the years, the unsatisfactory yield of existing treatments has prompted the search for new therapeutic approaches to HGGs (7). Among investigated techniques is sonodynamic therapy (SDT), which has proven in recent years to be a promising approach for treatment of intracranial tumors. It relies on the natural pharmacokinetics and tumor-selectivity of non-toxic sound-sensitive molecules, called sonosensitizers, which are able to locally magnify the cytotoxic and modulatory effects of low-frequency low-intensity ultrasound waves (8). Possible mechanisms of SDT include peroxidation of membrane lipids *via* peroxyl radicals, generated by activation of the sonosensitizer; physical destabilization of the cell membrane, allowing increased susceptibility of the cell to shear forces; and enhanced uptake of chemotherapy due to sonoporation (9). There are many different agents known to be effective sonosensitizers for SDT; the most common are porphyrin-based or xanthene-based. The ideal sonosensitizer should have no substantial *in vivo* toxicity, high selectivity for the target lesion, and a high clearance rate from healthy tissue (10).

The concept that porphyrin-based molecules could be used as sonosensitizers dates back to the employment of hematoporphyrin in photodynamic therapy and is based on the evidence that electronic excitations of this compound by ultrasound energy initiate a chemical process that eventually results in the formation of cytotoxic reactive oxygen species (ROS) (11). 5-aminolevulinic acid (5-ALA) is a porphyrin-based compound, often employed in SDT for glioma model due to its characteristic selectivity for tumor cells. In particular, 5-ALA is implicated in physiological heme synthesis and normally does not produce ROS. However, when an exogenous source of 5-ALA is administered, one of its deriving porphyrins - Protoporphyrin IX (PpIX) - accumulates in the intracellular compartment of tumor cells and, when activated by low-intensity ultrasound, generates cytotoxic ROS that in turn damage target cells (12). The selective accumulation of PpIX in HGG, but not in normal tissue, is explained by a variety of different mechanisms: the limited activity of ferrochelatase, an enzyme for PpIX metabolism to heme, in tumor cells; the increased capacity for converting 5-ALA to PpIX; enhanced uptake of the compound resulting from impairment of the BBB surrounding glial tumors (13–15). Due to this highly selective accumulation in glioma cells, 5-ALA is, to date, the most commonly investigated sonosensitizer for glioma-SDT (4).

Sodium Fluorescein (Na-Fl) is an organic xanthene-based compound often used as a fluorescent dye during surgical removal of malignant gliomas. Its selectivity for pathologic tissue after systemic administration is achieved through preferential accumulation in brain areas with impaired BBB and rapid washout from vessels and healthy tissue (16, 17). After intravenous administration, Na-Fl weakly binds to blood proteins; hence, the presence of both bound (66 kDa) and unbound protein (376 Da) in circulation. The latter is able to cross normal BBB and readily penetrate normal brain tissue, wherein its concentration is highly time-dependent and peaks between 15 and 30 minutes after administration (17).

Intrinsic characteristics of Na-Fl (i.e. high extinction coefficient and high fluorescence quantum yield in water) account for its photodynamic and sonodynamic activity when appropriately stimulated. In particular, ultrasonic irradiation of fluorescein results in the generation of singlet oxygen ($^1O_2$), which induces oxidative stress and resultantly injures surrounding tissue (18). Indeed, Na-Fl has only recently been investigated as a sonosensitizer for glioma-SDT, exhibiting efficacy and safety in an ectopic model of rat glioma (19).

Many preclinical studies have already investigated the efficacy of both 5-ALA and Na-Fl in treating gliomas. However, studies published to date have only employed small animal (i.e. rodent) models, typically with minor subsets of healthy subjects, and have been focused on tumor response, lending minimal insight into the effects of SDT on the surrounding brain parenchyma (4). Furthermore, sonication devices were mostly experimental, with only one study having employed a device currently in use for ultrasound therapy in humans (20). The objective of the present study is to demonstrate the feasibility and safety of SDT in a large animal model using both 5-ALA and Na-Fl as sonosensitizers for

in vivo application of SDT to healthy pigs using an MRI-guided FUS (MRgFUS) device (Insightec 220 kHz MRgFUS system).

MATERIALS AND METHODS

Study Design

Healthy adult pigs (Sus scrofa domesticus) underwent MRI-guided cerebral sonodynamic therapy. One animal was preliminarily employed as a test-pilot to assess workflow and feasibility and was sacrificed the same day of the procedure. Experimental subjects were randomized into two treatment arms - SDT with 5-ALA (n=3) and SDT with Na-Fl (n=5) - as summarized in **Table 1**. Subjects received the assigned sonosensitizer and underwent a craniotomy procedure and subsequent sonication *via* the MRgFUS system (ExAblate, Tirat Carmel, Israel). Ultrasound waves were focused on two target structures within a single cerebral hemisphere, employing the contralateral hemisphere of each subject as a direct internal control. Subjects underwent MRI imaging at day 1 and at day 7 after the procedure; at day 7 subjects received a second dose of the assigned sonosensitizer and, two to three hours later, they were euthanized; after sacrifice, subjects' brains were extracted and fixed for histopathological assessment. **Figure 1** summarizes the timeline of experimental treatments.

Subjects' Preparation

All procedures were performed at University of Virginia strictly following Animal Care and Use Committee (ACUC) guidelines (protocol approval #4152).

Two to three hours prior to the acoustic sonications, each subject received a full dose of either 5-ALA (20mg/Kg body weight) or Na-Fl (10mg/Kg body weight), namely the dose currently used in clinical practice for fluorescence-guided surgery, through the left lateral auricular vein with a peripheral venous line.

Surgical Procedure

Due to the peculiar anatomy of the porcine skull, which is not compatible with the geometry of the ExAblate's stereotaxic helmet, a craniotomy procedure was necessary to allow optimal coupling of brain tissues with the device. After administration of the sonosensitizer, subjects were brought to the veterinary facility at University of Virginia and positioned on the surgical table in a prone position.

Each subject subsequently received general anesthesia with Telazol/Xylazine 4-6/2 mg per kg intramuscularly (induction) and Isoflurane (maintenance).

After induction of anesthesia, the skin was epilated and disinfected with betadine and alcohol 70% and the sterile surgical field was prepared. The procedure began with a 35mm incision of the skin 10 mm from the midline and 10 mm anterior to the coronal suture and dissection of the subcutaneous tissues. Once the bone was exposed, a 5 cm-diameter wide fronto-parietal craniotomy was performed with rongeurs and a cutting burr to expose the region of brain superficial to the selected targets. Subsequently, sterile water was inserted into the cavity and the skin was closed over the brain without the interposition of the bone flap to allow the unhindered penetration of the ultrasound waves.

Sonication Procedure

Each subject was subsequently transported to the ExAblate 220 kHz MRgFUS device located at the University of Virginia

TABLE 1 | The table summarizes the subjects employed in the present studies, exemplifying the sonosensitizer administered, the areas of sonication, the number of spots sonicated, and the post-procedure scans performed.

#	Group	Mod	Areas	Locations	Sonications	Sub-spots	Post-procedure scans
1	Pilot	na	fPWM	1	6	4	na
			Th	/	/	/	
2	5-ALA	94	fPWM	2	6	4	Cube T2; T1
			Th	2	6	4	
3	5-ALA	95	fPWM	2	6	10	Sag Cube FLAIR
			Th	2	6	10	Sag CUBE T2
							Sag CUBE T1
4	5-ALA	95	fPWM	2	6	10	Sag Cube FLAIR
			Th	2	6	10	Sag CUBE T2
							Sag CUBE T1
5	Na-FL	95	fPWM	2	6	10	Sag Cube FLAIR
			Th	2	6	10	Sag CUBE T2
							Sag CUBE T1
6	Na-FL	OMISSIS	fPWM	na	na	na	na
		(95)	Th	na	na	na	
7	Na-FL	95	fPWM	2	6	10	Sag Cube FLAIR
			Th	2	6	10	Sag CUBE T2
							Sag CUBE T1
8	Na-FL	12	fPWM	2	7	10	Sag Cube FLAIR
			Th	2	7	10	Sag CUBE T2
							Sag CUBE T1
9	Na-FL	12	fPWM	2	7	10	Sag Cube FLAIR
			Th	2	7	10	Sag CUBE T2
							Sag CUBE T1

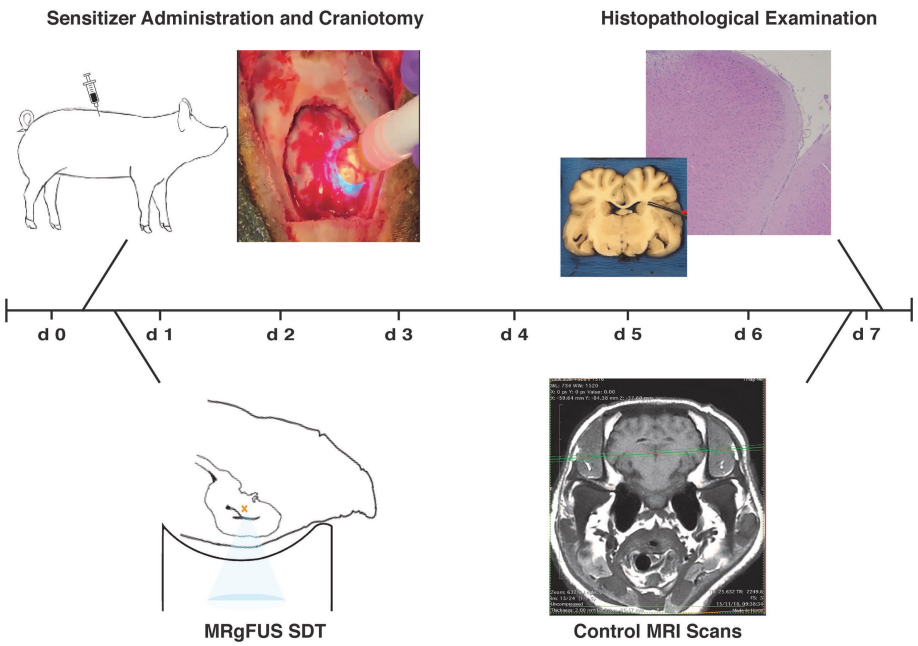

FIGURE 1 | Timeline of experimental treatments. Subjects were administered the assigned sensitizing compound right before undergoing craniotomy at day one. After the procedure, subjects were placed in prone position inside the Exablate device and received MRI-guided low-intensity insonation. On the day 3, MRI scans were acquired again to be later compared with pre-treatment tracking images. Upon sacrifice on the seventh day, brains were harvested for histopathological examination.

Focused Ultrasound Center, secured to a helmet and positioned supine on the MRI table of the device while maintained under general anesthesia.

Treatment targets were identified on the MRI using a 2D, multi-slice, balanced, steady-state acquisition (FIESTA) with whole-brain coverage. The sequence was repeated with prescribed slices oriented in the coronal, sagittal, and transverse orientation. Slices were prescribed to cover the entire brain volume. The resulting images presented strong contrast between gray/white matter and the ventricles, allowing stereotactic planning of the treatment targets. Conditions that might compromise the results, e.g. pre-existing lesions, inflammation or edema, were then ruled out (**Figure 2**).

The FUS treatment was administered with a power level of 1 W (0.57 acoustic power) to achieve a focused peak power of 2-3 W/cm^2. Peak pressure for this power level, measured with a hydrophone, was around 200 kPa. In order to maximize the

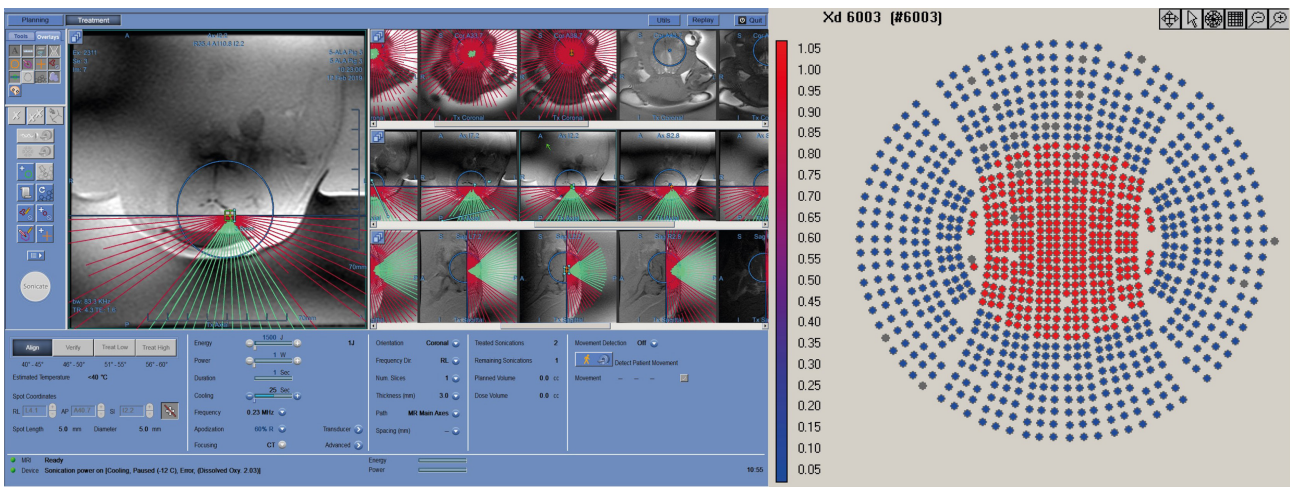

FIGURE 2 | T1- and T2-weighted images acquired after the sonication procedure.

treatment volume, we leveraged the 10% duty cycle (DC) of the ExAblate system chosen for the treatment sonication; the device's multi-element array has the ability to rapidly switch the sonication target by changing the phase of the 1024 elements in the transducer to move the focus of the transducer within a region roughly 2 cm in diameter (**Figure 3**). A sonication pattern was designed to raster the focus across 10 locations centered around the target location on the clinical software. As a result, each insonated region encompassed a rectangle roughly 10x10x15 mm, about the same size and shape of two dice stacked on top of one another with the center of the sonication target located between the two faces of the dice.

Post-Treatment Procedures and Examination

Immediately after the insonation, each subject was removed from the Insightec system and placed prone in an 8-channel imaging coil. MRI images (T1 and T2-weighted SPACE, 3D-MPRAGE, Diffusion-weighted MRI) were then acquired; diffusion-weighted sequences were considered particularly significant as an early indicator of post-treatment lesion (21). Contrast-enhanced T1 scans were not considered due to the lack of a pathological lesion to produce extravasation of Gadolinium, nor the necessity to asses contrast extravasation as for blood brain barrier opening. Acquisition parameters are described in **Table 2**.

Preliminarily, the test-pilot subject (pig #1), which had received 5-ALA administration, was euthanized immediately after completion of the FUS procedure in order to verify the feasibility of the present experimental protocol.

Conversely, all the other subjects were transported back to the animal nursery unit at University of Virginia after the procedure to be awakened and closely monitored. These subjects underwent further MRI scans at day 7 and were subsequently euthanized. Two to three hours prior euthanasia, each subject received a second dose of the assigned sensitizer (either 5-ALA, 20mg/Kg body weight, or Na-Fl, 10mg/Kg body weight), through the left lateral auricular vein with a peripheral venous line; the purpose of this procedure was to reproduce, at the ex vivo examination, the same parenchymal concentration of the compounds that was present at the time of the sonication.

Upon euthanasia (Euthasol 1ml/10lbs body weight, IV), the brains of all subjects were harvested for histopathological examination.

Histopathological Examination

After being harvested, brains were preserved in 10% neutral buffered formalin (Sigma-Aldrich, USA) for histological analysis.

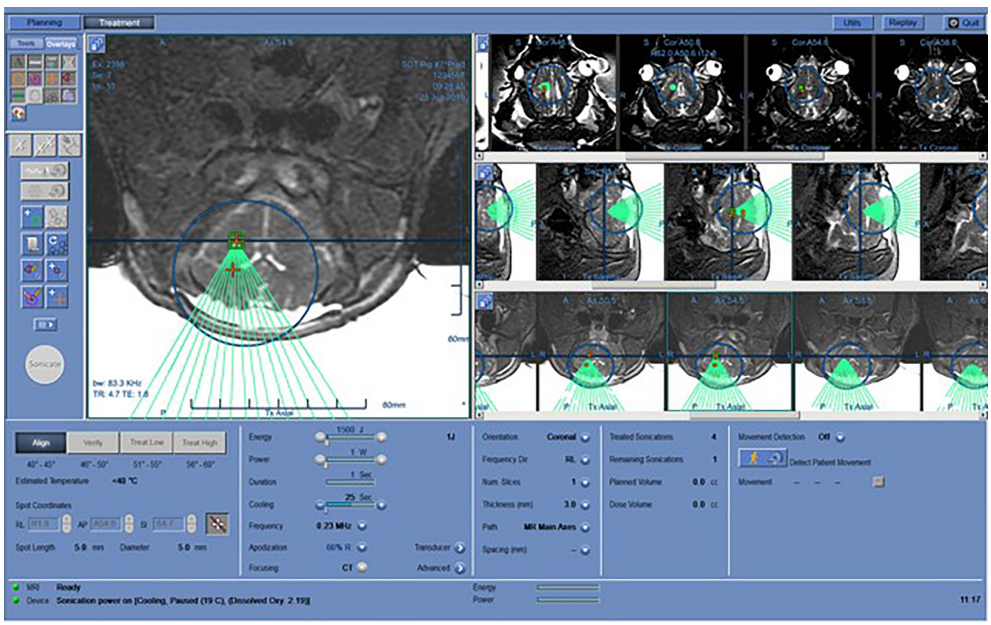

FIGURE 3 | Working layout of the Exablate system during insonation of one subject. The insonation pattern is superimposed on the pre-acquired MR images in different slices.

TABLE 2 | MRI acquisition parameters used immediately after insonation and at 7-day follow-up imaging.

Scan Type	TR (s)/TE (ms)/TI (ms)	FOV (mm)/Resolution (mm)	Bandwidth (kHz)/Echo train length	b-value s mm^{-1}/Directions
3D T1-w SPACE	0.6/15.8	160 x 160 x 272/0.5 x 0.5 x 1	244/28	
3D T2-w SPACE	3/109	160 x 160 x 272/0.5 x 0.5 x 1	244/130	
3D-MPRAGE	1.2/4.1/450	160 x 160 x 272/0.5 x 0.5 x 1	122/32	
DW	8/69	160 x 160 x 64/1.25 x 1.25 x 4	1953/128	1000/25

Brains were then cut in coronal sections; anatomical slices containing treated areas and surrounding regions were paired with corresponding intra-procedural MRI slices for comparison purposes.

Slices corresponding to target locations were first macroscopically inspected to identify any gross signs of damage resulting from sonication procedures. Subsequently, tissue sections from the bilateral thalami and periventricular areas were then sampled and processed for paraffin-embedding. Microscopic examination was performed on 5 µm-thick histologic sections stained by hematoxylin and eosin.

Fluorescence Quantification

The tip of the frontal lobe from the pigs' extracted brains were excised and employed to quantify PpIX and NA-Fl concentration, respectively.

- *5-ALA group*: the tip was minced into tiny pieces with sterile scissors and weighed. The brain tissue was suspended in 300ul Solvable (Sigma-Aldrich, USA) in a 45°C water bath for 15 minutes. Meanwhile, a final concentration of 200uM PpIX powder (purchased from Sigma-Aldrich, USA) in Solvable was prepared, and then serial dilutions of PpIX were prepared in 200ul Solvable in a 96-well assay plate (Costar, black plate, clear bottom with lid, Corning, USA) for a standard curve of PpIX. Transferred 200ul supernatant from the aforementioned brain tissue preparation tube. The fluorescence intensity was quantitated using SpectraMax iD3 multi-mode (Fluorescence, luminescence, absorbance) plate reader with the excitation wavelength of 405 nm and the emission wavelength of 635 nm (Molecular Devices, Biomolecular Analysis Facility, University of Virginia) (22).
- *Na-Fl group*: excised regions of cerebral tissue were immersed in a phosphate buffered saline bath and imaged using the IVIS Spectrum (PerkinElmer) for Na-FL fluorescence signal using 494/521 excitation/emission peak inputs and auto-exposure settings. The Living Images software package (PerkinElmer) was used for quantification of epifluorescence from images. Identical circular Regions of Interest (ROI) were applied to encompass individual tissues or a background region, following which Na-Fl fluorescence was quantified and reported as radiance.

RESULTS

Out of 9 total experiments performed, 1 subject (pig #6) was excluded from analysis since, during the closure of the scalp over the craniotomy, it suffered a direct injury to the non-sonicated hemisphere; histopathological examination showed a superficial subacute infarct with organizing subarachnoid and intraparenchymal hemorrhage, surrounding infarction of the cortex and significant inflammatory reaction comprised of lymphocytes, macrophages and eosinophils, while the left cortex showed focal organizing subarachnoid hemorrhage. Although ultimately excluded, this subject went through the whole experimental protocol until sacrifice on the seventh day. In the remaining subjects, the protocol was carried out without any relevant complications. Of note, during the sonication procedure, pig #8 was reported to have moved from reference position before completion of the treatment due to suboptimal fixation of the helmet. Nevertheless, after being repositioned, the treatment scheme was reinitiated, but the subject was ultimately not included in the analysis.

Overall, sonication procedure had a mean duration of 1 hour, 40 minutes, corresponding to 20 minutes for each location.

Fluorescence Quantification

- *5-ALA group*: fluorescence quantification confirmed the presence of PpIX in all the analyzed specimens. Fluorescence intensity of PpIX was 56,4 µmol/gm brain tissue in pig #2, 7438,4 µmol/gm brain tissue in pig #3 and 8375,5 µmol/gm brain tissue in pig #4. The difference among these results reflected the specific time lapse between the sonosensitizer administration and euthanasia in each subject; the low level of PpIX in subject #1, in particular, might be due to the fact that, due to technical constraints, this specific specimen had to be frozen at -80°C and, then, analyzed 48h after the harvest.
- *Na-Fl group*: epifluorescence imaging revealed noteworthy differential uptake of Na-Fl in cerebral tissues immediately following intervention. The brain exhibited the highest uptake of Na-Fl, approximately 2.1- and 1.2-fold higher than the brainstem and dura, respectively.

Sonication Procedures and Radiological Findings

In preclinical sonodynamic treatment studies performed to date, typically a 10% DC (where the transducer is on 10% of the time and off for 90%) has been used in order to provide a power sufficient to activate the sonosensitizer agent but avoid a thermal rise in the target and surrounding tissues (23–25). In our procedure, each sonication target was a series of 10 sub-sonications centered around the target chosen on the targeting software; by taking advantage of the fact that each sonication needed to be 10ms in length and a 10% DC, the 90% off time could be used to treat additional targets. So, the total ON-time for the transducer was almost 100%, but each spot received only a 10% DC, as usual. The steering used for each sonication are exemplified in **Table 3**.

The spot size for the 220kHz ExAblate system was approximately 4x10mm (full width, half maximum). This yielded a treatment volume roughly 10x10x15 mm in 20' (**Figure 4**).

In order to sonicate for the full 20 minutes required for the treatment, multiple sonications were required due to a limitation with the treatment software that only allowed a maximum 180 seconds per sonication. Sonications were restarted when each was finished (about 5-10 seconds between each sonication) for 6 times with a final 7th sonication lasting for 120 seconds to give a full 20 minutes. Sonications were typically apodized to about 80% to allow transmission through the craniotomy.

The radiological appearance of the target regions appeared indistinguishable from normative, healthy tissue on all scans (**Figure 5**). There were no indications of edema or hematoma throughout the whole brain, with the exception of subject #6, who, as mentioned above, suffered an injury during scalp closure.

TABLE 3 | The table shows the steering used for all sonication; coordinates are listed in mm.

Sonication 1	(0.0, 0.0, 3.0)
Sonication 2	(3.0, 3.0, 3.0)
Sonication 3	(-3.0, 3.0, 3.0)
Sonication 4	(-3.0, -3.0, 3.0)
Sonication 5	(3.0, -3.0, 3.0)
Sonication 6	(0.0, 0.0, -3.0)
Sonication 7	(3.0, 3.0, -3.0)
Sonication 8	(-3.0, 3.0, -3.0)
Sonication 9	(-3.0, -3.0, -3.0)
Sonication 10	(3.0, -3.0, -3.0)

Histopathological Findings

- *5-ALA group*: At macroscopic examination, coronal sections did not reveal any gross abnormalities at target areas (bilateral basal ganglia, thalamus, periventricular white matter). Multifocal areas of acute subarachnoid hemorrhage were present in pig #2 and pig #3, suggestive of terminal event. At histopathology, target areas (left thalamus and periventricular white matter) did not show any significant pathologic abnormality, including infarction, necrosis or hemorrhage; neurons and glial cells were intact, with no significant cellular alterations. Of note, microscopic intraparenchymal hemorrhages, without tissue reaction, were found in the lower portions of the thalamus of pig #2 and pig #3, suggestive of terminal event. Contralateral areas, serving as direct controls, were unremarkable both at macro and microscopic examination.
- *Na-FL group*: At macroscopic examination, subjects were completely unremarkable. At histopathology, target areas (left thalamus and periventricular white matter) did not reveal significant pathologic abnormalities including infarction, necrosis or hemorrhage. There was integrity of the neurons and glial cells with no significant cellular alterations. The contralateral areas were also unremarkable. Control areas of pigs #5, #8 and #9 were unremarkable. On the other hand, pig #7 showed organizing subarachnoid hemorrhage with gliosis of the subpial area of the right cortex.

DISCUSSION

The results of the present study demonstrate the safety of sonicating the healthy brain parenchyma after the administration of sonosensitizing agents in a large *in vivo* model. Moreover, considering the heterogeneous and complex cytoarchitecture of the encephalon, the safety of the procedure was assessed for both grey and white matter structures, represented by the thalamus and frontal periventricular white matter, respectively, demonstrating that neither of these areas are subjected to macro- and microscopic damage when treated with SDT. The presence of the sensitizing compounds within insonated brains was confirmed through analysis of the fluorescence output of the specimens of all the subjects. No clinical adverse events occurred during the procedure or survival phase of the experiment and no damage was observed either on neuroimaging, during or after the procedure, or on histopathological evaluation - with the exception of a single subject sustaining an injury during closure of the scalp. The multifocal areas of acute subarachnoid hemorrhage reported on histopathological analysis of certain subjects were suggestive of a terminal event and not attributable to the procedure.

Concerning brain tumors, different factors generally guide the choice of the most appropriate therapeutic approach. For example, localization is of paramount importance in brain tumor management, since deep masses are not usually well-suited for open surgery, which is potentially burdened by severe neurological morbidity. Other therapeutic strategies, such as

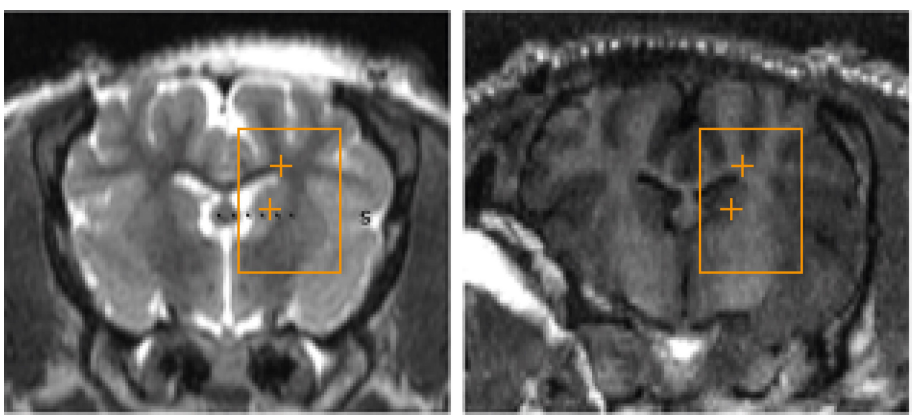

FIGURE 4 | Three-axial representation of the treatment-planning phase prior to insonation. Insonation targets are represented by orange cross signs within Basal Ganglia and Periventricular White Matter. Each location was composed of 10 sub-sonication spots that were alternately targeted by the tracking system to exploit the "off-duty" time of each single insonation.

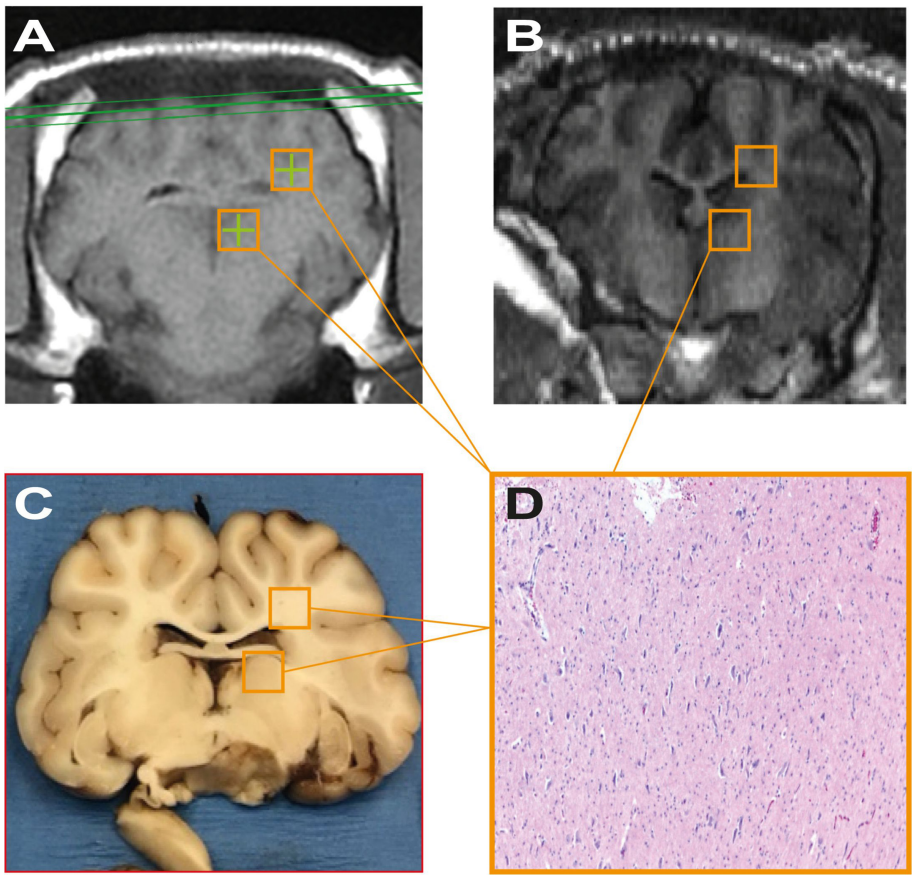

FIGURE 5 | **(A, B)** represent pre-treatment tracking images and post-procedure scans respectively, showing no significant differences attributable to the sonodynamic therapeutic protocol. Similarly, **(C, D)** were acquired during macroscopical examination and histopathological analysis of specimens and show no signs of necrosis or apoptotic phenomena after the treatment.

laser interstitial therapy or radiosurgery, have shown limited results in this context (7, 26, 27). In comparison, SDT may represent an innovative modality for the treatment of intracranial masses, as it exploits the ability of certain compounds (i.e. sonosensitizers) to be activated by ultrasound irradiation, thus locally exerting their biological effect in defined targets where they selectively accumulate. To this end, the interaction between the sensitizing agent and the lesion which selectively uptakes it acts as a "self-focusing mechanism" of this non-invasive treatment modality.

It is known that, in SDT, neither the low frequency insonation nor the sensitizing agent are able to appreciably treat any lesions when used alone; however, their simultaneous application can exert a cytotoxic effect (9).

This study aimed to push this paradigm one step further by demonstrating that even the simultaneous presence of both the ultrasound wave and the sensitizer is insufficient to produce significant effects, as there is the additional critical consideration of a "concentration effect" within the target lesion, be it neoplastic or otherwise. As no injuries were detected on clinical, radiological, and histopathological examinations following SDT, our results suggest that even if the presence of sonosensitizers had been confirmed in healthy brain tissues, this accumulation would be inconsequential. Indeed, in our subjects, the concentration of sensitizers was too low for determining a biological effect, since the absence of an area where these compounds can preferentially accumulate, such as a tumor. In light of this evidence, we postulate that three particular contemporary events must occur in order for SDT to render a cytotoxic effect: the administration of ultrasound and sonosensitizer and the presence of a lesion where the latter can reach a particular concentration, thus adding a further safety mechanism for SDT (**Figure 6**).

A crucial factor, which may hinder the future translation of SDT into clinical use, is the time required for the treatment; unlike sonication of small structures, as that performed, for example, for thalamic ventral intermediate nucleus (Vim) in essential tremor, the larger volumes which need to be treated in SDT for intracranial tumors require multiple sonications, and consequently, much longer treatment times. In contrast with small animals or *in vitro* models, this problem became particularly evident in the swine model employed herein.

In the present study, the time required for each procedure was drastically optimized by taking advantage of the low DC (10%) of

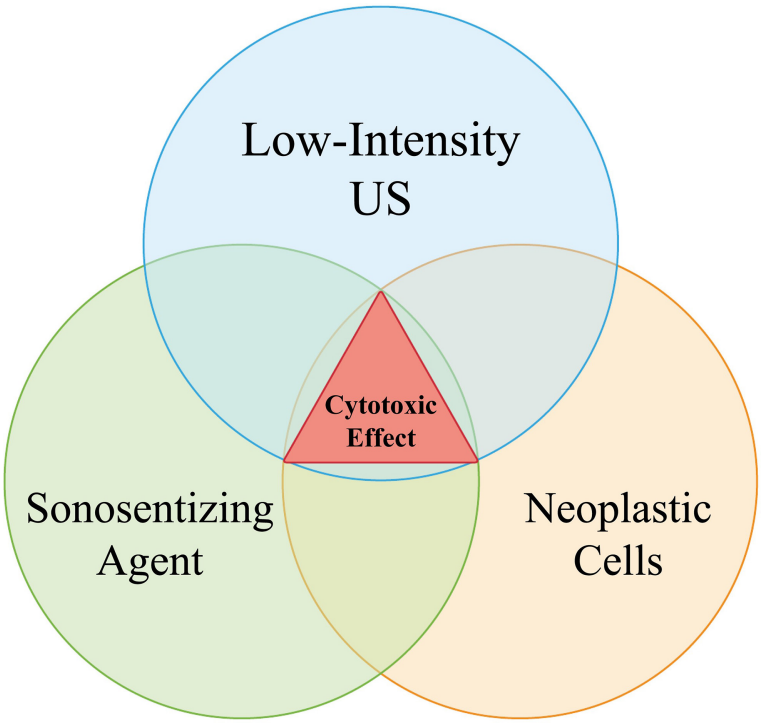

FIGURE 6 | The Venn Diagram explains the relation between sonosensitizer administration (5-ALA or Na-Fl), low-frequency sonication and tumor presence. The contemporary presence of all the three aforementioned events is required for a cytotoxic process to verify. As "tumor" here it is meant any lesion which is able to properly locally concentrate the administered sonosensitizers, granting the onset of their biological effects once activated by sound beams.

each sonication and rastering the sonication target in 10 sub-sonication areas, thus exploiting the 90% off-time of each DC by treating 9 additional spots. As a result, the total "ON" time for the transducer was almost 100%, but each spot received only a 10% DC, as commonly used. The aforementioned approach gives rise to a new sonication scheme, enabling treatment of larger volumes in the same amount of time and could be of great importance for translating SDT from animal models to clinical practice. On the other hand, it is noteworthy that such insonation strategy does not expose subject to higher energy levels, nor does it change the way each spot is treated per se; rather it exploits the silent "breaks" of traditional schemes to speed up the whole process.

Many preclinical studies have already investigated the safety and efficacy of both 5-ALA and Na-FL. Nonetheless, published experiences have generally employed small rodent models, with only minor subsets of healthy subjects (4); furthermore, sonication devices were mostly experimental, with only one study having employed a device currently in use for human ultrasonic treatments (20). To the best of our knowledge, this was the first proof of principle for intracranial MRI-guided SDT in a large animal model using a device that is in active clinical use. The porcine model allowed a more precise target definition, in a more similar way to the technique that would be used for clinical purposes in humans. Furthermore, the employed sonosensitizers are already approved for clinical usage in brain tumor surgery.

Even if HGGs are the most common and aggressive group of primary malignant tumors of the brain, there are other types of lesions which, despite their benign histological classification, comprise a group of challenging pathologies; this is attributable to their high local recurrence, aggressive behavior or deep location, e.g. chordomas or skull base meningiomas. If PpIX, the photo- and sono-dynamically active compound of 5-ALA, is known to accumulate in HGGs due to abnormal ferrochelatase activity in glial cells, its selectivity for these other tumor types is expected to be much less pronounced. The localization of Na-Fl, on the other hand is mainly dictated by BBB alterations and has been confirmed in different tumoral contexts, including meningiomas, hemangioblastomas, metastases, ependymomas, pilocytic astrocytomas, and schwannomas (28, 29). The safety of Na-Fl SDT, therefore, may open new hints towards future studies involving the treatment of different brain tumors beyond gliomas.

This study may bear some noteworthy future directions. First clinical experiences with SDT for brain tumors will likely rely on MRgFUS devices employing a stereotaxic frame; indeed, two clinical trials in the USA and Europe (NCT04559685 and NCT04845919 respectively) employing similar parameters and sensitizers' dosage were already approved. Future experimental designs are likely to benefit from the "rastered" insonation scheme herein proposed. This strategy will require further investigation to directly compare its efficacy with that of "classic" sonication modalities. Moving forward, SDT for brain

tumors might also benefit from approaches and devices that enable more agile and repeatable approaches to the disease management (30–32).

Limitations

The current study presents different limitations, among which the restricted sample size of the study; however, the decision to include only 9 specimens was made in order to minimize animal use by the Animal Care and Use Committee.

Furthermore, only one insonation protocol was tested in our experimental design for the same reason; however, the parameters employed in the study were derived from previous preclinical experiences (4, 19, 20, 33–36), the efficacy of which will be tested in one FDA and on CE approved clinical trial.

In this regard might sound limiting the absence of a pathological lesion in our experimental design to demonstrate concurrent effects of SDT towards it in the absence of damages to healthy tissues; it has to be kept in mind that the goal of the study was to prove that SDT does not affect brain tissue even when US beams are focused directly towards it. Of course, the present model does not indeed comprise a tumor marginal zone with compromised blood-brain barrier and potential higher concentration of the sensitizer, especially concerning Na-Fl. Furthermore, it has to be taken into account the absence of a validated porcine model of glioblastoma comparable to murine models employed in other studies. Future studies are warranted once this model will be readily available.

Tissue damage was only evaluated *via* H&E-stained histologic preparations, without further immunohistochemical or molecular assays; while these more complex methodologies are generally employed for tumor-bearing subjects (37–39), our present approach is consistent with other studies investigating safety of SDT in healthy specimens (40–42).

CONCLUSIONS

The current study demonstrated that insonation of both 5-ALA and Na-Fl is harmless from a clinical, radiological and histopathological point of view towards healthy brain tissue in absence of a lesion that is able to concentrate the aforementioned compounds to a determined level.

The ability of ultrasound to reach deep intracerebral structures may enable the possibility to treat lesions otherwise not amenable to benefit from open surgery.

With the results of the present study, new evidence in favor of SDT safety is provided, with the aim to ease its translation from experimental studies to clinical practice; this path, however, still has some hurdles. One major concern is that ultrasound procedures generally require long treatment sessions and this confines their application to small volumes; in order to overcome this problem, we propose a novel sonication procedure that exploits the duty cycle of SDT exposure conditions to expedite treatment time.

Finally, the current study suggests a new found flexibility to adjust the SDT treatment envelope to every lesion that is able to concentrate a particular sonosensitizer, in a manner appropriate for each compound's particular pharmacokinetic properties.

DATA AVAILABILITY STATEMENT

The original contributions presented in the study are included in the article/supplementary material. Further inquiries can be directed to the corresponding author.

ETHICS STATEMENT

The animal study was reviewed and approved by Animal Care & Use Committee (ACUC).

AUTHOR CONTRIBUTIONS

Conceptualization: FP, DM, KT, and ZX. Experimental procedure: FP, DM, KT, SA, JG, AF, and ZX. Data analysis: FP, LR, AD'A, MG, and EP. Writing, review and editing: LR, AD'A, MG, NS, JG, M-BL, AF, DM, SA, JS, ZX, and FP. Supervision: FP, FD, and JS. Project administration: FP, NS, DM, KT, and ZX. Funding acquisition: FP, JS, and ZX. All authors contributed to the article and approved the submitted version.

FUNDING

The present study was funded and supported by the Focused Ultrasound Foundation (Charlottesville, VA, USA).

REFERENCES

1. Eder K, Kalman B. Molecular Heterogeneity of Glioblastoma and its Clinical Relevance. *Oncol Res* (2014) 20(4):777–87. doi: 10.1007/s12253-014-9833-3
2. Tamimi AF, Juweid M. Epidemiology and Outcome of Glioblastoma. In: *Glioblastoma*. Codon Publications (2017). p. 143–53. Available at: https://exonpublications.com/index.php/exon/article/view/130.
3. Koshy M, Villano JL, Dolecek TA, Howard A, Mahmood U, Chmura SJ, et al. Improved Survival Time Trends for Glioblastoma Using the SEER 17 Population-Based Registries. *J Neurooncol* (2012) 107(1):207–12. doi: 10.1007/s11060-011-0738-7
4. Bilmin K, Kujawska T, Grieb P. Sonodynamic Therapy for Gliomas. Perspectives and Prospects of Selective Sonosensitization of Glioma Cells. *Cells* (2019) 8(11):1–11. doi: 10.3390/cells8111428

5. Bradshaw A, Wickremsekera A, Tan ST, Peng L, Davis PF, Itinteang T. Cancer Stem Cell Hierarchy in Glioblastoma Multiforme. *Front Surg* (2016) 3:21. doi: 10.3389/fsurg.2016.00021
6. Robin AM, Lee I, Kalkanis SN. Reoperation for Recurrent Glioblastoma Multiforme. *Neurosurg Clin N Am* (2017) 28(3):407–28. doi: 10.1016/j.nec.2017.02.007
7. Weller M, van den Bent M, Tonn JC, Stupp R, Preusser M, Cohen-Jonathan-Moyal E, et al. European Association for Neuro-Oncology (EANO) Guideline on the Diagnosis and Treatment of Adult Astrocytic and Oligodendroglial Gliomas. *Lancet Oncol* (2017) 18(6):e315–29. doi: 10.1016/S1470-2045(17)30194-8
8. Costley D, Mc Ewan C, Fowley C, McHale AP, Atchison J, Nomikou N, et al. Treating Cancer With Sonodynamic Therapy: A Review. *Int J Hyperth* (2015) 31(2):107–17. doi: 10.3109/02656736.2014.992484
9. McHale AP, Callan JF, Nomikou N, Fowley C, Callan B. Sonodynamic Therapy: Concept, Mechanism and Application to Cancer Treatment. *Adv Exp Med Biol* (2016) 880:429–50. doi: 10.1007/978-3-319-22536-4_22
10. Wang X, Jia Y, Wang P, Liu Q, Zheng H. Current Status and Future Perspectives of Sonodynamic Therapy in Glioma Treatment. *Ultrason Sonochem* (2017) 37:592–9. doi: 10.1016/j.ultsonch.2017.02.020
11. Rosenthal I, Sostaric JZ, Riesz P. Sonodynamic Therapy?? A Review of the Synergistic Effects of Drugs and Ultrasound. *Ultrason Sonochem* (2004) 11 (6):349–63. doi: 10.1016/j.ultsonch.2004.03.004
12. Guo S, Sun X, Cheng J, Xu H, Dan J, Shen J, et al. Apoptosis of THP-1 Macrophages Induced by Protoporphyrin IX-mediated Sonodynamic Therapy. *Int J Nanomedicine* (2013) 8:2239–46. doi: 10.2147/IJN.S43717
13. Teng L, Nakada M, Zhao SG, Endo Y, Furuyama N, Nambu E, et al. Silencing of Ferrochelatase Enhances 5-Aminolevulinic Acid-Based Fluorescence and Photodynamic Therapy Efficacy. *Br J Cancer* (2011) 104(5):798–807. doi: 10.1038/bjc.2011.12
14. Kinoshita M, Hynynen K. Mechanism of Porphyrin-Induced Sonodynamic Effect: Possible Role of Hyperthermia. *Radiat Res* (2006) 165(3):299–306. doi: 10.1667/rr3510.1
15. Kim JE, Cho HR, Xu WJ, Kim JY, Kim SK, Kim S-K, et al. Mechanism for Enhanced 5-Aminolevulinic Acid Fluorescence in Isocitrate Dehydrogenase 1 Mutant Malignant Gliomas. *Oncotarget* (2015) 6(24):20266–77. doi: 10.18632/oncotarget.4060
16. Acerbi F, Broggi M, Schebesch K-M, Höhne J, Cavallo C, De Laurentis C, et al. Fluorescein-Guided Surgery for Resection of High-Grade Gliomas: A Multicentric Prospective Phase II Study (Fluoglio). *Clin Cancer Res* (2018) 24(1):52–61. doi: 10.1158/1078-0432.CCR-17-1184
17. Folaron M, Strawbridge R, Samkoe KS, Filan C, Roberts DW, Davis SC. Elucidating the Kinetics of Sodium Fluorescein for Fluorescence-Guided Surgery of Glioma. *J Neurosurg* (2019) 131(3):724–34. doi: 10.3171/2018.4.JNS172644
18. Zou M, Zhang L, Wang J, Wang Q, Gao J, Fan P. Investigation on Interaction and Sonodynamic Damage of Fluorescein Derivants to Bovine Serum Albumin (BSA) Under Ultrasonic Irradiation. *Spectrochim Acta Part A Mol Biomol Spectrosc* (2013) 110:364–76. doi: 10.1016/j.saa.2013.03.073
19. Prada F, Sheybani N, Franzini A, Moore D, Cordeiro D, Sheehan J, et al. Fluorescein-Mediated Sonodynamic Therapy in a Rat Glioma Model. *J Neurooncol* (2020) 148(3):445–54. doi: 10.1007/s11060-020-03536-2
20. Yoshida M, Kobayashi H, Terasaka S, Endo S, Yamaguchi S, Motegi H, et al. Sonodynamic Therapy for Malignant Glioma Using 220-Khz Transcranial Magnetic Resonance Imaging-Guided Focused Ultrasound and 5-Aminolevulinic Acid. *Ultrasound Med Biol* (2019) 45(2):526–38. doi: 10.1016/j.ultrasmedbio.2018.10.016
21. Allen SP, Prada F, Xu Z, Gatesman J, Feng X, Sporkin H, et al. A Preclinical Study of Diffusion-Weighted MRI Contrast as an Early Indicator of Thermal Ablation. *Magn Reson Med* (2021) 85(4):2145–59. doi: 10.1002/mrm.28537
22. Takahashi K, Hasegawa T, Ishii T, Suzuki A, Nakajima M, Uno K, et al. Antitumor Effect of Combination of Hyperthermotherapy and 5-Aminolevulinic Acid (ALA). *Anticancer Res* (2013) 33(7):2861–6.
23. Feril LB, Kondo T, Cui Z-G, Tabuchi Y, Zhao Q-L, Ando H, et al. Apoptosis Induced by the Sonomechanical Effects of Low Intensity Pulsed Ultrasound in a Human Leukemia Cell Line. *Cancer Lett* (2005) 221(2):145–52. doi: 10.1016/j.canlet.2004.08.034
24. Hoogenboom M, Eikelenboom D, den Brok MH, Heerschap A, Fütterer JJ, Adema GJ. Mechanical High-Intensity Focused Ultrasound Destruction of Soft Tissue: Working Mechanisms and Physiologic Effects. *Ultrasound Med Biol* (2015) 41(6):1500–17. doi: 10.1016/j.ultrasmedbio.2015.02.006
25. Tsukahara K, Umemura S, Yoshizawa S. Experimental Investigation of Effect of Ultrasonic Duty Cycle on Generation of Reactive Oxygen Species for Highly Efficient Sonodynamic Treatment. *Jpn J Appl Phys* (2020) 59(SK): SKKE08. doi: 10.35848/1347-4065/ab82a5
26. Kamath AA, Friedman DD, Akbari SHA, Kim AH, Tao Y, Luo J, et al. Glioblastoma Treated With Magnetic Resonance Imaging-Guided Laser Interstitial Thermal Therapy: Safety, Efficacy, and Outcomes. *Neurosurgery* (2019) 84(4):836–43. doi: 10.1093/neuros/nyy375
27. Sheehan J. Stereotactic Radiosurgery for Glioblastoma—Time to Revisit This Approach. *World Neurosurg* (2012) 78(6):592–3. doi: 10.1016/j.wneu.2012.05.023
28. Minkin K, Naydenov E, Gabrovski K, Dimova P, Penkov M, Tanova R, et al. Intraoperative Fluorescein Staining for Benign Brain Tumors. *Clin Neurol Neurosurg* (2016) 149:22–6. doi: 10.1016/j.clineuro.2016.07.016
29. Acerbi F, Cavallo C, Schebesch K-M, Akçakaya MO, de Laurentis C, Hamamcioglu MK, et al. Fluorescein-Guided Resection of Intramedullary Spinal Cord Tumors: Results From a Preliminary, Multicentric, Retrospective Study. *World Neurosurg* (2017) 108:603–9. doi: 10.1016/j.wneu.2017.09.061
30. Chen K-T, Lin Y-J, Chai W-Y, Lin C-J, Chen P-Y, Huang C-Y, et al. Neuronavigation-Guided Focused Ultrasound (NaviFUS) for Transcranial Blood-Brain Barrier Opening in Recurrent Glioblastoma Patients: Clinical Trial Protocol. *Ann Transl Med* (2020) 8(11):673–3. doi: 10.21037/atm-20-344
31. Pouliopoulos AN, Wu S-Y, Burgess MT, Karakatsani ME, Kamimura HAS, Konofagou EE. A Clinical System for Non-Invasive Blood–Brain Barrier Opening Using a Neuronavigation-Guided Single-Element Focused Ultrasound Transducer. *Ultrasound Med Biol* (2020) 46(1):73–89. doi: 10.1016/j.ultrasmedbio.2019.09.010
32. Asquier N, Bouchoux G, Canney M, Martin C, Law-Ye B, Leclercq D, et al. Blood-Brain Barrier Disruption in Humans Using an Implantable Ultrasound Device: Quantification With MR Images and Correlation With Local Acoustic Pressure. *J Neurosurg* (2020) 132(3):875–83. doi: 10.3171/2018.9.JNS182001
33. D'Ammando A, Raspagliesi L, Gionso M, Franzini A, Porto E, Di Meco F, et al. Sonodynamic Therapy for the Treatment of Intracranial Gliomas. *J Clin Med [Internet]* (2021) 10(5):1101. doi: 10.3390/jcm10051101
34. Yamaguchi F, Asakura T, Takahashi H, Kitamura T, Teramoto A. Low Frequency Ultrasonication Induced Antitumor Effect in 5-Aminolevulinic Acid Treated Malignant Glioma. *J Cancer Ther* (2013) 04(01):170–5. doi: 10.4236/jct.2013.41025
35. Bilmin K, Kujawska T, Secomski W, Nowicki A, Grieb P. 5-Aminolevulinic Acid-Mediated Sonosensitization of Rat RG2 Glioma Cells In Vitro. *Folia Neuropathol* (2016) 3:234–40. doi: 10.5114/fn.2016.62233
36. Johansson A, Palte G, Schnell O, Tonn J-C, Herms J, Stepp H. 5-Aminolevulinic Acid-Induced Protoporphyrin IX Levels in Tissue of Human Malignant Brain Tumors. *Photochem Photobiol* (2010) 86(6):1373–8. doi: 10.1111/j.1751-1097.2010.00799.x
37. Suehiro S, Ohnishi T, Yamashita D, Kohno S, Inoue A, Nishikawa M, et al. Enhancement of Antitumor Activity by Using 5-ALA–mediated Sonodynamic Therapy to Induce Apoptosis in Malignant Gliomas: Significance of High-Intensity Focused Ultrasound on 5-ALA-SDT in a Mouse Glioma Model. *J Neurosurg* (2018) 129(6):1416–28. doi: 10.3171/2017.6.JNS162398
38. Ju D, Yamaguchi F, Zhan G, Higuchi T, Asakura T, Morita A, et al. Hyperthermotherapy Enhances Antitumor Effect of 5-Aminolevulinic Acid-Mediated Sonodynamic Therapy With Activation of Caspase-Dependent Apoptotic Pathway in Human Glioma. *Tumor Biol* (2016) 37(8):10415–26. doi: 10.1007/s13277-016-4931-3
39. Endo S, Kudo N, Yamaguchi S, Sumiyoshi K, Motegi H, Kobayashi H, et al. Porphyrin Derivatives-Mediated Sonodynamic Therapy for Malignant Gliomas In Vitro. *Ultrasound Med Biol* (2015) 41(9):2458–65. doi: 10.1016/j.ultrasmedbio.2015.05.007
40. Ohmura T, Fukushima T, Hirotomo S, Yoshizawa S, Inoue T, Kuroki M, et al. Sonodynamic Therapy With 5-Aminolevulinic Acid and Focused Ultrasound for Deep-Seated Intracranial Glioma in Rat. *Anticancer Res* (2011) 31 (7):2527–33.
41. Wu S-K, Santos MA, Marcus SL, Hynynen K. MR-Guided Focused Ultrasound Facilitates Sonodynamic Therapy With 5-Aminolevulinic Acid in a Rat Glioma Model. *Sci Rep* (2019) 9(1):10465. doi: 10.1038/s41598-019-46832-2

42. Jeong E-J, Seo S-J, Ahn Y-J, Choi K-H, Kim K-H, Kim J-K. Sonodynamically Induced Antitumor Effects of 5-Aminolevulinic Acid and Fractionated Ultrasound Irradiation in an Orthotopic Rat Glioma Model. *Ultrasound Med Biol* (2012) 38(12):2143–50. doi: 10.1016/j.ultrasmedbio.2012.07.026

Conflict of Interest: The authors declare that the research was conducted in the absence of any commercial or financial relationships that could be construed as a potential conflict of interest.

frontiers in Neurology

ORIGINAL RESEARCH
published: 16 July 2021
doi: 10.3389/fneur.2021.668656

High-Dose Fluorescein Reveals Unusual Confocal Endomicroscope Imaging of Low-Grade Glioma

Evgenii Belykh[1], *Naomi R. Onaka*[1], *Xiaochun Zhao*[1], *Irakliy Abramov*[1], *Jennifer M. Eschbacher*[2], *Peter Nakaji*[2†] *and Mark C. Preul*[1*]

[1] Department of Neurosurgery, The Loyal and Edith Davis Neurosurgical Research Laboratory, St. Joseph's Hospital and Medical Center, Barrow Neurological Institute, Phoenix, AZ, United States, [2] Department of Neuropathology, Barrow Neurological Institute, St. Joseph's Hospital and Medical Center, Phoenix, AZ, United States

Background: Fluorescence-guided brain tumor surgery using fluorescein sodium (FNa) for contrast is effective in high-grade gliomas. However, the effectiveness of this technique for visualizing noncontrast-enhancing and low-grade gliomas is unknown. This report is the first documented case of the concurrent use of wide-field fluorescence-guided surgery and confocal laser endomicroscopy (CLE) with high-dose FNa (40 mg/kg) for intraoperative visualization of tumor tissue cellularity in a nonenhancing glioma.

Case Description: A patient underwent fluorescence-guided surgery for a left frontal lobe mass without contrast enhancement on magnetic resonance imaging. The patient received 40 mg/kg FNa intravenously at the induction of anesthesia. Surgery was performed under visualization with a Yellow 560 filter and white-light wide-field imaging. Intraoperative CLE produced high-quality images of the lesion 1.5 h after FNa injection. Frozen-section analysis demonstrated findings comparable to those of intraoperative CLE visualization and consistent with World Health Organization (WHO) glioma grades II–III. The patient recovered without complications. Analysis of the permanent histologic sections identified the tumor as an anaplastic oligodendroglioma, IDH-mutant, 1p/19q co-deleted, consistent with WHO grade III because of discrete foci of hypercellularity and increased mitotic figures, but large regions of the lesion were low grade.

Conclusions: The use of high-dose FNa in this patient with a nonenhancing borderline low-grade/high-grade glioma produced actionable wide-field fluorescence imaging using the operating microscope and improved CLE visualization of tumor cellularity. Higher doses of FNa for intraoperative CLE imaging and possible simultaneous wide-field fluorescence surgical guidance in nonenhancing gliomas merit further investigation.

Keywords: confocal laser endomicroscopy, fluorescein sodium, fluorescence-guided surgery, low-grade glioma, nonenhancing glioma, oligodendroglioma

OPEN ACCESS

Edited by:
Talat Kiris, Koç University, Turkey

Reviewed by:
Dan Qi, Baylor Scott and White Health, United States
Francesco Acerbi, Fondazione IRCCS Istituto Neurologio Carlo Besta, Italy

****Correspondence:***
Mark C. Preul
Neuropub@barrowneuro.org

†Present address:
Peter Nakaji, Department of Neurosurgery, University of Arizona College of Medicine, Phoenix, AZ, United States

Specialty section:
This article was submitted to Neuro-Oncology and Neurosurgical Oncology, a section of the journal Frontiers in Neurology

Received: *16 February 2021*
Accepted: *17 June 2021*
Published: *16 July 2021*

Citation:
Belykh E, Onaka NR, Zhao X, Abramov I, Eschbacher JM, Nakaji P and Preul MC (2021) High-Dose Fluorescein Reveals Unusual Confocal Endomicroscope Imaging of Low-Grade Glioma. Front. Neurol. 12:668656. doi: 10.3389/fneur.2021.668656

INTRODUCTION

Fluorescein sodium (FNa) is a fluorescent biomarker available as a water-soluble dye that has been widely used in ophthalmology since the early 1960s. Moore et al. (1) reported anecdotal clinical use of fluorescein to help localize intracranial neoplasms as early as 1948. Although FNa has demonstrated utility in increasing the extent of resection in high-grade gliomas (HGG), its

efficacy has not been well-elucidated in low-grade gliomas (LGG), and there is currently a paucity of investigation on what FNa-guided resection may reveal when used for LGG (2–5). In a systematic review of fluorescence-guided glioma surgery, Senders et al. (6) identified 11 studies describing the use of FNa in glioma resection. All 11 studies included patients with HGG, whereas only three studies included patients with LGG.

FNa is commonly used for retinal angiographic procedures, and it has been shown to have few side effects with oral ingestion; the most common adverse effects are nausea and vomiting (7, 8). Additional adverse effects of intravenous FNa include postoperative yellow discoloration of urine at lower doses, such as 3–4 mg/kg, and skin or sclera discoloration at higher doses; nonetheless, overall, it is confirmed to be safe for patients (9). Only two cases of anaphylactic reactions have been reported after neurosurgical administration of FNa, both with an FNa dose of 20 mg/kg (10, 11).

FNa is useful in identifying intracranial malignancies because it extravasates from cerebral vessels in places where the blood-brain barrier has been damaged. This mechanism allows the dye to concentrate, localizing the area where tumor invasion has disrupted vascular integrity. The pattern of FNa extravasation is relatively unique in HGG compared to that in simple surgical trauma to brain tissue, and the pattern indicates a disruption in the blood-brain barrier (12). FNa is excited by light in 460–500 nm wavelengths, and it emits radiation in the 540–690 nm range. Light filters, such as the Yellow 560 filter (Carl Zeiss Meditec AG, Oberkochen, Germany), on surgical microscopes help to visualize the fluorescing tissue. However, visualization and surgical maneuvering during resection often require switching between the filter and wide-field white-light illumination. The range of FNa doses used for neurosurgical application has varied and has been subjectively divided into a "low-dose" (1–10 mg/kg) range that requires a fluorescence detection module on a neurosurgical operating microscope for identification and a "high-dose" (15–20 mg/kg or greater) range in which the naked eye can detect the fluorescent staining even without a fluorescence detection module (13).

In conjunction with dedicated fluorescein filters on surgical microscopes, the increasing use of intraoperative histopathologic examination with confocal laser endomicroscopy (CLE) using FNa has produced a tool for optically interrogating gliomas with a sensitivity and specificity comparable to the examination of a frozen section (14–18). Our institutional experience with CLE and low-dose FNa has been similar to that of others, albeit inconsistent for nonenhancing lesions and LGG. However, in this case report, we describe a situation in which high-dose FNa was administered during resection of an oligodendroglioma with the use of CLE, which produced unusually clear images of the LGG. This report contributes to the limited evidence for the possible use of FNa to visualize LGG, particularly with the aid of CLE. The CLE images indicate that a relatively high dose of FNa (e.g., 20–40 mg/kg) may produce a significant benefit in identifying tumors heretofore not labeled well with lower doses of FNa during fluorescence-guided surgery.

Abbreviations: CLE, confocal laser endomicroscopy; FET-PET, ^{18}F-fluoroethyl-L-tyrosine–positron emission tomography; FLAIR, fluid-attenuated inversion recovery; FNa, fluorescein sodium; HGG, high-grade gliomas; IDH, isocitrate dehydrogenase; LGG, low-grade gliomas; MRI, magnetic resonance imaging; WHO, World Health Organization; 5-ALA, 5-aminolevulinic acid.

CASE DESCRIPTION

A patient with a 4-year history of headaches was admitted for new-onset generalized seizure. Magnetic resonance imaging (MRI) showed a nonenhancing 1.6 × 1.3-cm heterogeneous posterior left frontal lobe mass just anterior to the precentral gyrus, with a surrounding abnormal high signal on T2-weighted and fluid-attenuated inversion recovery (FLAIR) imaging, interpreted as probably representing edema (**Figure 1**). The most likely differential diagnoses considered were metastatic disease and primary brain lesion. The patient gave voluntary informed consent to participate in the CLE imaging study, which was approved by the St. Joseph's Hospital and Medical Center Institutional Review Board (No. 10BN130). In the operating room, FNa was administered to the patient shortly after the induction of anesthesia. However, instead of the typical dose of 2–5 mg/kg, a higher dose of 40 mg/kg was administered. This higher dose was within the acceptable dosing range for FNa. When the tumor area was mapped for motor function, both the posterior and anterior regions immediately adjacent to the tumor showed some motor function. Yellow discoloration of the tissue was observed because of the higher FNa dose (**Figures 2A,B**). The dye concentrated in the area of the tumor, which allowed visualization of its borders, and the tumor was resected completely.

Four biopsies from within the tumor region (the last obtained about 1.5 h after FNa administration) were subjected to immediate intraoperative *ex vivo* CLE imaging (Convivo, Carl Zeiss Meditec AG). CLE imaging demonstrated hypercellular brain architecture, with abnormal cells suggestive of a cellular tumor in all biopsy specimens (**Figures 2C–G**). Histologic findings on frozen sections were consistent with glioma grades II–III, with the wide area majority characteristic of grade II glioma (**Figure 3**). Further histologic assessment of the permanent sections revealed variable cellular and infiltrative glioma with rounded oligodendroglial morphology and prominent perinuclear halos. The tumor was assigned the overall classification of anaplastic oligodendroglioma, isocitrate dehydrogenase (IDH)-mutant, 1p/19q codeleted, with ATRX expression because of the regions of more aggressive heterogeneity (discrete foci of hypercellularity and increased mitotic figures) but also extensive areas of lower-grade tumor.

CLE concurrent with high-dose FNa provided extremely clear images of cellular architecture, mitotic figures, endothelium of vessels, and swollen axons (**Figure 4**). The brightness and clarity of the CLE images revealed a distinct morphologic appearance not typically observed with lower-dose FNa, especially 1.5 h or longer after administration (but often in even less time). The patient tolerated this dose well, and the patient's postoperative yellowish skin discoloration resolved rapidly.

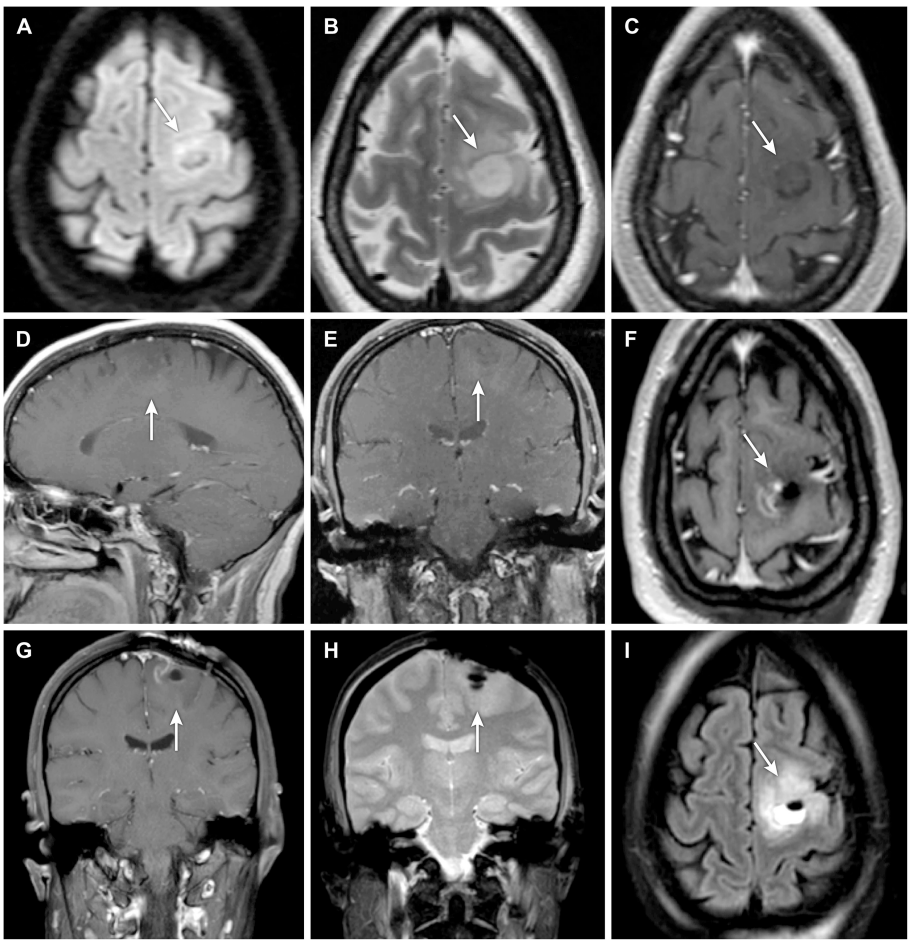

FIGURE 1 | (A–E) Preoperative and **(F–I)** postoperative magnetic resonance imaging (MRI) of a patient with a nonenhancing lesion (**A–I**, *arrows*) in the left precentral gyrus. Preoperative MRIs shown are **(A)** axial diffusion-weighted, **(B)** axial T2-weighted, **(C)** axial T1-weighted, **(D)** sagittal T1-weighted with contrast, and **(E)** coronal T1-weighted with contrast. Postoperative MRIs shown are **(F)** axial T1-weighted with contrast, **(G)** coronal T1-weighted with contrast, **(H)** coronal diffusion-weighted, and **(I)** axial diffusion-weighted. Used with permission from Barrow Neurological Institute, Phoenix, Arizona.

DISCUSSION

Gliomas are classified according to WHO grades I–IV, with LGG encompassing grades I and II. Still, they are representative of a heterogeneous group of tumors with wide variability in terms of prognosis and treatment. In the case description, we present the immunohistochemistry and pathologic characteristics identifying the tumor as an anaplastic oligodendroglioma, IDH-mutant, 1p/19q codeleted, with ATRX expression isolated within a vast majority of areas that were lower-grade glioma. Although the tumor was classified as a grade III glioma because of regions of increased aggressive characteristics, the prognostic significance of grade II vs. III in this tumor class compared with that of a nonanaplastic oligodendroglioma with an otherwise similar profile is not clearly understood, with the diagnostic criteria for histopathologic grading introducing subjectivity in interobserver variability in grading these lesions (19).

The tumor in this patient was categorized as grade II rather than grade III in the initial frozen-section analysis. It was noncontrast enhancing, which is a characteristic most often observed with LGG. The vast majority of this tumor was of a low-grade II glioma. The tumor was assigned the grade III classification because some localized regions were interpreted to be more aggressive. Low-grade tumors are often show localized areas or have heterogeneous regions in transition to more aggressive states.

Despite the grade III classification, our findings support the utility of high-dose FNa in the resection of LGG because the imaging correlated to the histology within the regions of lower-grade tumor.

The higher dose of 40 mg/kg FNa administered to the patient revealed fine intraoperative imaging characterization using CLE for areas of hypercellularity and tissue. The higher than usual dose of FNa produced unusually excellent contrast for the CLE visualization of the tumor. In conjunction with earlier studies commenting on the potential use of FNa in the resection of LGG, our report highlights several areas of interest, including the optimal dose of FNa and which

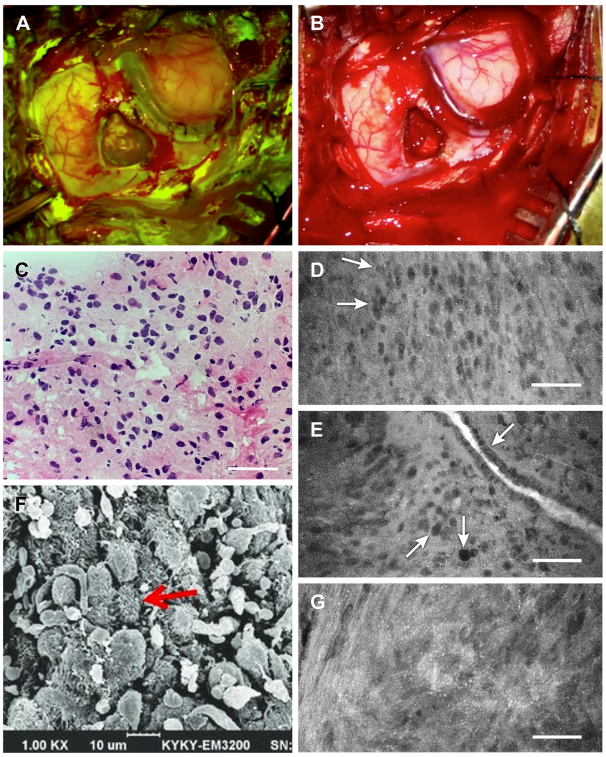

FIGURE 2 | Intraoperative tumor visualization. Exposure during tumor resection with **(A)** Yellow 560 filter and **(B)** standard white light. **(C)** Photograph of intraoperative frozen-tissue section slide interpreted as grade II glioma. **(D)** Confocal laser endomicroscopy (CLE) image showing subtle discrete cellular aggregates (*arrows*) within a relatively widespread area of cells interpreted as consistent with lower-grade glioma 1.5 h after injection of 40 mg/kg fluorescein sodium (FNa). **(E)** A vessel 1.5 h after injection of 40 mg/kg FNa showing irregular endothelium (*top arrow*), with a focus of cells indicating pleomorphism relative to surrounding cells (*center arrow*) and what appears to be a mitotic figure (*bottom arrow*). **(F)** Scanning electron microscopy (SEM) image showing glioma cell morphology with multiple small vesicles and protrusions. **(G)** CLE image of another tumor area demonstrates small bright dots that likely represent cell surface vesicles with fluorescein, which corresponds well to the SEM microscopy of the cells. These bright dots were visible throughout the tumor on CLE images. Scale 50 μm **(D,E,G)**. Panels **(A–E,G)** are used with permission from Barrow Neurological Institute, Phoenix, Arizona. Panel **(F)** is adapted from Lv D, Hu Z, Lu L, Lu H, Xu X. Three-dimensional cell culture: A powerful tool in tumor research and drug discovery. Oncol Lett. 2017; 14(6):6999-7010. Copyright of Institute of Pathology and Southwest Cancer Center and made available under Creative Commons Attribution 3.0 License (https://creativecommons.org/licenses/by/3.0).

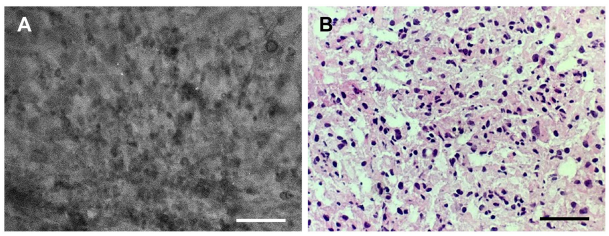

FIGURE 3 | Good correlation of the **(A)** confocal laser endomicroscopy image collocated with the **(B)** hematoxylin-eosin–stained frozen section interpreted as grade II glioma. Scale bars, 50 μm. Used with permission from Barrow Neurological Institute, Phoenix, Arizona.

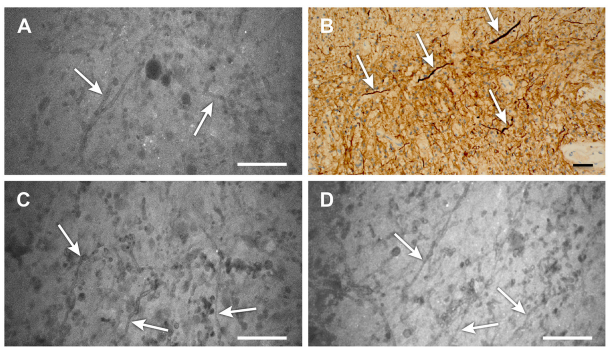

FIGURE 4 | (A–D) Confocal laser endomicroscopy (CLE) images showing areas of low-grade glioma **(A,C,D)** that reveal distinct strand-like structures or fibers throughout the tumor (scale 50 μm). **(B)** Image from the same area stained for neurofilaments (*arrows*) also shows these structures, which are likely swollen axons resulting from tumor edema (scale bar, 20 μm). We have not previously observed these detailed structures on CLE images with low-dose fluorescein sodium (FNa) staining. Their notable appearance here is likely related to the high dose of FNa used in this case. Used with permission from Barrow Neurological Institute, Phoenix, Arizona.

grades and characteristics of LGG may be most amenable for FNa-guided resection.

CLE With Low-Dose FNa for Low-Grade Glioma

Our previous experience with CLE for LGG demonstrated that FNa contrast was usually inadequate for clear visualization of histologic characteristics, especially 1 h or longer after administration of FNa (15). In each patient, 5 mg/kg FNa was injected, and intraoperative CLE was performed within a few minutes after its administration. In 66 patients, 8 grade II gliomas were identified, 10 grade III, and 3 grade IV. The exact histopathologic diagnosis of the tumors was not possible for every biopsy or every patient because of the lack of image contrast and clarity to view mitoses adequately enough to count them reliably.

Chen et al. (5) found that, in four gross total resections of LGG, three gliomas were clearly stained after injection of high-dose FNa (15–20 mg/kg). In preoperative MRIs, these three tumors also showed enhancement, which is generally found in higher tumor grades. However, in one patient whose LGG was nonenhancing on preoperative MRI, the staining was not clear. Notably, FNa still provided utility in this case because the surgeons could resect around nebulously stained areas, prompting Chen et al. (5) to conclude that FNa may be useful in treating LGG, although this aspect was not specifically evaluated in their investigation.

Schebesch et al. (4) reported five patients with nonenhancing preoperative MRIs but gliomas positive for FET-PET (^{18}F-fluoroethyl-L-tyrosine–positron emission tomography), which they referred to as nonenhancing gliomas. All five patients received 5 mg/kg FNa, and the Yellow 560 filter was used as needed. These investigators found that, despite the lack of

contrast enhancement on MRI in all patients, all five tumors demonstrated some degree of fluorescence, which correlated with PET metabolic activity. One grade II tumor was visible only under the fluorescence-detecting filter. Final grading identified two LGG and three HGG as grade III. Nonetheless, Schebesch et al. (4) concluded that the incorporation of FNa was helpful both in detecting lesions and in ascertaining their borders, regardless of grade.

Notably, in the report by Schebesch et al. (4), abnormalities were found in the FLAIR and T2 sequences of preoperative MRIs in all five patients in their series. These abnormalities may be sensitive markers of a damaged blood-brain barrier, and they may be present before the tumor becomes contrast-enhancing with progression. In the patient detailed in our case report, preoperative imaging showed similar findings in that the tumor was noncontrast enhancing, but there was a highly abnormal T2/FLAIR signal surrounding the mass. Ultimately, two of the five patients in the Schebesch et al. (4) report were found to have grade III anaplastic oligodendrogliomas, which was the same diagnosis as in our patient. Further studies using FNa may permit elaboration of the characteristics of each tumor subtype under visualization with FNa, and our findings in combination with those previously reported by other authors compel further exploration in future studies.

CLE With High-Dose FNa for Low-Grade Glioma

Extrapolating from the existing literature and from our observations as detailed in this report, we believe that the application of FNa is influenced by its dosing, both in terms of visualization with or without the Yellow 560 filter and with its beneficial administration in patients with lower grades of glioma. In a study of FNa-guided resection of glioblastoma, Shinoda et al. (20) found that high doses of FNa (20 mg/kg) produced usable fluorescence that was viewable under white-light illumination, without the need for an operating microscope Yellow 560 filter. Their report supports the evaluation that higher doses of FNa can better identify the tumor area and borders. However, their results were obtained from imaging of high-grade lesions with an ostensibly larger degree of blood-brain barrier disruption. Thus, the results may not be translatable to gliomas demonstrating nonenhancement on MRIs. Unlike 5-aminolevulinic acid (5-ALA), which does not usually demonstrate cellular uptake in low-grade tumors, high-dose FNa may provide fluorescent visualization and discrimination of the cellular architecture and tumor margin zone.

The question of whether to use FNa when dealing with either low-grade or high-grade tumors is thus germane for wide-field operative microscopy and CLE imaging. Currently, the intraoperative redosing of FNa is used as an off-label FNa application in the United States. In most cases, FNa is administered at the beginning of the surgery (21), as we have performed it early on. However, exposure of the tumor and the beginning of resection, as well as later inspection of surgical margins, may require many minutes to hours before the use of imaging such as CLE. In our experience, we have begun to delay FNa administration until after anesthesia induction but immediately before surgical work begins on the tumor, which allows for brighter and clearer images on CLE imaging. However, the timing of FNa administration is a judgment call because later administration of FNa after accessing the tumor or beginning its surgical resection may highlight surgically damaged tissue as viewed with wide-field imaging, making it almost useless for delineating tumor margin. In most instances, the FNa signal on wide-field imaging is confined to the tumor before it progressively saturates surrounding tissue. This characteristic of FNa can be confusing or disconcerting on wide-field imaging because of the fluorescence of nonrelevant tissues, areas of bleeding, or areas with disruption of tissue during the normal process of surgery.

In many cases where 2–5 mg/kg FNa was administered early in the procedure, we acquired CLE imaging that was suboptimal, uninterpretable, or too dark. Thus, we have redosed the FNa to acquire improved CLE images (16). In the current case report, the single 40 mg/kg FNa dose produced a signal that remained bright and produced excellent CLE images even 1.5 h after administration. This case is fortuitous in that it may show implications for very-high-dose FNa administration, where in the past, FNa fluorescence has not been particularly delineative of LGG when used with wide-field operative microscopy.

The two cases where anaphylactic reactions occurred minutes after FNa injection showed decreased blood pressure, bradycardia or tachycardia, and flushing over the infusion anatomical area (10, 11). These patients responded to adrenaline, atropine, prednisolone, and dopamine administration. Surgeries were halted, and the patients were moved to the intensive care unit. In both cases, elevated laboratory values of tryptase were found, while in one case, the IgE value was also increased. In both instances, the patients fully recovered, and one report cited the occurrence of such a reaction for the first time in 121 patients injected with FNa for neurosurgery (10).

When the goal is to produce actionable fluorescence image surgical guidance with a wide-field fluorescence detection system, especially when using CLE, a higher dose of FNa may be of more benefit if only one dose is administered at the beginning of an operation. This approach may be particularly useful when using sensitive imaging such as CLE for discriminating the histoarchitecture of tumor margins, especially for LGG tissue that may not be as amenable to 5-ALA fluorescence guidance. Simultaneous use of fluorophores such as 5-ALA and FNa may be an option for low-grade tumors or nonenhancing tumors. Although 5-ALA has not been shown to delineate low-grade tumors well, isolated regions of low-grade gliomas often transition to a more metabolically aggressive type. The use of 5-ALA may discriminate those isolated regions, whereas high-dose FNa could help define the general tumor area of low-grade tissue and margins. Of course, the logistics of administering the different fluorophores for optimal uptake by tumor cells should be considered. FNa dose-escalation studies in LGG may be useful to define the minimal dosage that allows better interpretation of CLE images to delineate the histologic tumor features and, importantly, the tumor margins or invaded regions. CLE is currently in its infancy regarding *in vivo* surgical application.

Cases such as ours may indicate a need for expanded or explorative fluorescence techniques.

CONCLUSIONS

This case report demonstrates the excellent quality available with dual-fluorescence visualization (wide-field operative microscope Yellow 560 fluorescence navigation and CLE imaging) with a high dose of FNa in a patient with a nonenhancing glioma up to 1.5 h after FNa administration. This report supports the investigation of higher doses of FNa in nonenhancing gliomas and gliomas suspected to be a lower grade that usually do not exhibit 5-ALA-mediated fluorescence. Given the highly informative images, the minimal adverse effects of FNa, and the good postoperative outcome of this case, higher doses of FNa (20–40 mg/kg) should be considered or trialed with intraoperative CLE.

DATA AVAILABILITY STATEMENT

The raw data supporting the conclusions of this article will be made available by the authors, without undue reservation.

ETHICS STATEMENT

The studies involving human participants were reviewed and approved by St. Joseph's Hospital and Medical Center Institutional Review Board for Human Research. The patients and participants provided written informed consent to participate in this study.

AUTHOR CONTRIBUTIONS

EB, PN, and MP: study planning and coordination. EB and IA: acquisition of confocal images. EB, NO, XZ, and IA: processing and organizing of the data and confocal images. EB, XZ, IA, JE, PN, and MP: assessment of confocal images. EB, NO, and MP: writing the draft. MP: final approval. All authors: review of the draft.

FUNDING

This research was supported by funds from the Barrow Neurological Foundation, the Women's Board of the Barrow Neurological Institute, and the Newsome Family Endowment in Neurosurgery to MP.

ACKNOWLEDGMENTS

We thank the staff of the Neuroscience Publications office at Barrow Neurological Institute for assistance with manuscript preparation.

REFERENCES

1. Moore GE, Peyton WT, French LA, Walker WW. The clinical use of fluorescein in neurosurgery; the localization of brain tumors. *J Neurosurg.* (1948) 5:392–8. doi: 10.3171/jns.1948.5.4.0392
2. Acerbi F, Cavallo C, Broggi M, Cordella R, Anghileri E, Eoli M, et al. Fluorescein-guided surgery for malignant gliomas: a review. *Neurosurg Rev.* (2014) 37:547–57. doi: 10.1007/s10143-014-0546-6
3. Hong J, Chen B, Yao X, Yang Y. Outcome comparisons of high-grade glioma resection with or without fluorescein sodium-guidance. *Curr Probl Cancer.* (2019) 43:236–44. doi: 10.1016/j.currproblcancer.2018.07.007
4. Schebesch KM, Brawanski A, Doenitz C, Rosengarth K, Proescholdt M, Riemenschneider MJ, et al. Fluorescence-guidance in non-gadolinium enhancing, but FET-PET positive gliomas. *Clin Neurol Neurosurg.* (2018) 172:177–82. doi: 10.1016/j.clineuro.2018.07.011
5. Chen B, Wang H, Ge P, Zhao J, Li W, Gu H, et al. Gross total resection of glioma with the intraoperative fluorescence-guidance of fluorescein sodium. *Int J Med Sci.* (2012) 9:708–14. doi: 10.7150/ijms.4843
6. Senders JT, Muskens IS, Schnoor R, Karhade AV, Cote DJ, Smith TR, et al. Agents for fluorescence-guided glioma surgery: a systematic review of preclinical and clinical results. *Acta Neurochir (Wien).* (2017) 159:151–67. doi: 10.1007/s00701-016-3028-5
7. Hara T, Inami M, Hara T. Efficacy and safety of fluorescein angiography with orally administered sodium fluorescein. *Am J Ophthalmol.* (1998) 126:560–4. doi: 10.1016/S0002-9394(98)00112-3
8. Kwan AS, Barry C, McAllister IL, Constable I. Fluorescein angiography and adverse drug reactions revisited: the Lions Eye experience. *Clin Exp Ophthalmol.* (2006) 34:33–8. doi: 10.1111/j.1442-9071.2006.01136.x
9. Schebesch KM, Proescholdt M, Hohne J, Hohenberger C, Hansen E, Riemenschneider MJ, et al. Sodium fluorescein-guided resection under the YELLOW 560 nm surgical microscope filter in malignant brain tumor surgery–a feasibility study. *Acta Neurochir (Wien).* (2013) 155:693–9. doi: 10.1007/s00701-013-1643-y
10. Dilek O, Ihsan A, Tulay H. Anaphylactic reaction after fluorescein sodium administration during intracranial surgery. *J Clin Neurosci.* (2011) 18:430–1. doi: 10.1016/j.jocn.2010.06.012
11. Tanahashi S, Lida H, Dohi S. An anaphylactoid reaction after administration of fluorescein sodium during neurosurgery. *Anesth Analg.* (2006) 103:503. doi: 10.1213/01.ANE.0000227205.37935.10
12. Belykh E, Shaffer KV, Lin C, Byvaltsev VA, Preul MC, Chen L. Blood-brain barrier, blood-brain tumor barrier, and fluorescence-guided neurosurgical oncology: delivering optical labels to brain tumors. *Front Oncol.* (2020) 10:739. doi: 10.3389/fonc.2020.00739
13. Schebesch KM, Brawanski A, Hohenberger C, Hohne J. Fluorescein sodium-guided surgery of malignant brain tumors: history, current concepts, and future project. *Turk Neurosurg.* (2016) 26:185–94. doi: 10.5137/1019-5149.JTN.16952-16.0
14. Belykh E, Miller EJ, Patel AA, Yazdanabadi MI, Martirosyan NL, Yagmurlu K, et al. Diagnostic accuracy of a confocal laser endomicroscope for in vivo differentiation between normal injured and tumor tissue during fluorescein-guided glioma resection: laboratory investigation. *World Neurosurg.* (2018) 115:e337–e48. doi: 10.1016/j.wneu.2018.04.048
15. Martirosyan NL, Eschbacher JM, Kalani MY, Turner JD, Belykh E, Spetzler RF, et al. Prospective evaluation of the utility of intraoperative confocal laser endomicroscopy in patients with brain neoplasms using fluorescein sodium: experience with 74 cases. *Neurosurg Focus.* (2016) 40:E11. doi: 10.3171/2016.1.FOCUS15559
16. Belykh E, Zhao X, Ngo B, Farhadi DS, Byvaltsev VA, Eschbacher JM, et al. Intraoperative confocal laser endomicroscopy *ex vivo* examination of tissue microstructure during fluorescence-guided brain tumor surgery. *Front Oncol.* (2020) 10:599250. doi: 10.3389/fonc.2020.599250

17. Acerbi F, Pollo B, De Laurentis C, Restelli F, Falco J, Vetrano IG, et al. *Ex vivo* fluorescein-assisted confocal laser endomicroscopy (CONVIVO(R) System) in patients with glioblastoma: results from a prospective study. *Front Oncol.* (2020) 10:606574. doi: 10.3389/fonc.2020.606574
18. Hohne J, Schebesch KM, Zoubaa S, Proescholdt M, Riemenschneider MJ, Schmidt NO. Intraoperative imaging of brain tumors with fluorescein: confocal laser endomicroscopy in neurosurgery. Clinical and user experience. *Neurosurg Focus.* (2021) 50:E19. doi: 10.3171/2020.11.FOCUS20783
19. Olar A, Wani KM, Alfaro-Munoz KD, Heathcock LE, van Thuijl HF, Gilbert MR, et al. IDH mutation status and role of WHO grade and mitotic index in overall survival in grade II-III diffuse gliomas. *Acta Neuropathol.* (2015) 129:585–96. doi: 10.1007/s00401-015-1398-z
20. Shinoda J, Yano H, Yoshimura S, Okumura A, Kaku Y, Iwama T, et al. Fluorescence-guided resection of glioblastoma multiforme by using high-dose fluorescein sodium. Technical note. *J Neurosurg.* (2003) 99:597–603. doi: 10.3171/jns.2003.99.3.0597
21. Acerbi F, Broggi M, Broggi G, Ferroli P. What is the best timing for fluorescein injection during surgical removal of high-grade gliomas? *Acta Neurochir (Wien).* (2015) 157:1377–8. doi: 10.1007/s00701-015-2455-z

Conflict of Interest: The authors declare that the research was conducted in the absence of any commercial or financial relationships that could be construed as a potential conflict of interest.

frontiers in Oncology

REVIEW
published: 30 July 2021
doi: 10.3389/fonc.2021.699301

5-ALA in Suspected Low-Grade Gliomas: Current Role, Limitations, and New Approaches

*Barbara Kiesel[1], Julia Freund[1], David Reichert[2,3], Lisa Wadiura[1], Mikael T. Erkkilae[2], Adelheid Woehrer[4], Shawn Hervey-Jumper[5], Mitchel S. Berger[5] and Georg Widhalm[1]**

[1] Department of Neurosurgery, Medical University of Vienna, Vienna, Austria, [2] Center for Medical Physics and Biomedical Engineering, Medical University of Vienna, Vienna, Austria, [3] Christian Doppler Laboratory OPTRAMED, Medical University of Vienna, Vienna, Austria, [4] Department of Neurology, Institute for Neuropathology and Neurochemistry, Medical University of Vienna, Vienna, Austria, [5] Department of Neurological Surgery, University of California San Francisco (UCSF), San Francisco, CA, United States

OPEN ACCESS

Edited by:
Morgan Broggi, Istituto Neurologico Carlo Besta (IRCCS), Italy

Reviewed by:
Alessandro Della Puppa, University of Florence, Italy
Marco Riva, University of Milan, Italy

***Correspondence:**
Georg Widhalm
georg.widhalm@meduniwien.ac.at

Specialty section:
This article was submitted to Neuro-Oncology and Neurosurgical Oncology, a section of the journal Frontiers in Oncology

Received: *23 April 2021*
Accepted: *19 July 2021*
Published: *30 July 2021*

Citation:
Kiesel B, Freund J, Reichert D, Wadiura L, Erkkilae MT, Woehrer A, Hervey-Jumper S, Berger MS and Widhalm G (2021) 5-ALA in Suspected Low-Grade Gliomas: Current Role, Limitations, and New Approaches. Front. Oncol. 11:699301. doi: 10.3389/fonc.2021.699301

Radiologically suspected low-grade gliomas (LGG) represent a special challenge for the neurosurgeon during surgery due to their histopathological heterogeneity and indefinite tumor margin. Therefore, new techniques are required to overcome these current surgical drawbacks. Intraoperative visualization of brain tumors with assistance of 5-aminolevulinic acid (5-ALA) induced protoporphyrin IX (PpIX) fluorescence is one of the major advancements in the neurosurgical field in the last decades. Initially, this technique was exclusively applied for fluorescence-guided surgery of high-grade glioma (HGG). In the last years, the use of 5-ALA was also extended to other indications such as radiologically suspected LGG. Here, we discuss the current role of 5-ALA for intraoperative visualization of focal malignant transformation within suspected LGG. Furthermore, we discuss the current limitations of the 5-ALA technology in pure LGG which usually cannot be visualized by visible fluorescence. Finally, we introduce new approaches based on fluorescence technology for improved detection of pure LGG tissue such as spectroscopic PpIX quantification fluorescence lifetime imaging of PpIX and confocal microscopy to optimize surgery.

Keywords: 5-ALA, suspected LGG, anaplastic foci, spectroscopic PpIX analysis, fluorescence lifetime imaging, confocal microscopy

Abbreviations: 5-ALA, 5-aminolevulinic acid; AED, Antiepileptic drugs; ATRX, Alpha thalassemia/intellectual disability X-linked; DNET, Dysembryoplastic neuroepithelial tumor; CLE, Confocal laser endomicroscopy; CMOS, Complementary metal-oxide semiconductor; EOR, Extent of resection; FAD, Flavin adenine dinucleotide; FDA, U.S. Food and Drug administration; FD-FLIM, Frequency-domain-FLIM; FET, ^{18}F-fluoroethyl-L-tyrosine; FLAIR, Fluid-attenuated inversion recovery; FLIM, Fluorescence lifetime imaging; GBM, Glioblastoma; HGG, High-grade glioma; IDH, Isocitrate dehydrogenase; LGG, Low-grade glioma; MET, ^{11}C-methionine; MGMT, O6-methylguanine-methyltransferase; MRI, Magnetic resonance imaging; NAD(P)H, Nicotinamide adenine dinucleotide (phosphate); PDD, Photodynamic diagnosis; PET, Positron emission tomography; PpIX, Protoporphyrin IX.

INTRODUCTION

Neurosurgical resection constitutes the primary treatment in low-grade gliomas (LGG), but still remains challenging due to their histopathological heterogeneity as well as infiltrative growth pattern into the surrounding brain parenchyma (1–5). Thus, incomplete resection of LGG and histopathological undergrading of gliomas is not uncommon in the routine neurosurgical practice (6–14). In the last decades, different techniques were introduced into the neurosurgical operating room for improved intraoperative visualization of LGG tissue such as neuronavigation with multimodal imaging data, intraoperative MRI and advanced ultrasound (15–24).

Aside from these techniques, intraoperative visualization of brain tumor tissue with assistance of 5-aminolevulinic acid (5-ALA) induced fluorescence represents one of the most powerful methods for visualization of tumor tissue during surgery (7, 8, 25–31). Initially, this innovative fluorescence technique was exclusively applied during tumor resection of high-grade gliomas (HGG) (7, 8, 25, 29, 32). According to the data from a randomized controlled multicenter phase III trial, the rate of complete resections as well as the progression-free survival was significantly higher in HGG patients with 5-ALA fluorescence-guided surgery as compared to conventional white-light microscopy (7). Therefore, the 5-ALA fluorescence technique is current standard for resection of HGG in many neurosurgical departments around the world (7). Based on these promising observations in HGG, 5-ALA was increasingly applied also in patients with radiologically suspected LGG in the last years (24, 33–36). Here, we discuss the current role, limitations and new approaches of 5-ALA fluorescence during surgery of suspected LGG.

LOW-GRADE GLIOMAS

LGG represent a heterogenous group of astrocytic and oligodendroglial tumors and account for approximately 20% of all primary brain tumors with an incidence rate of 5.2 per 100 000 persons per year (5, 37–41). These tumors predominately affect a younger patient population in the 2nd to 4th decade (5). The median survival rate of patients suffering from LGG ranges from 5 to 13 years (5, 39–42). This wide range of survival rates in LGG are most likely due to differences in clinical, histopathological and molecular/genetic factors. In this sense, patient age and clinical performance status as well as histopathological and molecular genetic factors such as 1p19q co-deletion, isocitrate dehydrogenase (IDH) mutational status, O6-methylguanine-methyltransferase (MGMT) promotor methylation status and alpha thalassemia/intellectual disability X-linked (ATRX) mutation play an important role for patient prognosis in such tumors (13, 40, 43, 44). Additionally, several studies demonstrated the importance of the extent of resection (EOR) on progression-free and overall survival in patients suffering from LGG (5, 11, 21, 45–48). Thus, the neurosurgical aim of surgery in LGG represents maximal safe resection with preservation of neurological function to allow optimal patient prognosis (11, 45–48).

Magnetic resonance imaging (MRI) represents the gold standard for precise diagnosis of suspected LGG (49–57). On T1-weighted sequences, suspected LGG shows an hypointense lesion usually without contrast-media enhancement (49–57). A circumscribed area of contrast-enhancement within an otherwise non-enhancing tumor frequently indicates the occurrence of intratumoral malignant progression within the so-called "anaplastic focus" (6, 10, 58–64). For preoperative identification of intratumoral anaplastic foci within initially suspected LGG, advanced MRI techniques such as MRI spectroscopy, diffusion-weighted imaging, perfusion-weighted imaging as well as positron emission tomography (PET) using amino acids are powerful techniques (6, 23, 24, 54, 56, 59, 65).

CURRENT TECHNIQUES AND LIMITATIONS OF INTRAOPERATIVE LGG VISUALIZATION

At present, the use of intraoperative neuronavigation systems to optimize surgery of suspected LGG is routinely applied (22–24, 66). In this sense, navigation with T2-weighted/FLAIR sequences supports the neurosurgeon to improve intraoperative visualization of LGG tissue especially at the tumor margin in order to achieve the neurosurgical goal of a complete tumor resection according to the current Response Assessment in Neuro-Oncology (RANO) (51, 67, 68).

Although neuronavigation systems are routinely applied, this technique lacks accuracy in the course of glioma resection due to the so-called "brain-shift" leading to significant inaccuracy in image guidance since neuronavigation is based on preoperative image data (69–71). Thus, the occurrence of brain-shift during surgery of suspected LGG might impede precise detection of the tumor margin and the anaplastic focus (24, 58, 71, 72). Furthermore, insufficient intraoperative identification of LGG tissue as well as insufficient differentiation of intratumoral focal HGG tissue representing the anaplastic focus within LGG tissue represents a major challenge for the neurosurgeon (73, 74). Therefore, incomplete resection is reported in up to 88% of cases in surgery of LGG and histopathological undergrading is not uncommon in the routine neurosurgical practice (11, 13, 48, 75).

To overcome these current limitations of glioma surgery, intraoperative MRI was introduced into the neurosurgical field for improved visualization of residual tumor tissue during resection of LGG (16–18, 62, 76–79). This powerful intraoperative technique demonstrated to significantly increase the rate of complete glioma resections (80). However, this technique suffers from specific limitations as intraoperative MRI is not widely available due to its high costs (81). Moreover, specific departments routinely apply intraoperative ultrasound for real-time visualization of tumor tissue during LGG surgery (20, 82). Nevertheless, this technique is dependent from large experience of the performing neurosurgeon and thus this tool is infrequently used (82, 83).

Consequently, new and innovative widely available intraoperative techniques are required to overcome the above-mentioned current limitations in order to improve visualization

of LGG tissue and intratumoral heterogeneity of diffusely infiltrating gliomas during surgery.

FLUORESCENCE-GUIDED SURGERY IN NEUROSURGERY

Intraoperative visualization of brain tumor tissue with the assistance of fluorescence is unaffected by brain-shift and thus might overcome the current limitations of surgery in suspected LGG (7, 32, 84, 85). Already in 1948, Moore et al. reported their first observations of visible fluorescence using fluorescein in different types of brain tumors (86). Since 1992, the fluorescent dye 5-ALA was increasingly applied for intraoperative visualization of tumor tissue in different medical disciplines such as urology and dermatology (87, 88). In 1998, Stummer et al. reported the use of this well-tolerated fluorescent dye for fluorescence-guided surgery in the first patients in the neurosurgical field as well (89). In 2000, the authors published the first clinical study including 52 consecutive patients suffering from HGG (8). In this study, Stummer et al. observed strong 5-ALA fluorescence in HGG tissue, whereas normal brain tissue did not show any visible fluorescence during surgery (8). Based on these first promising findings, Stummer et al. initiated in a further step a randomized controlled multicenter phase III trial investigating the impact of 5-ALA fluorescence-guided resection on EOR and progression-free survival in HGG (7). According to their data, this study showed that 5-ALA fluorescence-guided surgery improves the rate of complete resection of the contrast-media enhancing tumor resulting in a significantly prolonged progression-free survival as compared to conventional white-light resections (7). Consequently, 5-ALA was approved for resection of HGG in the European Union in 2007. Following this approval, fluorescence-guided surgery using 5-ALA became more and more attractive in the neurosurgical field as it is relatively inexpensive, widely available and has little side effects (7, 29, 30, 32). Ten years later, 5-ALA was approved by the FDA for intraoperative visualization of suspected HGG in the United States as well (85).

METHODS

In this review, we performed a literature search to discuss the current role, limitations, and new approaches of 5-ALA fluorescence during surgery of suspected LGG. For this purpose, we performed a literature research using Pubmed to screen the MEDLINE database for relevant publications. To cover all relevant publications, we used different search criteria such as "5-ALA", "glioma", "LGG" and "PET". Additionally, we also included "HGG" in our search criteria as we aimed to identify cohorts including "radiologically suspected LGG" which may present as neuropathologically confirmed HGG. Therefore, our literature review also covers cohorts including HGG as well as LGG cases with the application of 5-ALA.

5-ALA FLUORESCENCE IN LGG

Based on these auspicious findings in HGG, the application of 5-ALA was also investigated in LGG in the last years. In this sense, Ishihara et al. reported in 2007 altogether 6 patients including 2 LGG, 2 HGG and 2 GBM that were investigated *ex-vivo* after 5-ALA administration (90). Interestingly, only samples from HGG and GBM demonstrated macroscopic visible 5-ALA fluorescence, whereas in all LGG samples no visible fluorescence was observed (90). Additionally, Stummer et al. described one single patient with focal malignant transformation showing visible 5-ALA fluorescence in the contrast-enhancing area, but no fluorescence in the non-enhancing LGG part (89). As these studies only included single cases, larger patient cohorts were needed.

In 2010, Widhalm et al. evaluated in the first clinical study the intraoperative application of 5-ALA in 19 cases of radiologically suspected LGG (58). In this first *in-vivo* study, the 5-ALA fluorescence status was analyzed during resection and demonstrated that a subgroup of these suspected LGG showed visible fluorescence in a circumscribed intratumoral area (58). Interestingly, histopathological analysis revealed 8 LGG cases which did not show any visible 5-ALA fluorescence (58). Notably, all tumors showing visible intratumoral fluorescence were histopathologically classified as WHO grade III gliomas resulting in a positive predictive value of focal 5-ALA fluorescence for WHO grade III glioma of 100% (58). Additionally, gliomas with visible 5-ALA fluorescence showed a significantly higher proliferation rate (MIB-1: 20 *vs* 6%, p=0.001) compared to gliomas without visible fluorescence (58). In conclusion, Widhalm et al. suggested 5-ALA fluorescence as a promising tool to intraoperatively visualize anaplastic foci within initially suspected LGG (58). In addition, the authors hypothesized that 5-ALA fluorescence might optimize tissue sampling and subsequently improves postoperative treatment allocation in suspected LGG patients (58).

In a further study conducted by Ewelt et al. these initial findings suggesting that visible 5-ALA fluorescence in suspected LGG is a predictive marker for high-grade histology were confirmed in an independent cohort (91). Of these 30 included tumors, 13 were diagnosed as WHO grade II, 15 as WHO grade III and two as WHO grade IV gliomas (91). Visible fluorescence was observed in 13 of 30 patients in this study (91). According to histopathological analysis, the majority of WHO grade III and IV gliomas demonstrated visible fluorescence (2 of 2 GBM, 10 of 15 WHO grade III gliomas; 70%) (91). In contrast, only one of 11 WHO grade II gliomas showed visible fluorescence (91).

In a subsequent clinical study, Widhalm et al. analyzed 59 patients with a suspected LGG consisting of 26 HGG and 33 LGG (26). In this study, 85% of all WHO grade III gliomas showed focal fluorescence, whereas 91% of WHO grade II gliomas revealed no visible fluorescence (26). According to detailed histopathological analysis, the authors found a significantly higher mitotic rate, cell density, nuclear pleomorphism and proliferation rate in intratumoral areas with focal 5-ALA fluorescence compared to areas without visible fluorescence (26). These findings resulted in a positive predictive value of visible 5-ALA fluorescence for WHO grade III histology of 85% (26). In this study, the authors confirmed their initial findings of their pilot study that 5-ALA is a powerful and reliable intraoperative marker for anaplastic foci identification independent of brain-shift (26). Additionally, this study reported a significant correlation of focal 5-ALA fluorescence with specific histopathological parameters of anaplasia (26).

The largest patient cohort up to date of 166 tumors lacking characteristic GBM imaging features included 82 WHO grade II, 76 WHO grade III and 8 WHO grade IV gliomas (92). This study was published in 2016 by Jaber et al. and correlated 5-ALA with MRI, PET, proliferation index and molecular genetics (92). According to the data, WHO grade histology and proliferation index correlated with visible 5-ALA fluorescence, however, no correlation was found with MGMT promoter methylation status, IDH1 mutational status or 1p19q co-deletion (92). Furthermore, fluorescing WHO grade III gliomas showed a significantly higher proliferation index as compared to tumors without visible fluorescence (92). Interestingly, no difference of proliferation index was noted in WHO grade II gliomas with visible fluorescence and no visible fluorescence, respectively (92). In brief, this study confirmed that visible 5-ALA fluorescence is associated with high-grade histology and increased proliferation index (92). However, the authors concluded that further analysis to identify the impact of 5-ALA fluorescence in a subgroup of WHO grade II gliomas are needed (92).

An additional study published in 2017 by Saito et al. evaluated the association between 5-ALA fluorescence and proliferation rate as well as molecular markers including IDH1 mutational status and 1p19q co-deletion in a series of WHO grade II, III and IV gliomas (93). In this study, univariate analysis indicated that 5-ALA fluorescence is significantly related to proliferation rate as well as IDH1 mutational status and 1p19q co-deletion (93). According to multivariate analysis, only IDH1 status remained statistically significant (93). In detail, gliomas with visible 5-ALA fluorescence showed a significantly higher rate of IDH1 wildtype tumors (93). However, this high rate of visible fluorescence in IDH1 wildtype tumors might be explained by the high number of WHO grade IV gliomas with IDH1 wildtype included in this analysis (93).

In 2019, Jaber et al. evaluated the impact of visible 5-ALA induced fluorescence in a study cohort including only histopathologically confirmed pure LGG (36). In this study, 74 patients with pure LGG were analyzed and visible 5-ALA fluorescence was observed in 16 of 74 (22%) cases (36). Interestingly, progression-free survival, malignant transformation-free survival and overall survival were shorter in tumors showing visible 5-ALA fluorescence as compared to non-fluorescing LGG (36). However, in this study only overall survival was statistically significant (36). According to these findings, the authors proposed that postoperative adjuvant therapies might be early considered in patients with histopathologically confirmed LGG and visible 5-ALA fluorescence (36). Additionally, Jaber et al. suggested shorter intervals during MRI follow-up examinations should be considered (36).

In a further study in the same year, Goryaynov et al. reported the presence of visible 5-ALA fluorescence in a markedly higher portion of LGG patients (52%) (94). However, this study not only included diffusely infiltrating gliomas WHO grade II, but also pilocytic astrocytoma, gemistocytic astrocytoma and desmoplastic infantile ganglioglioma (94). With regard to a subgroup analysis, only 29% of astrocytoma WHO grade II showed visible fluorescence which is in accordance with earlier publications (26, 36, 58, 94). An overview of the literature is given in **Table 1** and an illustrative case is provided in **Figure 1**.

5-ALA FLUORESCENCE AND PET IMAGING

In the literature, different studies also correlated PET imaging with visible 5-ALA fluorescence in diffusely infiltrating gliomas (36, 92, 95–98). In this sense, Stockhammer et al. first reported in 2009 that the standardized uptake value of PET related to normal brain using ^{18}F-fluoroethyl-L-tyrosine (FET) was significantly higher in tumor areas with 5-ALA fluorescence as compared to normal brain with absence of visible fluorescence (95). This study cohort consisted mainly of patients suffering from glioblastomas (n=11 of 13 patients) (95).

In a study published in 2010 including only WHO grade II and III gliomas, Widhalm et al. correlated PET imaging using ^{11}C-methionine (MET) with focal 5-ALA fluorescence (58). In this study, the maximal tumor to normal brain ratio (PET_{max}) was significantly higher in the focal 5-ALA fluorescence glioma group as compared to gliomas with lack of fluorescence (58). Furthermore, the authors observed that focal fluorescence always correlated topographically with the MET-PET hotspot verified by intraoperative navigation (58). In a subsequent study with a larger patient cohort, Widhalm et al. confirmed this interesting observation and reported that focal fluorescence correlated topographically in all gliomas with a distinct PET hotspot (26). These data indicate that focal 5-ALA fluorescence is able to intraoperatively identify intratumoral areas with highest metabolic activity according to MET-PET (26, 58). Therefore, the authors advocate the combined use of PET imaging and 5-ALA fluorescence to optimize tissue sampling during surgery of suspected LGG (26, 58). In this sense, PET is a clinically reliable method for preoperative identification of anaplastic foci within suspected LGG and 5-ALA fluorescence is subsequently useful for intraoperative detection of such PET hotspots independent of brain-shift (26, 58).

In a subsequent study published in 2011 Floeth et al. investigated the preoperative FET-PET, contrast media enhancement on MRI and intraoperative 5-ALA fluorescence in 38 glioma samples (33). The study cohort consisted of biopsies from 17 LGG and 21 HGG (33). In biopsies of HGG, 86% of cases showed a metabolic hotspot on FET-PET as compared to visible 5-ALA fluorescence/contrast-enhancing area on MRI which was present in 57% of cases (33). Interestingly, all gliomas with visible 5-ALA fluorescence showed a metabolic hotspot on FET-PET (33). Despite this positive correlation of visible 5-ALA fluorescence and FET-PET, the authors postulated that FET-PET is more sensitive for glioma tissue detection especially in LGG compared to 5-ALA fluorescence (33).

Another study by Ewelt et al. published in 2011 analyzed the FET-PET uptake and its correlation with 5-ALA fluorescence in 30 gliomas (91). In this study, all tumors with intraoperative visible fluorescence were positive on preoperative FET-PET (91). Moreover, FET-PET/5-ALA positive biopsies were found in 71% of HGG, whereas this constellation was observed in only 8% of LGG (91). Furthermore, the FET-PET tracer uptake was significantly higher in tissue samples with visible fluorescence (FET-PET uptake always >1.6) as compared to samples with

TABLE 1 | Studies in the literature with primary focus on visible 5-ALA fluorescence including LGG (WHO grade II).

Publication	Year	Total	Histopathological diagnosis		Positive 5-ALA Fluorescence	
		n	*n*		*n*	*(%)*
Ishihara et al.	2007	6	2	WHO° II	0/2	(0)
			2	WHO° III	2/2	(100)
			2	WHO° IV	2/2	(100)
Widhalm et al.	2010	17	8	WHO° II	0/8	(0)
			9	WHO° III	8/9	(89)
Ewelt et al.	2011	30	13	WHO° II	1/13	(8)
			15	WHO° III	10/15	(67)
			2	WHO° IV	2/2	(100)
Widhalm et al.	2013	59	33	WHO° II	4/33	(12)
			26	WHO° III	23/26	(88)
Jaber et al.	2016	166	82	WHO° II	19/82	(23)
			76	WHO° III	66/76	(87)
			8	WHO° IV	7/8	(88)
Saito et al.	2017	60	8	WHO° II	2/8	(25)
			17	WHO° III	9/17	(53)
			35	WHO° IV	31/35	(89)
Jaber et al.	2019	74	74	WHO° II	16/74	(22)
Goryaynov et al.	2019	27	20	WHO° II	7/20	(35)
			4	Pilocytic astrocytoma	4/4	(100)
			2	Gemistocytic astrocytoma	2/2	(100)
			1	Desmoplastic infantile ganglioglioma	1/1	(100)

5-ALA, 5-aminolevulinic acid; WHO, World Health Organization.

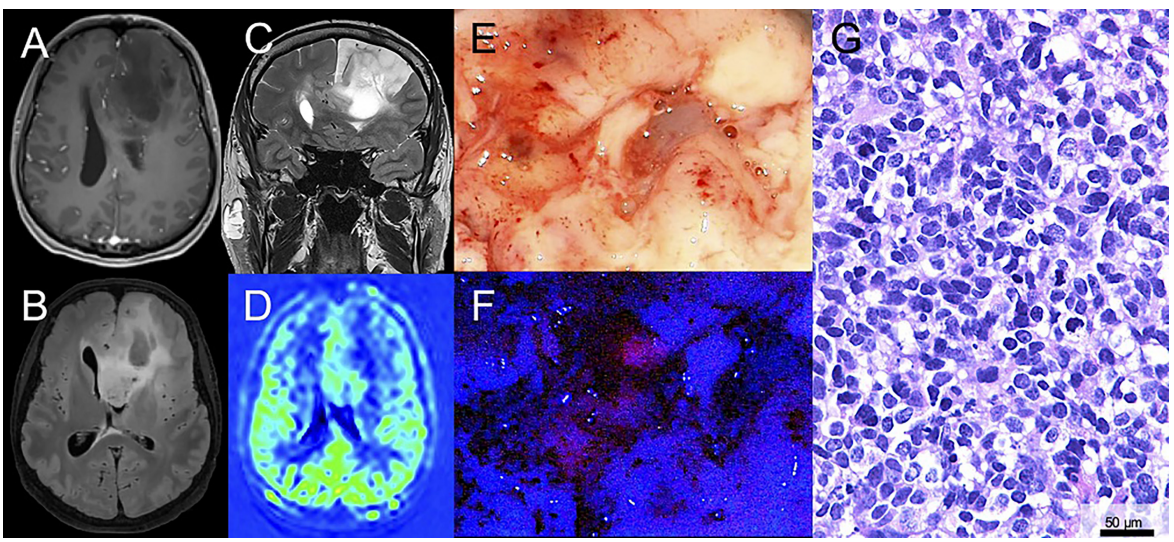

FIGURE 1 | Illustrative case of a patient with a suspected low-grade glioma (LGG) with surgical resection after 5-ALA administration. **(A)** Magnetic resonance imaging of a 43-year-old male patient reveals a suspected LGG in the left frontal lobe. On T1-weighted sequences no significant contrast-media enhancement is observed. **(B, C)** On fluid-attenuated inversion recovery (FLAIR) and T2-weighted sequences the lesion is hyperintense. **(D)** Perfusion imaging shows no hyperperfusion. **(E)** During surgical tumor resection, conventional white-light microscopy was used. **(F)** Additionally, the microscope was repeatedly switched to violet-blue excitation light and an intratumoral area of visible fluorescence was detected. **(G)** Histopathological analysis revealed an anaplastic astrocytoma WHO grade III (IDH mutated).

absence of fluorescence (91). Therefore, the authors concluded in this study that a positive preoperative FET-PET is highly predictive for visible 5-ALA fluorescence during glioma surgery (91). In a further study, this group reported in 2016 that a FET-PET uptake ratio >1.85 predicted visible 5-ALA fluorescence in gliomas with absence of characteristic glioblastoma features based on preoperative MRI (92).

A detailed histopathological analysis of cell density in 11 glioma patients was performed in 2012 by Arita et al. and the authors correlated cell density to MET-PET and 5-ALA fluorescence (99). In this study, cell density was observed to correlate with MET-PET tracer uptake and positive 5-ALA fluorescence (99). Interestingly, MET-PET uptake showed no correlation with areas with positive or negative fluorescence in this study (99). However, this study was limited by its small sample size of included patients (n=11 patients) (99). An overview of the literature is given in **Table 2**.

CURRENT LIMITATIONS OF 5-ALA IN SUSPECTED LGG

Although 5-ALA fluorescence-guided procedures represent one of the most important advancements in the neurosurgical field, specific limitations are associated with this technique. First of all, the vast majority of pure LGG do not produce sufficient 5-ALA induced PpIX accumulation and thus visible fluorescence is usually absent during surgery in these tumors (26, 58, 91, 100). Therefore, 5-ALA is usually not useful for improved definition of the tumor margin during surgery of pure LGG (75, 101, 102). Furthermore, 5-ALA is not capable to visualize a subgroup of suspected LGG with presence of an intratumoral anaplastic focus by visible fluorescence during surgery (58, 91). Finally, visible 5-ALA induced fluorescence underlies a subjective observation based on the performing neurosurgeon and is thus associated with an interobserver variability (103, 104). Thus, intratumoral areas with only vague 5-ALA fluorescence might not be recognized by certain neurosurgeons. Consequently, further advancements of this innovative fluorescence technique are necessary to overcome these current limitations in the future.

QUANTITATIVE SPECTROSCOPIC MEASUREMENT OF 5-ALA INDUCED PpIX ACCUMULATION

In the last years, novel technologies for improved fluorescence detection in brain tumors were introduced in the neurosurgical field. One of the most promising methods represents quantitative spectroscopic analysis of 5-ALA induced PpIX accumulation. In this sense, spectroscopic analysis is capable to measure the characteristic fluorescence signal of PpIX with typical emission peaks at 635nm and 710nm (90, 102, 104–106).

In a study performed by Utsuki et al. in 2006, the authors analyzed the potential of intraoperative laser spectroscopy in 6 patients with brain tumors (105). This promising approach was able to detect tumor tissue by laser spectroscopy at a peak of 636 nm after 5-ALA administration despite the absence of visible fluorescence (105).

In a further study, Ishihara et al. reported an *ex-vivo* quantitative analysis of 5-ALA induced PpIX fluorescence intensity using spectroscopy in 2007 (90). In this study, 65 samples of 6 glioma patients (2 WHO grade II, 2 WHO grade III and 2 WHO grade IV gliomas, respectively) were quantitatively analyzed and correlated with fluorescence intensity and specific histopathological criteria (90). According to the data, proliferation index, CD31-mircovessel density and the vascular endothelial growth factor correlated with

TABLE 2 | Studies in the literature with comparison of PET and visible 5-ALA fluorescence including LGG (WHO grade II).

Publication	Year	Total	Histopathological diagnosis		Positive 5-ALA fluorescence		PET tracer	PET T/N ratio	
		n	*n*		*n*	*(%)*		*5-ALA pos*	*5-ALA neg*
Stockhammer et al.	2009	13	1	WHO° II	1/1	(100)	FET	2.321	1.142
			1	WHO° III	1/1	(100)		***p<0.0001***	
			11	WHO° IV	11/11	(100)			
Widhalm et al.	2010	17	8	WHO° II	0/8	(0)	MET	2.3	1.2
			9	WHO° III	8/9	(89)		***p=0.037***	
Floeth et al.	2011	30	13	WHO° II	1/13	(8)	FET	*n.d.*	*n.d.*
			15	WHO° III	8/15	(53)			
			2	WHO° IV	2/2	(100)			
Ewelt et al.	2011	30	13	WHO° II	1/13	(8)	FET	2.82	1.33
			15	WHO° III	9/15	(60)		***p=0.026***	
			2	WHO° IV	2/2	(100)			
Arita et al.	2012	11	2	WHO° II	*n.d.*	*n.d.*	MET	1.66	1.41
			2	WHO° III				*p=0.367*	
			7	WHO° IV					

5-ALA, 5-aminolevulinic acid; FET, O-[2- (18F)fluoroethyl]-L-tyrosine; MET, methionine; n.d., no data; PET, positron emission tomography.
T/N ratio, tumor to normal brain ratio; WHO, World Health organization.
Bold = significant.

spectroscopic fluorescence intensity (90). These observations indicated that a higher proliferation rate might trigger 5-ALA fluorescence as the proliferation index was the strongest histopathological marker correlated with fluorescence intensity (90). Most importantly, tumor tissue of LGG with absence of visible fluorescence could be detected by quantitative spectroscopic analysis of fluorescence intensity (90).

In 2011, Valdes et al. reported a quantitative *ex-vivo* analysis using "PpIX fluorimetry" to measure 5-ALA induced PpIX concentrations in 23 patients with low-grade and high-grade gliomas (107). Interestingly, none of the four WHO grade I gliomas and only one of two included WHO grade II gliomas showed visible fluorescence (107). In this study, the authors analyzed PpIX concentrations measured by PpIX fluorimetry and the proliferation rate of all together 133 tissue samples (107). According to the data, Valdes et al. found significantly higher levels of PpIX concentrations and proliferation rates in samples with visible fluorescence as compared to non-fluorescing specimens (107). It is of note that 40% of the tumor positive samples with absence of visible fluorescence with conventional 5-ALA microscopy demonstrated significant PpIX concentrations (>0.1 μg/mL) (107). These *ex-vivo* data demonstrated the potential ability of quantitative spectroscopic PpIX analysis to visualize also non-fluorescing tumor tissue as well as anaplastic foci within suspected LGG without any visible fluorescence (107).

In a further step, Valdes et al. developed a novel fiberoptic probe connected to a spectrometer also for intraoperative use to measure intratumoral PpIX concentrations during surgery (101). The authors reported the first *in-vivo* application of this hand-held fiberoptic probe during surgery in a small patient cohort of 14 different brain tumors (101). In detail, the study cohort consisted of 2 LGG, 3 HGG, 6 meningiomas and 3 brain metastases (101). In this study, the PpIX concentration was measured intraoperatively during different time points of resection/intratumoral areas and corresponding tissue biopsies were collected (101). Additionally, control data were investigated from normal brain and dura mater (101). According to the data, the authors found significant differences in PpIX concentrations between all measured tumors and normal brain (101, 102). Therefore, this first *in-vivo* study demonstrated the feasibility of this innovative approach in different common brain tumors (101).

In a subsequent study published in 2015, Valdes et al. analyzed the value of their fiberoptic probe also in a small series of LGG including altogether 12 patients (34). In detail, two oligodendrogliomas, two gangliogliomas, one ependymoma, three dysembryoplastic neuroepithelial tumors (DNETs), three oligoastrocytomas, and one pleomorphic xanthoastrocytoma were included (34). According to the data, the authors confirmed the poor diagnostic accuracy of the conventional visual 5-ALA fluorescence technology in LGG (34). However, significant PpIX concentrations were measured in LGG by using the fiberoptic probe according to these preliminary data (34). In detail, quantitative fluorescence PpIX measurement with the intraoperative fiberoptic probe was able to markedly increase the diagnostic accuracy for detection of LGG tissue as compared to 38% for qualitative visible fluorescence (34).

Based on these promising preliminary data, Widhalm et al. applied this fiberoptic probe in addition to conventional visual 5-ALA fluorescence technology in a study published in 2019 during surgery of 22 suspected diffusely infiltrating LGG (35). In this study, final histology after surgical resection revealed a WHO grade II in 8 cases, WHO grade III glioma in 10 cases and WHO grade IV glioma in 3 cases (35). With assistance of 5-ALA visual 5-ALA microscopy, visible fluorescence was present in circumscribed areas in the majority of HGG (79%), whereas visible fluorescence was absent in all LGG (35). By using the fiberoptic probe, a significantly higher mean PpIX concentration was found in fluorescing samples as compared to non-fluorescing tissue samples (35). Furthermore, a significant correlation of PpIX concentrations and the percentage of tumor cells was observed in this study (35). Moreover, this study reported a significant correlation between the maximum PpIX concentration and overall tumor grade (35). Altogether, the authors conclude that conventional 5-ALA visual 5-ALA microscopy is especially useful to identify intratumoral anaplastic foci to avoid the risk of histopathological undergrading (35). The additional use of quantitative PpIX analysis represents a powerful technique for improved intraoperative detection of LGG tissue that is generally characterized by absence of visible fluorescence in order to maximize the extent of resection (35).

In a further study from 2019, Martinez-Moreno et al. applied a handheld spectroscopic probe in a series of 68 patients with diffusely infiltrating gliomas (WHO grades II-IV) (108). With *ex-vivo* spectroscopic analysis, significant differences in the median fluorescence intensity values were found in certain parameters of malignancy as well as a significant correlation between fluorescence intensity and proliferation rate (108). These data demonstrated the value of such spectroscopic probes to visualize intratumoral histopathological heterogeneity in diffusely infiltrating gliomas for improved tissue sampling and detection of the tumor margin (108).

CONFOCAL MICROSCOPY AND 5-ALA FLUORESCENCE

Another innovative technique for improved detection of brain tumor tissue represents confocal microscopy combined with fluorescence technology (75, 109–113). In contrast to spectroscopic analysis, confocal microscopy is able to visualize fluorescing tissue by generating images with high contrast micron-scale spatial resolution (75, 109–113). The development of handheld probes provided new insight into the tumor enabling real time images of 5-ALA induced fluorescence at a 1000x magnification (75).

In 2011, Sanai et al. utilized confocal microscopy enabled through a handheld probe in order to visualize 5-ALA fluorescence during surgery of 10 LGG (WHO grades I and II gliomas) (75). Although none of the 10 LGG demonstrated visible fluorescence, confocal microscopy was able to visualize fluorescing tumor cells within LGG tissue (75). Therefore, the authors conclude that this innovative technique is useful to improve the detection of LGG tissue as well as their tumor margin in order to increase the rate of extent of resection (75).

Another approach was introduced by the group of Preul et al. with the combined use of intraoperative confocal laser endomicroscopy (CLE) and the fluorescence dye "fluorescein sodium" (110–113). In contrast to 5-ALA, this fluorescent dye is administered intravenously (110–113). By this innovative approach, the authors observed a high specificity and sensitivity for detection of glioma tissue (94% and 91%, respectively) and meningioma tissue (93% and 97%, respectively) comparable to those for conventional frozen sections (110–113). Therefore, the authors conclude that this technique will optimize in future surgery of brain tumors and intraoperative decision-making (110–113).

FLUORESCENCE LIFETIME IMAGING OF PpIX

Apart from intensity-based and spectroscopic measurements fluorescence can be analyzed in respect to its temporal decay dynamics (114–117). The fluorescence lifetime is the average time delay between the excitation of a fluorophore and the subsequent emission of fluorescence (114–118). It depends both on the intrinsic molecular properties and the direct cellular environment (118). FLIM has been widely used to measure the cellular redox states of the coenzymes nicotinamide adenine dinucleotide (phosphate) (NAD(P)H) and flavin adenine dinucleotide (FAD), which have shown to indicate metabolic re-programming in cancer cells (119–121). FLIM for the sensitive detection of PpIX in photodynamic diagnosis (PDD), however, has gained interest only recently (114–117).

In intensity-based PDD the detection of weak PpIX fluorescence is limited by the autofluorescence of the brain parenchyma (122). When excited in the blue region of the spectrum, the main contributors to tissue autofluorescence emitting above 600nm are flavins, lipofuscin-like lipopigments, vitamin A and endogenous porphyrins (122). This background fluorescence can be stronger than the actual PpIX fluorescence (122). Sensitive detection therefore inherently requires the distinction between PpIX and autofluorescence, which essentially corresponds to the specificity of the PpIX detection (122). As described in the previous sections, spectroscopic and hyperspectral techniques have been proposed to quantify PpIX concentrations (35, 123, 124). FLIM of PpIX constitutes a complementary approach as it allows to distinguish spectrally overlapping fluorophores based on their temporal decay characteristics (35, 116, 123, 124). Autofluorescence and 5-ALA induced PpIX fluorescence lifetimes in an orthotopic mouse model have been reported by Kantelhardt et al. using a multiphoton time-domain FLIM system (125). While lifetimes from 0.8 to 2.0ns were measured for brain parenchyma, cytoplasmic PpIX increased the lifetime to 2.9 ns in U87 GBM derived cell lines (125). Autofluorescence in both murine white and gray matter was measured to be 1.4 ns, whereas cells with a higher metabolic activity exceeded those values (>1.7 ns) (126). Russel et al. measured the lifetime of PpIX to be 16.4ns in organic solvent and 6.3 ns for mitochondrial PpIX in rat prostate adenocarcinoma cells incubated with 5-ALA (127). Similarly, a lifetime of 7.4ns was reported in 5-ALA incubated epithelial rat cells (128). Erkkilae et al. recently proposed the use of a frequency-domain FLIM (FD-FLIM) system based on a dual-tap CMOS camera for *ex-vivo* imaging of human brain tumor specimens collected during 5-ALA fluorescence-guided resection (114). While a mean fluorescence lifetime of 15.1ns was measured for a GBM WHO grade IV, lifetimes of up to 4.8ns were reported for an oligodendroglioma WHO grade II in a follow up study (116). In an extended pilot study, the median of the measured lifetimes of 3 LGG was 2.5ns, where 100 randomly selected measurement points were evaluated for each specimen (115). Likewise, tumor infiltrated brain of LGG and HGG showed increased lifetimes (12 samples, 3.2ns). In contrast, a median autofluorescence lifetime of 1.9 ns was reported for 2 non-pathological specimens (115).

FLIM of PpIX adds a third dimension to intensity-based and spectrally resolved techniques (117). Data suggest that weak PpIX accumulations, as found in LGG and infiltrated brain, increase the lifetime respective to non-pathological parenchyma. Further studies are required to determine the extent to which PpIX fluorescence can be detected within a dominating autofluorescence background. The homodyne detection scheme inherent to FD-FLIM facilitates the integration into surgical microscopes with long working distances (117). Clinical translation would therefore be consistent with surgical workflows and allow for combining sensitive wide-field PpIX detection with pre-operative stereotactic navigation data (117). Note that in FD-FLIM the measured lifetime is a weighted average composed of all excited fluorophores (117). Future studies should focus on combining spectrally-resolved methods with FD-FLIM to gain insight into the interplay of PpIX and autofluorescence. Also, time-domain FLIM techniques have been integrated into hand-held probes and could be used to reconstruct the multi-exponential decays of the mixed autofluorescence and PpIX signal (129, 130). Eventually, a combination of time- and spectrally resolved methods integrated into probes and wide-field visualization platforms could enhance LGG tissue detection in PDD and assist the neurosurgeon in a multitude of visualization tasks. An illustrative case is provided in **Figure 2**.

PHARMACEUTICALS' INFLUENCE ON 5-ALA FLUORESCENCE

The reason for the presence of visible fluorescence in pure LGG and in contrast, the absence of fluorescence in a group of gliomas with focal malignant histopathological characteristics are not fully clarified so far (25, 36, 58, 59, 131). The intake of antiepileptic drugs (AED) and/or dexamethasone prior to surgery has been discussed in the literature as a potentially influencing factor on 5-ALA fluorescence (94, 131–133). Two *in-vitro* studies analyzed the effect of different AED and/or dexamethasone on the metabolism of PpIX in malignant glioma cell lines (132, 133). The authors found a decreased amount of PpIX produced in these cells after the combination with dexamethasone as well as several AED, except Levetiracetam (132, 133). In line with these results, a first *in-vivo* study reported visible 5-ALA fluorescence more frequently in patients without preoperative intake of AED compared to patients with AED treatment in a series of 27 LGGs (94).

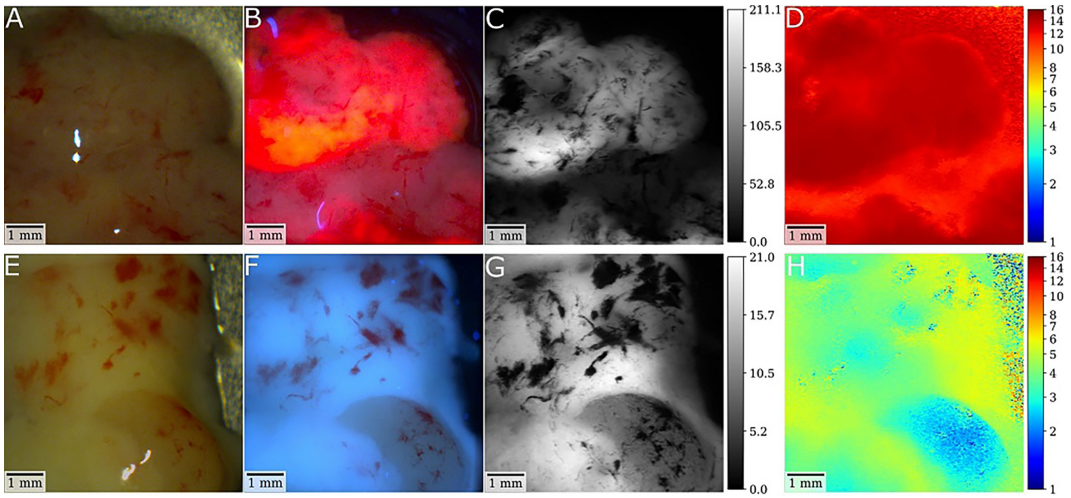

FIGURE 2 | Illustrative cases of a glioblastoma (GBM) and low-grade glioma (LGG) with postsurgical *ex-vivo* analysis with fluorescence lifetime imaging after preoperative 5-ALA administration. **(A, B)** In the first patient, white-light and fluorescence camera images show the tumor core of an IDH-wild-type GBM specimen. For the fluorescence image, the laser was scanned rapidly across the tissue with the integration time of the camera being set to 2 seconds. Note the strong visible PpIX fluorescence of the sample. Demodulated fluorescence intensity [mV_{RMS}] and fluorescence lifetime [ns] images of a raster-scanning FD-FLIM system are shown in **(C, D)**. As depicted by the color-coding, strong PpIX fluorescence led to increased lifetimes up to 15.3ns with a mean lifetime of 13.4ns. **(E, F)** In the second patient, respective images show a tissue specimen of an IDH mutated low-grade astrocytoma **(G, H)**. While no fluorescence was visible intraoperatively, the lifetime was increased from about 2.4 to 5.5ns, which is higher than the 0.8 to 2ns expected for non-pathological brain parenchyma. Thus, this tumor tissue could be visualized by fluorescence lifetime imaging.

However, this study did not only include diffusely infiltrating gliomas, but also ganglioglioma and pilocytic astrocytoma (94).

In a further study, Wadiura et al. investigated the influence of AED and dexamethasone on visible 5-ALA fluorescence in 110 newly diagnosed, suspected diffusely infiltrating LGG (131). According to the data, no independent correlation was found between the visible fluorescence status and the intake of dexamethasone/AED (131). According to these findings of the largest series to date, the treatment of AED/dexamethasone can be prescribed safely prior to fluorescence-guided surgery of LGG (131). However, future studies are warranted with the aim to detect even subtle alterations in intratumoral PpIX accumulation based on the potential influence of these frequently used drugs in neurosurgical patients using quantitative methods.

VALUE OF OTHER FLUOROPHORES IN LGG

Aside from 5-ALA other fluorophores were additionally investigated for fluorescence guided resection in HGG as well as LGG. One alternative to 5-ALA for intraoperative fluorescence represents sodium fluorescein (134–137). Sodium fluorescein is a technique for intraoperative fluorescence-guided resection in HGG, however, it showed no benefit in LGG surgery as no intraoperative yellow fluorescence was evident in LGG tissue (138, 139). A further fluorophore was investigated by Akimoto et al. analyzing talaporfin sodium for intraoperative photodiagnosis for malignant glioma (140). Aside from HGG and other tumor entities, also LGG cases were investigated in their study cohort and revealed at least weak fluorescence (140).

CONCLUSION

The 5-ALA fluorescence technology is especially useful to visualize intratumoral regions with malignant transformation (anaplastic foci) within initially suspected LGG to avoid the risk of histopathological undergrading. However, the current 5-ALA technique is limited by the frequent absence of visible fluorescence within pure LGG. Recently, new approaches were introduced for improved detection of pure LGG tissue such as quantitative spectroscopic PpIX measurement, FLIM of PpIX and confocal microscopy. Consequently, further studies should clarify if these promising techniques are capable to reliably detect pure LGG tissue during surgery in order to maximize the extent of resection and improve the patient prognosis.

AUTHOR CONTRIBUTIONS

BK, JF, DR, LW, ME, AW, SH-J, MB, and GW substantially contributed to the conception and design of the work. BK, JF, DR, LW, and GW were responsible for data acquisition, analysis or interpretation of data for the work. BK, JF, DR, LW, ME, AW, SH-J, MB, and GW drafting the work or revising it critically for important intellectual content. All authors contributed to the article and approved the submitted version.

REFERENCES

1. Jakola AS, Skjulsvik AJ, Myrmel KS, Sjavik K, Unsgard G, Torp SH, et al. Surgical Resection *Versus* Watchful Waiting in Low-Grade Gliomas. *Ann Oncol* (2017) 28(8):1942–8. doi: 10.1093/annonc/mdx230
2. Yordanova YN, Moritz-Gasser S, Duffau H. Awake Surgery for WHO Grade II Gliomas Within "Noneloquent" Areas in the Left Dominant Hemisphere: Toward a "Supratotal" Resection. *Clin article. J Neurosurg* (2011) 115 (2):232–9. doi: 10.3171/2011.3.JNS101333
3. Pallud J, Fontaine D, Duffau H, Mandonnet E, Sanai N, Taillandier L, et al. Natural History of Incidental World Health Organization Grade II Gliomas. *Ann Neurol* (2010) 68(5):727–33. doi: 10.1002/ana.22106
4. Pallud J, Varlet P, Devaux B, Geha S, Badoual M, Deroulers C, et al. Diffuse Low-Grade Oligodendrogliomas Extend Beyond MRI-Defined Abnormalities. *Neurology* (2010) 74(21):1724–31. doi: 10.1212/WNL.0b013e3181e04264
5. Louis DN, Ohgaki H, Wiestler OD, Cavenee WKInternational Agency for Research on Cancer, World Health Organization. *WHO Classification of Tumours of the Central Nervous System*. Revised 4th ed. Vol. 408. Lyon: International Agency for Research on Cancer (IARC (2016).
6. Kunz M, Thon N, Eigenbrod S, Hartmann C, Egensperger R, Herms J, et al. Hot Spots in Dynamic (18)FET-PET Delineate Malignant Tumor Parts Within Suspected WHO Grade II Gliomas. *Neuro Oncol* (2011) 13(3):307–16. doi: 10.1093/neuonc/noq196
7. Stummer W, Pichlmeier U, Meinel T, Wiestler OD, Zanella F, Reulen HJ, et al. Fluorescence-Guided Surgery With 5-Aminolevulinic Acid for Resection of Malignant Glioma: A Randomised Controlled Multicentre Phase III Trial. *Lancet Oncol* (2006) 7(5):392–401. doi: 10.1016/S1470-2045(06)70665-9
8. Stummer W, Novotny A, Stepp H, Goetz C, Bise K, Reulen HJ. Fluorescence-Guided Resection of Glioblastoma Multiforme by Using 5-Aminolevulinic Acid-Induced Porphyrins: A Prospective Study in 52 Consecutive Patients. *J Neurosurg* (2000) 93(6):1003–13. doi: 10.3171/jns.2000.93.6.1003
9. Albert FK, Forsting M, Sartor K, Adams HP, Kunze S. Early Postoperative Magnetic Resonance Imaging After Resection of Malignant Glioma: Objective Evaluation of Residual Tumor and Its Influence on Regrowth and Prognosis. *Neurosurgery* (1994) 34(1):45–60discussion –1. doi: 10.1227/00006123-199401000-00008
10. Paulus W, Peiffer J. Intratumoral Histologic Heterogeneity of Gliomas. *A Quantitative Study. Cancer* (1989) 64(2):442–7. doi: 10.1002/1097-0142(19890715)64:2<442::AID-CNCR2820640217>3.0.CO;2-S
11. Smith JS, Chang EF, Lamborn KR, Chang SM, Prados MD, Cha S, et al. Role of Extent of Resection in the Long-Term Outcome of Low-Grade Hemispheric Gliomas. *J Clin Oncol* (2008) 26(8):1338–45. doi: 10.1200/JCO.2007.13.9337
12. Sanai N, Polley MY, Berger MS. Insular Glioma Resection: Assessment of Patient Morbidity, Survival, and Tumor Progression. *J Neurosurg* (2010) 112 (1):1–9. doi: 10.3171/2009.6.JNS0952
13. Capelle L, Fontaine D, Mandonnet E, Taillandier L, Golmard JL, Bauchet L, et al. Spontaneous and Therapeutic Prognostic Factors in Adult Hemispheric World Health Organization Grade II Gliomas: A Series of 1097 Cases: Clinical Article. *J Neurosurg* (2013) 118(6):1157–68. doi: 10.3171/2013.1.JNS121
14. Sanai N, Eschbacher J, Hattendorf G, Coons SW, Preul MC, Smith KA, et al. Intraoperative Confocal Microscopy for Brain Tumors: A Feasibility Analysis in Humans. *Neurosurgery* (2011) 68(2 Suppl Operative):282–90: discussion 90. doi: 10.1227/NEU.0b013e318212464e
15. Leroy HA, Delmaire C, Le Rhun E, Drumez E, Lejeune JP, Reyns N. High-Field Intraoperative MRI and Glioma Surgery: Results After the First 100 Consecutive Patients. *Acta Neurochir (Wien)* (2019) 161(7):1467–74. doi: 10.1007/s00701-019-03920-6
16. Seifert V, Gasser T, Senft C. Low Field Intraoperative MRI in Glioma Surgery. *Acta Neurochir Suppl* (2011) 109:35–41. doi: 10.1007/978-3-211-99651-5_6
17. Senft C, Bink A, Franz K, Vatter H, Gasser T, Seifert V. Intraoperative MRI Guidance and Extent of Resection in Glioma Surgery: A Randomised, Controlled Trial. *Lancet Oncol* (2011) 12(11):997–1003. doi: 10.1016/S1470-2045(11)70196-6
18. Senft C, Bink A, Heckelmann M, Gasser T, Seifert V. Glioma Extent of Resection and Ultra-Low-Field iMRI: Interim Analysis of a Prospective Randomized Trial. *Acta Neurochir Suppl* (2011) 109:49–53. doi: 10.1007/978-3-211-99651-5_8
19. Senft C, Schoenes B, Gasser T, Platz J, Bink A, Franz K, et al. Feasibility of Intraoperative MRI Guidance for Craniotomy and Tumor Resection in the Semisitting Position. *J Neurosurg Anesthesiol* (2011) 23(3):241–6. doi: 10.1097/ANA.0b013e31821bc003
20. Bo HK, Solheim O, Kvistad KA, Berntsen EM, Torp SH, Skjulsvik AJ, et al. Intraoperative 3D Ultrasound-Guided Resection of Diffuse Low-Grade Gliomas: Radiological and Clinical Results. *J Neurosurg* (2019) 132 (2):518–29. doi: 10.3171/2018.10.JNS181290
21. Hervey-Jumper SL, Berger MS. Maximizing Safe Resection of Low- and High-Grade Glioma. *J Neurooncol* (2016) 130(2):269–82. doi: 10.1007/s11060-016-2110-4
22. Conti Nibali M, Rossi M, Sciortino T, Riva M, Gay LG, Pessina F, et al. Preoperative Surgical Planning of Glioma: Limitations and Reliability of Fmri and DTI Tractography. *J Neurosurg Sci* (2019) 63(2):127–34. doi: 10.23736/S0390-5616.18.04597-6
23. Mert A, Gan LS, Knosp E, Sutherland GR, Wolfsberger S. Advanced Cranial Navigation. *Neurosurgery* (2013) 72 Suppl 1:43–53. doi: 10.1227/NEU.0b013e3182750c03
24. Mert A, Kiesel B, Wohrer A, Martinez-Moreno M, Minchev G, Furtner J, et al. Introduction of a Standardized Multimodality Image Protocol for Navigation-Guided Surgery of Suspected Low-Grade Gliomas. *Neurosurg Focus* (2015) 38(1):E4. doi: 10.3171/2014.10.FOCUS14597
25. Widhalm G, Minchev G, Woehrer A, Preusser M, Kiesel B, Furtner J, et al. Strong 5-Aminolevulinic Acid-Induced Fluorescence Is a Novel Intraoperative Marker for Representative Tissue Samples in Stereotactic Brain Tumor Biopsies. *Neurosurgical Rev* (2012) 35(3):381–91:discussion 91. doi: 10.1007/s10143-012-0374-5
26. Widhalm G, Kiesel B, Woehrer A, Traub-Weidinger T, Preusser M, Marosi C, et al. 5-Aminolevulinic Acid Induced Fluorescence Is a Powerful Intraoperative Marker for Precise Histopathological Grading of Gliomas With non-Significant Contrast-Enhancement. *PloS One* (2013) 8(10): e76988. doi: 10.1371/journal.pone.0076988
27. Millesi M, Kiesel B, Woehrer A, Hainfellner JA, Novak K, Martinez-Moreno M, et al. Analysis of 5-Aminolevulinic Acid-Induced Fluorescence in 55 Different Spinal Tumors. *Neurosurg Focus* (2014) 36(2):E11. doi: 10.3171/2013.12.FOCUS13485
28. Kiesel B, Millesi M, Woehrer A, Furtner J, Bavand A, Roetzer T, et al. 5-ALA-Induced Fluorescence as a Marker for Diagnostic Tissue in Stereotactic Biopsies of Intracranial Lymphomas: Experience in 41 Patients. *Neurosurg Focus* (2018) 44(6):E7. doi: 10.3171/2018.3.FOCUS1859
29. Kiesel B, Mischkulnig M, Woehrer A, Martinez-Moreno M, Millesi M, Mallouhi A, et al. Systematic Histopathological Analysis of Different 5-Aminolevulinic Acid-Induced Fluorescence Levels in Newly Diagnosed Glioblastomas. *J Neurosurg* (2018) 129(2):341–53. doi: 10.3171/2017.4.JNS162991
30. Millesi M, Kiesel B, Wöhrer A, Mercea PA, Bissolo M, Roetzer T, et al. Is Intraoperative Pathology Needed If 5-Aminolevulinic-Acid-Induced Tissue Fluorescence Is Found in Stereotactic Brain Tumor Biopsy? *Neurosurgery* (2020) 86(3):366–73. doi: 10.1093/neuros/nyz086
31. Millesi M, Kiesel B, Mazanec V, Wadiura LI, Wöhrer A, Herta J, et al. 5-ALA Fluorescence for Intraoperative Visualization of Spinal Ependymal Tumors and Identification of Unexpected Residual Tumor Tissue: Experience in 31 Patients. *J Neurosurg Spine* (2020) 4:1–9. doi: 10.3171/2020.6.SPINE20506
32. Widhalm G. Intra-Operative Visualization of Brain Tumors With 5-Aminolevulinic Acid-Induced Fluorescence. *Clin Neuropathol* (2014) 33 (4):260–78. doi: 10.5414/NP300798
33. Floeth FW, Sabel M, Ewelt C, Stummer W, Felsberg J, Reifenberger G, et al. Comparison of (18)F-FET PET and 5-ALA Fluorescence in Cerebral Gliomas. *Eur J Nucl Med Mol Imaging* (2011) 38(4):731–41. doi: 10.1007/s00259-010-1690-z
34. Valdes PA, Jacobs V, Harris BT, Wilson BC, Leblond F, Paulsen KD, et al. Quantitative Fluorescence Using 5-Aminolevulinic Acid-Induced Protoporphyrin IX Biomarker as a Surgical Adjunct in Low-Grade Glioma Surgery. *J Neurosurg* (2015) 123(3):771–80. doi: 10.3171/2014.12.JNS14391
35. Widhalm G, Olson J, Weller J, Bravo J, Han SJ, Phillips J, et al. The Value of Visible 5-ALA Fluorescence and Quantitative Protoporphyrin IX Analysis for Improved Surgery of Suspected Low-Grade Gliomas. *J Neurosurg* (2019) 10:1–10. doi: 10.3171/2019.1.JNS182614
36. Jaber M, Ewelt C, Wolfer J, Brokinkel B, Thomas C, Hasselblatt M, et al. Is Visible Aminolevulinic Acid-Induced Fluorescence an Independent

Biomarker for Prognosis in Histologically Confirmed (World Health Organization 2016) Low-Grade Gliomas? *Neurosurgery* (2019) 84(6):1214–24. doi: 10.1093/neuros/nyy365
37. Rasmussen BK, Hansen S, Laursen RJ, Kosteljanetz M, Schultz H, Norgard BM, et al. Epidemiology of Glioma: Clinical Characteristics, Symptoms, and Predictors of Glioma Patients Grade I-IV in the the Danish Neuro-Oncology Registry. *J Neurooncol* (2017) 135(3):571–9. doi: 10.1007/s11060-017-2607-5
38. Bauchet L. Epidemiology of Diffuse Low Grade Gliomas. In: Duffau H, editor. *Diffuse Low-Grade Gliomas in Adults*. Cham: Springer International Publishing (2017). p. 13–53. doi: 10.1007/978-3-319-55466-2_2
39. Diwanji TP, Engelman A, Snider JW, Mohindra P. Epidemiology, Diagnosis, and Optimal Management of Glioma in Adolescents and Young Adults. *Adolesc Health Med Ther* (2017) 8:99–113. doi: 10.2147/AHMT.S53391
40. Lombardi G, Barresi V, Castellano A, Tabouret E, Pasqualetti F, Salvalaggio A, et al. Clinical Management of Diffuse Low-Grade Gliomas. *Cancers (Basel)* (2020) 12(10):3008. doi: 10.3390/cancers12103008
41. Ohgaki H, Kleihues P. Population-Based Studies on Incidence, Survival Rates, and Genetic Alterations in Astrocytic and Oligodendroglial Gliomas. *J Neuropathol Exp Neurol* (2005) 64(6):479–89. doi: 10.1093/jnen/64.6.479
42. Buckner JC, Shaw EG, Pugh SL, Chakravarti A, Gilbert MR, Barger GR, et al. Radiation Plus Procarbazine, CCNU, and Vincristine in Low-Grade Glioma. *N Engl J Med* (2016) 374(14):1344–55. doi: 10.1056/NEJMoa1500925
43. Franceschi E, Mura A, De Biase D, Tallini G, Pession A, Foschini MP, et al. The Role of Clinical and Molecular Factors in Low-Grade Gliomas: What is Their Impact on Survival? *Future Oncol* (2018) 14(16):1559–67. doi: 10.2217/fon-2017-0634
44. McGirt MJ, Chaichana KL, Attenello FJ, Weingart JD, Than K, Burger PC, et al. Extent of Surgical Resection is Independently Associated With Survival in Patients With Hemispheric Infiltrating Low-Grade Gliomas. *Neurosurgery* (2008) 63(4):700–7author reply 7–8. doi: 10.1227/01.NEU.0000325729.41085.73
45. Hervey-Jumper SL, Berger MS. Role of Surgical Resection in Low- and High-Grade Gliomas. *Curr Treat Options Neurol* (2014) 16(4):284. doi: 10.1007/s11940-014-0284-7
46. Aghi MK, Nahed BV, Sloan AE, Ryken TC, Kalkanis SN, Olson JJ. The Role of Surgery in the Management of Patients With Diffuse Low Grade Glioma: A Systematic Review and Evidence-Based Clinical Practice Guideline. *J Neurooncol* (2015) 125(3):503–30. doi: 10.1007/s11060-015-1867-1
47. Soffietti R, Baumert BG, Bello L, von Deimling A, Duffau H, Frenay M, et al. Guidelines on Management of Low-Grade Gliomas: Report of an EFNS-EANO Task Force. *Eur J Neurol* (2010) 17(9):1124–33. doi: 10.1111/j.1468-1331.2010.03151.x
48. Sanai N, Berger MS. Glioma Extent of Resection and Its Impact on Patient Outcome. *Neurosurgery* (2008) 62(4):753–64discussion 264–6. doi: 10.1227/01.neu.0000318159.21731.cf
49. Fouke SJ, Benzinger T, Gibson D, Ryken TC, Kalkanis SN, Olson JJ. The Role of Imaging in the Management of Adults With Diffuse Low Grade Glioma: A Systematic Review and Evidence-Based Clinical Practice Guideline. *J Neurooncol* (2015) 125(3):457–79. doi: 10.1007/s11060-015-1908-9
50. Schäfer ML, Maurer MH, Synowitz M, Wüstefeld J, Marnitz T, Streitparth F, et al. Low-Grade (WHO II) and Anaplastic (WHO III) Gliomas: Differences in Morphology and MRI Signal Intensities. *Eur Radiol* (2013) 23(10):2846–53. doi: 10.1007/s00330-013-2886-y
51. van den Bent MJ, Wefel JS, Schiff D, Taphoorn MJ, Jaeckle K, Junck L, et al. Response Assessment in Neuro-Oncology (a Report of the RANO Group): Assessment of Outcome in Trials of Diffuse Low-Grade Gliomas. *Lancet Oncol* (2011) 12(6):583–93. doi: 10.1016/S1470-2045(11)70057-2
52. Guillevin R, Herpe G, Verdier M, Guillevin C. Low-Grade Gliomas: The Challenges of Imaging. *Diagn Interv Imaging* (2014) 95(10):957–63. doi: 10.1016/j.diii.2014.07.005
53. Shaver MM, Kohanteb PA, Chiou C, Bardis MD, Chantaduly C, Bota D, et al. Optimizing Neuro-Oncology Imaging: A Review of Deep Learning Approaches for Glioma Imaging. *Cancers (Basel)* (2019) 11(6):829. doi: 10.3390/cancers11060829
54. Choi YS, Ahn SS, Chang JH, Kang SG, Kim EH, Kim SH, et al. Machine Learning and Radiomic Phenotyping of Lower Grade Gliomas: Improving Survival Prediction. *Eur Radiol* (2020) 30(7):3834–42. doi: 10.1007/s00330-020-06737-5
55. Clarke JL, Chang SM. Neuroimaging: Diagnosis and Response Assessment in Glioblastoma. *Cancer J* (2012) 18(1):26–31. doi: 10.1097/PPO.0b013e318244d7c8
56. Norden AD, Pope WB, Chang SM. Current Concepts in Brain Tumor Imaging. *Am Soc Clin Oncol Educ Book* (2012) 32:119–24. doi: 10.14694/EdBook_AM.2012.32.119
57. Larsen J, Hoggard N, McKevitt FM. Imaging in Low-Grade Glioma: A Guide for Neurologists. *Pract Neurol* (2018) 18(1):27–34. doi: 10.1136/practneurol-2017-001686
58. Widhalm G, Wolfsberger S, Minchev G, Woehrer A, Krssak M, Czech T, et al. 5-Aminolevulinic Acid is a Promising Marker for Detection of Anaplastic Foci in Diffusely Infiltrating Gliomas With Nonsignificant Contrast Enhancement. *Cancer* (2010) 116(6):1545–52. doi: 10.1002/cncr.24903
59. Widhalm G, Krssak M, Minchev G, Wohrer A, Traub-Weidinger T, Czech T, et al. Value of 1H-Magnetic Resonance Spectroscopy Chemical Shift Imaging for Detection of Anaplastic Foci in Diffusely Infiltrating Gliomas With non-Significant Contrast-Enhancement. *J Neurol Neurosurg Psychiatry* (2011) 82(5):512–20. doi: 10.1136/jnnp.2010.205229
60. Chaichana KL, McGirt MJ, Laterra J, Olivi A, Quinones-Hinojosa A. Recurrence and Malignant Degeneration After Resection of Adult Hemispheric Low-Grade Gliomas. *J Neurosurg* (2010) 112(1):10–7. doi: 10.3171/2008.10.JNS08608
61. van den Bent MJ, Afra D, de Witte O, Ben Hassel M, Schraub S, Hoang-Xuan K, et al. Long-Term Efficacy of Early *Versus* Delayed Radiotherapy for Low-Grade Astrocytoma and Oligodendroglioma in Adults: The EORTC 22845 Randomised Trial. *Lancet* (2005) 366(9490):985–90. doi: 10.1016/S0140-6736(05)67070-5
62. Martin C, Alexander E3rd, Wong T, Schwartz R, Jolesz F, Black PM. Surgical Treatment of Low-Grade Gliomas in the Intraoperative Magnetic Resonance Imager. *Neurosurg Focus* (1998) 4(4):e8. doi: 10.3171/foc.1998.4.4.11
63. Pallud J, Capelle L, Taillandier L, Fontaine D, Mandonnet E, Guillevin R, et al. Prognostic Significance of Imaging Contrast Enhancement for WHO Grade II Gliomas. *Neuro Oncol* (2009) 11(2):176–82. doi: 10.1215/15228517-2008-066
64. White ML, Zhang Y, Kirby P, Ryken TC. Can Tumor Contrast Enhancement be Used as a Criterion for Differentiating Tumor Grades of Oligodendrogliomas? *AJNR Am J Neuroradiol* (2005) 26(4):784–90.
65. Ellenbogen JR, Walker C, Jenkinson MD. Genetics and Imaging of Oligodendroglial Tumors. *CNS Oncol* (2015) 4(5):307–15. doi: 10.2217/cns.15.37
66. Mert A, Buehler K, Sutherland GR, Tomanek B, Widhalm G, Kasprian G, et al. Brain Tumor Surgery With 3-Dimensional Surface Navigation. *Neurosurgery* (2012) 71(2 Suppl Operative):ons286–94discussion ons94–5. doi: 10.1227/NEU.0b013e31826a8a75
67. Verburg N, de Witt Hamer PC. State-of-the-Art Imaging for Glioma Surgery. *Neurosurg Rev* (2020) 44(3):1331–43. doi: 10.1007/s10143-020-01337-9
68. Vogelbaum MA, Jost S, Aghi MK, Heimberger AB, Sampson JH, Wen PY, et al. Application of Novel Response/Progression Measures for Surgically Delivered Therapies for Gliomas: Response Assessment in Neuro-Oncology (RANO) Working Group. *Neurosurgery* (2012) 70(1):234–43discussion 243–4. doi: 10.1227/NEU.0b013e318223f5a7
69. Skrinjar O, Nabavi A, Duncan J. Model-Driven Brain Shift Compensation. *Med Image Anal* (2002) 6(4):361–73. doi: 10.1016/S1361-8415(02)00062-2
70. Nabavi A, Black PM, Gering DT, Westin CF, Mehta V, Pergolizzi RS Jr, et al. Serial Intraoperative Magnetic Resonance Imaging of Brain Shift. *Neurosurgery* (2001) 48(4):787–97discussion 97–8. doi: 10.1227/00006123-200104000-00019
71. Nimsky C, Ganslandt O, Cerny S, Hastreiter P, Greiner G, Fahlbusch R. Quantification of, Visualization of, and Compensation for Brain Shift Using Intraoperative Magnetic Resonance Imaging. *Neurosurgery* (2000) 47(5):1070–9discussion 9–80. doi: 10.1097/00006123-200011000-00008
72. Gerard IJ, Kersten-Oertel M, Petrecca K, Sirhan D, Hall JA, Collins DL. Brain Shift in Neuronavigation of Brain Tumors: A Review. *Med Image Anal* (2017) 35:403–20. doi: 10.1016/j.media.2016.08.007
73. Barker FG2nd, Chang SM, Huhn SL, Davis RL, Gutin PH, McDermott MW, et al. Age and the Risk of Anaplasia in Magnetic Resonance-Nonenhancing Supratentorial Cerebral Tumors. *Cancer* (1997) 80(5):936–41. doi: 10.1002/(SICI)1097-0142(19970901)80:5<936::AID-CNCR15>3.0.CO;2-X
74. Ginsberg LE, Fuller GN, Hashmi M, Leeds NE, Schomer DF. The Significance of Lack of MR Contrast Enhancement of Supratentorial Brain Tumors in Adults: Histopathological Evaluation of a Series. *Surg Neurol* (1998) 49(4):436–40. doi: 10.1016/S0090-3019(97)00360-1

75. Sanai N, Snyder LA, Honea NJ, Coons SW, Eschbacher JM, Smith KA, et al. Intraoperative Confocal Microscopy in the Visualization of 5-Aminolevulinic Acid Fluorescence in Low-Grade Gliomas. *J Neurosurg* (2011) 115(4):740–8. doi: 10.3171/2011.6.JNS11252
76. Fahlbusch R, Nimsky C. Intraoperative MRI Developments. *Neurosurg Clin N Am* (2005) 16(1):xi–xiii. doi: 10.1016/j.nec.2004.07.012
77. Gasser T, Szelenyi A, Senft C, Muragaki Y, Sandalcioglu IE, Sure U, et al. Intraoperative MRI and Functional Mapping. *Acta Neurochir Suppl* (2011) 109:61–5. doi: 10.1007/978-3-211-99651-5_10
78. Nimsky C, Ganslandt O, Fahlbusch R. Functional Neuronavigation and Intraoperative MRI. *Adv Tech Stand Neurosurg* (2004) 29:229–63. doi: 10.1007/978-3-7091-0558-0_6
79. Nimsky C, Ganslandt O, Buchfelder M, Fahlbusch R. Intraoperative Visualization for Resection of Gliomas: The Role of Functional Neuronavigation and Intraoperative 1.5 T MRI. *Neurol Res* (2006) 28 (5):482–7. doi: 10.1179/016164106X115125
80. Mohammadi AM, Sullivan TB, Barnett GH, Recinos V, Angelov L, Kamian K, et al. Use of High-Field Intraoperative Magnetic Resonance Imaging to Enhance the Extent of Resection of Enhancing and Nonenhancing Gliomas. *Neurosurgery* (2013) 74(4):339–50. doi: 10.1227/NEU.0000000000000278
81. Makary M, Chiocca EA, Erminy N, Antor M, Bergese SD, Abdel-Rasoul M, et al. Clinical and Economic Outcomes of Low-Field Intraoperative MRI-Guided Tumor Resection Neurosurgery. *J Magn Reson Imaging* (2011) 34 (5):1022–30. doi: 10.1002/jmri.22739
82. Jenkinson MD, Barone DG, Bryant A, Vale L, Bulbeck H, Lawrie TA, et al. Intraoperative Imaging Technology to Maximise Extent of Resection for Glioma. *Cochrane Database Syst Rev* (2018) 1(1):Cd012788. doi: 10.1002/14651858.CD012788.pub2
83. Unsgaard G, Rygh OM, Selbekk T, Müller TB, Kolstad F, Lindseth F, et al. Intra-Operative 3D Ultrasound in Neurosurgery. *Acta Neurochir (Wien)* (2006) 148(3):235–53:discussion 53. doi: 10.1007/s00701-005-0688-y
84. Stepp H, Stummer W. 5-ALA in the Management of Malignant Glioma. *Lasers Surg Med* (2018) 50(5):399–419. doi: 10.1002/lsm.22933
85. Hadjipanayis CG, Stummer W. 5-ALA and FDA Approval for Glioma Surgery. *J Neurooncol* (2019) 141(3):479–86. doi: 10.1007/s11060-019-03098-y
86. Moore GE, Peyton WT, French LA, Walker WW. The Clinical Use of Fluorescein in Neurosurgery; the Localization of Brain Tumors. *J Neurosurg* (1948) 5(4):392–8. doi: 10.3171/jns.1948.5.4.0392
87. Kriegmair M, Baumgartner R, Knuchel R, Stepp H, Hofstadter F, Hofstetter A. Detection of Early Bladder Cancer by 5-Aminolevulinic Acid Induced Porphyrin Fluorescence. *J Urol* (1996) 155(1):105–9discussion 9–10. doi: 10.1016/S0022-5347(01)66559-5
88. Fritsch C, Becker-Wegerich PM, Schulte KW, Neuse W, Lehmann P, Ruzicka T, et al. [Photodynamic Therapy and Breast-Plasty of a Extensive Superficial Trunk Skin Basalioma of the Breast. An Effective Combination Therapy with Photodynamic Diagnosis]. *Hautarzt* (1996) 47(6):438–42. doi: 10.1007/s001050050447
89. Stummer W, Stocker S, Wagner S, Stepp H, Fritsch C, Goetz C, et al. Intraoperative Detection of Malignant Gliomas by 5-Aminolevulinic Acid-Induced Porphyrin Fluorescence. *Neurosurgery* (1998) 42(3):518–25discussion 25–6. doi: 10.1097/00006123-199803000-00017
90. Ishihara R, Katayama Y, Watanabe T, Yoshino A, Fukushima T, Sakatani K. Quantitative Spectroscopic Analysis of 5-Aminolevulinic Acid-Induced Protoporphyrin IX Fluorescence Intensity in Diffusely Infiltrating Astrocytomas. *Neurol Med Chir (Tokyo)* (2007) 47(2):53–7:discussion 7. doi: 10.2176/nmc.47.53
91. Ewelt C, Floeth FW, Felsberg J, Steiger HJ, Sabel M, Langen KJ, et al. Finding the Anaplastic Focus in Diffuse Gliomas: The Value of Gd-DTPA Enhanced MRI, FET-PET, and Intraoperative, ALA-Derived Tissue Fluorescence. *Clin Neurol Neurosurg* (2011) 113(7):541–7. doi: 10.1016/j.clineuro.2011.03.008
92. Jaber M, Wolfer J, Ewelt C, Holling M, Hasselblatt M, Niederstadt T, et al. The Value of 5-Aminolevulinic Acid in Low-Grade Gliomas and High-Grade Gliomas Lacking Glioblastoma Imaging Features: An Analysis Based on Fluorescence, Magnetic Resonance Imaging, 18F-Fluoroethyl Tyrosine Positron Emission Tomography, and Tumor Molecular Factors. *Neurosurgery* (2016) 78(3):401–11:discussion 11. doi: 10.1227/NEU.0000000000001020
93. Saito K, Hirai T, Takeshima H, Kadota Y, Yamashita S, Ivanova A, et al. Genetic Factors Affecting Intraoperative 5-Aminolevulinic Acid-Induced Fluorescence of Diffuse Gliomas. *Radiol Oncol* (2017) 51(2):142–50. doi: 10.1515/raon-2017-0019
94. Goryaynov SA, Widhalm G, Goldberg MF, Chelushkin D, Spallone A, Chernyshov KA, et al. The Role of 5-ALA in Low-Grade Gliomas and the Influence of Antiepileptic Drugs on Intraoperative Fluorescence. *Front Oncol* (2019) 9:423. doi: 10.3389/fonc.2019.00423
95. Stockhammer F, Misch M, Horn P, Koch A, Fonyuy N, Plotkin M. Association of F18-Fluoro-Ethyl-Tyrosin Uptake and 5-Aminolevulinic Acid-Induced Fluorescence in Gliomas. *Acta Neurochir (Wien)* (2009) 151 (11):1377–83. doi: 10.1007/s00701-009-0462-7
96. Müther M, Koch R, Weckesser M, Sporns P, Schwindt W, Stummer W. 5-Aminolevulinic Acid Fluorescence-Guided Resection of 18F-FET-PET Positive Tumor Beyond Gadolinium Enhancing Tumor Improves Survival in Glioblastoma. *Neurosurgery* (2019) 85(6):E1020–e9. doi: 10.1093/neuros/nyz199
97. Kim YI, Cho KG, Jang SJ. Comparison of Dual-Time Point 18F-FDG PET/CT Tumor-to-Background Ratio, Intraoperative 5-Aminolevulinic Acid Fluorescence Scale, and Ki-67 Index in High-Grade Glioma. *Med (Baltimore)* (2019) 98(8):e14397. doi: 10.1097/MD.0000000000014397
98. Pala A, Reske SN, Eberhardt N, Scheuerle A, König R, Schmitz B, et al. Diagnostic Accuracy of Intraoperative Perfusion-Weighted MRI and 5-Aminolevulinic Acid in Relation to Contrast-Enhanced Intraoperative MRI and (11)C-Methionine Positron Emission Tomography in Resection of Glioblastoma: A Prospective Study. *Neurosurgical Rev* (2019) 42(2):471–9. doi: 10.1007/s10143-018-0987-4
99. Arita H, Kinoshita M, Kagawa N, Fujimoto Y, Kishima H, Hashimoto N, et al. (1)(1)C-Methionine Uptake and Intraoperative 5-Aminolevulinic Acid-Induced Fluorescence as Separate Index Markers of Cell Density in Glioma: A Stereotactic Image-Histological Analysis. *Cancer* (2012) 118 (6):1619–27. doi: 10.1002/cncr.26445
100. Sanai N, Polley M-Y, McDermott MW, Parsa AT, Berger MS. An Extent of Resection Threshold for Newly Diagnosed Glioblastomas. *J Neurosurg* (2011) 115(1):3–8. doi: 10.3171/2011.2.JNS10998
101. Valdes PA, Leblond F, Kim A, Harris BT, Wilson BC, Fan X, et al. Quantitative Fluorescence in Intracranial Tumor: Implications for ALA-Induced Ppix as an Intraoperative Biomarker. *J Neurosurg* (2011) 115(1):11–7. doi: 10.3171/2011.2.JNS101451
102. Valdés PA, Kim A, Leblond F, Conde OM, Harris BT, Paulsen KD, et al. Combined Fluorescence and Reflectance Spectroscopy for *in Vivo* Quantification of Cancer Biomarkers in Low- and High-Grade Glioma Surgery. *J BioMed Opt* (2011) 16(11):116007. doi: 10.1117/1.3646916
103. Tonn JC, Stummer W. Fluorescence-Guided Resection of Malignant Gliomas Using 5-Aminolevulinic Acid: Practical Use, Risks, and Pitfalls. *Clin Neurosurg* (2008) 55:20–6.
104. Haj-Hosseini N, Richter J, Andersson-Engels S, Wardell K. Optical Touch Pointer for Fluorescence Guided Glioblastoma Resection Using 5-Aminolevulinic Acid. *Lasers Surg Med* (2010) 42(1):9–14. doi: 10.1002/lsm.20868
105. Utsuki S, Oka H, Sato S, Suzuki S, Shimizu S, Tanaka S, et al. Possibility of Using Laser Spectroscopy for the Intraoperative Detection of Nonfluorescing Brain Tumors and the Boundaries of Brain Tumor Infiltrates. *Tech note. J Neurosurg* (2006) 104(4):618–20. doi: 10.3171/jns.2006.104.4.618
106. Melo TB, Reisaeter G. The Physicochemical State of Protoporphyrin IX in Aqueous Solution Investigated by Fluorescence and Light Scattering. *Biophys Chem* (1986) 25(1):99–104. doi: 10.1016/0301-4622(86)85070-0
107. Valdes PA, Kim A, Brantsch M, Niu C, Moses ZB, Tosteson TD, et al. Delta-Aminolevulinic Acid-Induced Protoporphyrin IX Concentration Correlates With Histopathologic Markers of Malignancy in Human Gliomas: The Need for Quantitative Fluorescence-Guided Resection to Identify Regions of Increasing Malignancy. *Neuro Oncol* (2011) 13(8):846–56. doi: 10.1093/neuonc/nor086
108. Martínez-Moreno M, Kiesel B, Woehrer A, Mischkulnig M, Furtner J, Timelthaler G, et al. *Ex-Vivo* Analysis of Quantitative 5-ALA Fluorescence Intensity in Diffusely Infiltrating Gliomas Using a Handheld Spectroscopic Probe: Correlation With Histopathology, Proliferation and Microvascular Density. *Photodiagnosis Photodyn Ther* (2019) 27:354–61. doi: 10.1016/j.pdpdt.2019.05.013
109. Valdes PA, Roberts DW, Lu FK, Golby A. Optical Technologies for Intraoperative Neurosurgical Guidance. *Neurosurg Focus* (2016) 40(3):E8. doi: 10.3171/2015.12.FOCUS15550
110. Belykh E, Miller EJ, Carotenuto A, Patel AA, Cavallo C, Martirosyan NL, et al. Progress in Confocal Laser Endomicroscopy for Neurosurgery and

Technical Nuances for Brain Tumor Imaging With Fluorescein. *Front Oncol* (2019) 9:554. doi: 10.3389/fonc.2019.00554
111. Belykh E, Zhao X, Ngo B, Farhadi DS, Byvaltsev VA, Eschbacher JM, et al. Intraoperative Confocal Laser Endomicroscopy *Ex Vivo* Examination of Tissue Microstructure During Fluorescence-Guided Brain Tumor Surgery. *Front Oncol* (2020) 10:599250. doi: 10.3389/fonc.2020.599250
112. Martirosyan NL, Georges J, Eschbacher JM, Cavalcanti DD, Elhadi AM, Abdelwahab MG, et al. Potential Application of a Handheld Confocal Endomicroscope Imaging System Using a Variety of Fluorophores in Experimental Gliomas and Normal Brain. *Neurosurg Focus* (2014) 36(2): E16. doi: 10.3171/2013.11.FOCUS13486
113. Martirosyan NL, Eschbacher JM, Kalani MY, Turner JD, Belykh E, Spetzler RF, et al. Prospective Evaluation of the Utility of Intraoperative Confocal Laser Endomicroscopy in Patients With Brain Neoplasms Using Fluorescein Sodium: Experience With 74 Cases. *Neurosurg Focus* (2016) 40(3):E11. doi: 10.3171/2016.1.FOCUS15559
114. Erkkila MT, Bauer B, Hecker-Denschlag N, Madera Medina MJ, Leitgeb RA, Unterhuber A, et al. Widefield Fluorescence Lifetime Imaging of Protoporphyrin IX for Fluorescence-Guided Neurosurgery: An *Ex Vivo* Feasibility Study. *J Biophotonics* (2019) 12(6):e201800378. doi: 10.1002/jbio.201800378
115. Erkkilä MT, Reichert D, Gesperger J, Kiesel B, Roetzer T, Mercea PA, et al. Macroscopic Fluorescence-Lifetime Imaging of NADH and Protoporphyrin IX Improves the Detection and Grading of 5-Aminolevulinic Acid-Stained Brain Tumors. *Sci Rep* (2020) 10(1):20492. doi: 10.1038/s41598-020-77268-8
116. Reichert D, Erkkila MT, Holst G, Hecker-Denschlag N, Wilzbach M, Hauger C, et al. Towards Real-Time Wide-Field Fluorescence Lifetime Imaging of 5-ALA Labeled Brain Tumors With Multi-Tap CMOS Cameras. *BioMed Opt Express* (2020) 11(3):1598–616. doi: 10.1364/BOE.382817
117. Erkkilä MT, Reichert D, Hecker-Denschlag N, Wilzbach M, Hauger C, Leitgeb RA, et al. Surgical Microscope With Integrated Fluorescence Lifetime Imaging for 5-Aminolevulinic Acid Fluorescence-Guided Neurosurgery. *J BioMed Opt* (2020) 25(7):1–7. doi: 10.1117/1.JBO.25.7.071202
118. Berezin MY, Achilefu S. Fluorescence Lifetime Measurements and Biological Imaging. *Chem Rev* (2010) 110(5):2641–84. doi: 10.1021/cr900343z
119. Marcu L, Hartl BA. Fluorescence Lifetime Spectroscopy and Imaging in Neurosurgery. *IEEE J Sel Top Quantum Electron* (2012) 18(4):1465–77. doi: 10.1109/JSTQE.2012.2185823
120. Chorvat DC A. Multi-Wavelength Fluorescence Lifetime Spectroscopy: A New Approach to the Study of Endogenous Fluorescence in Living Cells and Tissues. *Laser Phys Lett* (2009) 6:175–93. doi: 10.1002/lapl.200810132
121. Schaefer PM, Kalinina S, Rueck A, von Arnim CAF, von Einem B. NADH Autofluorescence-a Marker on Its Way to Boost Bioenergetic Research. *Cytometry A* (2019) 95(1):34–46. doi: 10.1002/cyto.a.23597
122. Croce AC, Bottiroli G. Autofluorescence Spectroscopy and Imaging: A Tool for Biomedical Research and Diagnosis. *Eur J Histochem* (2014) 58(4):2461. doi: 10.4081/ejh.2014.2461
123. Valdes PA, Jacobs VL, Wilson BC, Leblond F, Roberts DW, Paulsen KD. System and Methods for Wide-Field Quantitative Fluorescence Imaging During Neurosurgery. *Opt Lett* (2013) 38(15):2786–8. doi: 10.1364/OL.38.002786
124. Jermyn M, Gosselin Y, Valdes PA, Sibai M, Kolste K, Mercier J, et al. Improved Sensitivity to Fluorescence for Cancer Detection in Wide-Field Image-Guided Neurosurgery. *BioMed Opt Express* (2015) 6(12):5063–74. doi: 10.1364/BOE.6.005063
125. Kantelhardt SR, Diddens H, Leppert J, Rohde V, Huttmann G, Giese A. Multiphoton Excitation Fluorescence Microscopy of 5-Aminolevulinic Acid Induced Fluorescence in Experimental Gliomas. *Lasers Surg Med* (2008) 40 (4):273–81. doi: 10.1002/lsm.20623
126. Kantelhardt SR. Multiphoton Microscopy and Fluorescence Lifetime Imaging: Applications in Biology and Medicine. In: K König, editor. Berlin/Boston: Walter de Gruyter GmbH & Co KG (2018). p. 450.
127. Russell J, Diamond KR, Collins TJ, Tiedje HF, Hayward J, Farrell T, et al. Characterization of Fluorescence Lifetime of Photofrin and Delta-Aminolevulinic Acid Induced Protoporphyrin IX in Living Cells Using Single- and Two-Photon Excitation. *IEEE J Selected Topics Quantum Electron* (2008) 14:158–66. doi: 10.1109/JSTQE.2007.912896
128. Kress M, Meier T, Steiner R, Dolp F, Erdmann R, Ortmann U, et al. Time-Resolved Microspectrofluorometry and Fluorescence Lifetime Imaging of Photosensitizers Using Picosecond Pulsed Diode Lasers in Laser Scanning Microscopes. *J BioMed Opt* (2003) 8(1):26–32. doi: 10.1117/1.1528595
129. Yankelevich DR, Ma D, Liu J, Sun Y, Sun Y, Bec J, et al. Design and Evaluation of a Device for Fast Multispectral Time-Resolved Fluorescence Spectroscopy and Imaging. *Rev Sci Instrum* (2014) 85(3):034303. doi: 10.1063/1.4869037
130. Sun Y, Hatami N, Yee M, Phipps J, Elson DS, Gorin F, et al. Fluorescence Lifetime Imaging Microscopy for Brain Tumor Image-Guided Surgery. *J BioMed Opt* (2010) 15(5):056022. doi: 10.1117/1.3486612
131. Wadiura LI, Mischkulnig M, Hosmann A, Borkovec M, Kiesel B, Rotzer T, et al. Influence of Corticosteroids and Antiepileptic Drugs on Visible 5-Aminolevulinic Acid Fluorescence in a Series of Initially Suspected Low-Grade Gliomas Including World Health Organization Grade II, III, and IV Gliomas. *World Neurosurg* (2020) 137:e437–e46. doi: 10.1016/j.wneu.2020.01.243
132. Lawrence JE, Steele CJ, Rovin RA, Belton RJJr., Winn RJ. Dexamethasone Alone and in Combination With Desipramine, Phenytoin, Valproic Acid or Levetiracetam Interferes With 5-ALA-Mediated Ppix Production and Cellular Retention in Glioblastoma Cells. *J Neurooncol* (2016) 127(1):15–21. doi: 10.1007/s11060-015-2012-x
133. Hefti M, Albert I, Luginbuehl V. Phenytoin Reduces 5-Aminolevulinic Acid-Induced Protoporphyrin IX Accumulation in Malignant Glioma Cells. *J Neurooncol* (2012) 108(3):443–50. doi: 10.1007/s11060-012-0857-9
134. Coburger J, Nabavi A, Konig R, Wirtz CR, Pala A. Contemporary Use of Intraoperative Imaging in Glioma Surgery: A Survey Among EANS Members. *Clin Neurol Neurosurg* (2017) 163:133–41. doi: 10.1016/j.clineuro.2017.10.033
135. Cavallo C, De Laurentis C, Vetrano IG, Falco J, Broggi M, Schiariti M, et al. The Utilization of Fluorescein in Brain Tumor Surgery: A Systematic Review. *J Neurosurg Sci* (2018) 62(6):690–703. doi: 10.23736/S0390-5616.18.04480-6
136. Zhang ZZ, Shields LB, Sun DA, Zhang YP, Hunt MA, Shields CB. The Art of Intraoperative Glioma Identification. *Front Oncol* (2015) 5:175. doi: 10.3389/fonc.2015.00175
137. Hansen RW, Pedersen CB, Halle B, Korshoej AR, Schulz MK, Kristensen BW, et al. Comparison of 5-Aminolevulinic Acid and Sodium Fluorescein for Intraoperative Tumor Visualization in Patients With High-Grade Gliomas: A Single-Center Retrospective Study. *J Neurosurg* (2019) 4:1–8. doi: 10.3171/2019.6.JNS191531
138. Xiang Y, Zhu XP, Zhao JN, Huang GH, Tang JH, Chen HR, et al. Blood-Brain Barrier Disruption, Sodium Fluorescein, and Fluorescence-Guided Surgery of Gliomas. *Br J Neurosurg* (2018) 32(2):141–8. doi: 10.1080/02688697.2018.1428731
139. Schebesch KM, Brawanski A, Hohenberger C, Hohne J. Fluorescein Sodium-Guided Surgery of Malignant Brain Tumors: History, Current Concepts, and Future Project. *Turk Neurosurg* (2016) 26(2):185–94. doi: 10.5137/1019-5149.JTN.16952-16.0
140. Akimoto J, Fukami S, Ichikawa M, Mohamed A, Kohno M. Intraoperative Photodiagnosis for Malignant Glioma Using Photosensitizer Talaporfin Sodium. *Front Surg* (2019) 6:12. doi: 10.3389/fsurg.2019.00012

Conflict of Interest: JF receives financial research support by NX Development Corp.

The remaining authors declare that the research was conducted in the absence of any commercial or financial relationships that could be construed as a potential conflict of interest.

frontiers in Oncology

ORIGINAL RESEARCH
published: 30 September 2021
doi: 10.3389/fonc.2021.668661

Redosing of Fluorescein Sodium Improves Image Interpretation During Intraoperative *Ex Vivo* Confocal Laser Endomicroscopy of Brain Tumors

Irakliy Abramov[1], *Alexander B. Dru*[1], *Evgenii Belykh*[2], *Marian T. Park*[1], *Liudmila Bardonova*[1] *and Mark C. Preul*[1]*

[1] *The Loyal and Edith Davis Neurosurgical Research Laboratory, Department of Neurosurgery, Barrow Neurological Institute, St. Joseph's Hospital and Medical Center, Phoenix, AZ, United States,* [2] *Department of Neurosurgery, Rutgers New Jersey Medical School, Newark, NJ, United States*

OPEN ACCESS

Edited by:
Constantinos G. Hadjipanayis, Mount Sinai Health System, United States

Reviewed by:
Randy D'Amico, Lenox Hill Hospital, United States
Francesco Acerbi, Fondazione IRCCS Istituto Neurologio Carlo Besta (IRCCS), Italy

***Correspondence:**
Mark C. Preul
Neuropub@barrowneuro.org

Specialty section:
This article was submitted to Neuro-Oncology and Neurosurgical Oncology, a section of the journal Frontiers in Oncology

Received: *16 February 2021*
Accepted: *13 September 2021*
Published: *30 September 2021*

Citation:
Abramov I, Dru AB, Belykh E, Park MT, Bardonova L and Preul MC (2021) Redosing of Fluorescein Sodium Improves Image Interpretation During Intraoperative Ex Vivo Confocal Laser Endomicroscopy of Brain Tumors. Front. Oncol. 11:668661. doi: 10.3389/fonc.2021.668661

Background: Fluorescein sodium (FNa) is a fluorescence agent used with a wide-field operating microscope for intraoperative guidance and with confocal laser endomicroscopy (CLE) to evaluate brain tissue. Susceptibility of FNa to degradation over time may affect CLE image quality during prolonged surgeries. This study describes improved characteristics of CLE images after intraoperative redosing with FNa.

Methods: A retrospective analysis was performed using CLE images obtained *ex vivo* from samples obtained during tumor resections with FNa-based fluorescence guidance with a wide-field operating microscope. The comparison groups included CLE images acquired after FNa redosing (redose imaging group), images from the same patients acquired after the initial FNa dose (initial-dose imaging group), and images from patients in whom redosing was not used (single-dose imaging group). A detailed assessment of image quality and interpretation regarding different FNa dosage and timing of imaging after FNa administration was conducted for all comparison groups.

Results: The brightest and most contrasting images were observed in the redose group compared to the initial-dose and single-dose groups ($P<0.001$). The decay of FNa signal negatively correlated with brightness (rho = -0.52, $P<0.001$) and contrast (rho = -0.57, $P<0.001$). Different doses of FNa did not significantly affect the brightness ($P=0.15$) or contrast ($P=0.09$) in CLE images. As the mean timing of imaging increased, the percentage of accurately diagnosed images decreased ($P=0.03$).

Conclusions: The decay of the FNa signal is directly associated with image brightness and contrast. The qualitative interpretation scores of images were highest for the FNa redose imaging group. Redosing with FNa to improve the utility of CLE imaging should be considered a safe and beneficial strategy during prolonged surgeries.

Keywords: brain tumors, confocal laser endomicroscopy, fluorescein sodium, fluorescence-guided neurosurgery, glioblastoma, image interpretation, redosing

1 INTRODUCTION

Intraoperative confocal laser endomicroscopy (CLE) is an emerging technology that evaluates brain tissue and pathologic tumor tissue *via* optical fluorescence-based interrogation. CLE technology produces images with resolution at cellular dimensions and displays them to the surgeon and pathologist in real time. CLE has the potential to maximize safe brain tumor resection and improve the positive yield and result time of tissue biopsy, particularly compared to frozen section biopsy, which may require significant time to return information vital to the progress of the surgical procedure. Unlike conventional clinical tools used for diagnostic work-up or in the operating room, CLE can provide real-time histopathologic information to distinguish tumor, non-tumor, and normal tissues *in vivo*. Thus, CLE can potentially improve tumor resection at the margin (1, 2).

To induce sufficient image contrast, either intravenous or topical exogenous fluorescence agents are used with CLE. Fluorescein sodium (FNa) was the first agent used for neurosurgical imaging based on its the previous success in gastroenterological CLE imaging (3). Since then, has been adopted as a fluorescence contrast for the first clinical-grade CLE system that has achieved US Food and Drug Administration (FDA) approval for use in neurosurgery. FNa has peak excitation at 494 nm and peak emission at 521 nm (4). When subjected to light at a wavelength of 560 nm, intravenously administered FNa emits a yellow-green fluorescence that marks the regions of blood-brain barrier (BBB) disruption (5, 6).

The initial clinical studies on research-grade CLE systems for brain tumor imaging with FNa were performed in the early 2010s in several centers (7–9). These studies involved the FNa administration protocol used in gastroenterology, specifically, the intravenous injection of an FNa bolus (5 ml) during the resection about 5 minutes before CLE imaging. During this same period, FNa was also being studied for use in neurosurgery as an intraoperative fluorescence contrast agent for wide-field guidance with an improved fluorescence filter set in the operating microscope (10, 11). These studies identified timing for FNa administration at the induction of anesthesia with a dose of 2 to 5 mg/kg. This timing and dosage have been used in a number of studies and have since become widely used in Europe and the United States.

We began assessing a CLE system for intraoperative neurosurgical use in 2016. The operation of this CLE system was based on the FNa Yellow 560 (Carl Zeiss Meditec AG, Oberkochen, Germany) fluorescence guidance protocol with FNa administration at the induction of anesthesia, a protocol that had already been established. The initial step in the use of the clinical-grade CLE system was to assess its performance in an *ex vivo* imaging environment. Our observations revealed that FNa signal intensity on CLE images was not always adequate to delineate the tissue at the time of surgical actions on the tumor when administered after anesthesia induction. This situation caused us to administer a second dose of FNa in order to achieve interpretable images and assess our imaging findings in greater detail. All fluorescence agents, including FNa, have a limited window of time during which their signal is optimal for visualization, after which they are subject to washout, metabolism, excretion, and photobleaching (12). Although some level of degradation is desirable so that fluorophores are excreted, a short half-life can compromise the contrast needed to accurately visualize tumor tissue morphology when longer observation is necessary or especially when actionable images are required for surgical decision-making. Therefore, effective deployment of CLE requires a refinement of dosing strategies and an appropriate choice of fluorescence dyes.

Preclinical animal-model studies and human clinical studies of brain tumors have reported promising results using FNa-based CLE for examining the histoarchitecture of and around brain tumors (13–18). However, FNa has a short half-life and is susceptible to degradation over time, which may affect CLE image interpretation during prolonged surgeries (19, 20). This shortcoming was circumvented with redosing with FNa, which we observed was beneficial for improving the clarity of CLE tissue visualization (18). Hence, redosing may provide histologic imaging information leading to more optimal tumor resection.

In this study, we describe these improved characteristics of CLE images when visualizing tumor tissue after FNa redosing. Through detailed image analysis, we assessed and quantified the enhanced quality of CLE images after FNa redosing in patients who underwent routine fluorescence-guided brain tumor resection using the Yellow 560 filter of the operating microscope together with *ex vivo* CLE imaging. This cohort was previously generally described by Belykh et al. (18). In this report, we analyze the differences in dosing strategies, diagnostic interpretation, and fluorescence signal strength and decay in addition to image quality. This report is the first to focus on FNa redosing to improve clinical CLE imaging of human brain tumor tissue.

2 MATERIAL AND METHODS

2.1 Study Design

Between August 2018 and May 2019, 47 adult patients (≥18 years) with brain tumors underwent FNa-guided surgery accompanied by *ex vivo* CLE imaging at Barrow Neurological Institute (Phoenix, Arizona) (18). The study was approved by the St. Joseph's Hospital and Medical Center Institutional Review Board for Human Research (No. 10BN130), and informed consent was obtained from patients. FNa was administered intravenously at the induction of anesthesia at a dose of 2 mg/kg or 5 mg/kg and could be redosed as such up to four times. Multiple tissue samples obtained during tumor resection were imaged using a CLE station (CONVIVO, Carl Zeiss Meditec, AG, Oberkochen, Germany) in the same operating room. FNa redosing (5 mg/kg) was performed when image brightness during tumor resection was considered inadequate by the neurosurgeon, based on interpretation of the CLE images. CLE

Abbreviations: 5-ALA, 5-aminolevulinic acid; BBB, blood–brain barrier; CLE, confocal laser endomicroscopy; FDA, Food and Drug Administration; FNa, fluorescein sodium; H&E, hematoxylin and eosin; ICG, indocyanine green; NIR, near infrared; PpIX, protoporphyrin IX; SD, standard deviation.

images were compared to the co-located conventional histologic hematoxylin and eosin (H&E)–stained images from the tissue biopsy preparations.

Seven patients had FNa redosed at some time during their surgery, but 1 case of redosing was excluded because the bandpass and longpass filters of the CLE system were used to manually increase the brightness of CLE images during surgery. All images from the remaining 6 redosing cases (4 gliomas, 1 metastasis, 1 choroid plexus carcinoma) were evaluated in this study. Each case was composed of multiple CLE optical biopsies or "spots" with a total of thousands of still CLE images.

Three FNa dose comparison imaging groups were generated for this analysis:

1) The redose imaging group (n=6) was composed of the cases where redose of FNa occurred during surgery. The redose occurred once, with FNa administered (2 to 5 mg/kg) according to the neurosurgeon's assessment that the FNa signal did not sufficiently yield clear, interpretable, actionable CLE images.
2) The initial-dose imaging group (n=6) was composed of the same 6 cases as above, but the CLE images evaluated and compared were those obtained before the patient was redosed. Thus, the FNa signal was assessed in the same group of patients at their initial dosing at the beginning of the surgical procedure and then when the neurosurgeon deemed it necessary to acquire informative guidance to progress with tumor resection or assessment of the tumor resection area.
3) A single-dose imaging group (n=9) was composed of the 9 remaining cases of glioma where an FNa redose was not administered, but that were regarded to have image qualities similar to the initial-dose imaging group and where the neurosurgeon did not request FNa redose. The glioma cases were chosen because they were most similar in pathological character to the redose imaging group of cases.

2.2 Image Analysis

Our analysis included intensity value assessments of images, image quality at different FNa dosages, diagnostic accuracy, and the timing of imaging after FNa administration for all three groups.

The collected images were processed using Fiji open-source software (21). The specific intensity measurements were selected to evaluate image quality objectively. Each image was assessed according to two intensity modalities, brightness and contrast, reported in software program-defined optical density units. Brightness was defined as the mean gray value within the selected image. The value was calculated from the sum of the gray values of all the pixels in the selection divided by the number of pixels. Contrast was defined as the standard deviation (SD) of the gray values used to generate the mean gray value. Values of intensity modalities from different groups were compared to each other and for different FNa doses. Also, the mean brightness and contrast values of different biopsy spots were assessed by different imaging acquisition times after FNa administration.

2.3 Image Evaluation

To assess how the quality of a CLE image affects its interpretation, 7 reviewers with different levels of experience in interpreting CLE images assessed the images (2 experienced neurosurgeons, 1 experienced neuropathologist, 2 inexperienced neurosurgeons, 2 inexperienced non-neurosurgeons). Each reviewer reviewed and subjectively graded the CLE images for quality on a scale of 1 to 5, with 5 being the highest quality, optimally clear image. No information was provided to reviewers regarding diagnosis, frozen section description, preoperative imaging, surgical procedure, or lesion location. CLE images that were recognized to show abnormal cells or pathologic vessels were graded as "lesional". "Normal" CLE images were defined by the presence of overwhelming or total normal brain tissue within the image. CLE images were considered "noninterpretable" based on an inability or difficulty to distinguish morphological structures. Images showing obvious artifacts, such as probe motion, acquisition problems, etc., were excluded. The overall interpretation of CLE images and H&E histologic sections was compared among different groups to define the diagnostic accuracy.

2.4 Statistical Analysis

Statistical analysis was performed using GraphPad Prism 9 (GraphPad Software, Inc., La Jolla, CA). Continuous variables were presented as means with standard deviations (SDs). Categorical variables were described using counts and percentages. The differences in intensity values and timing of imaging between the two groups were assessed with a Mann-Whitney U-test. Categorical variables in subgroups were compared with the chi-square test. The Spearman correlation coefficient was used to assess the association between the timing of imaging and intensity values. A P value < 0.05 was considered significant.

3 RESULTS

3.1 Descriptive Analysis

From 8854 available images, 1503 were excluded due to blackout signal or motion artifacts. Additionally, 335 images acquired with the CLE Z-stack image acquisition mode were excluded because the automatically recorded range of images from different focal depths represents an alternate image acquisition process that obstructs the analysis of image intensity. A total of 7016 images from 49 CLE imaging biopsies from the three imaging groups were identified for analysis: 1) the redose imaging group had 12 biopsies (2184 images); 2) the initial-dose imaging group had 18 biopsies (2535 images); and, 3) the single-dose imaging group had 19 biopsies (2297 images).

FNa dosing was 5 mg/kg per the redosing protocol for all 12 CLE imaging biopsies from the redose imaging group. FNa was administered at a dose of 5 mg/kg in 8 of 18 biopsies (44%) in the initial-dose imaging group and 2 of 19 biopsies (12%) in the single-dose imaging group, whereas 10 of 18 CLE imaging biopsies (56%) in the initial-dose imaging group and 17 of 19

CLE imaging biopsies (88%) in the single-dose imaging group were acquired at a FNa dose of 2 mg/kg.

CLE optical biopsy acquisition occurred at a mean (SD) of 6.4 (3.8) min after FNa administration in the redose imaging group, at 93.9 (50.1) min in the initial-dose imaging group, and at 123.2 (35.9) min in the single-dose imaging group.

3.2 Analysis of Image Intensity

3.2.1 Overall

The brightness and contrast values for images in the redose imaging group were higher than for images in the initial-dose imaging group (P<0.001) (**Figures 1**, **2**). Similarly, the images in the initial-dose imaging group had higher values of intensity modalities than in the single-dose imaging group (P<0.001).

3.2.2 FNa Dosing

Overall, mean (SD) brightness and contrast of images acquired at a FNa dose of 5 mg/kg were 71.7 (20.1) and 28.3 (7.0), respectively; at a dose of 2 mg/kg, results were 71.3 (22.4) and 24.3 (5.8), respectively. These different doses of FNa did not significantly affect the brightness (P=0.15) or contrast (P=0.09) of the CLE images (**Figure 3**). Images from the initial-dose imaging group were brighter and had better contrast than in the single-dose imaging group regardless of the difference of FNa dose (P<0.001). Further analysis on the timing of imaging after administration of FNa in these groups revealed a significant difference: images from the initial-dose imaging group were acquired at a shorter mean (SD) time when compared to the single-dose imaging group (93.9 [50.1] min *vs.* 123.2 [35.9] min, respectively; P=0.002).

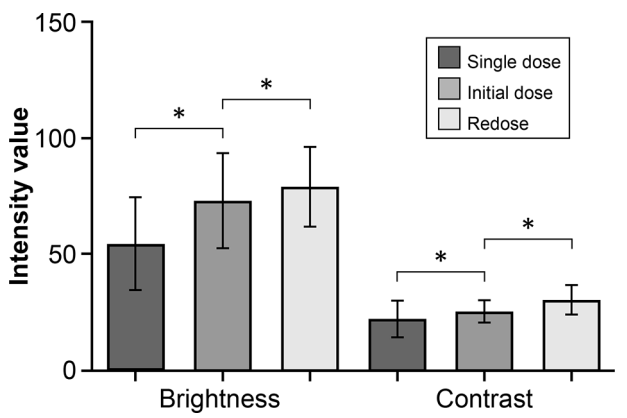

FIGURE 1 | Bar plot showing a comparison of the mean (SD) intensity modalities in the fluorescein sodium redose, initial-dose, and single-dose groups. The top and bottom whisker marks indicate the SD. *P < 0.001. The mean (SD) values of brightness and contrast of images are 79.1 (17.2) and 30.5 (6.3), respectively, in the redose group; 73.1 (20.4) and 25.4 (4.9) in the initial-dose group; and 54.6 (20.0) and 22.2 (7.9) in the single-dose group. The values are reported in units of optical density defined by Fiji open-source analytic software. Brightness is the mean gray value, calculated by the sum of the gray values of all the pixels in the selection divided by the number of pixels. Contrast is the SD of gray values used to generate the mean. SD, standard deviation. *Used with permission from Barrow Neurological Institute, Phoenix, Arizona.*

3.2.3 Timing of Imaging

The brightness and contrast values for each CLE optical biopsy from the three groups and the timing of imaging are shown in **Table 1**. The analysis of intensity values at different imaging time points after FNa administration revealed a moderate correlation between the imaging timing and image brightness for CLE biopsies (rho = -0.52, P<0.001) (**Figure 4A**). Similarly, a moderate correlation was observed between the imaging timing and image contrast for CLE biopsies (rho = -0.57, P<0.001) (**Figure 4B**).

3.3 Interpretation of Images

A qualitative assessment of images on a 1-to-5 scale showed that the highest mean (SD) scores were associated with images from the redose imaging group (4.5 [0.6]), followed by the initial-dose imaging group (2.3 [0.2]) and single-dose imaging group (2.3 [0.1]). Results of interpretation of CLE biopsies for each reviewer are shown in **Table 2**. When using images from the redose imaging group, the diagnostic accuracy was 83% regardless of reviewer experience. As the mean timing of imaging increased, the percentage of accurately diagnosed images decreased among reviewers and was significantly different for both experienced neurosurgeons (both P=0.03) and an experienced neuropathologist (P=0.03). No significant difference was observed in the diagnostic accuracy of groups by either inexperienced neurosurgeon (P=0.2 and P=0.1) or by the inexperienced non-neurosurgeons (both P=0.3).

4 DISCUSSION

FNa, which has been approved by the FDA for use in neurosurgery, is most frequently used in cerebrovascular and neuro-oncological procedures and is now also used with CLE. Although initially limited to ophthalmology, the use of FNa in neurosurgical applications was first reported in 1948 for localizing brain tumors (22). Its use in neurosurgery has expanded since the introduction of integrated fluorescence filters, such as the Yellow 560 filter, in clinical-grade operating microscopes (6, 10, 11, 19). Intravenous administration of FNa results in the extravasation of the compound in areas of disrupted BBB, such as those caused by a tumor (17).

CLE imaging technology allows neoplasm assessment through the presence of augmented fluorescence signals and real-time identification of abnormal tissue (15, 18). These novel handheld portable imaging systems have cellular-dimension resolution and can even allow visualization of subcellular structures. Optimization of these systems is being explored for maximal or better-informed tumor resection or tissue interrogation, particularly at the tumor margin, while preserving adjacent healthy brain tissue. Such technology may inform whether tumor invasion has occurred into exquisitely functional cortex, and thus whether resection should be halted.

Previously, our prospective clinical study examined the diagnostic accuracy of *ex vivo* intraoperative FNa-based CLE optical biopsies (18). In this study, we analyzed and described the improved features of the CLE images after FNa redosing and

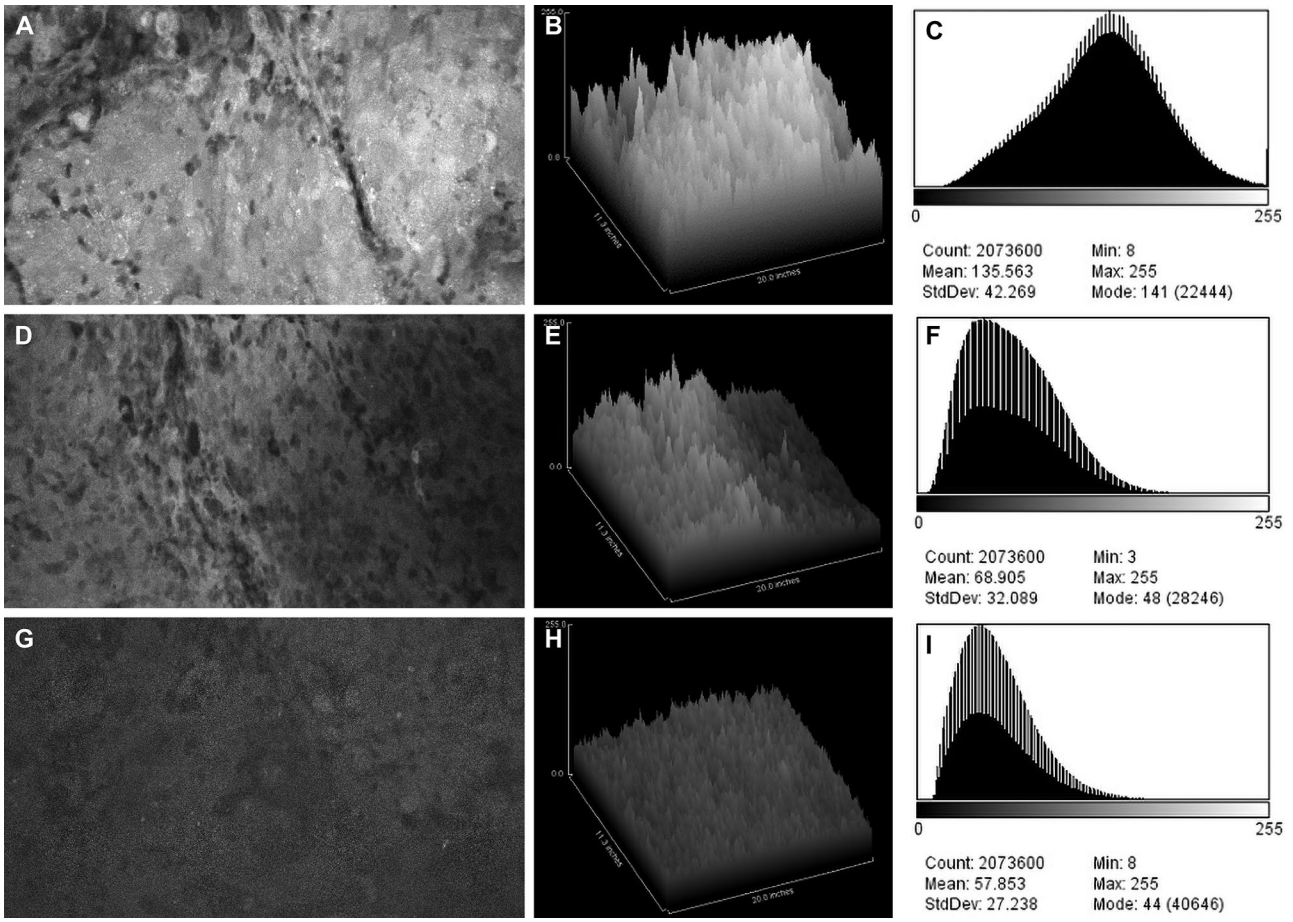

FIGURE 2 | Confocal laser endomicroscopy (CLE) images and data from **(A–C)** the fluorescein sodium redose, **(D–F)** initial-dose, and **(G–I)** single-dose groups. A CLE image **(A, D, G)** from each group is shown with a corresponding three-dimensional surface plot of pixel intensities **(B, E, H)** and a histogram of intensity values **(C, F, I)**. Count, number of pixels; Mean, brightness; StdDev, contrast; Min and Max, minimum and maximum gray values within the image; Mode, most frequently occurring gray value within the selection corresponds to the highest peak in the histogram. *Used with permission from Barrow Neurological Institute, Phoenix, Arizona.*

assessed image quality as the decay of FNa increased. Currently, FNa redosing is allowed at our institution under the parameters of institutional review board protocol for neurosurgical procedures, whereas in Europe, FNa redosing is not specified under the regulations and is therefore not performed.

Our study has shown improved CLE imaging results after the redosing of FNa during surgery. The first FNa dose was administered according to the wide-field fluorescence guidance protocol employing the operating microscope Yellow 560 module at the start of the anesthesia. CLE imaging could be performed successfully at this time parallel to the Yellow 560 imaging; however, in cases of insufficient FNa signal intensity and poor CLE image quality, redosing FNa (similar to its administration as per initial gastrointestinal protocol) can be performed to improve CLE image brightness, contrast, and overall quality for interpretation. Occasionally, CLE imaging acquisition occurs in a delayed fashion following FNa administration, which may result in decreased image quality, (i.e., darker, less interpretable images) as assessed by the operating neurosurgeon. In such cases, we have redosed the patient with FNa. We have not redosed patients with FNa multiple times, but our surgical protocol would allow up to four redosings at the low-dose parameters prescribed.

4.1 Image Intensity Analysis

The pharmacokinetics of intravenous FNa redistribution is nearly instantaneous, compared to the oral pathway and the time required for 5-aminolevulinic acid (5-ALA) distribution (23), which makes redosing of the latter infeasible. The 5-ALA metabolite induces protoporphyrin IX (PpIX) accumulation in tumor cells and takes longer to produce fluorescence than FNa (24). Intensity analysis is measured differently for 5-ALA than FNa because 5-ALA fluorescence emanates from cells, whereas FNa accumulates in the extracellular space. After oral administration of 5-ALA (20 mg/kg), peak fluorescence is expected in about 6 to 8 hours (25–27), with a fluorescence accumulation satisfactory for operation at around 3 hours. Fluorescence is eliminated with a terminal half-life of approximately 1 to 3 hours (27).

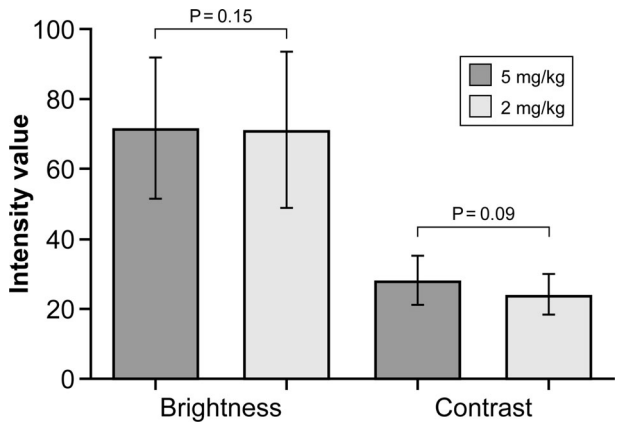

FIGURE 3 | Bar plot showing mean (SD) intensity modalities for confocal laser endomicroscopy images acquired after a fluorescein sodium dose of 5 mg/kg or 2 mg/kg. Whisker bars indicate the SD. The values are reported in units of optical density defined by Fiji open-source analytic software. Brightness is the mean gray value, calculated by the sum of the gray values of all the pixels in the selection divided by the number of pixels, and contrast is the SD of gray values used to generate the mean. *Used with permission from Barrow Neurological Institute, Phoenix, Arizona.*

This study assesses a central question relevant to the use of CLE for neurosurgery, which is a focus of the few centers currently permitted to use this technology. Only recently has one system been approved by the US FDA and European Medicines Agency for use in clinical neurosurgical work, which our institute and several other European centers are using. However, only in the United States is redosing of FNa permitted, thus our group of patients provides valuable data to guide administration of FNa. Ideally, the initial dose should be closer to the time of imaging as we have observed a time-associated decay of FNa fluorescence, with a corresponding decrease in CLE image quality. As a result, we investigated the benefit of FNa redosing because of its time-dependent degradation.

In the European centers using FNa, and initially in our center, FNa was administered shortly after the induction of anesthesia. However, after many minutes had passed in the performance of the craniotomy and start of tumor resection, it was observed that the CLE imaging was not optimal and could not be interpreted reliably. The FNa administration technique was then changed at our center so that FNa was administered nearer to the time that tumor resection was begun. Even after this change in administering FNa, many minutes may pass from the start of the tumor resection to the final stages of resection in which tumor extensions are evaluated in restricted or remote locations or where the tumor margins are unclear or suspicious within the resection bed. These final circumstances in tumor surgery, especially for invasive gliomas, often involve critical surgical decisions of whether to extend or curtail the surgical maneuvers toward optimizing the resection. During this time, the signal of FNa may deteriorate significantly and may require the administration of a redose to produce actionable CLE images. Redosing appears to be safe and effective, because the initial FNa dose is relatively low, and the resulting redose of FNa may provide exquisitely improved histological imaging information.

Our results demonstrated that among the three comparison groups, the brightest and most contrasting images were observed in the redose imaging group, when compared to the initial-dose imaging group and single-dose imaging group ($P<0.001$) (**Figure 5**). However, a significant difference in intensity values was observed between images after the initial FNa dose and images from the selected cases where an FNa redose was not used ($P<0.001$). The single-dose imaging group was initially hypothesized to have similar image qualities to the initial-dose imaging group because the acquisition of CLE images occurred at a relatively similar time after administration of a single FNa dose in both groups (93.9 [50.1] min *vs.* 123.2 [35.9] min). However, although we tried to match these groups for imaging timing, the difference of 30 minutes between these groups was substantial enough to affect the quality of images (**Figure 6**). This observation may be supported by the pharmakokinetics of FNa. We made every effort to exactly match the groups, and 30 minutes difference was as close as possible for the groups. These variances are the result of timely decisions made at surgery by the operating surgeon viewing and assessing the CLE images.

4.2 Timing of CLE Imaging

Approximately 80% of FNa binds weakly to plasma proteins, mainly to albumin, and the remaining 20% is the free salt (28, 29). Therefore, both forms of the fluorophore are initially present in systemic circulation before permeating through a damaged BBB and concentrating at the tumor site (30). Within 1 hour of intravenous administration, FNa is rapidly metabolized in the liver to fluorescein monoglucuronide, which also exhibits fluorescent properties but to a much lesser degree (20, 28, 31). Blair et al. (20) have reported that 4 to 5 hours after intravenous FNa injection, almost all plasma fluorescence is due to the weakly illuminating fluorescein monoglucuronide. Plasma elimination half-lives of fluorescein and fluorescein monoglucuronide are 23.5 and 264 minutes, respectively (20), with complete renal clearance by 24 to 32 hours (28, 32).

Given the time-dependent kinetics and limited signal duration of FNa and 5-ALA, the fluorescence strength of a given fluorophore can degrade over the course of an operation. The analysis of all CLE images obtained at different time intervals showed a gradual decrease in image quality as the signal decayed, resulting in darker images ($P<0.001$) and worse contrast ($P<0.001$) (**Figure 4**). In other words, FNa redosing was beneficial for the maintenance of image quality and higher diagnostic accuracy. However, due to the nonselective passive permeability of FNa, it may induce false-positive fluorescence in areas with surgical damage and edema that are classically present at tumor margins (19).

The problem of image quality degradation over time may be also related to the *ex vivo* nature of the analysis; with *in vivo* acquisition, this problem might be attenuated. *Ex vivo* CLE analysis could involve additional time to prepare the tissue sample for imaging. However, our setup for CLE imaging was directly within the operating room with tissue samples imaged within seconds after removal. Thus, we believe that these data

TABLE 1 | Image brightness, contrast, and timing for each CLE optical biopsy by FNa dosing groups.

FNa Group:CLE biopsy no.	Brightness*	Contrast*	Time after FNa dose, min
Redose			
1	88.2	33.2	5
2	95.0	25.2	10
3	88.7	31.2	15
4	72.9	26.8	3
5	76.8	34.6	5
6	51.2	31.7	5
7	51.1	23.0	5
8	78.7	29.6	5
9	76.7	39.9	5
10	73.2	27.5	3
11	97.8	28.3	2
12	89.2	29.5	10
Initial dose			
1	52.8	25.2	13
2	53.4	25.1	180
3	71.0	26.0	150
4	64.0	24.4	60
5	60.4	28.5	65
6	55.5	29.2	70
7	54.1	21.3	60
8	61.3	26.2	60
9	72.3	28.3	70
10	57.8	25.8	90
11	60.4	26.7	120
12	85.6	27.0	60
13	88.7	25.6	60
14	93.7	25.1	60
15	91.2	27.7	60
16	89.0	25.3	90
17	70.2	24.9	90
18	77.8	19.6	105
Single dose			
1	60	27.4	180
2	52	24.6	180
3	61	26.8	180
4	43	15.1	120
5	65	21.8	120
6	52.9	17	120
7	74.1	23.6	120
8	24.2	9.8	90
9	24	11.7	90
10	15.1	6.8	110
11	32.6	12.9	170
12	53.4	25.7	90
13	51.3	20.6	110
14	50.8	18.9	180
15	63.3	26.2	90
16	67.8	24.7	90
17	68.8	25.5	90
18	71	27	90
19	66	25	120

**Values are reported in units of optical density defined by Fiji open-source analytic software. Brightness is the mean gray value, calculated by the sum of the gray values of all the pixels in the selection divided by the number of pixels, and contrast is the standard deviation of gray values used to generate the mean.*

reflect closely what may occur with human *in vivo* FNa CLE imaging. We have observed similar results with repeated FNa dosing during *in vivo* imaging in animal tumor studies (17).

4.3 CLE Image Interpretation

Analysis of the reviewers' interpretations of CLE images showed that the diagnostic accuracy for CLE biopsies obtained after redose was 83% regardless of the reviewer's level of experience with CLE or in interpreting CLE images. This reveals obvious interpretable improvement in image quality. When analyzing images, the reviewers were blinded to patient and surgical data; thus, their CLE diagnostic accuracy would be expected to substantially increase if other clinical and surgical information were provided as normally occurs in patient management and

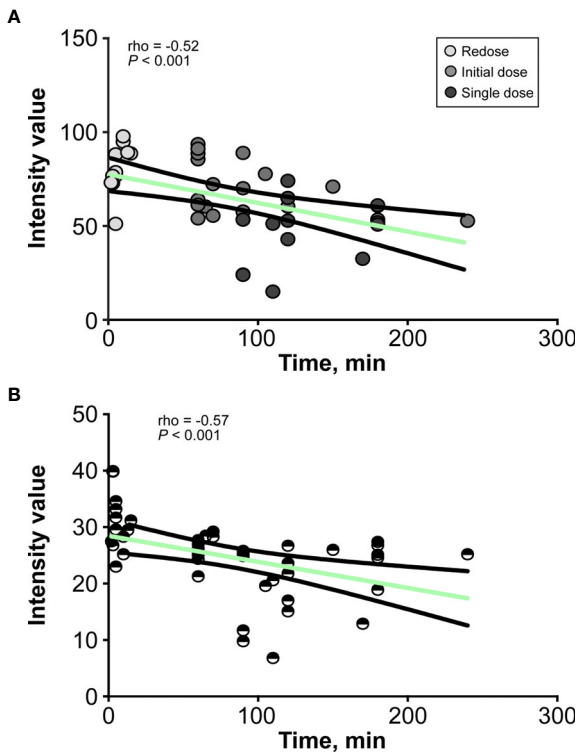

FIGURE 4 | Line graphs show the relationship between **(A)** the brightness and **(B)** the contrast of the confocal laser endomicroscopy image and the decay of fluorescein sodium in minutes. The values are reported in units of optical density defined by Fiji open-source analytic software. Brightness is the mean gray value, calculated by the sum of the gray values of all the pixels in the selection divided by the number of pixels, and contrast is the standard deviation of gray values used to generate the mean. *Used with permission from Barrow Neurological Institute, Phoenix, Arizona.*

operative situations. All 7 reviewers demonstrated a higher percentage of accurate diagnoses in the analysis of redose imaging group versus initial-dose imaging group and single-dose imaging group; however, there was a significant increase in diagnostic accuracy across the 3 groups for the experienced neurosurgeons and neuropathologist (**Table 2**). This finding likely indicates a more rigorous interpretation of CLE images by more experienced users familiar with the CLE system and images. Regardless, the longer the time from FNa dosing to CLE imaging generates poorer or less interpretable images. Similarly, subjective assessment of image quality showed that images from the redose imaging group were interpreted as the highest quality, which is supported by our intensity analysis. Standard deviation scores for image quality assessment were relatively low regardless of the reviewers' experience, which indicates that the improvement in the quality of images was obvious.

4.4 Safety Profile of FNa

The safety profile of FNa is well established, as confirmed in cross-sectional surveys, randomized studies, and prospective cohorts (33–38). Of note, patients with severe liver diseases may experience prolonged yellow skin discoloration after FNa administration due to slower excretion of the fluorophore (22). Rare anaphylactic reactions from FNa injection have been reported (39), but it has been less of a concern in recent neurosurgical applications, especially because FNa can be administered at lower doses using specific filters like Yellow 560 (11). In addition, FNa is devoid of the drawbacks associated with the metabolic fluorophore 5-ALA, which are the high cost and the need for patients to avoid sunlight and bright indoor light for 24 hours after administration due to porphyrin-related skin sensitivity (40, 41).

We reported that 1 patient who was administered 40 mg/kg of FNa experienced a yellow tinging of the skin that resolved within 48 hours, with no other adverse reactions (18, 42) (**Figure 7**). However, it is not clear whether FNa doses higher than administered in our study would result in a longer duration or a higher quality of signal since we did not observe significantly different brightness (P=0.15) and contrast (P=0.09) values between the different low FNa doses administered to the patients of this study.

4.5 Other Fluorophores

Recent studies have reported preliminary work on the simultaneous use of FNa and 5-ALA to provide fluorescent effects that would better discriminate pathologic tissue (27, 28). Suero Molina et al. (43) used a long-pass filter that allowed light to pass between 545 and 740 nm to allow simultaneous

TABLE 2 | Diagnostic accuracy of interpretation of CLE biopsies by reviewer.

	FNa Dosing Group			P value
	Redose, n=12	Initial dose, n=18	Single dose, n=19	
Mean timing, min*	6.4 ± 3.8	93.9 ± 50.1	123.2 ± 35.9	
Diagnostic accuracy, no. (%)				
Experienced neuropathologist	10 (83)	13 (72)	9 (47)	0.03
Experienced neurosurgeon	10 (83)	13 (72)	9 (47)	0.03
Experienced neurosurgeon	10 (83)	13 (72)	9 (47)	0.03
Inexperienced neurosurgeon	10 (83)	7 (39)	10 (53)	0.2
Inexperienced neurosurgeon	10 (83)	14 (78)	11 (58)	0.1
Inexperienced non-neurosurgeon	10 (83)	10 (56)	12 (63)	0.3
Inexperienced non-neurosurgeon	10 (83)	11 (61)	12 (63)	0.3

CLE, confocal laser endomicroscopy; FNa, fluorescein sodium.
**Mean timing of CLE biopsy imaging after FNa administration.*

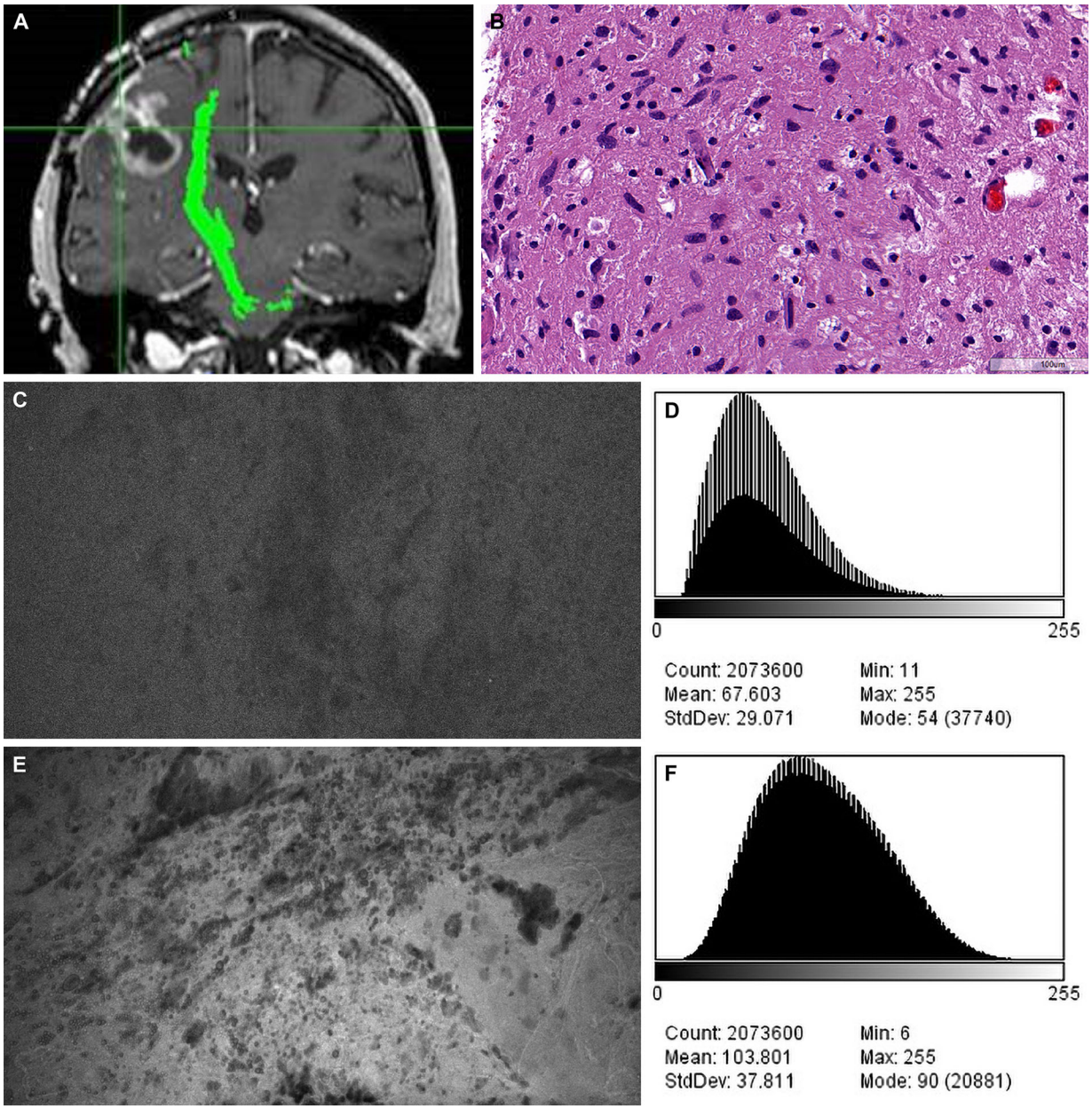

FIGURE 5 | Case example of confocal laser endomicroscopy (CLE) images acquired after fluorescein sodium (FNa) redosing. **(A)** Coronal T1-weighted magnetic resonance image with contrast. Biopsy specimens were obtained from the enhancing tumor in the left frontal lobe. **(B)** A diagnosis of high-grade glioma was made on the basis of H&E staining of the biopsy specimens. **(C)** A CLE image acquired 95 minutes after initial FNa injection lacks clarity and was regarded as noninterpretable. **(D)** A histogram corresponding to the image in C shows intensity values of the CLE image acquired after the initial FNa dose. **(E)** A marked increase in brightness and contrast of the CLE image was observed after FNa redosing. **(F)** A histogram corresponding to E shows the intensity values of the CLE image acquired after FNa redosing. Count, number of pixels; Mean, brightness; StdDev, contrast; Min and Max, minimum and maximum gray values within the image; Mode, most frequently occurring gray value within the selection corresponds to the highest peak in the histogram. *Used with permission from Barrow Neurological Institute, Phoenix, Arizona.*

visualization of FNa and PpIX fluorescence with appropriate light illumination. The investigators reported that FNa provided an enhanced background for 5-ALA fluorescence; tumor tissue was detected as a red-orange fluorescence due to dual-labeling of PpIX and FNa (43). Whether simultaneous FNa and 5-ALA administration could provide additional benefit to help surgically manage invasive brain tumors merit further investigation, especially as it relates to CLE-based tissue interrogation.

Other intraoperative fluorophore options include indocyanine green (ICG) and topical fluorescence stains. ICG has prior

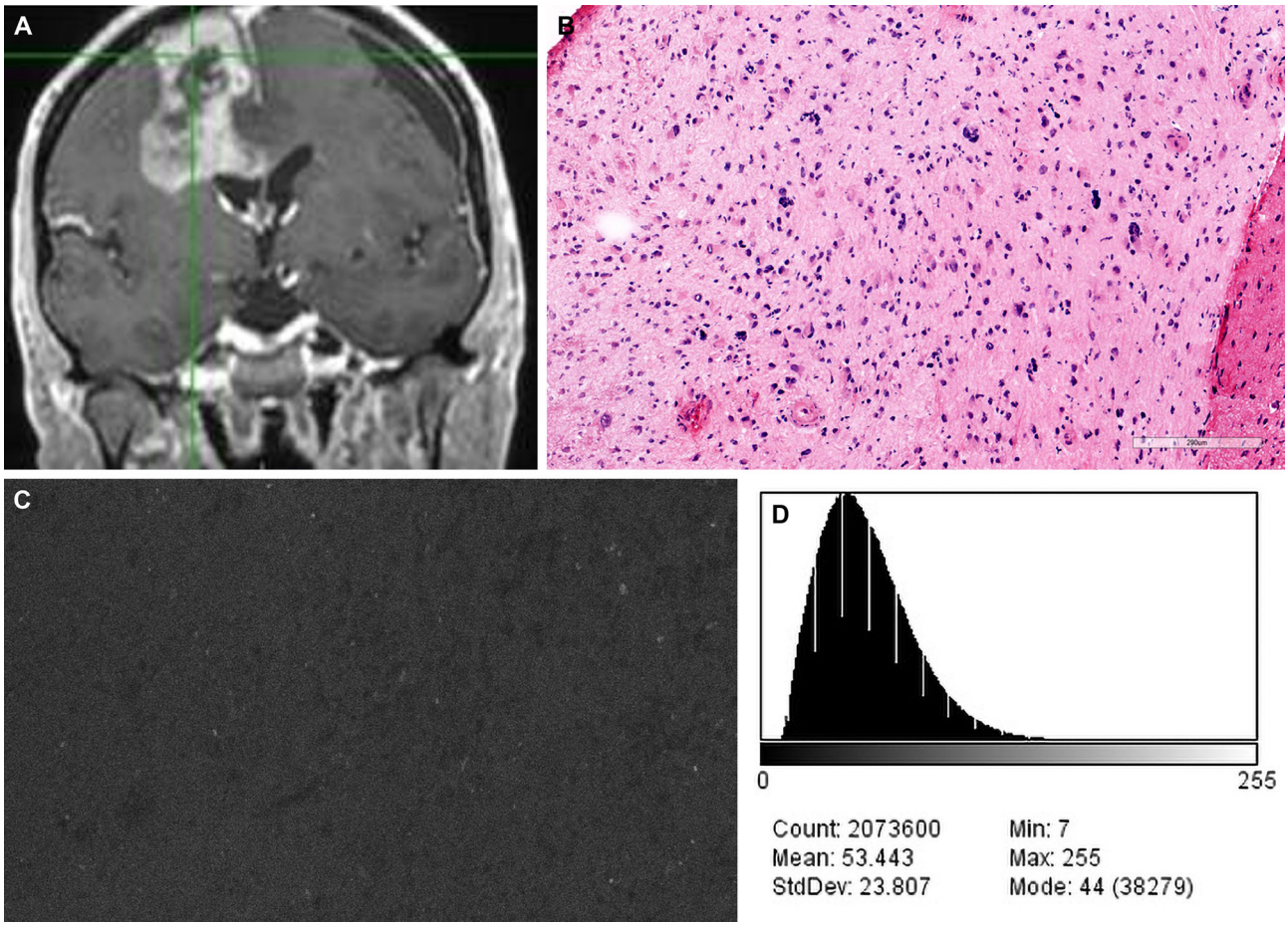

FIGURE 6 | Case example of confocal laser endomicroscopy (CLE) images acquired after a single dose of fluorescein sodium (FNa) before the concept of redosing was introduced. **(A)** Coronal T1-weighted magnetic resonance image with contrast. Biopsy specimens were obtained from the enhancing tumor in the left frontal lobe. **(B)** A diagnosis of high-grade glioma was made on the basis of H&E staining of biopsy specimens. **(C)** A CLE image acquired 180 minutes after FNa injection is dark and noninterpretable. **(D)** A corresponding histogram shows the intensity values of the CLE image. Count, number of pixels; Mean, brightness; StdDev, contrast; Min and Max, minimum and maximum gray values within the image; Mode, most frequently occurring gray value within the selection corresponds to the highest peak in the histogram. *Used with permission from Barrow Neurological Institute, Phoenix, Arizona.*

applications in neurosurgery, most commonly in cerebrovascular neurosurgery for angiography (28, 44). However, unlike FNa and 5-ALA, ICG is a near-infrared (NIR) fluorophore (peak excitation = 805 nm, peak emission = 835 nm), which leads to enhanced tissue penetration and less absorption of light by hemoglobin and other tissue proteins (45). ICG binds to plasma proteins, thereby remaining intravascular; however, in cases of BBB breakdown, ICG was taken up by the tumor cells (46). In a technique known as second-window ICG with the enhanced permeability and retention effects of both intra- and extra-axial neoplasms, administration of ICG 16 to 30 hours before surgery as a bolus allowed enhanced visualization of many brain tumors (47).

Currently, although CLE systems are used in research environments, ICG and other NIR fluorophores cannot be detected within the laser operating range of the clinical-grade FDA-approved CLE imaging system used in this study. Additional limitations of these fluorophores include a high false-positive rate due to the unspecific labeling of any tissue with altered vasculature, the need for specific NIR sensors in microscopes and/or exoscopes, and washout from any ambient light source. Topical contrast agents like acriflavine, acridine orange, and cresyl violet have been used for CLE (48), but they may not be suitable for *in vivo* application because of possible mutagenic effects (49). Currently, only FNa is approved for use with CLE (15), but next-generation targeted fluorophores may be appropriate for redosing or re-administration intraoperatively on demand.

Simultaneous imaging of different fluorophores is possible, but they cannot necessarily be administered simultaneously, as 5-ALA must be administered orally hours before the surgery, and ICG is best administered hours before surgery for optimal uptake by tumor cells (46). Although 5-ALA and ICG appear to label tissue at the cellular level, there are no approved CLE systems for their use in neurosurgery. Therefore, considerations of redosing these fluorophores with a CLE system are irrelevant at this time,

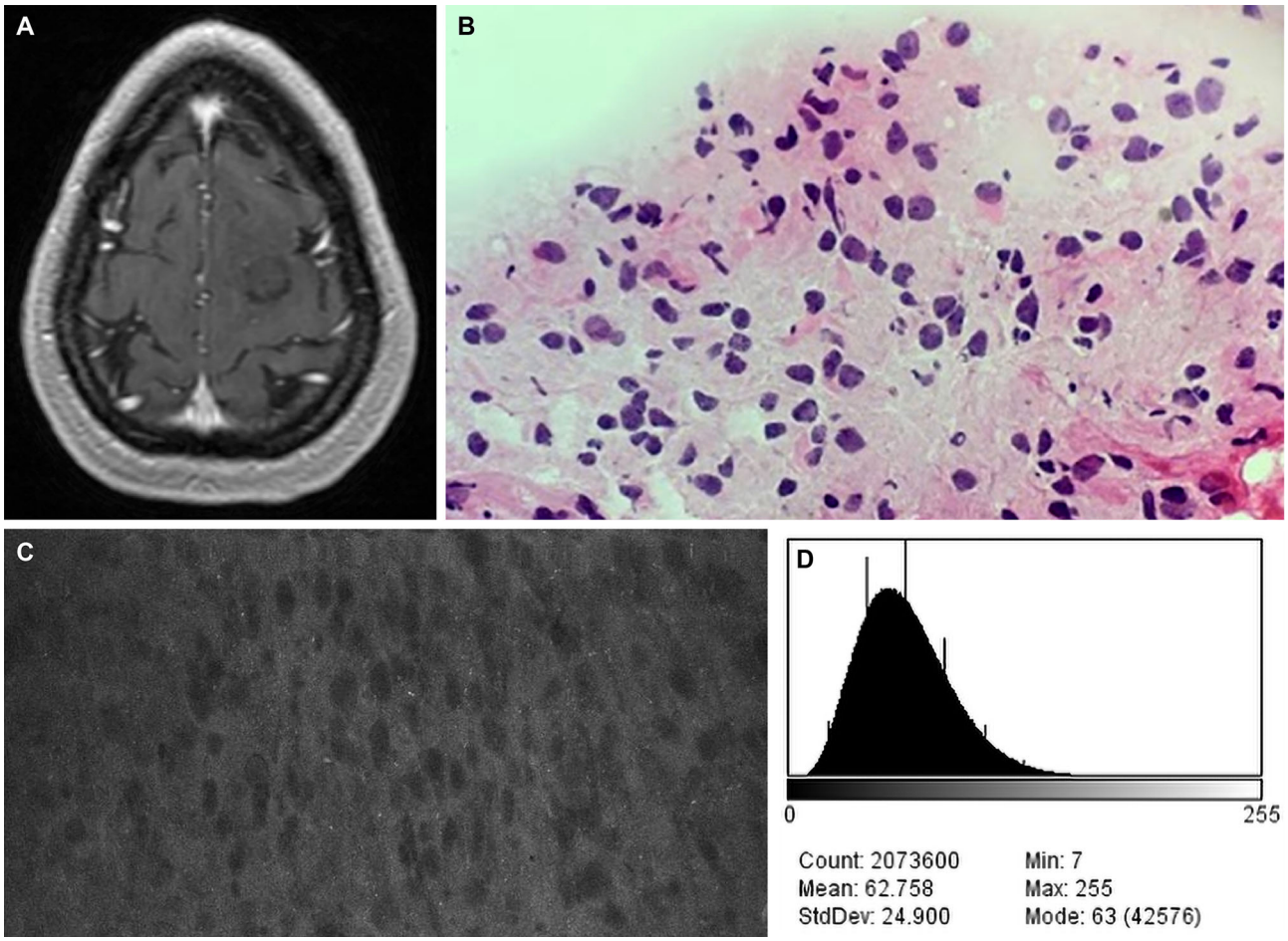

FIGURE 7 | Case example of CLE images acquired at a fluorescein sodium (FNa) dose of 40 mg/kg. **(A)** Axial T1-weighted magnetic resonance image with contrast. Biopsy specimens were obtained from the nonenhancing tumor in the left frontal lobe. **(B)** A diagnosis of low-grade glioma was made on the basis of H&E staining of biopsy specimens. **(C)** A CLE image acquired 90 minutes after FNa injection appears to be relatively dark, but tumor cells are still present. **(D)** A corresponding histogram shows the intensity values of the CLE image. Count, number of pixels; Mean, brightness; StdDev, contrast; Min and Max, minimum and maximum gray values within the image; Mode, most frequently occurring gray value within the selection corresponds to the highest peak in the histogram. *Used with permission from Barrow Neurological Institute, Phoenix, Arizona*.

and for 5-ALA such consideration would seem to be especially complex. Thus, although FNa is not taken up by cells in the same way as 5-ALA or ICG, in our experience, CLE with FNa contrast labelling demonstrates reasonable and useful histoarchitectural feature recognition and a good correlation of pathology compared to H&E stained histologic examination. Further delineation of the optimal timing of administration of these fluorophores alone and together with FNa is warranted.

4.6 CLE Technique Incorporation Into Surgery

CLE-guided tumor surgery using FNa fluorescence contrast is an emerging technology. CLE is not wide-field imaging such as that obtained by an operating microscope with fluorescence detection modules. Wide-field fluorescence imaging with the operating microscope does not show cellular resolution, but reveals a greater detection area of fluorescence signal, which is often vague or indeterminate at the margins. The so-called "contrast labeling" of tissue seen in FNa-based CLE provides histologic imaging information on the cellular level. CLE provides cellular resolution but is limited to a small field of view of histoarchitecture. It is also more sensitive to changes in fluorescence signal intensity and quality. Because this imaging system is so new, there has not been time to validate CLE imaging compared with wide-field operating microscope FNa imaging. These studies, which would seem to be advantageous for combining the two imaging techniques, especially for examination at the margins of invasive tumors, are underway. Currently, there are no guidelines or protocols as to when the initial dose of FNa should be administered in CLE-guided tumor surgery, and no other studies on the "redosing" of FNa exist. The relatively short half-life of FNa may affect the quality of images obtained with CLE; therefore, it is important to identify the optimal timing for planning of resection and intraoperative visualization of tumor histoarchitecture.

Unlike wide-field FNa-guided tumor resection, FNa-based CLE-guided resection provides surgeons and pathologists with histopathological information in real time, allowing them to distinguish between tumor and normal brain tissue and increasing the potential for an optimal tumor resection. The small field of view of CLE may not allow an exact tissue diagnosis, but it can help identify abnormal histoarchitecture. CLE offers an "optical biopsy," because of its ability to image at cellular or subcellular resolution, and it can therefore provide greater positive yield of tissue biopsies. CLE does not require tissue biopsy, as opposed to the tissue biopsy acquired with the use of the operating microscope and fluorescence detection modules. The surgeon and pathologist can interact in real time to interpret the CLE imaging produced on the fly.

Although the current FNa-based CLE system can be used without wide-field FNa fluorescence operating microscope technique, it would seem that the most reasonable and optimal use of FNa CLE would be its incorporation as an adjunctive tissue interrogation technology to surgery conducted with FNa *via* visualization using the operating microscope. It is also important to recognize that despite the benefit of FNa redosing seen in *ex vivo* conditions reported here, such redosing may interfere in the discrimination of the intra-axial tumoral tissue and normal brain tissue in the presence of surgical trauma during FNa-guided surgery. There may be iatrogenic leakage of FNa into the extracellular space, especially in the areas such as the tumor resection bed. In the first few seconds to minutes after administration, FNa defines the tumor well as viewed with the fluorescence module of the operating microscope, especially for high-grade gliomas, but then signal begins to emanate from surrounding surgical tissues, such as muscle or even scalp, as FNa distributes. Such FNa signal overage may become overwhelming when viewed through the operating microscope. Theoretically, CLE should be more sensitive in detecting changes in FNa signal, and thus the rationale to use repeated but low doses of FNa that will not overwhelm the fluorescence viewing system of the operating microscope. These redoses would be used when the CLE images have been determined to be inadequate for histoarchitecture discrimination and surgical decision-making.

4.7 Study Limitations

In the present sample of cases, only 6 patients were studied who underwent FNa reinjection, which is a low number for a powerful statistical analysis. However, although only 6 redosing cases were included, thousands of images were analyzed in each group. The cases studied mainly included gliomas and not tumors such as meningiomas, where there may be different FNa fluorescence characteristics. The principal use of CLE may find similar application in meningiomas where it may be used to image the dura to detect tumor invasion. FNa signal decay and retention is dependent on BBB permeability and hence may be different for various histopathological types of lesions. However, the CLE system was designed to be used mainly with primary invasive brain tumors.

Redosing of FNa was performed relatively late in our study period, as the idea had not been contemplated early on. At other times, redosing was not done because there was limited tissue sampling or no further tissue sampling was performed. At other times, the surgeon did not want to redose. Planning a future prospective multicenter study is reasonable, with FNa administration timing and dosing as structured as possible. In this study, we have not investigated the effect of the FNa redosing on wide-field operating microscope imaging results or its effectiveness in optimizing surgical resection.

Although most artifacts were excluded in the image analysis, red blood cells can still produce dark signals that may appear on CLE images with a different frequency. An abundance of such artifacts can directly affect the mean brightness and contrast of the image. In addition, alterations of the image acquisition filter systems should be widely explored to alter and improve image characteristics. As experience with CLE increases, more sophisticated technology for image processing and implementation of machine learning for image interpretation may be used.

5 CONCLUSIONS

The decay of the FNa signal revealed by CLE *ex vivo* imaging was directly associated with image intensity. Image brightness, contrast, and quality, and therefore interpretation, were improved with FNa redosing. However, given the diversity of factors influencing FNa metabolism and the individual surgical situation, the decision to redose a patient with FNa should be made for every clinical situation uniquely. This study demonstrates that FNa redosing, at least at 2 to 5 mg/kg, should be considered a safe and beneficial manipulation during prolonged resections of tumors and where CLE imaging is employed to interrogate the tumor and associated tissue region.

DATA AVAILABILITY STATEMENT

The raw data supporting the conclusions of this article will be made available by the authors, without undue reservation.

ETHICS STATEMENT

The studies involving human participants were reviewed and approved by the Institutional Review Board for Human Research at St. Joseph's Hospital and Medical Center. The patients/participants provided their written informed consent to participate in this study.

AUTHOR CONTRIBUTIONS

Study planning and coordination: MCP, IA. Acquisition of confocal images: EB. Processing and organizing of the data and confocal images: IA, AD, and MCP. Assessment of confocal images: IA, AD, MTP, LB, and MCP. Statistical analysis: IA. Writing a draft: IA, MTP, AD, and MCP. Review of the draft: all authors. Final approval: MCP. All authors contributed to the article and approved the submitted version.

FUNDING

This study was supported by funds from the Newsome Chair in Neurosurgery Research held by MCP and from Barrow Neurological Foundation.

ACKNOWLEDGMENTS

We thank the Neuroscience Publications staff at Barrow Neurological Institute for assistance with manuscript preparation.

REFERENCES

1. Zehri AH, Ramey W, Georges JF, Mooney MA, Martirosyan NL, Preul MC, et al. Neurosurgical Confocal Endomicroscopy: A Review of Contrast Agents, Confocal Systems, and Future Imaging Modalities. *Surg Neurol Int* (2014) 5:60. doi: 10.4103/2152-7806.131638
2. Belykh E, Cavallo C, Gandhi S, Zhao X, Veljanoski D, Izady Yazdanabadi M, et al. Utilization of Intraoperative Confocal Laser Endomicroscopy in Brain Tumor Surgery. *J Neurosurg Sci* (2018) 62(6):704–17. doi: 10.23736/S0390-5616.18.04553-8
3. Neumann H, Kiesslich R, Wallace MB, Neurath MF. Confocal Laser Endomicroscopy: Technical Advances and Clinical Applications. *Gastroenterology* (2010) 139(2):388–92, 92 e1-2. doi: 10.1053/j.gastro.2010.06.029
4. Pogue BW, Gibbs-Strauss S, Valdes PA, Samkoe K, Roberts DW, Paulsen KD. Review of Neurosurgical Fluorescence Imaging Methodologies. *IEEE J Sel Top Quantum Electron* (2010) 16(3):493–505. doi: 10.1109/JSTQE.2009.2034541
5. Belykh E, Shaffer KV, Lin C, Byvaltsev VA, Preul MC, Chen L. Blood-Brain Barrier, Blood-Brain Tumor Barrier, and Fluorescence-Guided Neurosurgical Oncology: Delivering Optical Labels to Brain Tumors. *Front Oncol* (2020) 10:739. doi: 10.3389/fonc.2020.00739
6. Schebesch KM, Proescholdt M, Hohne J, Hohenberger C, Hansen E, Riemenschneider MJ, et al. Sodium Fluorescein-Guided Resection Under the YELLOW 560 Nm Surgical Microscope Filter in Malignant Brain Tumor Surgery–a Feasibility Study. *Acta Neurochir (Wien)* (2013) 155(4):693–9. doi: 10.1007/s00701-013-1643-y
7. Sanai N, Eschbacher J, Hattendorf G, Coons SW, Preul MC, Smith KA, et al. Intraoperative Confocal Microscopy for Brain Tumors: A Feasibility Analysis in Humans. *Neurosurgery* (2011) 68(2 Suppl Operative):282–90; discussion 90. doi: 10.1227/NEU.0b013e318212464e
8. Eschbacher J, Martirosyan NL, Nakaji P, Sanai N, Preul MC, Smith KA, et al. In Vivo Intraoperative Confocal Microscopy for Real-Time Histopathological Imaging of Brain Tumors. *J Neurosurg* (2012) 116(4):854–60. doi: 10.3171/2011.12.JNS11696
9. Schlosser HG, Suess O, Vajkoczy P, van Landeghem FK, Zeitz M, Bojarski C. Confocal Neurolasermicroscopy in Human Brain - Perspectives for Neurosurgery on a Cellular Level (Including Additional Comments to This Article). *Cent Eur Neurosurg* (2010) 71(1):13–9. doi: 10.1055/s-0029-1237735
10. Acerbi F, Broggi M, Eoli M, Anghileri E, Cuppini L, Pollo B, et al. Fluorescein-Guided Surgery for Grade IV Gliomas With a Dedicated Filter on the Surgical Microscope: Preliminary Results in 12 Cases. *Acta Neurochir (Wien)* (2013) 155(7):1277–86. doi: 10.1007/s00701-013-1734-9
11. Acerbi F, Broggi M, Eoli M, Anghileri E, Cavallo C, Boffano C, et al. Is Fluorescein-Guided Technique Able to Help in Resection of High-Grade Gliomas? *Neurosurg Focus* (2014) 36(2):E5. doi: 10.3171/2013.11.FOCUS13487
12. Belykh E, Miller EJ, Patel AA, Bozkurt B, Yagmurlu K, Robinson TR, et al. Optical Characterization of Neurosurgical Operating Microscopes: Quantitative Fluorescence and Assessment of PpIX Photobleaching. *Sci Rep* (2018) 8(1):12543. doi: 10.1038/s41598-018-30247-6
13. Sankar T, Delaney PM, Ryan RW, Eschbacher J, Abdelwahab M, Nakaji P, et al. Miniaturized Handheld Confocal Microscopy for Neurosurgery: Results in an Experimental Glioblastoma Model. *Neurosurgery* (2010) 66(2):410–7. doi: 10.1227/01.NEU.0000365772.66324.6F
14. Foersch S, Heimann A, Ayyad A, Spoden GA, Florin L, Mpoukouvalas K, et al. Confocal Laser Endomicroscopy for Diagnosis and Histomorphologic Imaging of Brain Tumors In Vivo. *PLoS One* (2012) 7(7):e41760. doi: 10.1371/journal.pone.0041760
15. Martirosyan NL, Eschbacher JM, Kalani MY, Turner JD, Belykh E, Spetzler RF, et al. Prospective Evaluation of the Utility of Intraoperative Confocal Laser Endomicroscopy in Patients With Brain Neoplasms Using Fluorescein Sodium: Experience With 74 Cases. *Neurosurg Focus* (2016) 40(3):E11. doi: 10.3171/2016.1.FOCUS15559
16. Belykh E, Patel AA, Miller EJ, Bozkurt B, Yagmurlu K, Woolf EC, et al. Probe-Based Three-Dimensional Confocal Laser Endomicroscopy of Brain Tumors: Technical Note. *Cancer Manag Res* (2018) 10:3109–23. doi: 10.2147/CMAR.S165980
17. Belykh E, Miller EJ, Patel AA, Yazdanabadi MI, Martirosyan NL, Yagmurlu K, et al. Diagnostic Accuracy of a Confocal Laser Endomicroscope for In Vivo Differentiation Between Normal Injured And Tumor Tissue During Fluorescein-Guided Glioma Resection: Laboratory Investigation. *World Neurosurg* (2018) 115:e337–e48. doi: 10.1016/j.wneu.2018.04.048
18. Belykh E, Zhao X, Ngo B, Farhadi DS, Byvaltsev VA, Eschbacher JM, et al. Intraoperative Confocal Laser Endomicroscopy Ex Vivo Examination of Tissue Microstructure During Fluorescence-Guided Brain Tumor Surgery. *Front Oncol* (2020) 10:599250. doi: 10.3389/fonc.2020.599250
19. Stummer W, Suero Molina E. Fluorescence Imaging/Agents in Tumor Resection. *Neurosurg Clin N Am* (2017) 28(4):569–83. doi: 10.1016/j.nec.2017.05.009
20. Blair NP, Evans MA, Lesar TS, Zeimer RC. Fluorescein and Fluorescein Glucuronide Pharmacokinetics After Intravenous Injection. *Invest Ophthalmol Vis Sci* (1986) 27(7):1107–14.
21. Schindelin J, Arganda-Carreras I, Frise E, Kaynig V, Longair M, Pietzsch T, et al. Fiji: An Open-Source Platform for Biological-Image Analysis. *Nat Methods* (2012) 9(7):676–82. doi: 10.1038/nmeth.2019
22. Moore GE, Peyton WT, French LA, Walker WW. The Clinical Use of Fluorescein in Neurosurgery; the Localization of Brain Tumors. *J Neurosurg* (1948) 5(4):392–8. doi: 10.3171/jns.1948.5.4.0392
23. Hadjipanayis CG, Widhalm G, Stummer W. What is the Surgical Benefit of Utilizing 5-Aminolevulinic Acid for Fluorescence-Guided Surgery of Malignant Gliomas? *Neurosurgery* (2015) 77(5):663–73. doi: 10.1227/NEU.0000000000000929
24. Colditz MJ, Leyen K, Jeffree RL. Aminolevulinic Acid (ALA)-Protoporphyrin IX Fluorescence Guided Tumour Resection. Part 2: Theoretical, Biochemical and Practical Aspects. *J Clin Neurosci* (2012) 19(12):1611–6. doi: 10.1016/j.jocn.2012.03.013
25. Stummer W, Stocker S, Novotny A, Heimann A, Sauer O, Kempski O, et al. In Vitro and In Vivo Porphyrin Accumulation by C6 Glioma Cells After Exposure to 5-Aminolevulinic Acid. *J Photochem Photobiol B* (1998) 45(2-3):160–9. doi: 10.1016/s1011-1344(98)00176-6
26. Stummer W, Stocker S, Wagner S, Stepp H, Fritsch C, Goetz C, et al. Intraoperative Detection of Malignant Gliomas by 5-Aminolevulinic Acid-Induced Porphyrin Fluorescence. *Neurosurgery* (1998) 42(3):518–25; discussion 25-6. doi: 10.1097/00006123-199803000-00017
27. Stummer W, Stepp H, Wiestler OD, Pichlmeier U. Randomized, Prospective Double-Blinded Study Comparing 3 Different Doses of 5-Aminolevulinic Acid for Fluorescence-Guided Resections of Malignant Gliomas. *Neurosurgery* (2017) 81(2):230–9. doi: 10.1093/neuros/nyx074
28. Zhao X, Belykh E, Cavallo C, Valli D, Gandhi S, Preul MC, et al. Application of Fluorescein Fluorescence in Vascular Neurosurgery. *Front Surg* (2019) 6:52. doi: 10.3389/fsurg.2019.00052
29. Delori FC, Castany MA, Webb RH. Fluorescence Characteristics of Sodium Fluorescein in Plasma and Whole Blood. *Exp Eye Res* (1978) 27(4):417–25. doi: 10.1016/0014-4835(78)90020-9
30. Diaz RJ, Dios RR, Hattab EM, Burrell K, Rakopoulos P, Sabha N, et al. Study of the Biodistribution of Fluorescein in Glioma-Infiltrated Mouse Brain and Histopathological Correlation of Intraoperative Findings in High-Grade Gliomas Resected Under Fluorescein Fluorescence Guidance. *J Neurosurg* (2015) 122(6):1360–9. doi: 10.3171/2015.2.JNS132507
31. McLaren JW, Brubaker RF. Measurement of Fluorescein and Fluorescein Monoglucuronide in the Living Human Eye. *Invest Ophthalmol Vis Sci* (1986) 27(6):966–74.

32. Belykh E, Martirosyan NL, Yagmurlu K, Miller EJ, Eschbacher JM, Izadyyazdanabadi M, et al. Intraoperative Fluorescence Imaging for Personalized Brain Tumor Resection: Current State and Future Directions. *Front Surg* (2016) 3:55. doi: 10.3389/fsurg.2016.00055
33. Yannuzzi LA, Rohrer KT, Tindel LJ, Sobel RS, Costanza MA, Shields W, et al. Fluorescein Angiography Complication Survey. *Ophthalmology* (1986) 93 (5):611–7. doi: 10.1016/s0161-6420(86)33697-2
34. Kwiterovich KA, Maguire MG, Murphy RP, Schachat AP, Bressler NM, Bressler SB, et al. Frequency of Adverse Systemic Reactions After Fluorescein Angiography. Results of a Prospective Study. *Ophthalmology* (1991) 98(7):1139–42. doi: 10.1016/s0161-6420(91)32165-1
35. Kwan AS, Barry C, McAllister IL, Constable I. Fluorescein Angiography and Adverse Drug Reactions Revisited: The Lions Eye Experience. *Clin Exp Ophthalmol* (2006) 34(1):33–8. doi: 10.1111/j.1442-9071.2006.01136.x
36. Wallace MB, Meining A, Canto MI, Fockens P, Miehlke S, Roesch T, et al. The Safety of Intravenous Fluorescein for Confocal Laser Endomicroscopy in the Gastrointestinal Tract. *Aliment Pharmacol Ther* (2010) 31(5):548–52. doi: 10.1111/j.1365-2036.2009.04207.x
37. Teixidor P, Arraez MA, Villalba G, Garcia R, Tardaguila M, Gonzalez JJ, et al. Safety and Efficacy of 5-Aminolevulinic Acid for High Grade Glioma in Usual Clinical Practice: A Prospective Cohort Study. *PLoS One* (2016) 11(2): e0149244. doi: 10.1371/journal.pone.0149244
38. Stummer W, Pichlmeier U, Meinel T, Wiestler OD, Zanella F, Reulen HJ, et al. Fluorescence-Guided Surgery With 5-Aminolevulinic Acid for Resection of Malignant Glioma: A Randomised Controlled Multicentre Phase III Trial. *Lancet Oncol* (2006) 7(5):392–401. doi: 10.1016/S1470-2045(06)70665-9
39. Dilek O, Ihsan A, Tulay H. Anaphylactic Reaction After Fluorescein Sodium Administration During Intracranial Surgery. *J Clin Neurosci* (2011) 18 (3):430–1. doi: 10.1016/j.jocn.2010.06.012
40. Tonn JC, Stummer W. Fluorescence-Guided Resection of Malignant Gliomas Using 5-Aminolevulinic Acid: Practical Use, Risks, and Pitfalls. *Clin Neurosurg* (2008) 55:20–6.
41. Acerbi F, Cavallo C, Broggi M, Cordella R, Anghileri E, Eoli M, et al. Fluorescein-Guided Surgery for Malignant Gliomas: A Review. *Neurosurgical Rev* (2014) 37(4):547–57. doi: 10.1007/s10143-014-0546-6
42. Belykh E, Onaka NR, Zhao X, Abramov I, Eschbacher JM, Nakaji P, et al. High-Dose Fluorescein Reveals Unusual Confocal Endomicroscope Imaging of Low-Grade Glioma. *Front Neurol* (2021) 12:668656. doi: 10.3389/fneur.2021.668656
43. Suero Molina E, Ewelt C, Warneke N, Schwake M, Muther M, Schipmann S, et al. Dual Labeling With 5-Aminolevulinic Acid and Fluorescein in High-Grade Glioma Surgery With a Prototype Filter System Built Into a Neurosurgical Microscope: Technical Note. *J Neurosurg* (2019) 132 (6):1724–30. doi: 10.3171/2018.12.JNS182422
44. Raabe A, Beck J, Gerlach R, Zimmermann M, Seifert V. Near-Infrared Indocyanine Green Video Angiography: A New Method for Intraoperative Assessment of Vascular Flow. *Neurosurgery* (2003) 52(1):132–9; discussion 9. doi: 10.1097/00006123-200301000-00017
45. Cho SS, Salinas R, Lee JYK. Indocyanine-Green for Fluorescence-Guided Surgery of Brain Tumors: Evidence, Techniques, and Practical Experience. *Front Surg* (2019) 6:11. doi: 10.3389/fsurg.2019.00011
46. Martirosyan NL, Cavalcanti DD, Eschbacher JM, Delaney PM, Scheck AC, Abdelwahab MG, et al. Use of In Vivo Near-Infrared Laser Confocal Endomicroscopy With Indocyanine Green to Detect the Boundary of Infiltrative Tumor. *J Neurosurg* (2011) 115(6):1131–8. doi: 10.3171/2011.8.JNS11559
47. Zeh R, Sheikh S, Xia L, Pierce J, Newton A, Predina J, et al. The Second Window ICG Technique Demonstrates a Broad Plateau Period for Near Infrared Fluorescence Tumor Contrast in Glioblastoma. *PLoS One* (2017) 12 (7):e0182034. doi: 10.1371/journal.pone.0182034
48. Martirosyan NL, Georges J, Eschbacher JM, Cavalcanti DD, Elhadi AM, Abdelwahab MG, et al. Potential Application of a Handheld Confocal Endomicroscope Imaging System Using a Variety of Fluorophores in Experimental Gliomas and Normal Brain. *Neurosurg Focus* (2014) 36(2): E16. doi: 10.3171/2013.11.FOCUS13486
49. Charalampaki P, Javed M, Daali S, Heiroth HJ, Igressa A, Weber F. Confocal Laser Endomicroscopy for Real-Time Histomorphological Diagnosis: Our Clinical Experience With 150 Brain and Spinal Tumor Cases. *Neurosurgery* (2015) 62(Suppl 1):171–6. doi: 10.1227/NEU.0000000000000805

Conflict of Interest: The authors declare that the research was conducted in the absence of any commercial or financial relationships that could be construed as a potential conflict of interest.

Advantages of publishing in Frontiers

OPEN ACCESS
Articles are free to read for greatest visibility and readership

FAST PUBLICATION
Around 90 days from submission to decision

HIGH QUALITY PEER-REVIEW
Rigorous, collaborative, and constructive peer-review

TRANSPARENT PEER-REVIEW
Editors and reviewers acknowledged by name on published articles

Frontiers
Avenue du Tribunal-Fédéral 34
1005 Lausanne | Switzerland

Visit us: www.frontiersin.org
Contact us: frontiersin.org/about/contact

REPRODUCIBILITY OF RESEARCH
Support open data and methods to enhance research reproducibility

DIGITAL PUBLISHING
Articles designed for optimal readership across devices

FOLLOW US
@frontiersin

IMPACT METRICS
Advanced article metrics track visibility across digital media

EXTENSIVE PROMOTION
Marketing and promotion of impactful research

LOOP RESEARCH NETWORK
Our network increases your article's readership